Title
Crossed Molecular Beam Studies of Atmospheric Chemical Reaction Dynamics

Author
Zhang, J.

Publication Date
1993-04-01

LBL-34297
UC-401

Lawrence Berkeley Laboratory
UNIVERSITY OF CALIFORNIA

CHEMICAL SCIENCES DIVISION

Crossed Molecular Beam Studies of Atmospheric Chemical Reaction Dynamics

J. Zhang
(Ph.D. Thesis)

April 1993

Prepared for the U.S. Department of Energy under Contract Number DE-AC03-76SF00098

DISCLAIMER

LBL-34297
UC-401

CROSSED MOLECULAR BEAM STUDIES OF ATMOSPHERIC CHEMICAL REACTION DYNAMICS

Jingsong Zhang

(Ph.D. Thesis)

Department of Chemistry
University of California, Berkeley

and

Chemical Sciences Division, Lawrence Berkeley Laboratory
University of California, Berkeley, California 94720

April 1993

This work was supported by the Director, Office of Energy Research, Office of Basic Energy Sciences, Chemical Sciences Division, of the U.S. Department of Energy under Contract No. DE-AC03-76SF00098.

CROSSED MOLECULAR BEAM STUDIES OF ATMOSPHERIC CHEMICAL REACTION DYNAMICS

Jingsong Zhang

ABSTRACT

The dynamics of several elementary chemical reactions that are important in atmospheric chemistry are investigated. The reactive scattering of ground state chlorine or bromine atoms with ozone molecules and ground state chlorine atoms with nitrogen dioxide molecules is studied using a crossed molecular beams apparatus with a rotatable mass spectrometer detector.

The $Cl + O_3 \rightarrow ClO + O_2$ reaction has been studied at four collision energies ranging from 6 kcal/mole to 32 kcal/mole. The derived product center-of-mass angular and translational energy distributions show that the reaction has a direct reaction mechanism and that there is a strong repulsion on the exit channel. The ClO product is sideways and forward scattered with respect to the Cl atom, and the translational energy release is large. The Cl atom is most likely to attack the terminal oxygen atom of the ozone molecule.

The $Br + O_3 \rightarrow ClO + O_2$ reaction has been studied at five collision energies ranging from 5 kcal/mole to 26 kcal/mole. The derived product center-of-mass angular and translational energy distributions are quite similar to those in the Cl

+ O_3 reaction. The Br + O_3 reaction has a direct reaction mechanism similar to that of the Cl + O_3 reaction. The electronic structure of the ozone molecule seems to play the central role in determining the reaction mechanism in atomic radical reactions with the ozone molecule.

The Cl + NO_2 → ClO + NO reaction has been studied at three collision energies ranging from 10.6 kcal/mole to 22.4 kcal/mole. The center-of-mass angular distribution has some forward-backward symmetry, and the product translational energy release is quite large. The reaction proceeds through a short-lived complex whose lifetime is less than one rotational period. The experimental results seems to show that the Cl atom mainly attacks the oxygen atom instead of the nitrogen atom of the NO_2 molecule.

Table of Contents

ACKNOWLEDGEMENTS

I owe my foremost thanks to Prof. Yuan T. Lee. I am deeply grateful to Yuan for giving me the chance and encouragement to pursue research in chemical reaction dynamics. His scientific knowledge, intuition, and experimental skills have been invaluable sources of help for me. His enthusiasm and dedication to science have deeply inspired me. In addition to his scientific guidance, his integrity as a person as well as a scientist also greatly influenced me.

I also owe a great deal to the Lee group members. When I first started the experiments described in this thesis, I got a lot of help from Tzong-Tsong Miau. I am impressed by his knowledge of machining, electronics, and personal computers and by his carefulness about experimental techniques. It is also fun to work with him to solve computer problems. I was lucky to get my training on the 35" machine from Barbara Balko. I learned a great deal from her about running the big machine. She also showed me how to be a hard-working graduate student and how to face tough problems. Bob Continetti was very helpful to answer my questions about the machine, and I truly enjoyed talking with him. I also benefitted from him when he visited back in the lab, because I would often learn something that I never knew before.

I am deeply grateful to Floyd Davis and Arthur Suits for helping me to

start with the ozone beam source. They did a great job showing me every thing from safely handling ozone to obtaining a decent ozone molecular beam. I also got a lot of advice from them about the data fitting program. I am very thankful to James Chesko for keeping the YTLEE1 and YTLEE2 running, even though this task is getting more and more difficult. His efforts have really facilitated my thesis work. He also helped to shape my English in this thesis, and I wish his Chinese will improve. Jim Myers has been a useful source of knowledge, especially when I panicked in front of the computers. The test running of his XBEAM program was quite educative and helpful to me. Lately, I have benefitted from talking with him about thesis writing. I enjoy having Hongtao Hou and Jinchun Xie as the fellow group members. Hongtao and I have a lot in common, and I enjoy discuss many things with him, and I wish him the best in his experiments. It is a great pleasure to talk with Jinchun, and I find that I can learn a lot about lasers and other things from him. Laura Smoliar is always considerate and helpful, and I greatly appreciate her kindness. I am lucky to have friendly neighbors, the B-team, Pam Chu, Simon North, and Cheryl Longfellow. Mark Vrakking is a good officemate, and we can have very interesting conversations. I also would like to thank Allan Bracker, Doo Wan Boo, Martin Stemmler, Cindy Berrie, David Blank, Gangyu Liu, and the other Lee Group members for their assistance and kindness.

Ann Lawhead deserves a lot of credit for keeping the group running smoothly. Her experience with the LBL and campus paperwork and ability of

getting things done straight and fast saved us a lot of time and energy. I also greatly appreciate her kindness. Many people at LBL and on campus provided great help for my experimental problems, and I also learned a great deal from them about their field of expertise. Harry Chiladaskis kept Giauque Hall running smoothly, and quickly came to our rescue during emergence power shut-down. I wish to thank everybody in the Chemistry machine shop for their excellent technique support over the years. George, Ron, and Chuck were always very patient to go through my not-so-good drawings and managed to get the work done fast. I would like to thank all the people in instrument repair shop. Especially, thanks go to Yimin Xie. His efficient and quick repair on the mechanical pumps kept my experiments running. I wish to thank everyone in the Chemistry glass shop and Chemistry electronic shop for their support. I would also like to thank Joe Katz at LBL electronic shop for his assistance.

I would like to thank Prof. D. A. Shirley for his early guidance. I appreciate the help and kindness from Zhengqing Huang, Jane Medhurst, Roger van Zee, Laisheng Wang, and Phil Heimann. I am greatly indebted to my teachers in University of Science and Technology of China, especially Prof. Shuqin Yu, Prof. Fanao Kong, and Prof. Xingxiao Ma. Their support, their encouragement, their expectations, and their friendship have been so important to me over the years. I also appreciate all my other friends here and in China.

With out the support of my family, I would certainly not be able to achieve what I have today. My parents have always encouraged and supported my

efforts. I also thank my brother for his understanding and kindness. Finally, my wife, Qiuxia Amber Zhao, has been an essential part of my life as a graduate student in Berkeley. In the early years, she sent me a lot of encouragement and love over the Pacific, and late on, her sacrifices, love, understanding, and assistance have contributed to my graduate studies in invaluable ways.

This work was supported by the Director, Office of Energy Research, Office of Basic Energy Sciences, Chemical Sciences Division of the U. S. Department of Energy under Contract No. DE-AC03-76SF00098.

CHAPTER 1

INTRODUCTION

Chemical reaction dynamics involves the study of chemical reactions on a fundamental level with all reactants prepared in well defined states and under well controlled reaction conditions. A complete picture of a chemical reaction will be obtained if all the properties of the products and their distribution functions are measured. Many experimental techniques have been developed in the past decades and a lot of progress has been made.[1,2] Among the experimental tools to study the chemical reaction dynamics, the crossed molecular beams technique is especially powerful and elegant.[3-5]

In our group, the universal crossed molecular beam apparatus is used for reactive scattering experiments.[5,6] Two supersonic molecular beams are crossed at a fixed angle of 90°, and the product laboratory angular distribution and time-of-flight spectra at various laboratory angles are measured with a rotatable mass spectrometric detector. An electron impact ionizer is used in the mass spectrometer, therefore, the detector in our crossed molecular beam apparatus is applicable to most species of interest.

The crossed molecular beam studies have contributed significantly to the understanding of the basics of chemical reaction dynamics.[1-4] They also have

provided rich information for understanding the fundamental processes in combustion chemistry.[4,7] However, for another type of complicated and important "real life" chemistry, atmospheric chemistry, there have been very few crossed molecular beam studies.[8] If some of the fundamental processes are understood in great detail, a clearer picture for the modeling system in atmospheric chemistry will be obtained.

One very important subject in atmospheric chemistry is stratospheric ozone loss.[9,10] It is currently believed that ClO radical plays the central role of the ozone depletion cycles and that BrO radical is also significantly involved in the ozone depletion. The $Cl + O_3 \rightarrow ClO + O_2$ and $Br + O_3 \rightarrow BrO + O_2$ reactions, two reactions studied in the thesis, are the sources of ClO and BrO radicals in stratosphere, respectively. As for the $Cl + NO_2 \rightarrow ClO + NO$ reaction, the third reaction studied in this thesis, its reverse reaction $ClO + NO \rightarrow Cl + NO_2$ is important in the overall balance of odd oxygen in stratosphere. Of course, these reactions are interesting even only for the purpose of fundamental reaction dynamic studies. As we discuss in the following chapters, interesting and rich chemistry has been seen in these systems.

In Chapters 2 and 3, we will discuss the reactive scattering of the $Cl + O_3$ and $Br + O_3$ reactions. Ozone is an interesting molecule, and a large number of kinetic studies of the ozone reactions have been carried out.[11] The reaction dynamic study of the $Cl + O_3 \rightarrow ClO + O_2$ reaction could provide information for understanding the mechanism of the more complicated ozone reactions. The Br

+ O_3 reaction is studied along with the Cl + O_3 reaction to obtain systematic understanding of the ozone reactions with atomic radicals. The results from these two experiments are strikingly similar. The electronic structure of the ozone molecule should play the central role in determining the mechanism of these reactions, and the transition state structures in these reactions should closely resemble that of the stable ozone molecule. Finally, it might be interesting to extend this work to the I + O_3 reaction. It has been suggested that electron density could be transferred from the ozone molecule to the Cl atom or Br atom in the Cl + O_3 or Br + O_3 reaction;[12] however, in the I + O_3 reaction, the electron density is expected to be transferred in the reverse direction because of the much lower ionization potential of the iodine atom. If the electron density is indeed transferred from the I atom to the ozone molecule, different reaction dynamics might happen.

In the tradition of chemical dynamics, the progress of experimental studies is accompanied by that of theoretical studies. The reactive scattering experiments can provide some of the experimental measurements that can be most straightforwardly compared with the theoretical calculations. A semi-empiric study of the Cl + O_3 reaction has been available.[13] Its results qualitatively agree with our experimental results in the Cl + O_3 study; however, the ClO_3 potential energy surface (PES) certainly needs to be improved. We hope that the reactive scattering study of the Cl + O_3 and Br + O_3 reactions, as well as the study of the following Cl + NO_2 reaction, could stimulate more theoretical studies of these

reactions.

In Chapter 4 the reaction $Cl + NO_2 \rightarrow ClO + NO$ is discussed. For this endoergic reaction, besides the angular distribution and the time-of-flight spectra, the energy dependence of the reaction cross section, i.e., the excitation function, is also measured. The excitation function could provide rich information about the reaction dynamics as well. The molecular beams technique allows us to adjust the collision energy of the reactive scattering so that the excitation function could be measured. This reaction is found to be quite different from the $Cl + O_3$ and $Br + O_3$ reactions. It is shown that the reaction $Cl + NO_2 \rightarrow ClO + NO$ proceeds through a short-lived complex.

A large amount of dynamic information has been obtained from the reactive scattering experiments in this thesis; however, these experiments are carried out using only atomic radical beams. Of course, these atomic radical reactions are very important. However, the challenging goal in the reactive scattering experiments is to produce diatomic or polyatomic radical beams to extend the scope of the reactions that the crossed molecular beams technique could study. To extend the study of atmospheric chemistry using the crossed molecular beams technique, it would be helpful to produce ClO radical beam and OH radical beam. Reactions of ClO radical are certainly important because it plays the central role in the ozone destruction cycles. Reactions of OH radical are of fundamental importance not only in combustion chemistry but also in atmospheric chemistry. The crossed molecular beams studies of these reactions

will definitely provide detailed understandings of their reaction dynamics. Before I began the experiments in this thesis, I had started serious planning and designing for a photolytic OH radical source beam; however, no experiment had been able to be carried out. As time goes by, a trial on generating the ClO radical beam has been performed,[14] and intense OH radical beams are now becoming available.[15] In the near future, we might be able to see more crossed molecular beam studies of the atmospheric chemical reaction dynamics using diatomic or polyatomic radical beams.

REFERENCES

1. R. D. Levine and R. B. Bernstein, Molecular Reaction Dynamics and Chemical Reactivity (Oxford University Press, Oxford, 1987).
2. I. W. M. Smith, Kinetics and Dynamics of Elementary Gas Reactions (Butterworths, London, 1980).
3. D. R. Herschbach, Angew. Chem. Int. Ed. Engl. **26**, 1221 (1987).
4. a) Y. T. Lee, Angew. Chem. Int. Ed. Engl. **26**, 939 (1987).
   b) Y. T. Lee, Science, **236**, 793 (1987).
   c) Y. T. Lee, in Atomic and Molecular Beam Methods, Vol I, edited by G. Scoles, (Oxford University Press, Oxford, 1988).
5. Y. T. Lee, J. D. McDonald, P. R. LeBreton, and D. R. Herschbach, Rev. Sci. Instrum. **40**, 1402 (1969).
6. R. K. Sparks, Ph. D. Thesis, University of California, Berkeley (1979).
7. A. -M. Schmoltner, Ph. D. Thesis, University of California, Berkeley (1989).
8. D. van den Ende, S. Stolte, J. B. Cross, G. H. Kwei, and J. J. Valentini, J. Chem. Phys. **77**, 2206 (1982).
9. R. P. Wayne, Chemistry of Atmospheres (Clarendon Press, Oxford, 1991).
10. Scientific Assessment of Ozone Depletion: 1991, World Meteorological Organization, Global Ozone Research and Monitoring Project, Report No. 25 (1991).
11. a) S. Toby, Chem. Rev. **84**, 277 (1984).

b) R. Atkinson and W. P. L. Carter, Chem. Rev. **84**, 437 (1984).

12. D. W. Toohey, W. H. Brune, and J. G. Anderson, Int. J. Chem. Kinet. **20**, 131 (1988).

13. S. C. Farantos and J. N. Murrell, Int. J. Quan. Chem. **14**, 659 (1978).

14. H. F. Davis, private communication.

15. a) P. Andresen, D. Häusler, and H. W. Lülf, J. Chem. Phys. **81**, 571 (1984).

b) P. Andresen, N. Aristov, V. Beushausen, D. Häusler, and H. W. Lülf, J. Chem. Phys. **95**, 5763 (1991).

c) D. M. Sonnenfroh, R. G. Macdonald, and K. Liu, J. Chem. Phys. **94**, 6508 (1991).

d) M. Alagia, N. Balucani, P. Casavecchia, D. Stranges, and G. G. Volpi, J. Chem. Phys. **98**, 2459 (1993).

CHAPTER 2

CROSSED MOLECULAR BEAM STUDY OF THE REACTION Cl + O_3

ABSTRACT

The reaction of ground-state (^2P_J) Cl atom with ozone molecule was studied by the crossed molecular beams technique at four different center-of-mass (CM) collision energies ranging from 6 kcal/mole to 32 kcal/mole. The translational energy distribution and the center-of-mass angular distribution of the products were derived from the experimental measurements. The findings are as follows: A large fraction of the total available energy is channeled into the translational energy of the products. The ClO product is sideways and forward scattered with respect to the Cl atom. The translational energy release depends on the center-of-mass scattering angle. With the increase of collision energy, the fraction of the total available energy channeled into the translational energy of the products is increased, and the ClO product is also scattered in a more forward direction with respect to the Cl atom. The reaction Cl + O_3 is believed to proceed through a direct reaction mechanism. The Cl atom is most likely to attack the terminal oxygen atom of the ozone molecule. The exit channel of the ClO_3 potential energy surface is expected to have a strong repulsion.

I. INTRODUCTION

The reaction of $Cl + O_3 \rightarrow ClO + O_2$ is of fundamental importance in stratospheric chemistry.[1] The reaction is the source of the ClO radical; hence, it plays a key role in catalytic ozone destruction cycles. It is currently believed that the following two catalytic cycles are responsible for most of the Antarctic stratosphere ozone loss:[2-6]

(I) ClO Dimer Mechanism:[2]

$2 (Cl + O_3 \rightarrow ClO + O_2)$

$2ClO + M \rightarrow (ClO)_2$

$(ClO)_2 + h\nu \rightarrow Cl + ClOO$

$ClOO + M \rightarrow Cl + O_2 + M$

Net: $2O_3 \rightarrow 3O_2$

(II) ClO/BrO Mechanism:[3]

$Cl + O_3 \rightarrow ClO + O_2$

$Br + O_3 \rightarrow BrO + O_2$

$ClO + BrO \rightarrow Cl + Br + O_2$

Net: $2O_3 \rightarrow 3O_2$

Present calculations indicate that the ClO dimer mechanism (I) accounts for 75% and the ClO/BrO mechanism (II) accounts for 20% of the Antarctic stratosphere ozone loss.[3-6]

A large number of kinetic studies on the Cl + O_3 and similar reactions such as the Br + O_3 reaction have been carried out.[7-12] Measurements made in these studies of reaction rate constants and their temperature dependencies provide a valuable data base for stratospheric chemistry modeling. It has been found that for X + O_3 (X=O(^{3}P), F, Cl, and Br) reactions, with the exception of the H + O_3 reaction, the pre-exponential factors were all very close to 2.2×10^{-11} $cm^3 \cdot molecule^{-1} \cdot s^{-1}$ and, hence, were insensitive to the reaction exothermicity.[11,12] The rate coefficients for the reaction X + O_3 were found to correlate with the electron affinities of the radical atoms instead of with the reaction exothermicity.[9] For reactions of O_3 with diatomic radicals such as NO, OH, and SO, there was similarly little variation in the pre-exponential factors; rather, all such values were close to 2.2×10^{-12} $cm^3 \cdot molecule^{-1} \cdot s^{-1}$.[11,12] Largely on the basis of these findings, it was then suggested that the transition state structures of these reactions were insensitive to reactant X and that the bond lengths and frequencies of the transition state resembled those for the stable ozone molecule.[9,10] It was also suggested that the X + O_3 reactions proceeded via early transition states that best resembled reactant ozone.[9,10] The correlation of the radical electron affinities with the reaction rate constants was seen to suggest that in X + O_3 reactions electron density might have been transferred from the highest occupied ozone molecular

orbital to the singly occupied radical molecular orbital.[9,10]

Asymmetric ClO_3 (ClO·OO) has been postulated as a possible reaction intermediate.[13,14] However, Carter and Andrews' matrix reaction study of the Cl atom with the O_3 molecule showed no observable infrared absorptions for a possible asymmetric ClO_3 radical species under conditions favorable for its formation, suggesting that the asymmetric ClO_3 might not be a stable species even in the matrix.[15] Meanwhile, the ClO radical produced from this matrix reaction was clearly identified in the infrared absorption spectra. From these results, it may be surmised that if the asymmetric ClO_3 were the possible reaction intermediate of the Cl + O_3 reaction, this reaction probably would not proceed through a long-lived complex.

McGrath and Norrish carried out the pioneer flash photolysis study on Cl_2-O_3 and Br_2-O_3 systems.[16] Their flash photolysis light was filtered by a soda glass filter so that only the Cl_2 or the Br_2 molecule, and not the O_3 molecule in the Cl_2-O_3 or Br_2-O_3 mixture, could be dissociated. For the Cl_2-O_3 system, immediately after the flash photolysis of Cl_2 (delay time in the range of several μs), the strong v" = 0 progression of ClO was observed. The ClO product formed in this reaction showed vibrational excitation, with the maximum value of v" possibly being as high as 5. Some vibrational relaxation of the nascent ClO product might have occurred in the time scale of this flash photolysis study; however, it was quite evident that the ClO product from the Cl + O_3 reaction had considerable vibrational excitation. Similarly, the results from McGrath and Norrish's study

on the Br_2-O_3 system showed that the strong v" = 0 progression of BrO was accompanied by BrO absorption bands with v" up to 4. Clyne and Coxon studied the $Cl + O_3 \rightarrow ClO + O_2$ reaction by detecting the ClO radical using time-resolved electronic absorption spectrophotometry in a discharge-flow system.[17] ClO (v" = 0) was considered to be a major product of the reaction, and vibrationally excited products, if present, were not identified. However, due to the much longer time delay (~5 ms) in this experiment, the vibrationally excited ClO radical from the $Cl + O_3$ reaction probably had already relaxed down to the ground vibrational state (v" = 0) when it was detected.

Electronically excited oxygen molecule products $O_2(^1\Delta_g)$ and $O_2(^1\Sigma_g^+)$ are energetically possible (Fig. 1); however, they have not been observed in bulk thermal experiments. If $O_2(^1\Sigma_g^+)$ were produced in a bulk $Cl + O_3$ reaction system, it would react rapidly with the O_3 molecule to generate the oxygen atom product and the ground-state oxygen molecule product $O_2(^3\Sigma_g^-)$ in the reaction $O_2(^1\Sigma_g^+) + O_3 \rightarrow 2O_2(^3\Sigma_g^-) + O$. Vanderzanden and Birks tried to find the electronically excited product $O_2(^1\Sigma_g^+)$ in a flow $Cl + O_3$ reaction system by detecting the O atom as the product of the secondary reaction between the product $O_2(^1\Sigma_g^+)$ and O_3; to do so, they used NO + O + M chemiluminescence detection.[18] Under the assumption that all the oxygen atoms detected in their system originated from the secondary reaction of $O_2(^1\Sigma_g^+)$ with O_3, they were able to estimate the branching ratio of the $O_2(^1\Sigma_g^+)$ channel to be in the range of $(1\text{-}5) \times 10^{-3}$. Their overall method, however, did not allow them to detect the $O_2(^1\Delta_g)$ channel. Even if

$O_2(^1\Delta_g)$ were produced from the reaction Cl + O_3, the reaction of $O_2(^1\Delta_g)$ with O_3 was too slow to generate a detectable quantity of oxygen atoms. In a similar effort, Choo and Leu studied the formation of $O_2(^1\Delta_g)$ and $O_2(^1\Sigma_g^+)$ in the Cl + O_3 reaction using the flow-discharge/chemiluminescence detection method.[19] Because they too failed to detect any $O_2(^1\Delta_g)$ and $O_2(^1\Sigma_g^+)$ chemiluminescence signals in the Cl + O_3 reaction system, their work defined the upper limits of the branching ratios for $O_2(^1\Sigma_g^+)$ and $O_2(^1\Delta_g)$ as $\leq 0.5 \times 10^{-3}$ and $\leq 2.5 \times 10^{-2}$, respectively. Both studies showed that productions of the electronically excited oxygen molecules $O_2(^1\Delta_g)$ and $O_2(^1\Sigma_g^+)$ in the Cl + O_3 reaction were negligible.

So far there have been few theoretical studies of the Cl + O_3 reaction. Farantos and Murrell used the many-body expansion method to derive an analytic function for the potential energy surface (PES) of the ground-state $ClO_3(^2A)$.[20] In this functional form, relative to the energies of the separated atoms, the potential energy of ClO_3 was taken as a sum of the interaction energies of the atoms in pairs (V^i_{ClO} and V^i_{OO}), of the atoms in threes ($V^i_{ClO_2}$ and $V^i_{O_3}$), and a four-body term ($V^i_{ClO_3}$). Including all the two-, three-, and four-body terms, they located an early transition state for the collinear collision pathway in which Cl attacked along the line of one O-O bond. The reaction barrier height along this collinear pathway on the ClO_3 PES was 0.34 kcal/mole, an estimation which appeared to be consistent with the experimental measurement of a 0.5 kcal/mole activation energy for the Cl + O_3 reaction.[10] Classic trajectory calculations were carried out on this PES at four different collision energies corresponding to the

Maxwellian mean velocities that ranged from 200 K to 600 K with the O_3 molecule in its vibrational ground state. The rate constant at room temperature, which was calculated using the cross-sections ($\sigma(E_r)$) generated from the trajectory calculations, was 1.34×10^{-11} $cm^3 \cdot molecule^{-1} \cdot s^{-1}$; hence, it too was consistent with the experimental estimation, in this case the value of 1.2×10^{-11} $cm^3 \cdot molecule^{-1} \cdot s^{-1}$. The trajectory calculations also provided some insight into the dynamics of the Cl + O_3 reaction. It was calculated that at 300 K the ClO product was predominantly forward scattered with respect to the Cl atom in the center-of-mass system. The lack of forward-backward symmetry showed that there was no long-lived complex formation along this collinear pathway. Farantos and Murrell's calculations showed that at 300 K about 49% of the total available energy went into the translational energy of the product while 20% went into ClO vibrational energy and only 4% went into O_2 vibrational energy. ClO rotation took 19% of the total available energy while O_2 rotation took only 9%. The researchers also predicted that v = 1 was the most probable vibrational state of ClO but that vibrational states up to v = 8 would be populated while almost all the O_2 would be in the ground vibrational state. In their calculations, there was a large amount of vibrational energy in the ClO product due to the early transition state located in the entrance valley. The O-O bond length, however, did not change much in the reaction, and consequently there was much less vibrational excitation in the O_2 product. It is worthwhile to note that the stable symmetric ClO_3 (D_{3h} symmetry) was found to be -36 kcal/mole relative to the separated Cl and O_3,

and there was a substantial barrier (>90 kcal/mole) to reach this minimum from Cl + O_3 by a reaction path that maintained C_{3v} symmetry. The trajectories calculated for the collinear approach showed that the long-lived ClO_3 intermediate was not formed in the reaction.

Recently Rathmann and Schindler carried out *ab initio* calculations on the geometries and thermodynamic stabilities of three chlorine trioxides: $ClO{\cdot}O_2$ ($\Delta H_{f,0K}$ = 41 kcal/mole), $OCl{\cdot}O_2$ ($\Delta H_{f,0K}$ = 58 kcal/mole), and sym-ClO_3 ($\Delta H_{f,0K}$ = 48 kcal/mole).[21] It was shown that the formation of the asymmetric $ClO{\cdot}O_2$ adduct by association of O_2 and ClO was endothermic by 13 kcal/mole; in other words, the energy of the asymmetric $ClO{\cdot}O_2$ intermediate lies above that of the separated products ClO and O_2 (Fig. 1). Therefore, the Cl + O_3 reaction should not proceed through a long-lived complex if this asymmetric ClO_3 is the reaction intermediate. The authors also planned to investigate further the minimum energy path of the Cl + O_3 reaction.

Schaefer and co-workers have used *ab initio* quantum mechanical methods to determine the key features of the H + O_3 PES.[22] The authors expected the key features of the H + O_3 PES to be transferable to X + O_3 (X = Cl, OH, NO, and NH_2) systems because the electronic structure of ozone has played a dominant role in determining these key features. However, they could not locate a planar transition state for a direct O-atom abstraction; instead, they suggested that the H + O_3 reaction proceeded through a nonplanar pathway in which the H atom attacked vertically to the ozone molecule plane. Most of the reaction

exothermicity was released while the H-O bond was being formed channeling energy specifically into OH vibration, in accord with experimental results from the chemiluminescence work by Polanyi and co-workers.[23] However, the experiment also showed a large ratio of OH vibrational energy (90% of total available energy) to OH rotational energy (~ 3% of total energy); this result led the authors to suggest that the potential energy surface favored a collinear HOO approach and that the H + O_3 reaction was restricted to a narrow range of impact parameters.[23] There is certainly a discrepancy between the *ab initio* calculation and experimental results on the H + O_3 reaction. Furthermore, if indeed the key features of the H + O_3 PES were transferable to the Cl + O_3 system, they would be quite different from those found in the semi-empirical calculations.[20] An *ab initio* calculation of the Cl + O_3 system itself would be very helpful.

Information on the dynamics of the Cl + O_3 reaction is not yet very clear. The goal of the present work is to probe further the dynamics of the Cl + O_3 reaction under well-defined single collision conditions. We have carried out a crossed molecular beam study of this reaction at four different collision energies. The center-of-mass angular and translational energy distributions of the product ClO are derived from the experimental measurements. Using the obtained dynamic information, we hope to provide more insight into the mechanism of this important reaction. As far as what we know, this is the first crossed molecular beam study of the Cl + O_3 reaction.

II. EXPERIMENTAL

The universal crossed molecular beam apparatus used for the present study has previously been described in detail.[24,25] The beams and detector arrangement is shown in Fig. 2. Continuous supersonic chlorine atomic and ozone molecular beams were seeded and two-stage differentially pumped. The two beams were crossed at 90° in the main collision chamber held at a vacuum of approximate 10^{-7} torr. The scattered products were detected by a triply differentially pumped mass spectrometric detector which rotated in the plane of the two beams with respect to the center of collision. The mass spectrometric detector is composed of a Brink's-type electron impact ionizer,[26] an Extrel quadrupole mass spectrometer, and a scintillation-based Daly ion detector.[27] The typical electron energy was 180 eV, and the typical ion energy was 90 eV. The size of the collision zone was typically 3 x 3 x 3 mm^3, and under normal conditions the whole collision zone was viewed by the detector.

The chlorine atom beam was produced by thermal dissociation of Cl_2 in rare gas mixtures in a resistively heated high-density graphite[28] nozzle source which was designed in this laboratory by Valentini, Coggiola, and Lee.[29] Mixtures of 10% Cl_2 in argon, 10% Cl_2 in 8% argon and 82% helium, 5% Cl_2 in helium, and 1% Cl_2 in helium were used as seeded gas mixtures for this experiment. The high-temperature graphite source had a nozzle of 0.12 mm diameter and was heated to approximately 1400 °C-1600 °C. The nozzle temperature was constantly

monitored by type C (Tungsten-5%Rhenium vs. Tungsten-26%Rhenium) thermocouples on the graphite heater and frequently checked by an optical pyrometer and by pure noble gas time-of-flight temperature measurements as well. After correcting the optical pyrometric measurements for emissivity of graphite and absorption of the Plexiglass on the view port, the optical pyrometric measurements agreed reasonably well with the noble gas time-of-flight temperature measurements; hence, the optical pyrometric measurements were chosen as our temperature readings. A conical graphite skimmer with an orifice 1.0 mm in diameter was positioned 7.6 mm along the downstream of the nozzle. A set of collimating slits on the differential wall further defined the beam to 3° in full width and 3 mm x 3 mm in the collision region. The total stagnation pressure of the beam was typically 700 torr measured outside of the machine just before the gas mixture entered the molecular beam source. A large fraction of Cl_2 thermal dissociation had been observed by a direct measurement of $[Cl]/[Cl_2]$ ratio in the beam. The residual Cl_2 species was not a problem in this experiment, as later discussed in detail. Heating power for the high-temperature graphite source was carefully maintained constant throughout the experiment period to ensure a stable Cl atom beam with stable beam velocity. The Cl beam velocity was also often checked before and after a daily reactive scattering experiment. The Cl beam quality was quite stable during the whole experiment; this high density graphite source seemed to be very reliable for a long period of time even for the Cl beam. To maintain the durability of the beam-source pumping system,

perfluoropolyether (PFPE) pumping fluids (Fomblin 25/6 for mechanical pump and Fomblin 25/9 for diffusion pump) were used.

The ozone used in this experiment was generated by a commercial ozonator (OREC, model number 03v1-0). The output of the ozonator (10% ozone, 90% oxygen) was passed through a Pyrex trap with coarse silica gel cooled to -78 °C in a dry ice/acetone slush.[30-32] After 1-3 hours of running time (depending on the condition of the trap), a sufficient amount of deep blue ozone with a small amount of oxygen was adsorbed on the silica gel. The trap was then transferred to a thermostatically controlled variable low-temperature bath (FTS Multicool System, model number MC-4-60A-1), and the gas mixture was generated by passing rare gas to carry the desorbing ozone out of the trap. The gas mixture then passed through a 1 cm x 1 cm quartz flow cell just prior to its entry into the ozone molecular beam source. It is important to use only clean stainless steel components, glass components, and Teflon or stainless steel tubing in the transportation line in order to prevent other metals and impurities from catalytically decomposing the ozone. The ozone concentration was continuously monitored by measuring the ultraviolet absorption of the gas mixture in the quartz cell at wavelength 280 nm (Fig. 3). The wavelength 280 nm corresponds to one discrete line of the Hg lamp used as a light source in our experiment, and the concentration of the ozone gas mixture gave a reasonable transmission (~10%) at this wavelength.[12,33,34] The total stagnation pressure of the ozone beam was 300 torr. After running the ozone beam through the nozzle for 1-2 hours, the small

amount of O_2 in the silica gel trap would be well purged by the inert carrier gas, and the system would also be well passivated and stabilized. The stabilized mole fraction of ozone for our experiment was typically maintained at 7%. The ratio $[O_3]/[O_2]$ was typically ~ 3 determined from direct beam measurement. Some residual O_2 from the trap and a small amount of decomposition of O_3 in the beam were unavoidable. Since the $Cl + O_2$ reaction was energetically impossible in this experiment, the presence of O_2 in the beam was not a problem. If there were single O atoms in the ozone molecular beam, they might react with residual Cl_2 in the Cl atom beam and produce ClO; however, as later mentioned, this process is quite likely to be absent in our experiment. Because the ozone in the silica gel trap was gradually depleted, in order to maintain the ozone concentration unchanged, we constantly adjusted the temperature of the low-temperature bath following ozone UV-absorption measurements, i.e., ozone concentration measurements. The operation temperature of the trap was normally kept in the range of -60 °C to -30 °C to obtain a constant ozone concentration. The trap itself could be used up to 12 hours for ozone beams of reproducible intensity and velocity. The ozone beam source had a nozzle 0.12 mm in diameter. To minimize the formation of ozone dimers, the tip of the nozzle was heated to 80 °C. The temperature of the nozzle was measured by a Chromel-Alumel (type K) thermocouple fixed on the nozzle source tip and referenced to an ice water bath. The ozone molecular beam was skimmed by a stainless steel skimmer with a 0.5 mm diameter orifice placed at a nozzle-skimmer distance of 7.6 mm. The beam

was further defined by the collimating slits on the differential wall before it entered the main chamber. These slits gave a 3° beam full width and 3 mm x 3 mm beam size in the collision region.

The time-of-flight (TOF) technique was used to measure the velocity distributions of the Cl and O_3 beams. A stainless steel wheel 17.8 cm in diameter with four 0.78 mm slots equally spaced around its circumference was installed in front of the detector. The wheel was spun at 300 Hz, and the modulated beam was sampled straight into the detector through a 0.18 mm aperture. A homemade 4096-channel multichannel scaler (MCS)[35] interfaced with a computer that accumulated the data. The flight path from the wheel to the effective center of the ionizer was experimentally determined to be 30.1 cm. Various noble gas beams were chosen for this calibration process, and their calculated ideal beam velocities were used in determining the flight path. After using the appropriate offset time (ion flight time, wheel trigger time offset etc.) to correct the experimental time-of-flight spectra, a program KELVIN, which convoluted over the known apparatus functions to determine the beam speed (v) and speed ratio ($v/\Delta v$), was used to fit the corrected experimental time-of-flight spectra and obtain the Cl atom and ozone molecular beam velocity distributions.[36,37] The typical beam parameters are listed in Table 1. The most-probable collision energies E_{coll} and the spread of the collision energies are listed in Table 2.

Product TOF spectra from the reactive scattering were measured using the cross-correlation method.[38] A 17.8 cm diameter cross-correlation wheel was

mounted in front of the detector to replace the four-slot single-shot wheel and was spun at 392 Hz. The wheel has two identical 255-bit pseudorandom sequences of open and closed slots and was photoetched by PCM Products based on Lee group specifications. When spun at 392 Hz, the wheel gives nominal 5 μs/channel time resolution in the TOF spectra and 50% transmission. The detector was stationed at a particular laboratory angle to measure the product velocity distribution. Product ClO was monitored. The mass spectrometer was set at m/e = 51 with low resolution to detect more abundant $Cl^{35}O$ isotope species, while a small amount of $Cl^{37}O$ might have been collected as well. Total counting times ranged from 0.5 to 12 hours per angle.

Initially, an Extrel Model 14 High-Q Head, the high frequency inductor circuit for the quadrupole mass spectrometer, was used. Due to its large mass range, it lacked sufficient mass resolution. When the detector moved to within 25° of the ozone beam, the O_3 molecule (m/e = 48) elastically scattered by the noble carrier gas in the Cl beam started to leak into the ClO (m/e = 51) time-of-flight spectra. The reactive ClO TOF peak and the elastic O_3 TOF peak were nevertheless well separated by the flight time. An Extrel Model 13 High-Q Head was then installed and used throughout the experiment, and this High-Q head gave good mass separation. The contamination of the ozone elastic scattering peak within 25° of the ozone beam was reduced to ≤ 5% of the intensity of the reactive ClO peak. For the laboratory angles close to the O_3 beam, the O_3 elastic scattering time-of-flight spectra were measured along with the ClO reactive time-

of-flight spectra. The O_3 elastic scattering spectrum at one laboratory angle was scaled to the O_3 elastic scattering peak in the raw ClO time-of-flight spectrum at the same angle and subtracted away from the raw ClO time-of-flight spectrum. However, this type of correction was very small ($\leq 5\%$) and was only necessary for the ClO time-of-flight spectra at laboratory angles $\Theta \geq 65°$.

We also have to point out, when measuring ClO time-of-flight spectra near the Cl beam (within ~10° of the Cl beam), a small amount of slow effusive background from the Cl beam source showed up in the spectra. To correct this background, ClO time-of-flight spectra near the Cl beam with the O_3 beam on and with the O_3 beam off were measured, and the corrected ClO product time-of-flight spectra for those laboratory angles near the Cl beam were obtained by simply subtracting the O_3 beam-off spectra away from the O_3 beam-on spectra at the same laboratory angles. However, this type of background subtraction procedure was needed only for the ClO time-of-flight spectra within 10° of the Cl beam.

The ClO product angular distributions were measured by modulating the ozone beam using a 150 Hz tuning folk chopper (Bulova) with the time-of-flight wheel removed. At a particular angle, the signal with the ozone beam on and the signal with the ozone beam off were recorded in two separate channels in a dual-channel scaler (Joerger, model VS) with an appropriate gating originated from the tuning folk chopper. Subtracting the beam-off signal from the beam-on signal at a particular laboratory angle simply gave the net reactive signal at that angle. To correct for long-term drifts of the experimental conditions, a reference angle

(typically the one with near maximum intensity) was chosen. After a sequence of measurements at every 6-10 angles, data was twice taken at this reference angle. The set of data was then normalized by taking a linear interpolation based on the time at which a given angle was measured and the time between normalization measurements. Counting time at each angle in each normalization sequence ranged from 1 min to 3 mins, while the total counting times per angle summed from all the normalization sequences ranged from 8 to 30 mins.

To reduce the background species entering into the detector, a cryogenic copper cold panel was placed against the differential wall inside the main scattering chamber and facing the detector. It was cooled by being tightly clamped to the liquid-nitrogen cooled cold shield in the scattering chamber. Its temperature was typically about 90 K, which was monitored by a low temperature sensor (LakeShore). It was effective to reduce the ClO background for both time-of-flight and angular measurements.

III. RESULTS AND ANALYSIS

Laboratory angular and time-of-flight distributions were recorded at four different center-of-mass collision energies from 6 kcal/mole to 32 kcal/mole (Experimental conditions for three collision energies are listed in Table 2). The Newton diagrams for the three collision energies are shown in Figs. 4, 9, and 14.

The circles stand for the maximum range of the center-of-mass recoil velocity of the ClO product if all the available energy channels into the translational energy of the products. The angular and TOF distributions were recorded at m/e = 51, corresponding to $Cl^{35}O^+$.

The product angular distribution and time-of-flight spectra were fitted using a forward-convolution method. The FORTRAN program is an improved version based on the previous program written by Buss.[39] The goal of the analysis is to find the product angular and translational energy distributions in the center-of-mass frame. It starts with a trial form for the center-of-mass product flux-energy distribution, i.e., the center-of-mass double differential reaction cross section (DDC). In most of the cases, the center-of-mass product flux-energy distribution $I_{CM}(\theta, E_T)$ (where θ is the center-of-mass angle and E_T is the product translational energy) is assumed to have an energy-angle separable form and is expressed as a product of $T(\theta)$, the center-of-mass product angular distribution, and $P(E_T)$, the center-of-mass product relative translational energy distribution:

$$I_{CM}(\theta, E_T) = T(\theta) \cdot P(E_T) \qquad (1)$$

The program transforms this trial center-of-mass flux distribution into the laboratory frame flux distribution using the transformation Jacobian $I_{Lab}(\Theta,v) = I_{CM}(\theta,u) \cdot v^2/u^2$ and generates the laboratory frame angular distribution and time-of-flight spectra for each experimental laboratory angle after convoluting over the measured beam velocity distributions and the known apparatus functions such

as the spread of collision angles, the detector acceptance angle, and the length of the ionizer. The program scales the calculated spectra to the experimental data and makes the comparison. This is repeated so as to optimize the $T(\theta)$ and $P(E_T)$ iteratively until a best fit for the experimental data is found.

Initially, we tried to fit the data using a single set of uncoupled $T(\theta)$ and $P(E_T)$. We found that, for large laboratory angles ($\Theta > 40°$), the fittings for the time-of-flight spectra were reasonably good; however, for small laboratory angles (10°-25°), the calculated time-of-flight spectra were clearly too slow compared with the experimental data. A faster and forward contribution in the center-of-mass flux distribution was needed to make a satisfactory fit to our experimental data which had very good signal-to-noise ratio. It was then realized that the center-of-mass angular distribution $T(\theta)$ and the translational energy distribution $P(E_T)$ were nonseparable, i.e., the product translational energy release was dependent on the center-of-mass scattering angle. The translational energy release in the forward direction with respect the Cl atom in the center-of-mass frame was larger than that in the backward direction; thus, the ClO product was faster at the small laboratory angles.

To account for this coupling effect in a simplified way, we used a combination of different sets of uncoupled $T(\theta)$ and $P(E_T)$. The center-of-mass product flux distribution was expressed as the weighted sum of the products of different sets of $T(\theta)$ and $P(E_T)$:

$$I_{CM}(\theta, E_T) = \sum_{i=1}^{n} w_i \cdot T_i(\theta) \cdot P_i(E_T) \qquad (2)$$

Each $P_i(E_T)$ was normalized so that $\int P_i(E_T)dE_T = 1$. The total center-of-mass angular distribution could therefore be expressed as:

$$I_{CM}(\theta) = \int_0^{\infty} I_{CM}(\theta, E_T)dE_T = \sum_{i=1}^{n} w_i \cdot T_i(\theta) \qquad (3)$$

The product translational energy distribution at CM angle θ would be expressed in Eqn. 2 with the CM angle fixed at θ.

For our purposes, a trial $I_{CM}(\theta, E_T)$ combined from two different sets of $T(\theta)$ and $P(E_T)$ was used as input to the fitting program. $T(\theta)$ was chosen in a point form because the angular distribution of this reaction was unique. $P(E_T)$ was chosen in a RRK-type functional form for the convenience of parameter adjustment. After optimizing this trial $I_{CM}(\theta, E_T)$ function, quite satisfactory fittings to the experimental data were finally reached. The calculated and experimental laboratory angular distributions at three different collision energies are shown in Figs. 4, 9, and 14. The fitted and experimental laboratory time-of-flight spectra at three collision energies are in Figs. 5, 10, and 15. The average translational energy releases versus center-of-mass angle and the total center-of-mass angular distributions are in Figs. 6, 11, and 16. We also plot the relative

translational energy distributions at various center-of-mass angles in Figs. 7, 12, and 17. Using the optimized center-of-mass flux-energy distribution $I_{CM}(\theta, E_T)$, we plot the center-of-mass flux distributions in velocity space $I_{CM}(\theta, u)$ ($I_{CM}(\theta, u) \propto u \cdot I_{CM}(\theta, E_T)$) both in contour maps and in 3-dimensional curves in Figs. 8, 13, and 18.

The laboratory angular distributions are quite broad. At higher collision energies, the distributions show significant forward peak in front of the center-of-mass angle. With collision energy increased, the peak of the laboratory angular distribution is moved in the forward direction. There is, however, a fall-off region in the laboratory angles close to the Cl beam; the intensities within 10° of the Cl beam are constantly low. In the center-of-mass frame, the angular distributions are also quite broad, and they have larger intensities for the sideways scattering. The center-of-mass angular distributions do not have forward-backward symmetry. Instead, the large asymmetry with more forward contribution is present in the angular distributions. The peak of the center-of-mass angular distribution $T(\theta)$ shifts from 90° to 50° and 30° with the collision energy increased, and the peaks becomes more predominant as well.

The overall product translational energy release is large. The product laboratory velocity peaks far away from the center-of-mass velocity $\mathbf{V}_{CM}$. In the center-of-mass frame, all translational energy release probabilities $P(E_T)$ peak quite far away from 0 kcal/mole. The $P(E_T)$ curves are smooth and almost symmetric. The width of the translational energy release probability $P(E_T)$ gets wider with the

increase of the collision energy. We notice two more trends of the kinetic energy release of this reaction shown in Tables 3 and 4. First, with the collision energy increased, a larger fraction of the total available energy is channeled into translational energy. Second, with the collision energy increased, the angular dependence of the translational energy release becomes larger; i.e., the difference between the fast and slow translational energy releases becomes larger.

The possible presence of ClO contamination in the Cl beam which might give different translational energy distribution from that of the Cl + O_3 reaction was ruled out. First, no ClO in the Cl beam was detected. The main components of chemical interest in the Cl beam were Cl atom and Cl_2 molecule. O_3 and O_2 were the main components of chemical interest in the O_3 beam; there might also have been a small amount of O atom in the beam. The reaction channel of Cl with O_2 is too endothermic ($\Delta H^\circ \approx 55$ kcal/mole) to produce ClO. $Cl_2 + O_3$ is a very slow molecule-molecule endothermic reaction ($\Delta H^\circ \geq 13$ kcal/mole); it would not produce any ClO, and even if it did, the ClO product from this reaction would be too slow to contaminate the ClO TOF spectra of the Cl + O_3 reaction. The reaction $Cl_2 + O \rightarrow ClO + Cl$ is slightly exothermic ($\Delta H^\circ = -6.2$ kcal/mole); it deserves some attention. However, it would not present any problems either. First, Cl_2 and O were all minor species in the two beams, especially the O atom. The amount of the O atom in the ozone beam is almost negligible. Second, the reaction Cl + O_3 is faster than the reaction Cl_2 + O. Finally and most importantly, the velocity of the ClO produced in the Cl_2 + O reaction would be too slow to

interfere with the TOF spectra of the Cl + O_3 reaction. Parrish and Herschbach carried out an early and brief crossed molecular beam study of the Cl_2 + O reaction.[40] They showed that the reactive scattering of Cl_2 and O was consistent with a persistent complex mechanism. Grice and co-workers further studied this reaction in detail using crossed molecular beams technique at 3, 7, and 9 kcal/mole collision energies.[41-43] It was shown that the Cl_2 + O reaction proceeded via a short-lived collision complex. The ClO center-of-mass angular distribution of this reaction showed certain forward-backward symmetry with a stronger peak in the backward direction with respect to the Cl_2 molecule. The ClO flux was concentrated on the poles at 0° and 180° in the center-of-mass frame, and since the kinetic energy release was small, most of the product flux located around the relative velocity vector. In our experiment, the expected collision energies for the Cl_2 + O reaction would be 4, 9, and 21 kcal/mole, which were comparable to those in Grice's experiments. The possible ClO product from the Cl_2 + O reaction had to concentrate around the relative velocity vector; however, the ClO product from the Cl + O_3 reaction peaked very far away from the relative velocity vector. Therefore, even if there were ClO from the Cl_2 + O reaction, it would be so slow that it would not interfere in the ClO TOF spectra of the Cl + O_3 reaction.

We tried to detect any evidence of the reaction channel Cl + $O_3 \rightarrow ClO_2$ + O (Fig. 1). This reaction channel is open at over 17.4 kcal/mole collision energy. There are two types of ClO_2 isomers: ClOO and OClO. OClO is a stable molecule and could be observed by the mass spectrometer with the electron bombardment

ionizer. However, it might require a very large collision energy for the Cl atom to insert into the O_3 molecule to make OClO. We failed to detect any signal at m/e = 67 at high collision energies 26 kcal/mole and 32 kcal/mole. In ClOO molecule, however, Cl and O_2 are bonded by only about 5-6 kcal/mole.[44-46] The ClOO molecule may not be able to survive in the electron bombardment ionizer. At over 24 kcal/mole collision energy, ClOO might undergo further decomposition, then the whole process becomes a collision-induced dissociation of the O_3 molecule by the Cl atom collision. We detected no signal at m/e = 67 at high collision energies 26 kcal/mole and 32 kcal/mole. At m/e = 35 and 32, the background signals from both beams were very strong so we could not find any evidence of Cl or O_2 fragments from ClOO by inspecting the time-of-flight spectra at collision energies 26 kcal/mole and 32 kcal/mole. We think the reaction $Cl + O_3 \rightarrow ClO_2 + O$ is a very minor channel.

IV. DISCUSSION

A. The Mechanism of the Reaction $Cl + O_3 \rightarrow ClO + O_2$

The reaction $Cl + O_3$ is a direct reaction. The center-of-mass angular distribution does not have the typical forward-backward symmetry that a reaction via a persistent long-lived complex has,[47] and there is a strong angular dependence of the kinetic energy release. This conclusion is consistent with the

information from thermodynamic data. The energy levels of three ClO_3 isomers all lie above that of the ground-state products according to *ab initio* calculations[21] (Fig. 1). Experimental results from DeMore gave an upper limit of about 7 kcal/mole for the potential well of the asymmetric ClO_3.[48] Therefore, in the Cl + O_3 reaction, asymmetric ClO_3 could not be a persistent long-lived complex due to the lack of any significant potential well and due to the large amount of excess energy in the exit channel; in other words, the life-time of the asymmetric ClO_3 would be very short. Observations by Cater and Andrews in matrix spectroscopy work also confirmed that a long-lived complex was hardly involved in the Cl + O_3 reaction.[15]

The CM angular distribution at 6 kcal/mole collision energy shows a slight forward-backward symmetry (Fig. 16). It seems to peak at about 90° in the center-of-mass frame. If a long-lived complex existed at this low collision energy, the center-of-mass angular distribution with the peak around 90° would suggest that the long-lived complex be an oblate,[47] and the ClO product should be ejected perpendicularly to the plane of rotation of the long-lived complex. However, there is no force acting in this direction. Most likely the force ejecting ClO would be near the plane of the rotation. Furthermore, by the conservation of the total angular momentum, if the long-lived complex existed, the ClO product should be ejected close to the plane of the rotation instead. The initial orbital angular momentum **L** is large, while the initial rotational angular momentum of the reactant ozone **j** is small due to the supersonic expansion. Thus, the total angular

momentum J is effectively the initial orbital angular momentum: $\mathbf{J} \approx \mathbf{L}$. Because of the large exoergicity and the large translational energy release in the reaction, the relative velocity of the products becomes larger than the initial relative velocity of the reactants, so the final orbital angular momentum $\mathbf{L}'$ is also expected to be large for any reasonable exit impact parameter, and the final rotational angular momentum $\mathbf{j}'$ is not very large due to the small rotational excitation in the products. According to $\mathbf{L} \approx \mathbf{J} = \mathbf{L}' + \mathbf{j}'$, the final orbital angular momentum $\mathbf{L}'$ is estimated to point in the similar direction of the initial orbital angular momentum L, so the initial relative velocity and the final relative velocity should be more-or-less parallel to each other. Therefore, the products are supposed to decay near the plane of the rotation of the complex instead of perpendicularly out of the plane. However, the center-of-mass angular distribution of the long-lived complex decaying in the plane of the rotation should have peaks in 0° and 180° in the center-of-mass frame, which is not the observation of our experiment. This argument from the conservation of the angular momentum shows that a long-lived complex in the Cl + O_3 reaction would give rise to a symmetric center-of-mass angular distribution with peaks at 0° and 180° instead of with a peak at 90°, therefore, this argument implies that it is highly unlikely for the reaction to proceed through a long-lived complex. Furthermore, in the reaction mechanism we will discuss in the following paragraphs, the Cl atom is likely to attack the terminal oxygen atom of the ozone molecule in a coplanar pathway at the low collision energy, and the transition

state would likely be a prolate. Because of this coplanar collision pathway, **L** and **L′** are correlated so that they would be in the similar direction, and the ClO product is expected to be ejected near this collision plane. Again, if a long-lived collision complex existed, a center-of-mass angular distribution peaking at 0° and 180° should be expected. However, the experimental results rule out this possibility. Finally, the difference in the center-of-mass recoil velocity of the ClO product as a function of scattering angle also strongly suggests that there is not a long-lived complex in this reaction.

The electronic structure of the O_3 molecule plays an important role in the reaction mechanism.[22] The electronic configuration of the O_3 molecule in the C_{2v} symmetry in its ground state (1^1A_1) is given by[49-52] $\cdots(5a_1)^2(3b_2)^2(1b_1)^2(6a_1)^2(4b_2)^2(1a_2)^2(2b_1)^0$. In the molecular-orbital (MO) picture,[49-52] the $5a_1$ and $3b_2$ orbitals are the O-O σ bonds, and the terminal lone pairs form the $6a_1$ and $4b_2$ σ orbitals. The central O2pπ is the occupied $1b_1$, and the two terminal atomic O2pπ orbitals form the pair of the π molecular orbitals $1a_2$ and $2b_1$. The highest occupied molecular orbital (HOMO) of the O_3 molecule is $1a_2$ orbital, which is fully occupied by the 2 terminal O2pπ electrons. The center oxygen atom of the O_3 molecule has a closed outer shell with 8 electrons, and the terminal oxygen atom has only 7 outer electrons with a half-filled π orbital perpendicular to the plane of the ozone molecule. The O_3 molecule is characterized as a diradical with the two unpaired π electrons in the terminal oxygen atoms.[49]

The electronic structure of the ozone molecule would suggest that it is unlikely for the Cl atom to strike the central oxygen atom to make the reaction happen because of the high repulsion of the lone pairs of electrons on the central oxygen atom. If the Cl atom abstracted the central oxygen atom, the ClO product would be predominantly scattered in the backward direction, and the O_2 product formed from the two terminal O atoms should be highly vibrationally excited. However, the experimental facts that the ClO CM angular distribution is peaked predominantly sideways instead of in the backward direction, that the O_2 vibrational states are not highly excited, and that the O_2 product stays in the electronic ground state clearly indicate that the Cl atom is unlikely to attack the central O atom of the ozone molecule.

It is also unlikely for the Cl atom to insert into the O-O bond. Previous kinetic studies suggested that in this reaction the structure of the transition state closely resembled that of the stable ozone molecule.[7-12] We also studied the reaction Br + O_3 using the crossed molecular beams technique;[53] the results for both the Cl + O_3 and the Br + O_3 reactions are quite similar, suggesting that the configurations of the transition states in these two reactions are similar and that the Cl or Br atom probably does not insert to the O-O bond to make the structure of the transition state quite different from that of the stable ozone molecule. The insertion of the Cl atom into the O-O bond is also not favored by the frontier orbital theory.[54,55] In this pathway, there is no effective orbital overlap and interaction. Unless the collision energy is very high, this pathway is not expected

to be significant.

The Cl atom is very likely to attack the terminal oxygen atom. One way is that the Cl atom attacks the π orbital on the O_3 molecule perpendicularly from above the plane of the ozone molecule, which is similar to the way given in the *ab initio* calculations of the H + O_3 reaction by Schaefer and co-workers.[22] This is also the favorite way in the frontier orbital theory.[54,55] The HOMO of the O_3 molecule could be considered as two weakly coupled 2pπ orbitals on the two terminal oxygen atoms. If the singly occupied p orbital on the Cl atom descends vertically to the π orbital on the terminal oxygen atom, there is a net overlap between the two orbitals, and a σ bond in this direction is expected to form between the Cl atom and the terminal O atom of the ozone molecule. This type of interaction is symmetry-allowed according to the frontier orbital theory. This collision pathway should have a large impact parameter b since the center of mass of the ozone molecule is on the C_{2v} axis that goes through the central oxygen atom. The ClO product would be expected to be scattered in the forward direction. With the increasing collision energy, the forward scattering would become stronger. However, the significant amount of wide-angle scattering, especially in high collision energies, could not be explained by this consistent large impact parameter approach. Furthermore, in this picture, the impact parameter is nearly constant, and the approach geometry is nearly identical; the translational energy release is therefore not expected to vary much with the CM scattering angle. The strong angular dependence of the translational energy

shown in the experimental results could not fit into this picture. We would like to emphasize that this reaction pathway does not contribute to wide-angle reactive scattering and that this reaction path alone could not give rise to the strong dependence of the product translational energy release on the center-of-mass scattering angle. Therefore, this reaction pathway can not account for the whole picture of the Cl + O_3 reaction mechanism. However, it can describe the forward reactive scattering fairly well. As we will discuss further, if two possible reaction pathways are involved in the Cl + O_3 reaction, this out-of-plane reaction pathway, in which the Cl atom attacks the terminal oxygen of the ozone molecule perpendicularly to the ozone molecule plane, could well account for the forward scattering channel.

A coplanar reaction mechanism, in which the Cl atom attacks a terminal oxygen atom in the plane of the ozone molecule, could well explain the experimental results, especially for the sideways and wide-angle scattering. This coplanar collision is also allowed according to the frontier orbital theory. If the Cl atom approaches the terminal oxygen atom of the ozone molecule in a coplanar pathway with the singly occupied p orbital on the Cl atom oriented perpendicularly to the collision plane (i.e., as a π orbital), this singly occupied p orbital of the Cl atom would have net overlap with the π orbital on the terminal O atom, and this type of interaction is symmetry-allowed. In this reaction pathway, the Cl atom has a large range of attacking angles which correspond to a large range of impact parameters and, thus, in the experimental results, a wide

range of CM angles into which the product ClO is scattered. If the Cl atom approaches the ozone molecule along the direction of the terminal and terminal O atoms, the impact parameter is small, and some backward scattered ClO would be expected. Because this is a head-on collision, and because the initial translational energy is well coupled to the vibrational modes of the reaction intermediate in this type of collision, this collision approach would lead to more internal excitation of the reaction intermediate and cause less translational energy release in the backward direction. However, in this coplanar approach, the Cl atom could cause sideways and forward scattering, if it attacks other than in the small impact parameter approach (e.g., along the terminal O atom and central O atom direction, or perpendicularly to this direction). There is quite a strong repulsive force acting on the separating products; the translational energy release is very large. Even with the increasing of the collision energy, the ClO product is still pushed sideways by such a strong repulsion. The large translational energy release and the low forward scattering intensities within the CM angle 20° at all collision energies might be explained by this repulsive force.

At low collision energy (6 kcal/mole), the sideways repulsion is stronger than the forward impulse from the Cl atom, and most of the ClO product is sideways scattered. When the collision energy is increased, and the forward impulse becomes stronger and overcomes the sideways repulsion, the forward peak starts to be predominant. It is noticed that, with the increase of collision energy, the increase of the translational energy release for the small angle

scattering is larger than that for the large angle scattering (Figs. 19, 20). This might be understood in two ways. First, the large angle scattering corresponds to the small impact parameter (small b) approach, which causes more vibrational excitation of the reaction intermediate. The small angle scattering, however, corresponds to the large impact parameter (large b) collision, which causes less vibrational excitation of the intermediate. When the collision energy is increased, the small b collision could still distribute the initial translational energy into the vibrational energy of the products. However, the large b collision is more efficient to channel the initial translational energy into the translation of the products. Second, the translational energy release pattern has also to meet the constraint of the conservation of the angular momentum. Since the small b collision has a relatively small total angular momentum, thus, smaller final orbital angular momentum and rotational angular momentum, therefore, the relative velocity of the products and the translational energy of the products all have to be relatively small to meet this constraint. However, the large b collision allows larger angular momentum, and, thus, large relative velocity of the products and larger translational energy release. The increase of the width of the $P(E_T)$ curve with the increase in the collision energy might be due to the increased excitation of the reaction intermediate with the increased collision energy.

We have to point out that it is also possible for the Cl + O_3 reaction to proceed through two reaction mechanisms. Besides the coplanar approach in which the Cl atom attacks a terminal oxygen atom of the ozone molecule in the

plane, the out-of-plane reaction pathway in which the Cl atom attacks the terminal O atom vertically to the ozone molecule plane might also exist. As we have discussed, this out-of-plane collision pathway would give largely forward scattering, and it can not account for the wide angle scattering, thus, not the complete picture of the reaction mechanism. Nevertheless, this out-of-plane channel might account for the forward scattering very well. Because of the large impact parameter in this approach, the reaction intermediate may have smaller internal excitation, therefore, the product translational energy is larger relative to that in the wide angle scattering. It is noticed that the increase of the translational energy release with the collision energy at small center-of-mass angles is larger than that at wide center-of-mass angles, i.e., that the trend of the increase at small angles is different from that at the large angles (see Fig. 19). At wide center-of-mass scattering angles, the translational energy release increases gradually, but at small center-of-mass scattering angles, the translational energy release increases drastically. It is noteworthy that there seems to be a big jump in the translational energy release from E_{coll} = 6 kcal/mole to E_{coll} = 13.5 kcal/mole at CM angle 10°; but there is only smooth increase at CM angles 50° and 120° (Fig. 19). It almost seems that at E_{coll} = 6 kcal/mole the forward scattering channel with large translational energy release is not open, and the forward scattering channel seems to have a higher reaction barrier than the wide-angle scattering channel. We try to understand this phenomenon in two ways. In the first aspect, in a large impact parameter collision such as in the out-of-plane approach, the orbital angular

momentum **L** is large, therefore, there is fair amount of translational energy tied up to rotation. This amount of translational energy is consumed into the rotation as the centrifugal energy and can not be used to break the chemical bond. For E_{coll} = 6 kcal/mole, this amount of energy is estimated to be about 1 kcal/mole. In addition to this rotational energy, there is also an average reaction barrier of about 0.5 kcal/mole.[10] Therefore, at low collision energy E_{coll} = 6 kcal/mole, the translational energy is not very effective for the reaction with large impact parameter. However, with the increase of the collision energy up to E_{coll} = 32 kcal/mole, the translational energy tied up to the rotation increases only up to about 3 kcal/mole, and it is much smaller than the collision energy. Therefore, at high collision energies, the effect of the translational energy consumed in the rotation becomes much smaller, and the forward scattering from the out-of-plane collision (with large impact parameter) becomes open and becomes predominant as well. However, for the large angle scattering which has to come from the in-plane collision, the impact parameter is smaller, and the translational energy tied to rotation plays a smaller role. Therefore, the dependence on the collision energy for the large angle scattering is smaller. Of course, the analysis for the out-of-plane collision is also suitable for the large impact parameter collision in the in-plane approach. However, in the coplanar approach, the dependence on the impact parameter should be smooth and may not be very strong, so the large dependence of the translational energy release on the scattering angle may not only come from the in-plane pathway. In the second aspect, the out-of-plane

approach may indeed have a larger reaction barrier than the in-plane approach, so the forward scattering (out-of-plane pathway) has different collision energy dependence from the wide-angle scattering (in-plane pathway). At the low collision energy (6 kcal/mole), the out-of-plane channel is almost not open, however, at high collision energy, with a wide range of acceptance angles, this channel becomes significant. To summarize, the in-plane collision causes the sideways and wide angle scattering; it causes the forward scattering as well. However, an additional collision channel, the out-of-plane channel, is also possible. This channel results largely the forward scattering. It does not seem to have significant contribution at low collision energy E_{coll} = 6 kcal/mole, however, at higher collision energies, the out-of-plane channel may become quite predominant.

Our experimental results have a qualitative agreement with the conclusions from the semi-empirical calculations by Farantos and Murrell.[20] The Cl + O_3 reaction is a direct reaction; no long-lived complex is involved. The trajectory calculations also showed no evidence of the long-lived complex. The translational energy release is about 50% of the total available energy. Our conclusion that the Cl atom could attack the ozone molecule in a coplanar way is consistent with the collinear reaction pathway given by the functional form of the ClO_3 potential energy surface. However, the quantitative comparison between the experiment and the calculations is not satisfactory. The most noteworthy feature is the center-of-mass angular distribution. The calculations showed a predominant

forward scattering of the ClO product with respect to the Cl atom at about 1 kcal/mole thermal energy. The experimental CM angular distribution at 6 kcal/mole collision energy, the lowest in our experiment, is relatively flat and peaked sideways. Only with the increase of the collision energy to 13.5 kcal/mole and finally to 32 kcal/mole, does the CM angular distribution shift to the forward direction. Strictly speaking, this shift is not totally forward but forward-sideways. The intensity $I(\theta)$ for $\theta < 20°$ in the center-of-mass angular distribution is still consistently low even at the highest collision energy. One possible reason for these discrepancies is that the semi-empirical ClO_3 potential energy surface did not have a strong enough repulsion on the exit channel. The semi-empirical PES may not be sufficient; an *ab initio* calculation on the Cl + O_3 reaction, which is achievable now, is most desirable.[21] Our experimental results also suggest that an out-of-plane collision pathway with a higher reaction barrier is possible. However, this pathway was not investigated in Farantos and Murrell's study.[20] It would be very interesting for an *ab initio* study to explore this out-of-plane collision approach.

It is clear now that the Cl atom mainly attack the terminal oxygen atom of the ozone molecule. At low collision energy (6 kcal/mole), the ClO product is mainly sideways scattered, and the translational energy is about 40% of the total available energy. The coplanar collision channel seems to contribute dominantly at 6 kcal/mole collision energy. At high collision energies (13.5 kcal/mole and 32 kcal/mole), the ClO product is forward and sideways scattered. The forward

component might come from an out-of-plane collision pathway, and the translational energy is 50-70% of the total available energy; however, the in-plane pathway still gives significant amount of sideways scattering. The in-plane collision contributes significantly at all collision energies, especially at low collision energy; and the out-of-plane collision seems to open and become predominant at high collision energy (13.5 kcal/mole and 32 kcal/mole). Farantos and Murrell's semi-empirical studies gave a good account for the coplanar collision pathway, however, they failed to explore the possible out-of-plane approach.[20] The *ab initio* calculations on the $H + O_3$ reaction seems to have given very reasonable results for this system.[22] Because the H atom has only an s orbital and it can only have σ interaction, the out-of-plane approach could have net overlap between the s orbital of the H atom and the π orbital on the terminal O atom and is symmetry-allowed; the in-plane approach could not have the net overlap between the frontier orbitals and therefore is repulsive. However, the key features of the $H + O_3$ PES may not be totally transferable to the $Cl + O_3$ reaction.[22] In both reactions, the out-of-plane approaches are similar; however, our experimental results show that the in-plane collision channel in the $Cl + O_3$ reaction is quite significant, on the contrary, in the *ab initio* calculations, there is no coplanar collision pathway in the $H + O_3$ reaction.[22] This is mainly because the Cl atom has p orbitals and could have π-π interaction with the terminal O atom of the ozone molecule in a coplanar approach. Finally, in the experimental studies by Polanyi and co-workers,[23] the highly vibrationally excited OH product

may not be due to a narrow range of impact parameters, because the reduced mass of the reactants H and O_3 is extremely small and a large range of impact parameters would still correspond to very small orbital angular momentum. Therefore, an out-of-plane collision pathway in the H + O_3 reaction might also produce highly vibrationally excited OH product, and the experimental results and the *ab initio* calculations may be consistent.

It has been suggested that electron density is transferred from the HOMO of the ozone molecule to the singly occupied p-orbital on the Cl atom, because Cl atom has higher electron affinity (E. A.) but lower ionization potential (I. P.) than O_3 molecule.[9,10] In both the in-plane and the out-of-plane mechanisms, the frontier orbital interactions are symmetry-allowed, and both approaches are favored. Therefore, both types of attacks of the Cl atom on the terminal oxygen of the ozone molecule could initiate the Cl + O_3 reaction, and the electron density is expected to be transferred from the π orbital on the ozone molecule to the Cl atom, and this π bond is weakened. After disappearance of the old O-O bond and the formation of the new ClO bond, the stable O_2 and ClO species are generated, and the strong repulsion between the two products while the O-O bond is being cleaved channels large amount of energy into the translational energy of the products.

B. The Absence of the Electronically Exited O_2 Products

Three ClO + O_2 channels are energetically possible and spin-allowed (Fig.

1). Furthermore, all the three product channels are symmetry-allowed. In a coplanar collision pathway, the reaction proceeds through a C_s symmetry, the electronic states of the three product channels are correlated with those of the reactants via $^2A'$ or $^2A''$ states. In the out-of-plane approach (C_1 symmetry), the states of the products and the reactants are correlated via ^2A state. However, early experiments found no evidence of the formation of the electronically excited $O_2(^1\Delta_g)$ and $O_2(^1\Sigma_g^+)$ channels.[18,19] The translational energy release probability $P(E_T)$ in our experiment is quite smooth with no obvious breaks, suggesting that it is unlikely for the electronically excited O_2 product to form which might have quite different types of $P(E_T)$ from that of the ground- state O_2 product. However, because of the vibrational and rotational excitations of the products and the time-of-flight resolution in our experiment, it is not very conclusive to tell whether or not the electronically excited O_2 product is formed just by inspecting the translational energy release $P(E_T)$. It is noteworthy that the absence or the very minor presence of the electronically excited oxygen molecule product seems to be a general case in the radical and ozone reaction systems such as $Cl + O_3$,[18,19] $O(^3P) + O_3$,[56] $H(^2S) + O_3$,[56] and $NO(^2\Pi) + O_3$.[56,57] This phenomenon might be understandable from the point of view of the electronic structure of the ozone molecule. If the radical attacks a terminal oxygen atom, the O-O bond between this terminal oxygen atom and the central oxygen atom cleaves, and the remaining O-O part from the ozone molecule would undergo minimum energy and electronic structure change to form the O_2 molecule. The most likely state of

the O_2 molecule would be the ground state $O_2(^3\Sigma^-_g)$ because the old π orbitals on this O-O part remain unchanged. It is unlikely for the electronically excited O_2 molecule to form in the reaction, because, in order to form the excited singlet O_2 molecule, the unpaired electron on the central oxygen atom that is just released from the breaking of the O-O σ bond has to undergo large rearrangement to pair with the previously unpaired π electron on the terminal oxygen atom. If the radical attacks the central oxygen atom instead of the terminal oxygen atom, a large change of the O-O electronic structure could occur, and the electronically excited O_2 might form;[58] however, this approach again will encounter a very high barrier. Our experimental results also imply that the Cl atom would not likely attack the central oxygen atom of the ozone molecule. Following the above analysis, it would not be surprising that almost no electronically excited O_2 molecule is produced in the Cl + O_3 reaction.

C. The Absence of the ClOO and OClO Channels

The reaction channels $Cl + O_3 \rightarrow ClOO(^2A) + O(^3P)$ ($\Delta H^\circ \approx 17.4$ kcal/mole) and $Cl + O_3 \rightarrow OClO(^2A) + O(^3P)$ ($\Delta H^\circ \approx 19.5$ kcal/mole) are open at the high collision energies 26 kcal/mole and 32 kcal/mole. These two channels are also spin-allowed. However, we have not observed any evidence of any of the two channels. To produce OClO, the Cl atom has to insert into the ozone molecule, but the high repulsion barrier that is much larger than the collision energies will prohibit this reaction channel. In the coplanar pathway, when the Cl atom attacks

one terminal oxygen atom on the ozone molecule to form the asymmetric ClO_3 intermediate, it would be the O-O bond between this terminal oxygen atom and the central oxygen atom that is weakened the most and is being broken because of the strongest perturbation from the Cl atom. Thus, it is very unlikely for the other O-O bond to break to form the ClOO product. If the lifetime of the asymmetric ClO_3 were quite long, there might be some small probability to break the other O-O bond after the redistribution of the internal energy of the ClO_3 intermediate and to form the ClOO product. However, our conclusion that the lifetime of the asymmetric ClO_3 intermediate is very small implies that there is a very small probability for the ClOO channel in the Cl + O_3 reaction. Certainly, other collision pathways would encounter much higher barriers and ClOO is unlikely to be generated in the range of the collision energies in our experiment.

D. Spin-orbit States of the Reactant Cl Atom and the Product ClO Radical

The Cl atoms are in two spin-orbit states $Cl(^2P_{3/2})$ and $Cl(^2P_{1/2})$. The excited state $Cl(^2P_{1/2})$ is separated by 2.52 kcal/mole from the ground state $Cl(^2P_{3/2})$.[59] Before the supersonic expansion, under the assumption that the Cl atoms are in the Boltzmannian distribution, about 20% of the Cl atoms are in the spin-orbit excited state $Cl(^2P_{1/2})$ at 1800 °K temperature. However, after the supersonic expansion, the Cl atoms in the spin-orbit excited state could be partially relaxed. The translational temperature of the Cl atomic beam is estimated to be less than 200 K using the measured speed ratios.[60] The 882 cm^{-1} energy separation between

$Cl(^2P_{1/2})$ and $Cl(^2P_{3/2})$ states is comparable to the energy spacing of a low frequency vibrational mode in a polyatomic molecule. There is reasonable chance for the $Cl(^2P_{1/2})$ atoms to relax. If the electronic temperature T_{el} in the Cl beam is taken to be 1000 K, only 10% of the Cl atoms would be left in the excited state $Cl(^2P_{1/2})$ after the expansion. There are two possible spin-orbit states of the product ClO in the ground electronic state $^2\Pi$: $ClO(^2\Pi_{3/2})$ and $ClO(^2\Pi_{1/2})$, which are separated by 318 cm^{-1}.[61] The time-of-flight resolution and the spread of the collision energies in our experiment prevented us from getting any information about the reactivities of the two spin-orbit states of the Cl atom and the fine structure population of the ClO product. In general, however, the $Cl(^2P_{3/2})$ atom is found to be more reactive than the excited $Cl(^2P_{1/2})$ atom, and the Cl atom products are usually preferentially formed in the ground state $^2P_{3/2}$.[62] The reaction rate constant of the $Cl(^2P_{3/2}) + O_3$ reaction measured at 298 K by Clyne and Nip[7] was slightly larger than that of the $Cl(^2P_{1/2}) + O_3$ reaction measured at the same temperature. Because the Cl atoms in the ground spin-orbit state $^2P_{3/2}$ are dominant in the beam, and because ground-state $Cl(^2P_{3/2})$ atoms are more reactive than the excited $Cl(^2P_{1/2})$ atoms, if we assume that the non-adiabatic transition processes in the reaction are small, then most of the ClO products should be in the ground spin-orbit state $^2\Pi_{3/2}$.

E. Some Implications to the Atmospheric Chemistry

This study of the reaction mechanism of the $Cl + O_3$ reaction shows that

the Cl + O_3 reaction is a direct and fast reaction. The Cl atom strikes the terminal oxygen atom of the ozone molecule, and the strong repulsion between ClO and O_2 on the collision intermediate immediately force the products to flight apart. Meanwhile, the remaining O-O bond of the ozone molecule is not too perturbed and serves as a spectator, and the O_2 product should be vibrationally cold. Therefore, it is reasonable to speculate from the translational energy distributions that besides the large translational energy release, a substantial amount of energy is also channeled into the ClO vibration.

In the part of atmosphere where the vibrational relaxation is slow, the vibrationally excited ClO radical might be of some importance. The vibrationally excited ClO product in the Cl + O_3 reaction could certainly promote its reaction with certain atmospheric species in both laboratory measurement and in the stratosphere.[63,64]

V. CONCLUSIONS

We have studied the Cl + O_3 reaction using the crossed molecular beams technique. The center-of-mass product angular distribution and the translational energy distribution have been derived from the experimental results. The average translational energy of the products is found to be 40-70% of the total available energy. In the center-of-mass frame, the ClO product is sideways and forward

scattered. With the increase of the collision energy, the ClO product is scattered in a more forward direction with respect to the Cl atom. The translational energy distribution depends on the center-of-mass scattering angle; the translational energy release in the forward direction in the center-of-mass frame is larger than that in the backward direction.

The Cl + O_3 reaction is a direct reaction. The Cl atom would most likely attack the terminal oxygen atom on the ozone molecule. The exit channel on the ClO_3 potential energy surface is believed to have a strong repulsion. Besides the large translational energy release in the products, the ClO product is also expected to be vibrationally excited. Since the remaining O-O bond of the ozone molecule serves as a spectator in the reaction process, the O_2 product that the remaining O-O bond finally turns into should remain vibrationally cold. A measurement of the state distributions of the ClO and O_2 products would be helpful to complete the picture of the reaction mechanism. An *ab initio* calculation on the Cl + O_3 reaction is also desirable to compare with the results of this crossed molecular beam study.

VI. REFERENCES

1. R. P. Wayne, Chemistry of Atmospheres (Clarendon Press, Oxford, 1991).

2. L. T. Molina and M. J. Molina, J. Phys. Chem. **91**, 433 (1987).

3. M. B. McElroy, R. J. Salawitch, S. C. Wofsy, and J. A. Logan, Nature **321**, 759 (1986).

4. J. G. Anderson, D. W. Toohey, and W. H. Brune, Science **251**, 39 (1991).

5. J. W. Barrett, P. M. Solomon, R. L. de Zafra, M. Jaramillo, L. Emmons, and A. Parrish, Nature **336**, 455 (1988).

6. S. Solomon, Nature **347**, 347 (1990).

7. M. A. A. Clyne and W. S. Nip, J. Chem. Soc. Far. Trans. II **72**, 838 (1976).

8. M. S. Zahniser, F. Kaufman, and J. G. Anderson, Chem. Phys. Lett. **37**, 226 (1976).

9. D. W. Toohey, W. H. Brune, and J. G. Anderson, Int. J. Chem. Kinet. **20**, 131 (1988) and the references therein.

10. J. M. Nicovich, K. D. Kreutter, and P. H. Wine, Int. J. Chem. Kinet. **22**, 399 (1990) and the references therein.

11. R. Patrick and D. M. Golden, J. Phys. Chem. **88**, 491 (1984).

12. a) D. L. Baulch, R. A. Cox, R. F. Hampson Jr., J. A. Kerr, J. Troe, and R. T. Watson, J. Phys. Chem. Ref. Data. **9**, 295 (1980).

    b) D. L. Baulch, R. A. Cox, P. J. Crutzen, R. F. Hampson Jr., J. A. Kerr, J. Troe, and R. T. Watson, J. Phys. Chem. Ref. Data. **11**, 327 (1982).

13. S. S. Prasad and W. M. Adams, J. Photochem. **13**, 243 (1980).

14. S. S. Prasad, Nature **285**, 152 (1980).

15. R. O. Carter III, L. Andrews, J. Phys. Chem. **85**, 2351 (1981).

16. a) W. P. McGrath and R. G. W. Norrish, Z. Phys. Chem. **15**, 245 (1958).

b) W. P. McGrath and R. G. W. Norrish, Proc. Roy. Soc. A **254**, 317 (1960).

17. M. A. A. Clyne and J. A. Coxon, Proc. Roy. Soc. A **303**, 207 (1968).

18. J. W. Vanderzanden and J. W. Birks, Chem. Phys. Lett. **88**, 109 (1982).

19. K. Y. Choo and M. Leu, J. Phys. Chem. **89**, 4832 (1985).

20. S. C. Farantos and J. N. Murrell, Int. J. Quan. Chem. **14**, 659 (1978).

21. a) T. Rathmann and R. N. Schindler, Chem. Phys. Lett. **190**, 539 (1992).

b) T. Rathmann and R. N. Schindler, Ber. Bunsenges. Phys. Chem. **96**, 421 (1992).

22. a) M. M. L. Chen, R. W. Wetmore, and H. F. Schaefer III, J. Chem. Phys. **74**, 2938 (1981).

b) M. Dupuis, G. Fitzgerald, B. Hammond, W. A. Lester, and H. F. Schaefer III, J. Chem. Phys. **84**, 2691 (1986).

23. a) K. G. Anlauf, R. G. MacDonald, and J. C. Polanyi, Chem. Phys. Lett. **1**, 619 (1968).

b) J. C. Polanyi and J. J. Sloan, Int. J. Chem. Kinet. Symp. **1**, 51 (1975).

24. Y. T. Lee, J. D. McDonald, P. R. LeBreton, and D. R. Herschbach, Rev. Sci. Instrum. **40**, 1402 (1969).

25. R. K. Sparks, Ph. D. Thesis, University of California, Berkeley (1979).

26. G. O. Brink, Rev. Sci. Instrum. **37**, 857, 1626 (1966).

27. a) N. R. Daly, Rev. Sci. Instrum. **31**, 264 (1960).

b) H. M. Gibbs and E. D. Commins, Rev. Sci. Instrum. **37**, 1385 (1966).

28. Carborundum Co., Specialty Graphite Plant, Sanborn, New York.

29. J. J. Valentini, M. J. Coggiola, and Y. T. Lee, Rev. Sci. Instrum. **48**, 58 (1977).

30. G. A. Cook, A. D. Kiffer, C. V. Klumpp, A. H. Malik, and L. A. Spence, Ozone Chemistry and Technology, Adv. Chem. Ser. **21**, 44 (1959).

31. P. N. Clough and B. A. Thrush, Chem. and Ind. **19**, 1971 (1966).

32. L. F. Atyaksheva and G. I. Emel'yanova, Russ. J. Phys. Chem. **64**, 1741 (1990).

33. M. Griggs, J. Chem. Phys. **49**, 857 (1968).

34. L. T. Molina and M. J. Molina, J. Geophys. Res. **91**, D13, 14501 (1986).

35. P. S. Weiss, Ph. D. Thesis, University of California, Berkeley (1986).

36. M. F. Vernon, Ph. D. Thesis, University of California, Berkeley (1983).

37. D. J. Krajnovich, Ph. D. Thesis, University of California, Berkeley (1983).

38. a) K. Sköld, Nucl. Inst. Methods **63**, 114 (1968).

b) V. L. Hirshy and J. P. Aldridge, Rev. Sci. Instrum. **42**, 381 (1971).

c) G. Comsa, R. David, and B. J. Schumacher, Rev. Sci. Instrum. **52**, 789 (1981).

39. R. J. Buss, Ph. D. Thesis, University of California, Berkeley (1979).

40. D. D. Parrish and D. R. Herschbach, J. Amer. Chem. Soc. **95**, 6133 (1973).

41. P. A. Gorry, C. V. Nowikow, and R. Grice, Chem. Phys. Lett. **49**, 116 (1977).

42. P. A. Gorry, C. V. Nowikow, and R. Grice, Chem. Phys. Lett. **55**, 19 (1978).

43. P. A. Gorry, C. V. Nowikow, and R. Grice, Molec. Phys. **37**, 347 (1979).

44. J. M. Nicovich, K. D. Kreutter, C. J. Schackelford, and P. H. Wine, Chem. Phys. Lett. **179**, 367 (1991).

45. S. Baer, H. Hippler, R. Rahn, M. Siefke, N. Seitzinger, and J. Troe, J. Chem. Phys. **95**, 6463 (1991).

46. R. L. Mauldin, III, J. B. Burkholder, and A. R. Ravishankara, J. Phys. Chem. **96**, 2582 (1992).

47. a) W. B. Miller, S. A. Safron, and D. R. Herschbach, Discuss. Faraday Soc. **44**, 108 (1967).

b) W. B. Miller, Ph. D. Thesis, Harvard University (1969).

48. W. B. DeMore, Geophys. Res. Lett. **17**, 2353 (1990).

49. P. J. Hay and T. H. Dunning, Jr., J. Chem. Phys. **67**, 2290 (1977).

50. S. Rothenberg and H. F. Schaefer III, Molec. Phys. **21**, 317 (1970).

51. R. P. Messmer and D. R. Salahub, J. Chem. Phys. **65**, 779 (1976).

52. P. Borowski, K. Andersson, P.-Å. Malmqvist, and B. O. Roos, J. Chem. Phys. **97**, 5568 (1992).

53. J. S. Zhang, T. T. Miau, and Y. T. Lee (to be published).

54. K. Fukui, Reactivity and Structure Concepts in Organic Chemistry, Vol. 2: Theory of Orientation and Stereoselection (Springer-Verlag, New York, 1975).

55. K. Fukui, in Molecular Orbitals in Chemistry, Physics and Biology, edited by P.-O. Löwdin and B. Pullman (Academic, New York, 1964), p. 513.

56. N. Washida, H. Akimoto, and M. Okuda, Bull. Chem. Soc. Jpn. **53**, 3496 (1980).

57. M. Gauthier and D. R. Snelling, Chem. Phys. Lett. **20**, 178 (1973).

58. A. E. Redpath, M. Menzinger, and T. Carrington, Chem. Phys. **27**, 409 (1978).

59. C. E. Moore, Atomic Energy Levels, National Stand. Ref. Data Ser. (National Bureau of Standards, Washington DC, 1971).

60. D. R. Miller, in Atomic and Molecular Beam Methods, Vol I, edited by G. Scoles, (Oxford University Press, Oxford, 1988).

61. K. P. Huber and G. Herzberg, Molecular Spectra and Molecular Structure, IV. Constants of Diatomic Molecules, (Van Nostrand Reinhold Company, New York, 1979).

62. P. J. Dagdigian and M. L. Campbell, Chem. Rev. **87**, 1 (1987).

63. A. J. Colussi and S. P. Sander, Chem. Phys. Lett. **187**, 85 (1991).

64. V. Vaida, E. C. Richard, A. Jefferson, L. A. Cooper, R. Flesch, and E. Rühl, Ber. Bunsenges. Phys. Chem. **96**, 391 (1992).

VII. TABLES

TABLE I. Experimental Beam Parameters.

Beam description	Peak velocity (v_{pk}) ($x10^4$ cm/sec)	Speed Ratio ($v/\Delta v$)
Cl (1% Cl_2 in He)	33.2	5.5
Cl (10% Cl_2 in 82% He and 8% Ar)	22.7	5.4
Cl (10% Cl_2 in Ar)	14.1	6.7
O_3 (7% in He)	14.9	13.6
O_3 (7% in Ar)	6.4	12.5

TABLE II. Experimental Conditions.

Cl v_{pk} ($x10^4$ cm/s)	O_3 v_{pk} ($x10^4$ cm/s)	Collision Energy E_{coll} (kcal/mole)	$\Delta E_{coll}/E_{coll}$	$\Delta E_{coll}/E_{avl}$
33.2	14.9	32	31%	14%
22.7	6.4	13.5	34%	9%
14.1	6.4	6	25%	3%

TABLE III. Average Translational Energy Release.

Collision Energy E_{coll} (kcal/mole)	CM Angle 10° $\langle E_T/E_{avl} \rangle$	CM Angle 50° $\langle E_T/E_{avl} \rangle$	CM Angle 120° $\langle E_T/E_{avl} \rangle$	$(\Delta\langle E_T \rangle)_{max}$ kcal/mole
32	.66	.50	.49	12.2
13.5	.60	.47	.43	8.6
6	.43	.41	.37	2.7

TABLE IV. Peak Translational Energy Release.

Collision Energy E_{coll} (kcal/mole)	CM Angle 10° E_T^{peak}/E_{avl}	CM Angle 50° E_T^{peak}/E_{avl}	CM Angle 120° E_T^{peak}/E_{avl}	$(\Delta E_T^{peak})_{max}$ kcal/mole
32	.65	.55	.49	11.0
13.5	.56	.44	.42	7.2
6	.41	.40	.35	2.8

VIII. FIGURE CAPTIONS

Figure 1 Energy level diagram of the Cl + O_3 system. Thermodynamic data of three chlorine trioxides is derived from Ref. 21. All the other thermodynamic data is derived from Ref. 12b. The solid lines stand for the collision energies in the experiment.

Figure 2 Top view of the crossed molecular beam apparatus.

Figure 3 Schematic diagram of the ozone molecular beam source.

Figure 4 Upper: Laboratory angular distribution of the reaction Cl + O_3 at E_{coll} = 32 kcal/mole. The filled circles are for the experimental data. Error bars stand for 95% confidence limits. The solid lines are for the calculated laboratory angular distribution.

Lower: The Newton diagram for the reaction Cl + O_3 at E_{coll} = 32 kcal/mole. The circle stands for the maximum center-of-mass recoil velocity of the ClO product. The direction of Cl velocity vector is defined as 0°, and the direction of ozone velocity vector is 90°.

Figure 5 Laboratory time-of-flight spectra of the ClO product at E_{coll} = 32 kcal/mole. The circles are the experimental data points. The solid lines are the calculated spectra. (a) TOF spectra for the laboratory angles from -20° to 27.5°. (b) TOF spectra for the laboratory angles from 30° to 75°.

Figure 6 Upper: Average translational energy $\langle E_T \rangle$ at different center-of-

mass angles for E_{coll} = 32 kcal/mole.

Lower: Total relative center-of-mass angular distribution $I_{CM}(\theta)$ at E_{coll} = 32 kcal/mole. The maximum of the relative angular distribution is scaled to unit.

Figure 7 Translational energy release probability $P(E_T, \theta)$ at various center-of-mass angles for E_{coll} = 32 kcal/mole. Maximum probabilities are scaled to unit. The maximum translational energy in these plots is the total available energy for the reaction at the most probable collision energy E_{coll} = 32 kcal/mole.

Figure 8 Contour map and 3-D plot for the center-of-mass flux-velocity distribution $I_{CM}(\theta, u)$ at E_{coll} = 32 kcal/mole.

Figure 9 Same as Fig. 4 but at E_{coll} = 13.5 kcal/mole.

Figure 10 Same as Fig. 5 but at E_{coll} = 13.5 kcal/mole. (a) TOF spectra for the laboratory angles from -20° to 35°. (b) TOF spectra for the laboratory angles from 40° to 75°.

Figure 11 Same as Fig. 6 but at E_{coll} = 13.5 kcal/mole.

Figure 12 Same as Fig. 7 but at E_{coll} = 13.5 kcal/mole.

Figure 13 Same as Fig. 8 but at E_{coll} = 13.5 kcal/mole.

Figure 14 Same as Fig. 4 but at E_{coll} = 6 kcal/mole.

Figure 15 Same as Fig. 5 but at E_{coll} = 6 kcal/mole: TOF spectra for the laboratory angles from -15° to 75°.

Figure 16 Same as Fig. 6 but at E_{coll} = 6 kcal/mole.

Figure 17 Same as Fig. 7 but at E_{coll} = 6 kcal/mole.

Figure 18 Same as Fig. 8 but at E_{coll} = 6 kcal/mole.

Figure 19 Upper: The fractions of the average translational energy in the total available energy at different center-of-mass angles versus the collision energies.

Lower: The fractions of the peak translational energy release in the total available energy at different center-of-mass angles versus the collision energies.

Figure 20 The maximum difference in the average translational energy release at different center-of-mass angles versus the collision energies and the maximum difference in the peak translational energy release at different center-of-mass angles versus the collision energies.

Energy Level Diagram

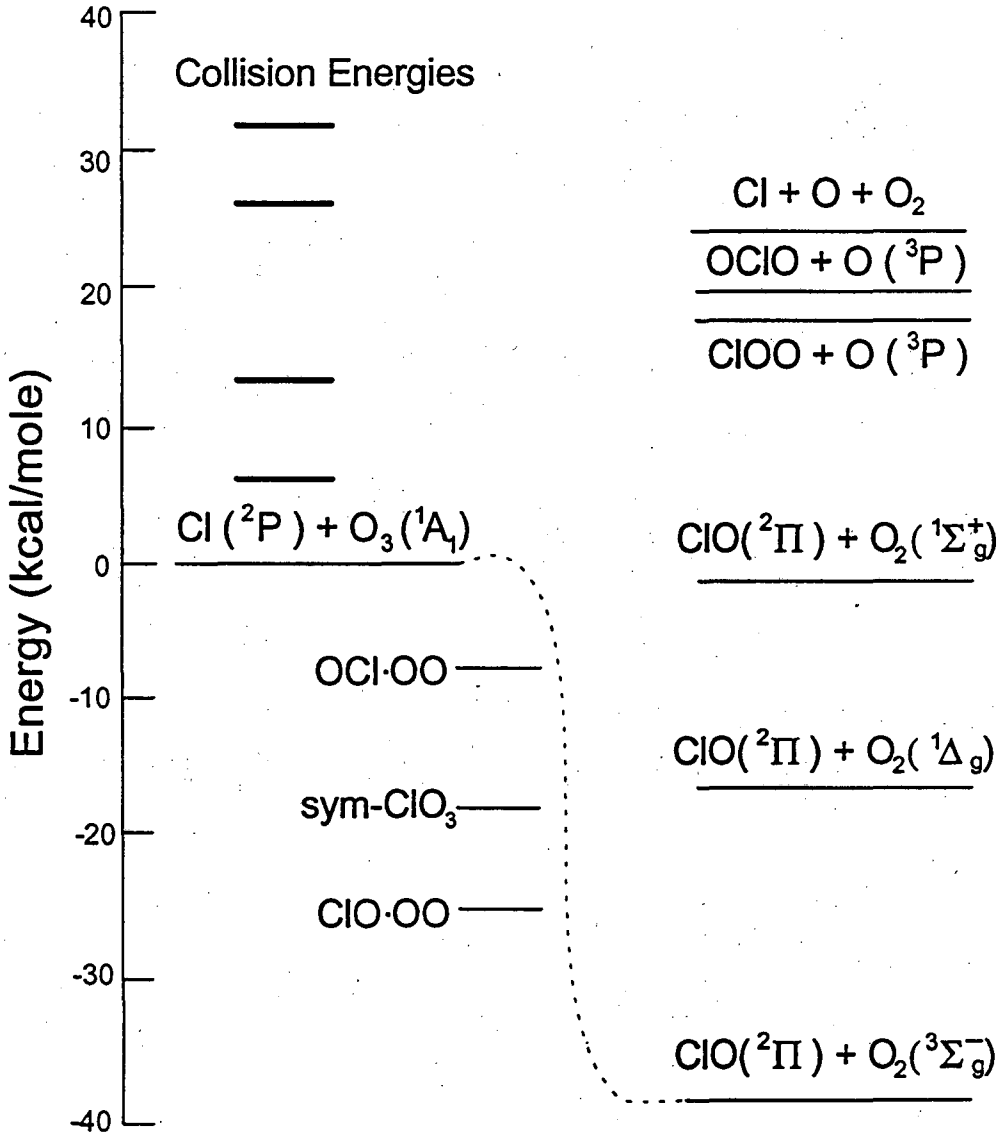

Figure 1

Crossed Molecular Beam Apparatus

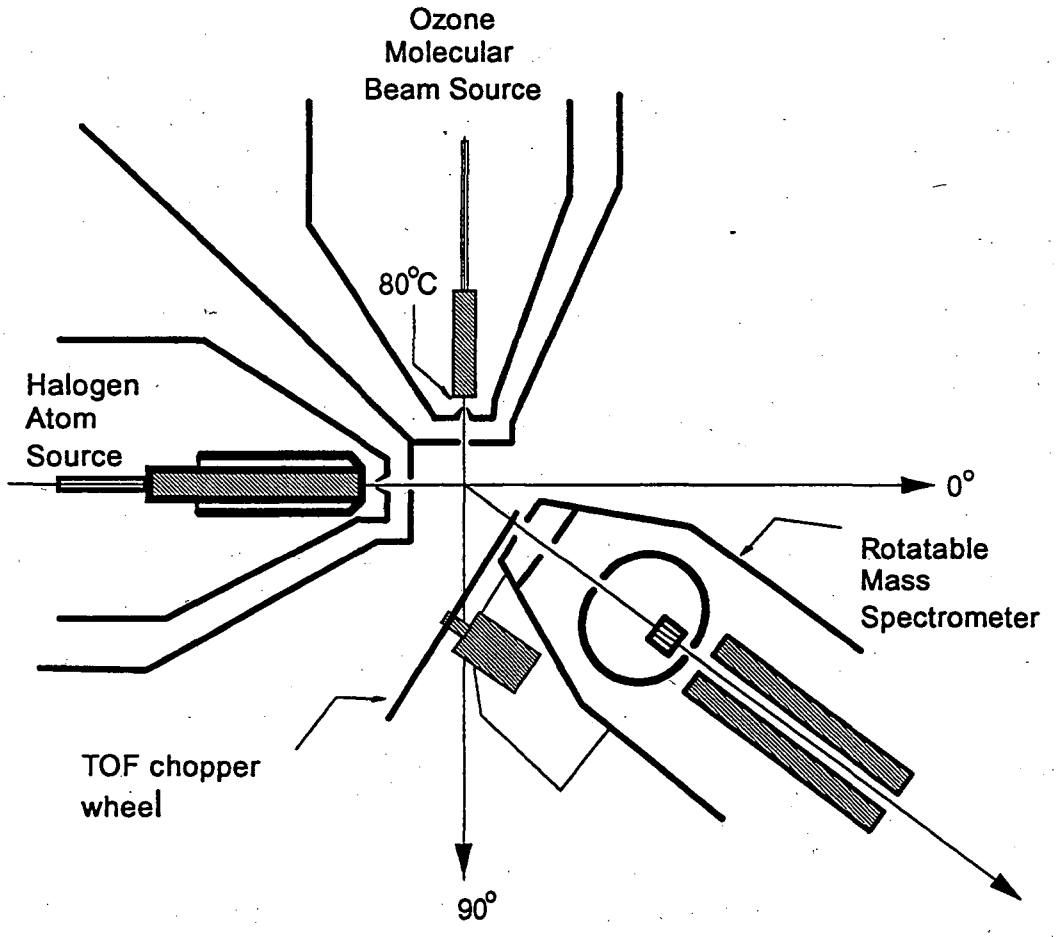

Figure 2

Ozone Molecular Beam Source Setup

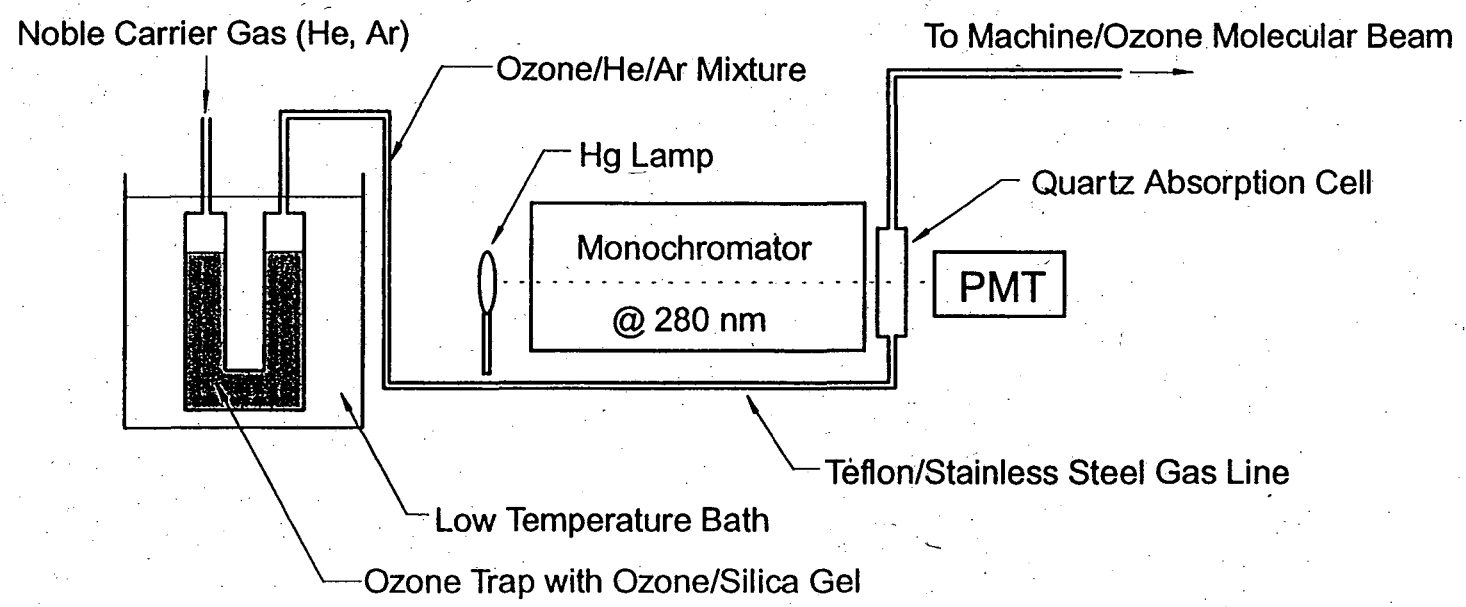

Figure 3

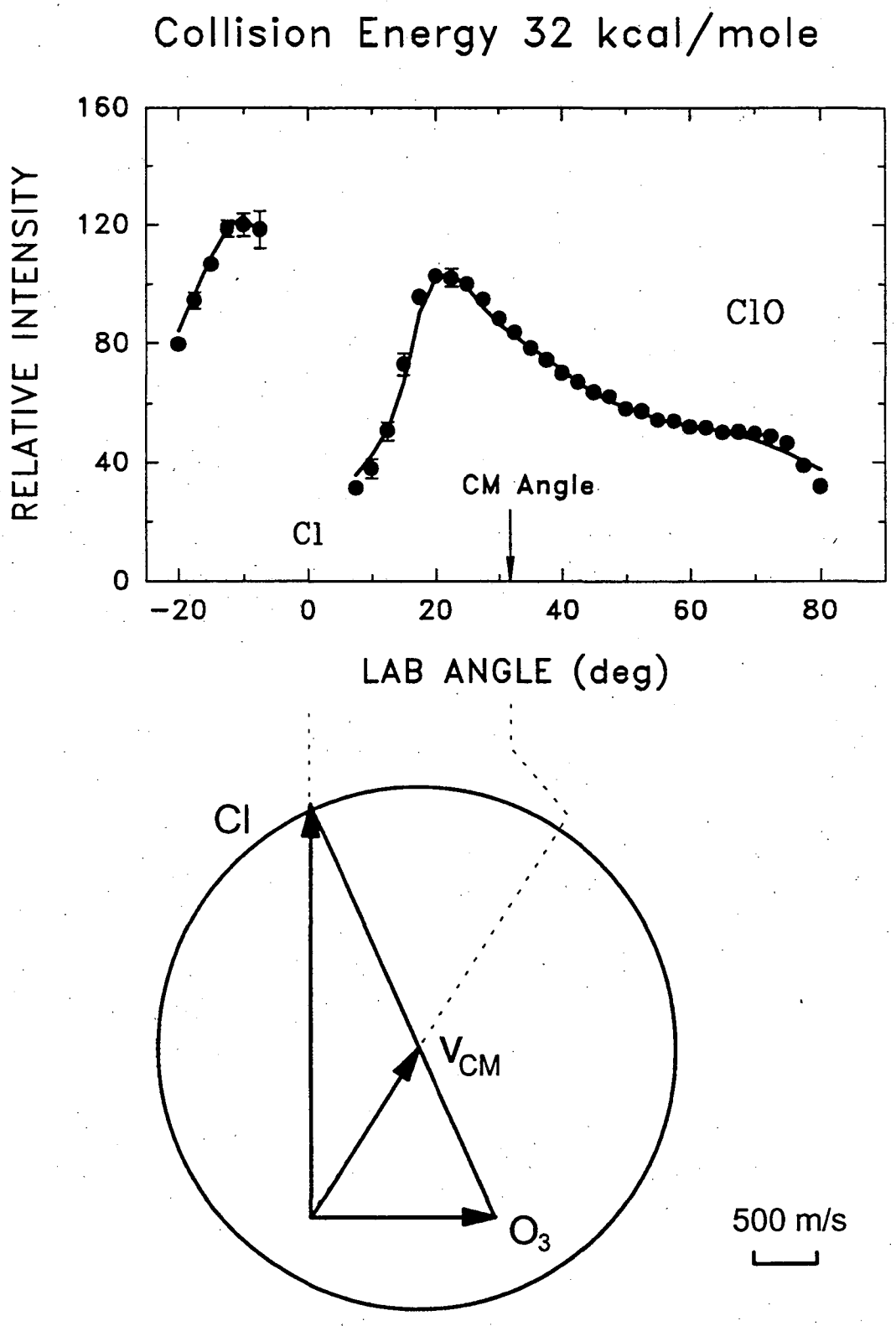
Collision Energy 32 kcal/mole
RELATIVE INTENSITY
160
120
80
40
0
−20
0
20
40
60
80
LAB ANGLE (deg)
ClO
Cl
CM Angle
Cl
V_{CM}
O_3
500 m/s

Figure 4

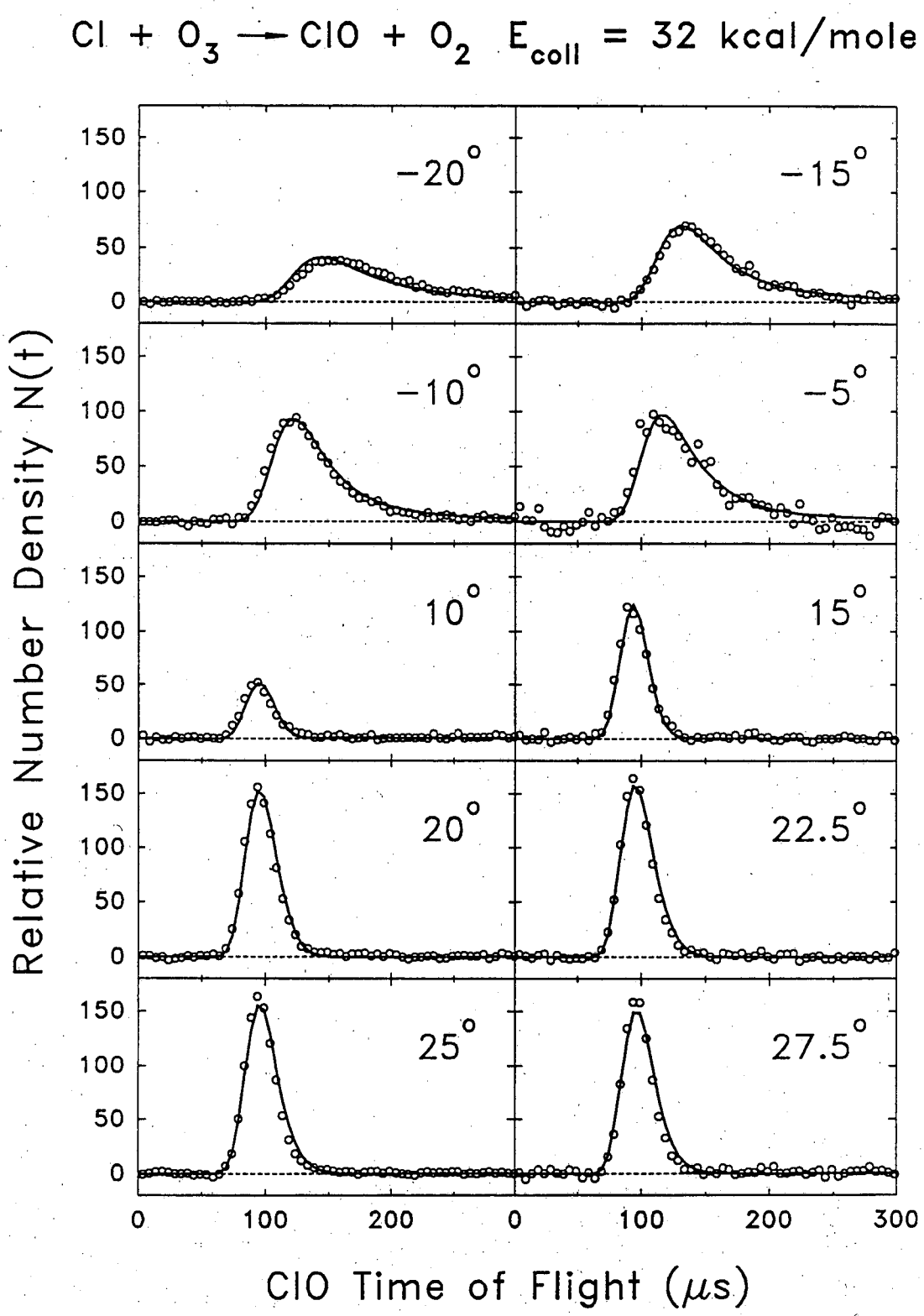
Cl + O3 → ClO + O2 Ecoll = 32 kcal/mole
Relative Number Density N(t)
−20°
−15°
−10°
−5°
10°
15°
20°
22.5°
25°
27.5°
150
100
50
0
0
100
200
300
ClO Time of Flight (μs)

Figure 5a

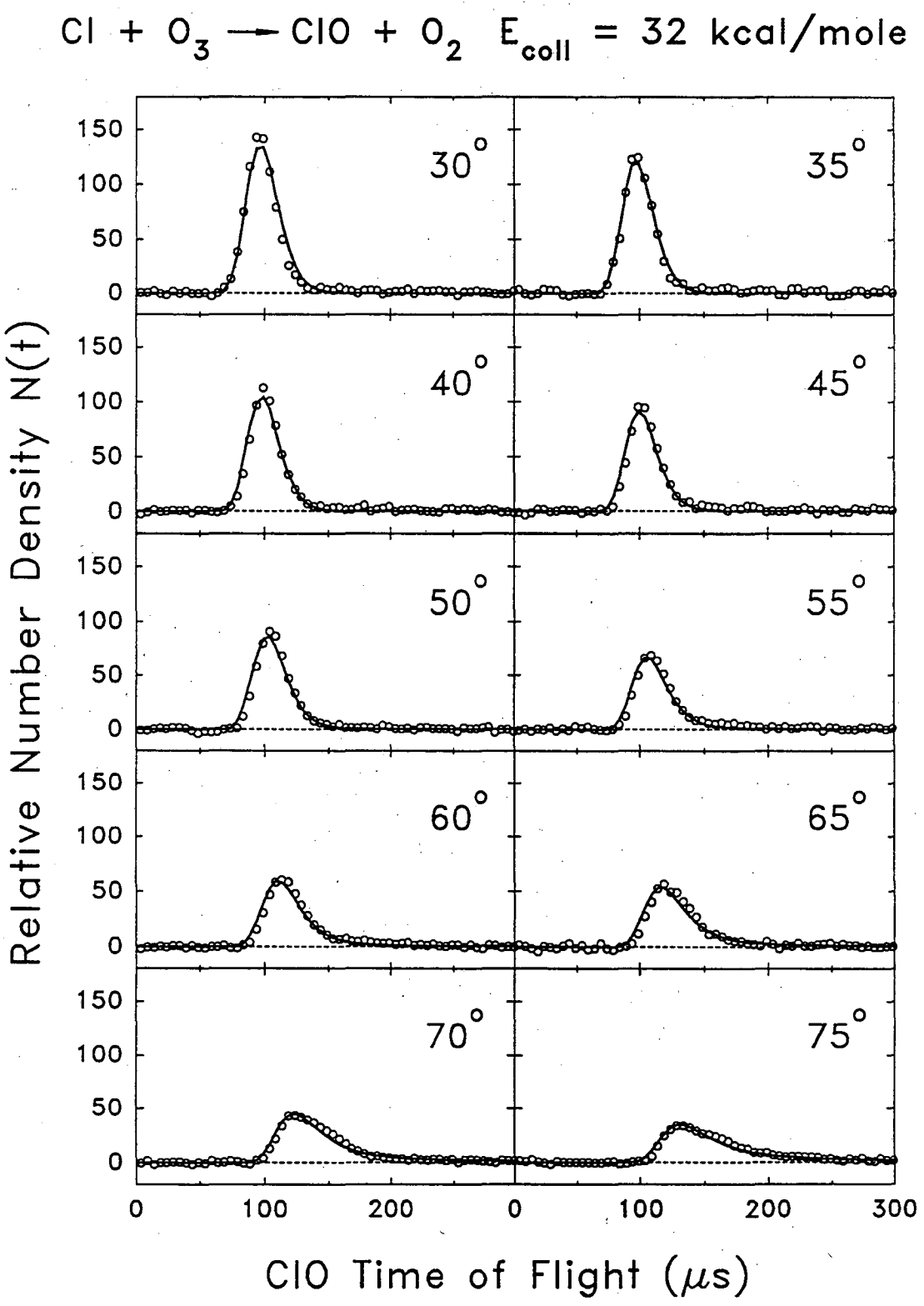
Cl + O3 → ClO + O2 Ecoll = 32 kcal/mole
Relative Number Density N(t)
30°
35°
40°
45°
50°
55°
60°
65°
70°
75°
150
100
50
0
0
100
200
300
ClO Time of Flight (μs)

Figure 5b

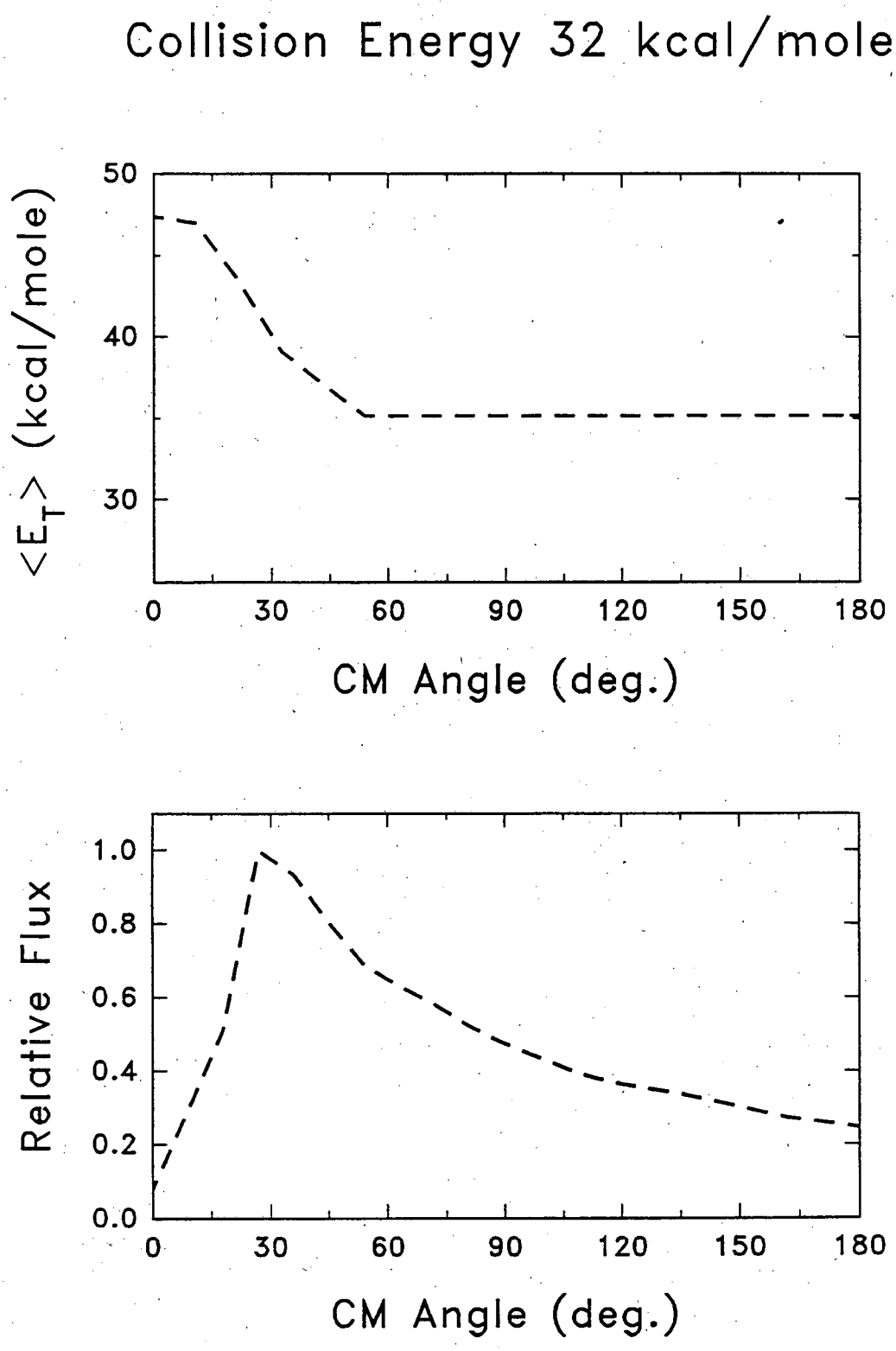
Collision Energy 32 kcal/mole
<E_T> (kcal/mole)
50
40
30
0
30
60
90
120
150
180
CM Angle (deg.)
Relative Flux
1.0
0.8
0.6
0.4
0.2
0.0
0
30
60
90
120
150
180
CM Angle (deg.)

Figure 6

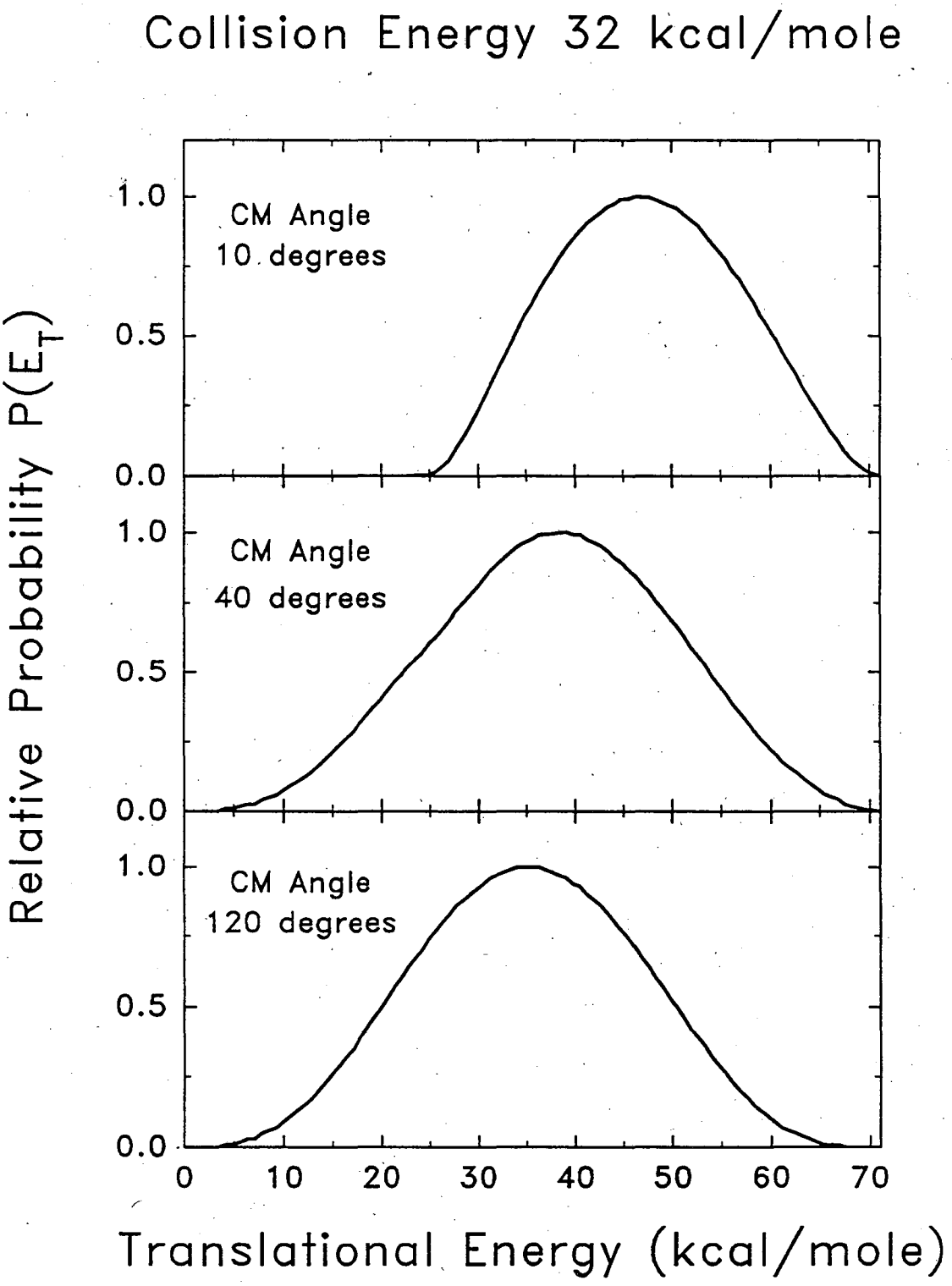
Collision Energy 32 kcal/mole
Relative Probability $P(E_T)$
CM Angle
10 degrees
CM Angle
40 degrees
CM Angle
120 degrees
1.0
0.5
0.0
0
10
20
30
40
50
60
70
Translational Energy (kcal/mole)

Figure 7

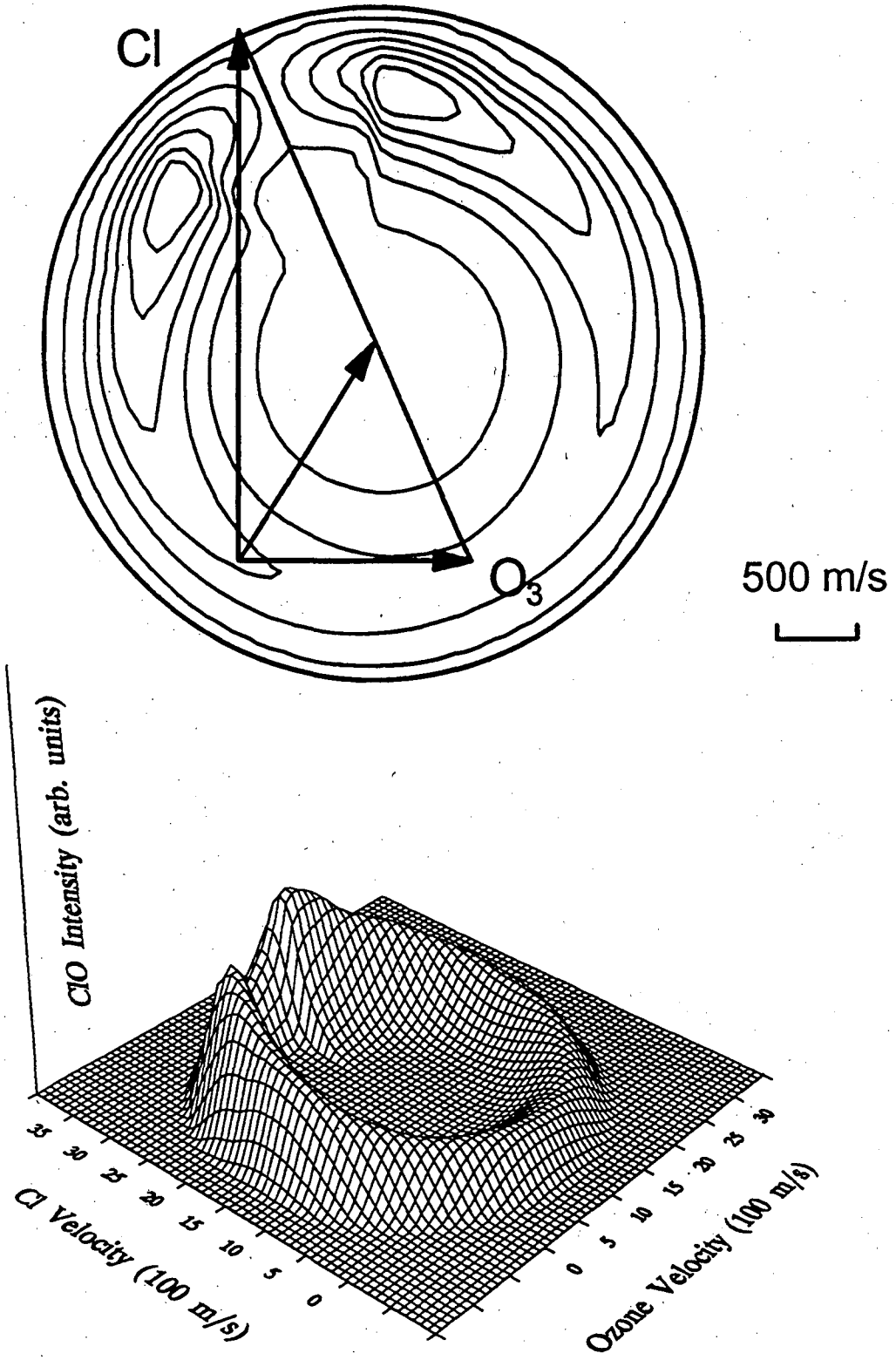
Cl
O_3
500 m/s
ClO Intensity (arb. units)
Cl Velocity (100 m/s)
Ozone Velocity (100 m/s)

Figure 8

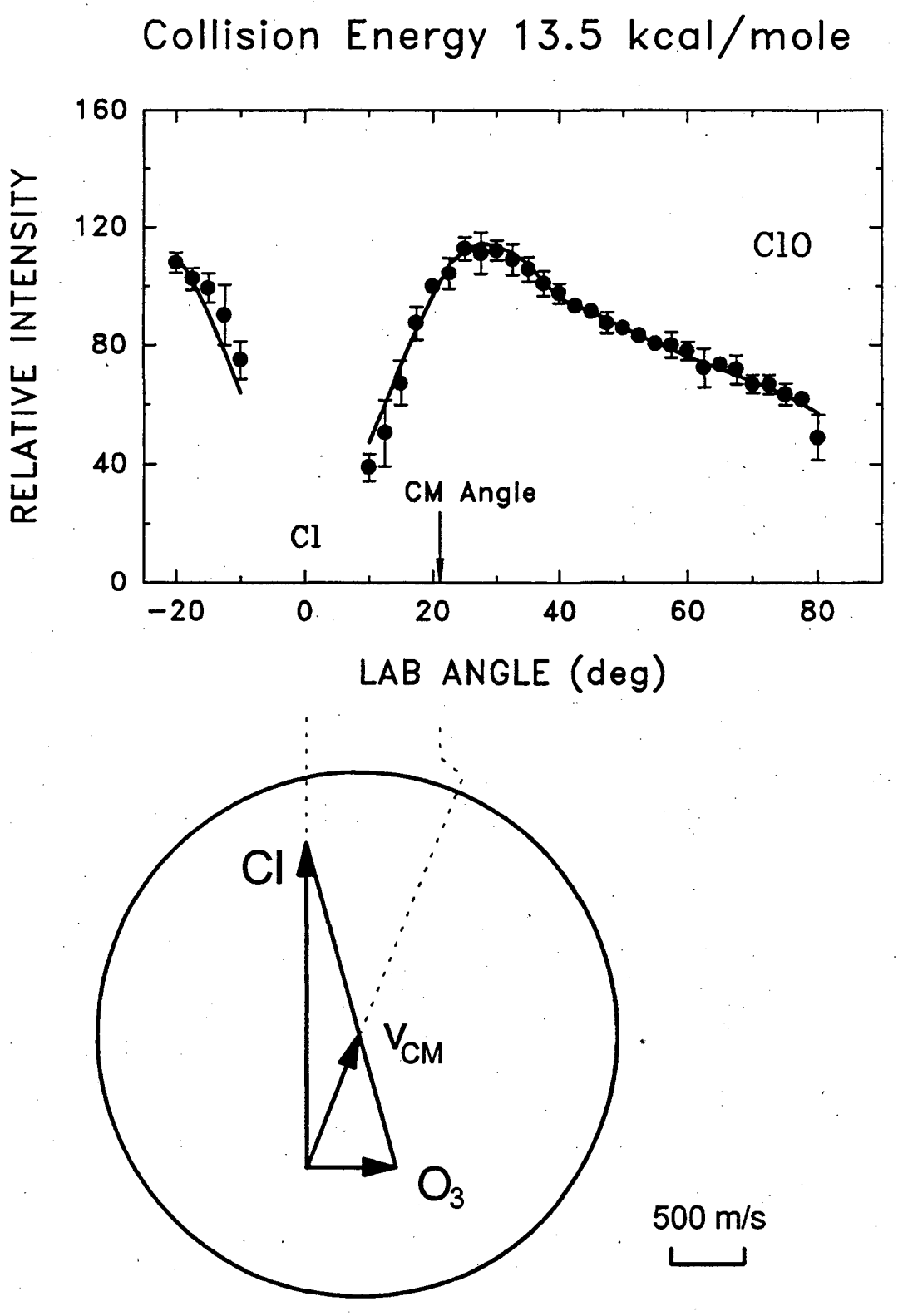
Collision Energy 13.5 kcal/mole
RELATIVE INTENSITY
160
120
80
40
0
ClO
CM Angle
Cl
−20
0
20
40
60
80
LAB ANGLE (deg)
Cl
V_{CM}
O_3
500 m/s

Figure 9

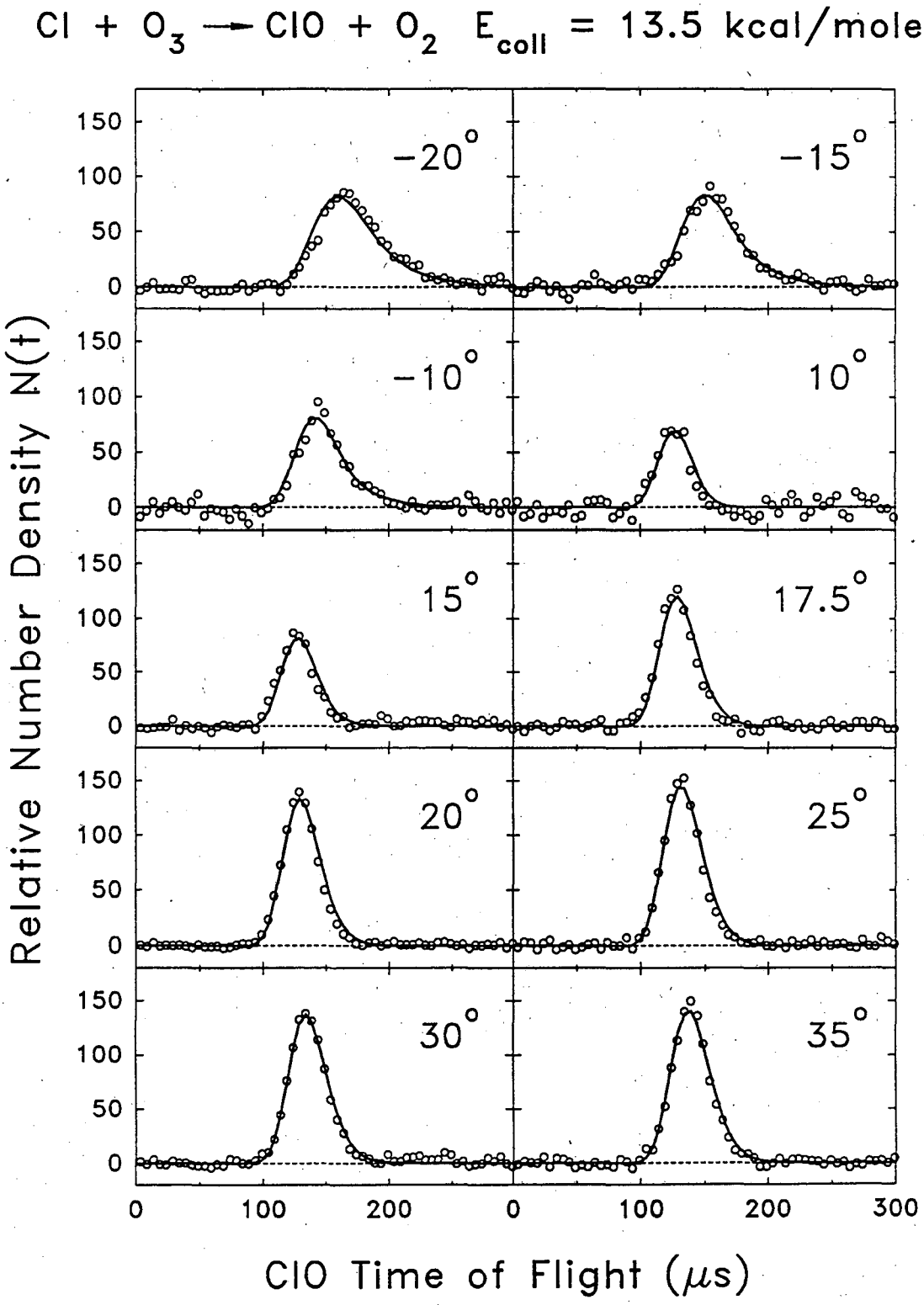
Cl + O3 → ClO + O2 Ecoll = 13.5 kcal/mole
Relative Number Density N(t)
ClO Time of Flight (μs)
−20°
−15°
−10°
10°
15°
17.5°
20°
25°
30°
35°
0
50
100
150
200
300

Figure 10a

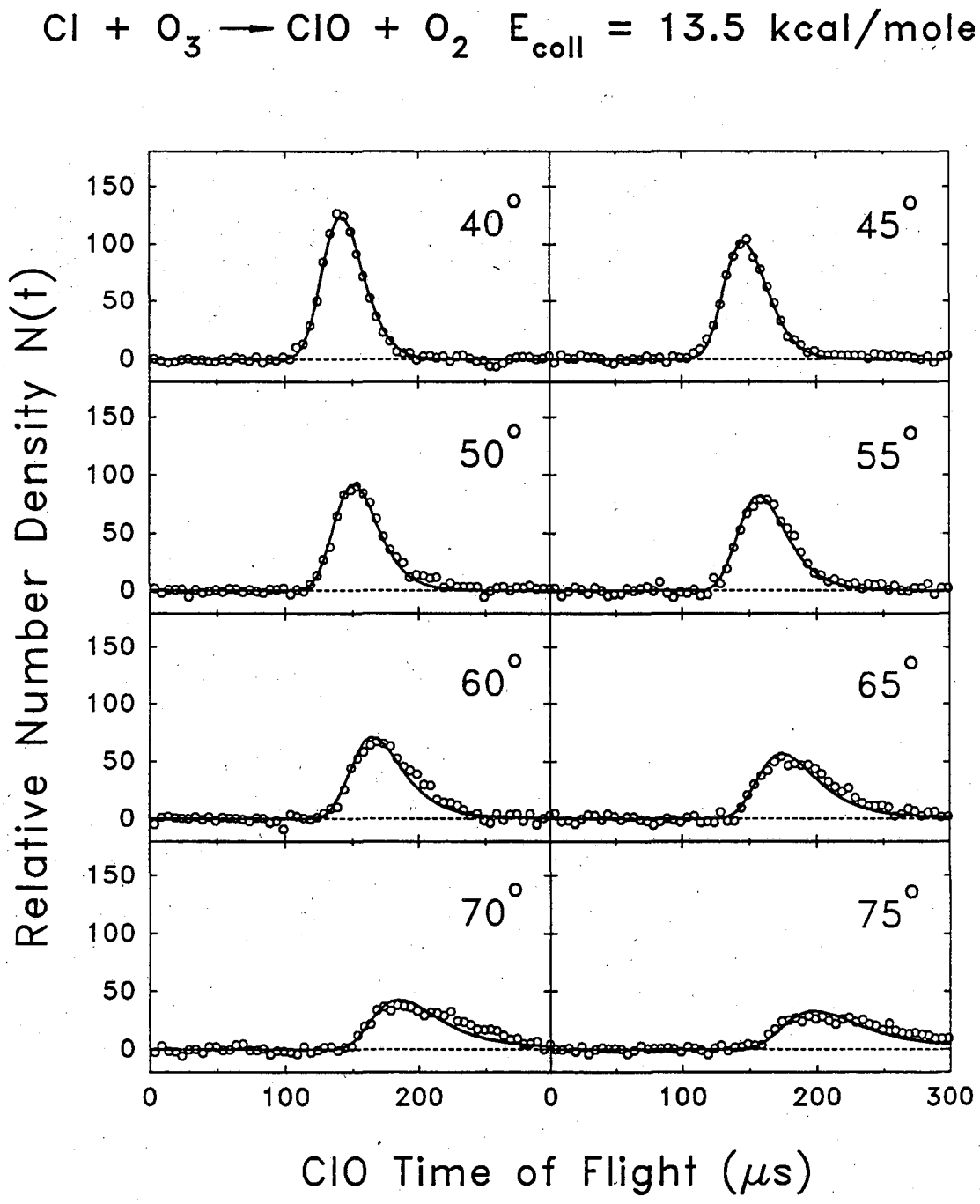
Cl + O3 → ClO + O2 Ecoll = 13.5 kcal/mole
Relative Number Density N(t)
40°
45°
50°
55°
60°
65°
70°
75°
150
100
50
0
0
100
200
300
ClO Time of Flight (μs)

Figure 10b

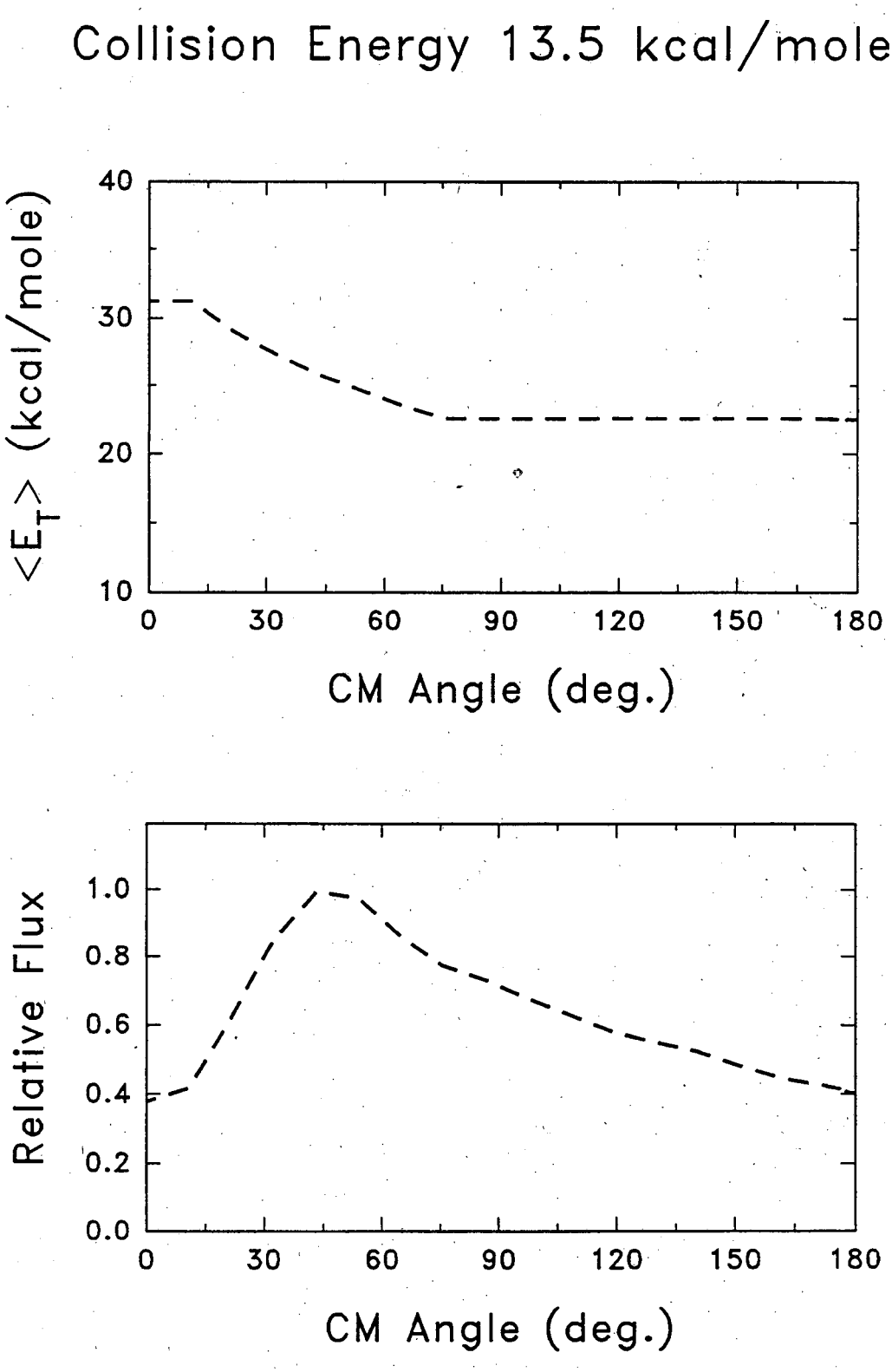
Collision Energy 13.5 kcal/mole
<E_T> (kcal/mole)
40
30
20
10
0
30
60
90
120
150
180
CM Angle (deg.)
Relative Flux
1.0
0.8
0.6
0.4
0.2
0.0
0
30
60
90
120
150
180
CM Angle (deg.)

Figure 11

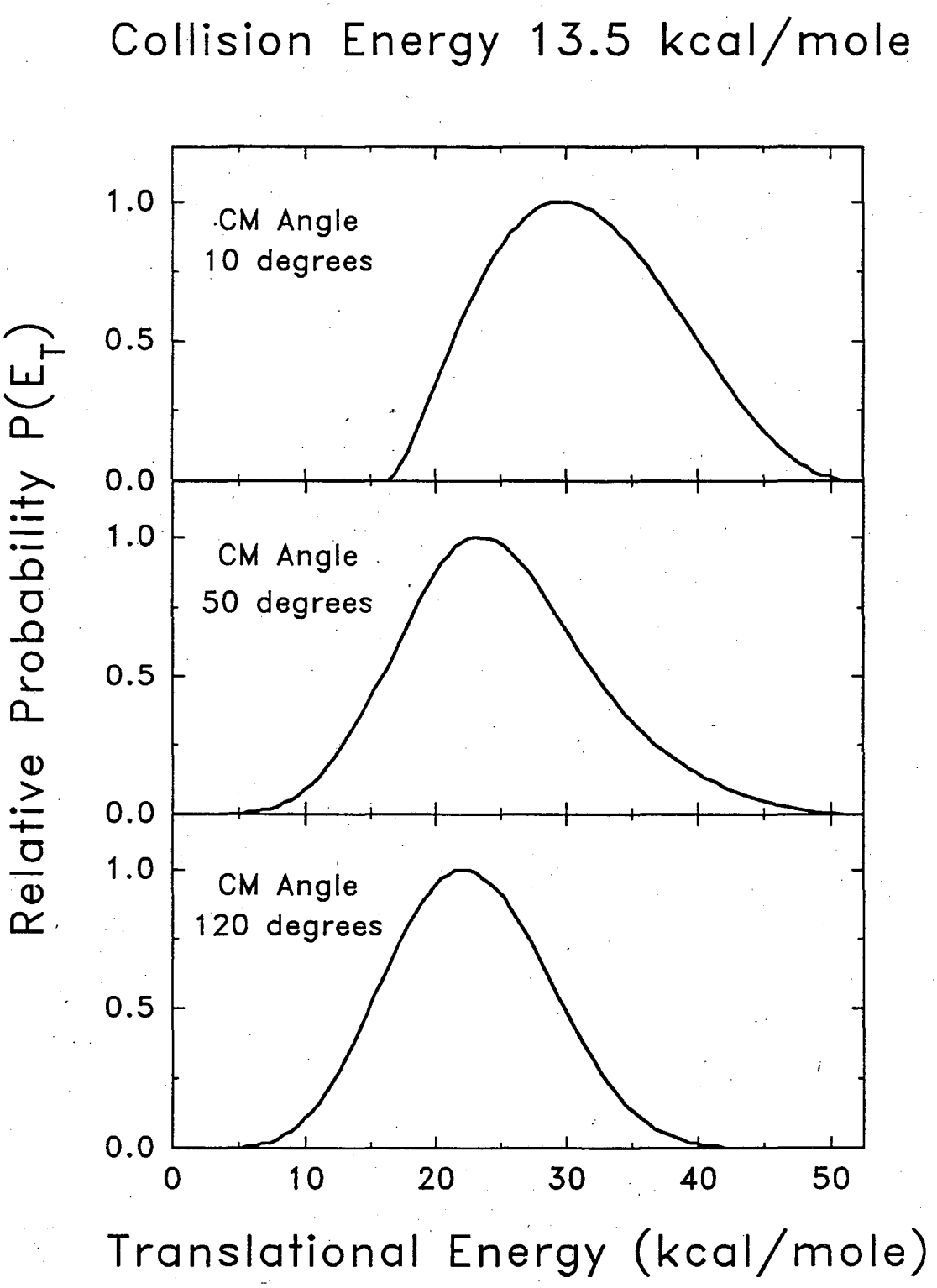
Collision Energy 13.5 kcal/mole
Relative Probability $P(E_T)$
CM Angle
10 degrees
CM Angle
50 degrees
CM Angle
120 degrees
1.0
0.5
0.0
0
10
20
30
40
50
Translational Energy (kcal/mole)

Figure 12

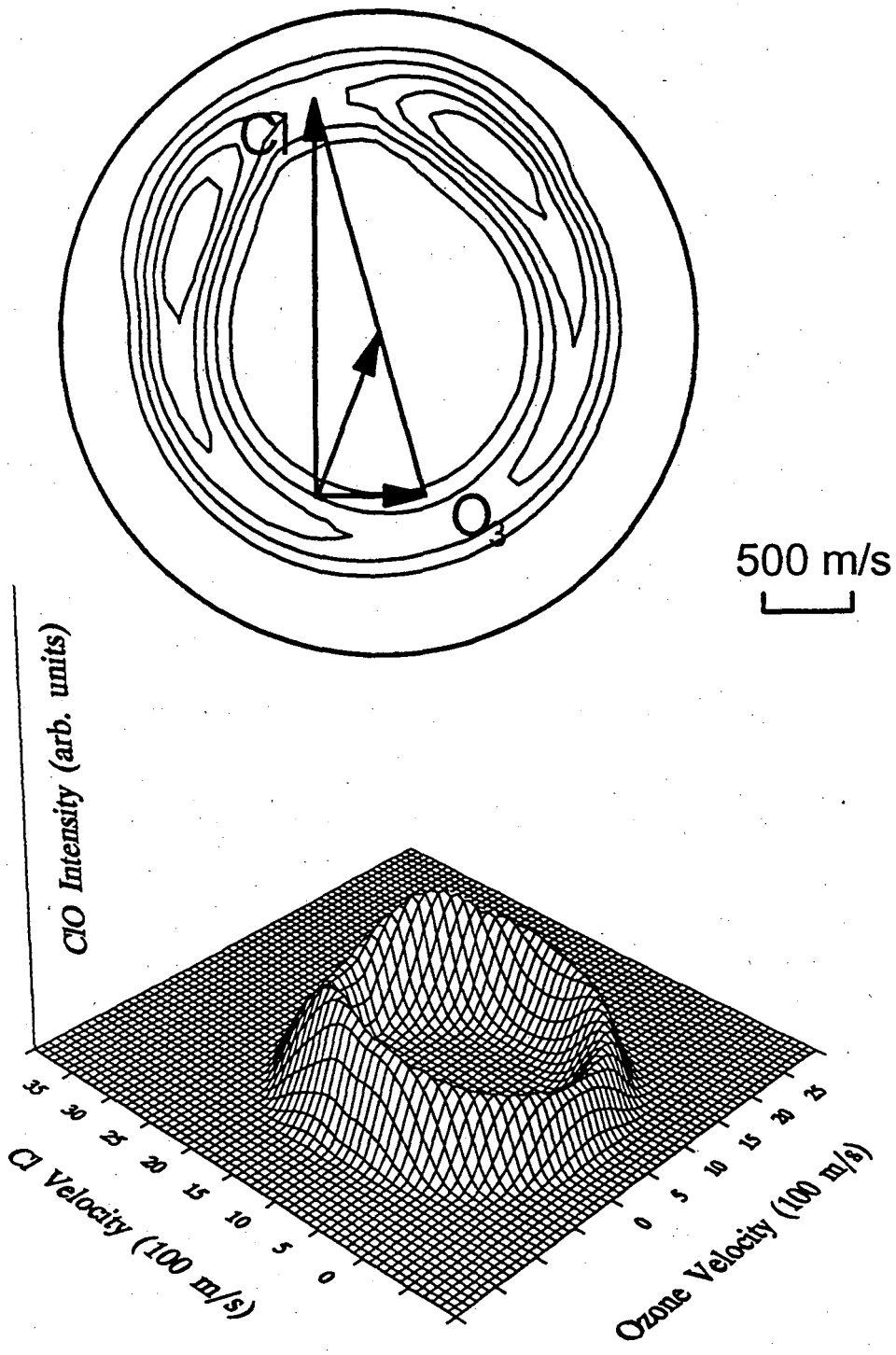
Cl
O3
500 m/s
ClO Intensity (arb. units)
Cl Velocity (100 m/s)
35 30 25 20 15 10 5 0
Ozone Velocity (100 m/s)
0 5 10 15 20 25

Figure 13

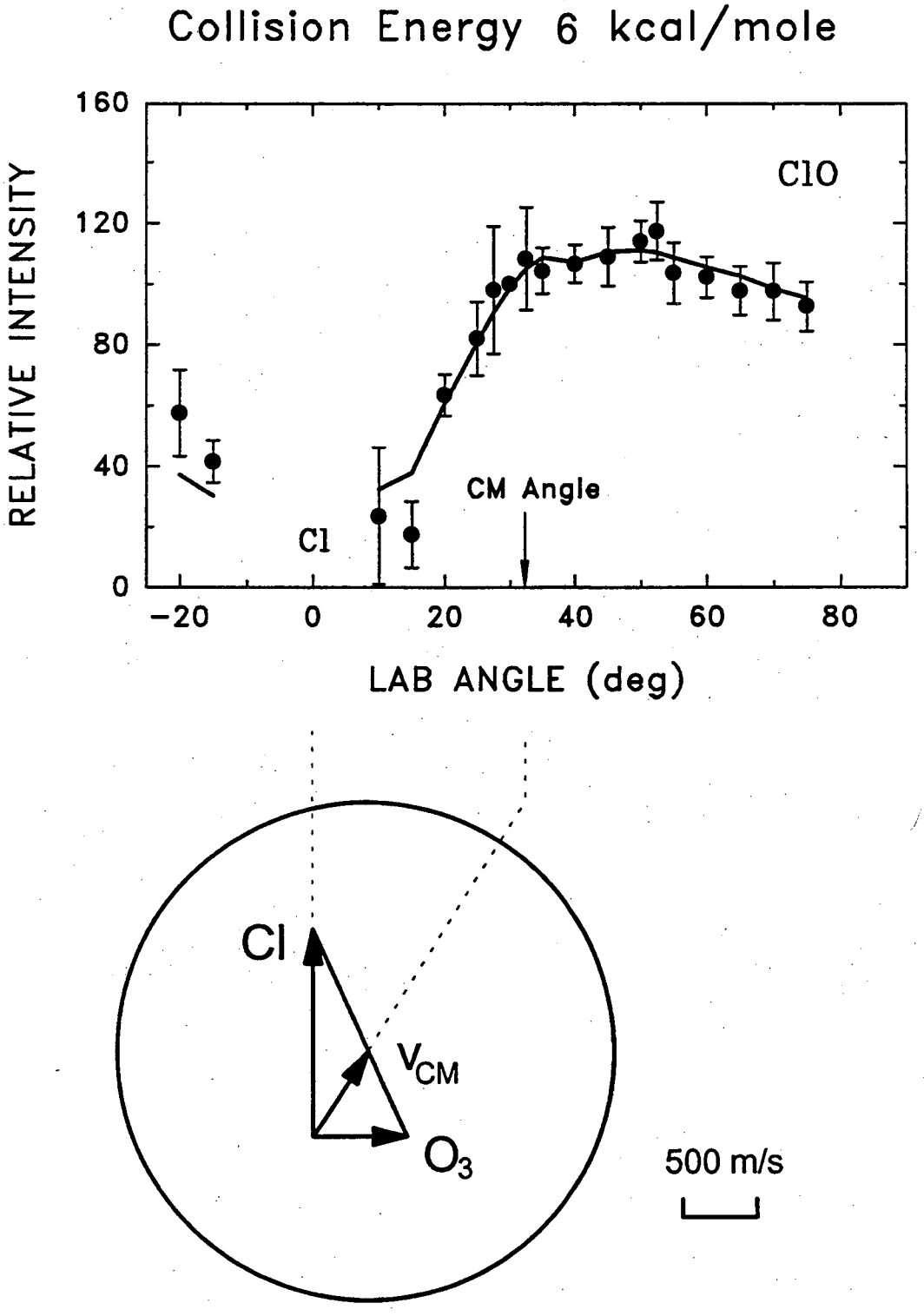
Collision Energy 6 kcal/mole
RELATIVE INTENSITY
160
120
80
40
0
ClO
Cl
CM Angle
−20
0
20
40
60
80
LAB ANGLE (deg)
Cl
V_{CM}
O_3
500 m/s

Figure 14

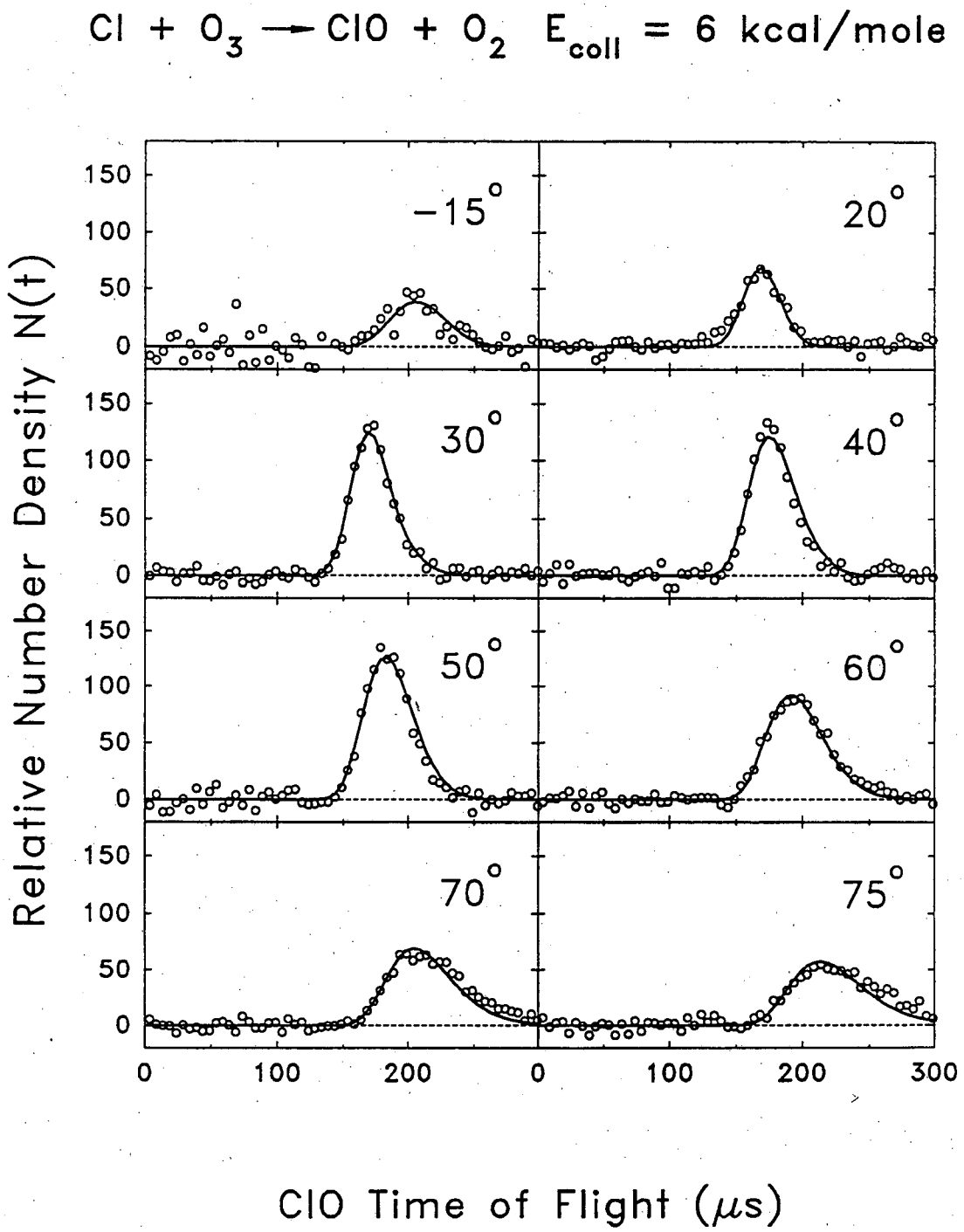
Cl + O3 → ClO + O2 Ecoll = 6 kcal/mole
Relative Number Density N(t)
−15°
20°
30°
40°
50°
60°
70°
75°
150
100
50
0
0
100
200
300
ClO Time of Flight (μs)

Figure 15

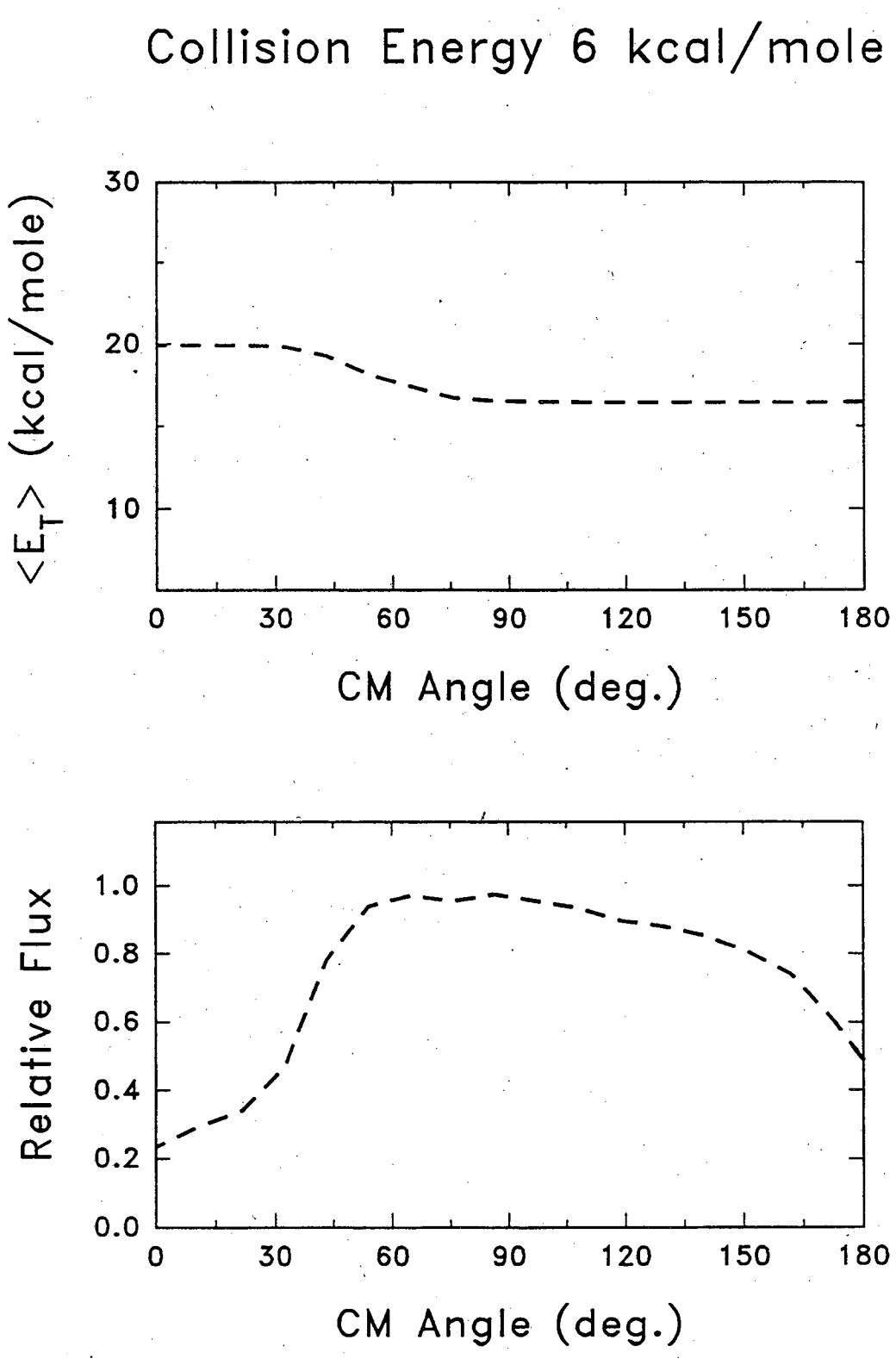
Collision Energy 6 kcal/mole
<E_T> (kcal/mole)
30
20
10
0
30
60
90
120
150
180
CM Angle (deg.)
Relative Flux
1.0
0.8
0.6
0.4
0.2
0.0
0
30
60
90
120
150
180
CM Angle (deg.)

Figure 16

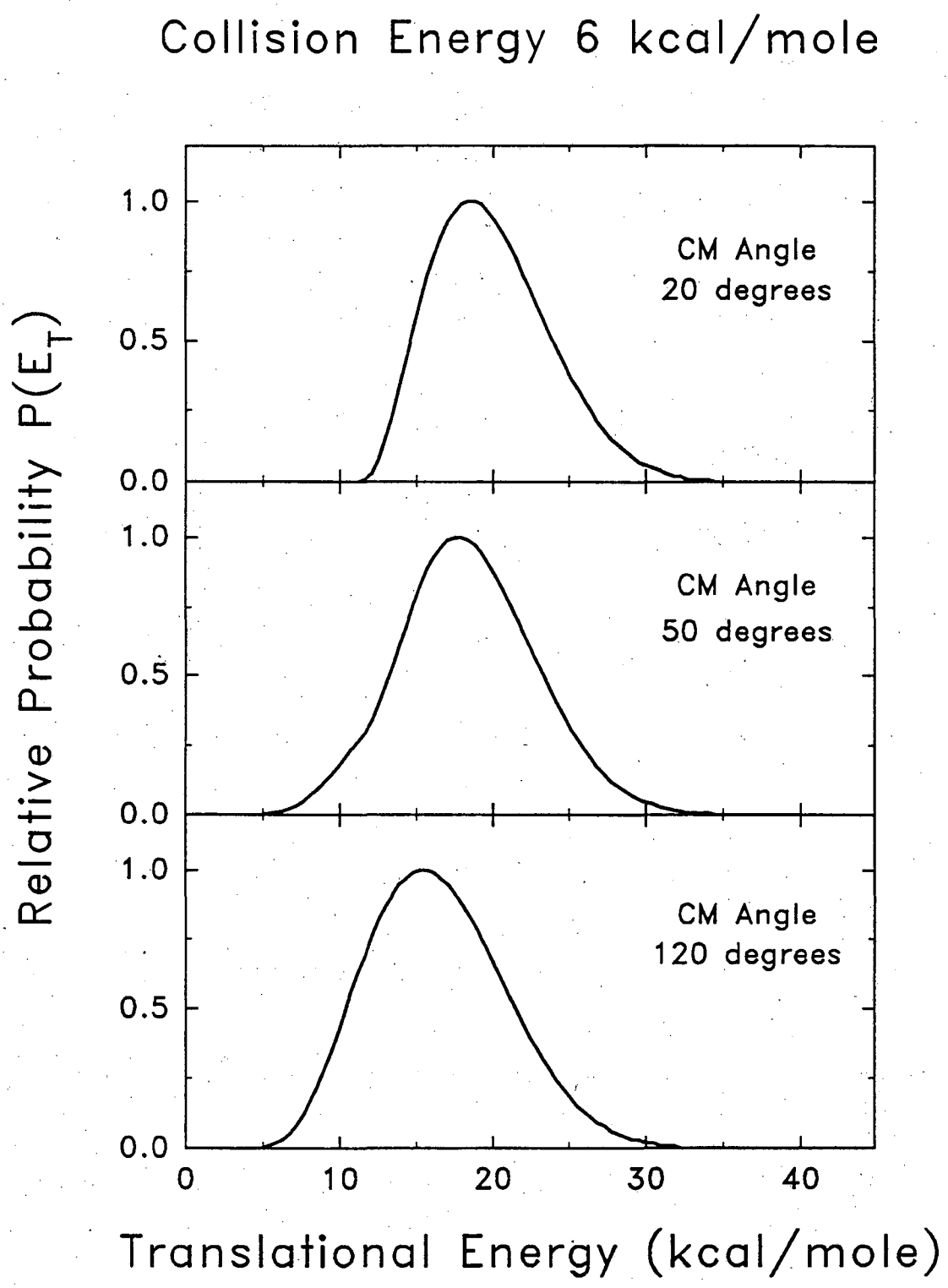
Collision Energy 6 kcal/mole
Relative Probability P(E_T)
1.0
0.5
0.0
CM Angle
20 degrees
CM Angle
50 degrees
CM Angle
120 degrees
0
10
20
30
40
Translational Energy (kcal/mole)

Figure 17

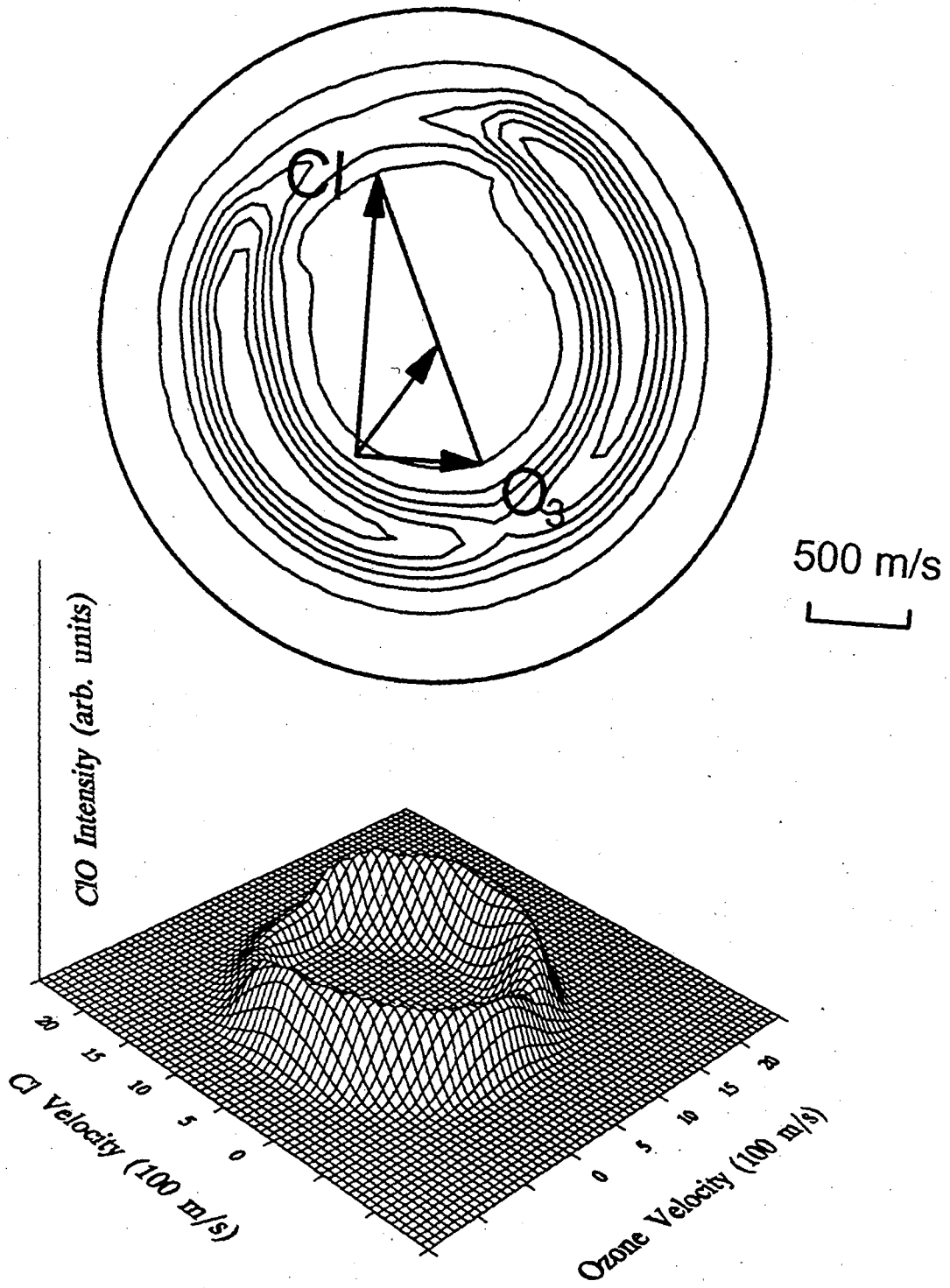
Cl
O_3
500 m/s
ClO Intensity (arb. units)
Cl Velocity (100 m/s)
20
15
10
5
0
Ozone Velocity (100 m/s)
0
5
10
15
20

Figure 18

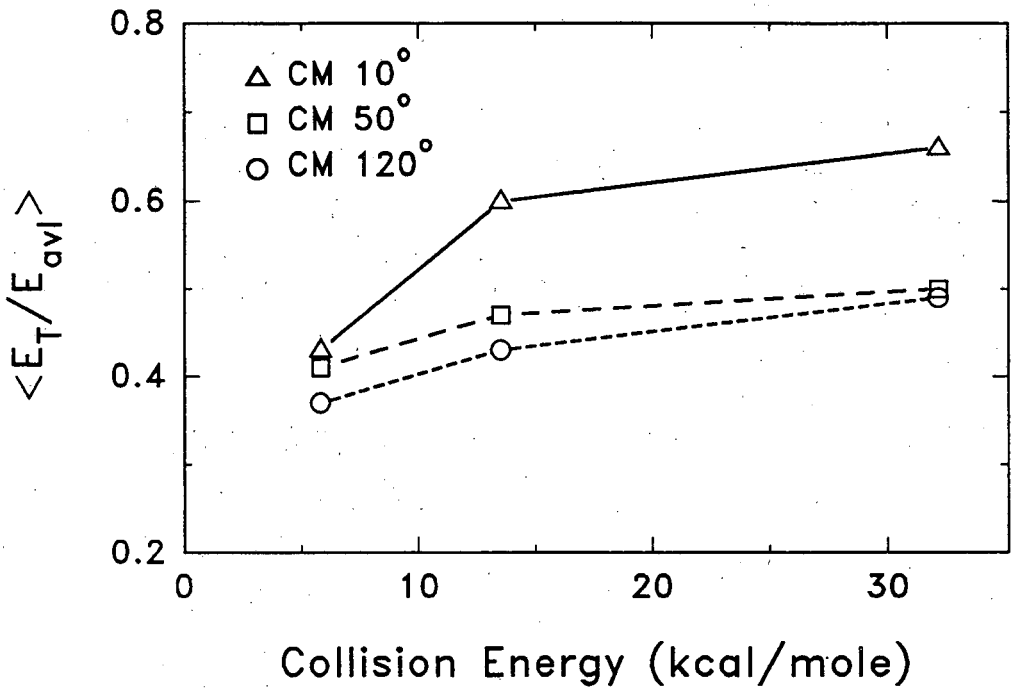
0.8
0.6
0.4
0.2
0
10
20
30
△ CM 10°
□ CM 50°
○ CM 120°
<E_T/E_avl>
Collision Energy (kcal/mole)

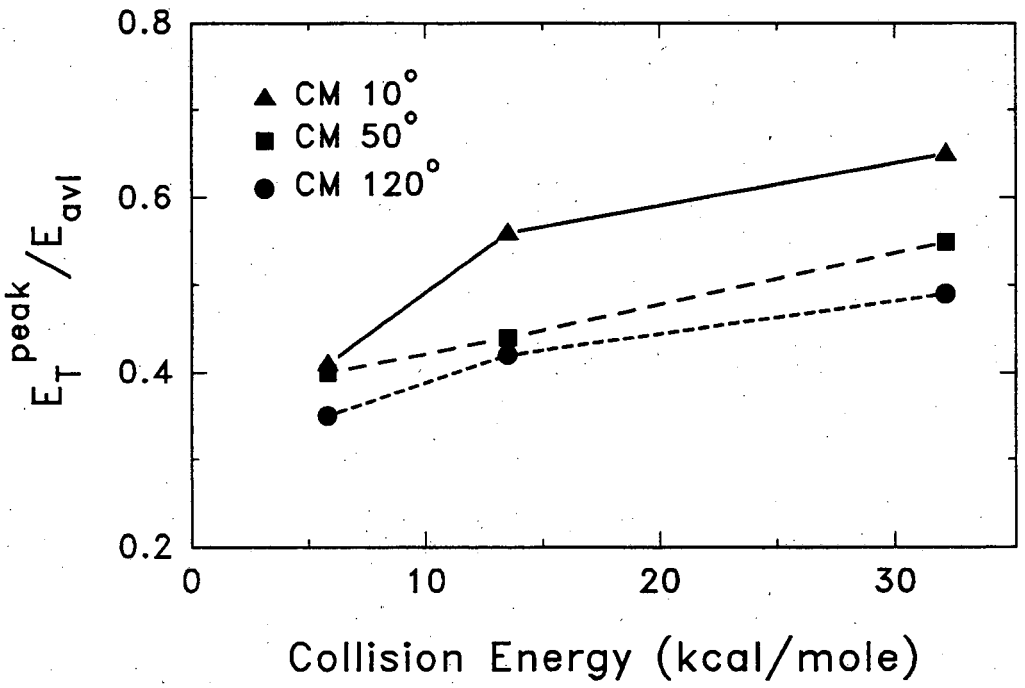
0.8
0.6
0.4
0.2
0
10
20
30
▲ CM 10°
■ CM 50°
● CM 120°
E_T^peak /E_avl
Collision Energy (kcal/mole)

Figure 19

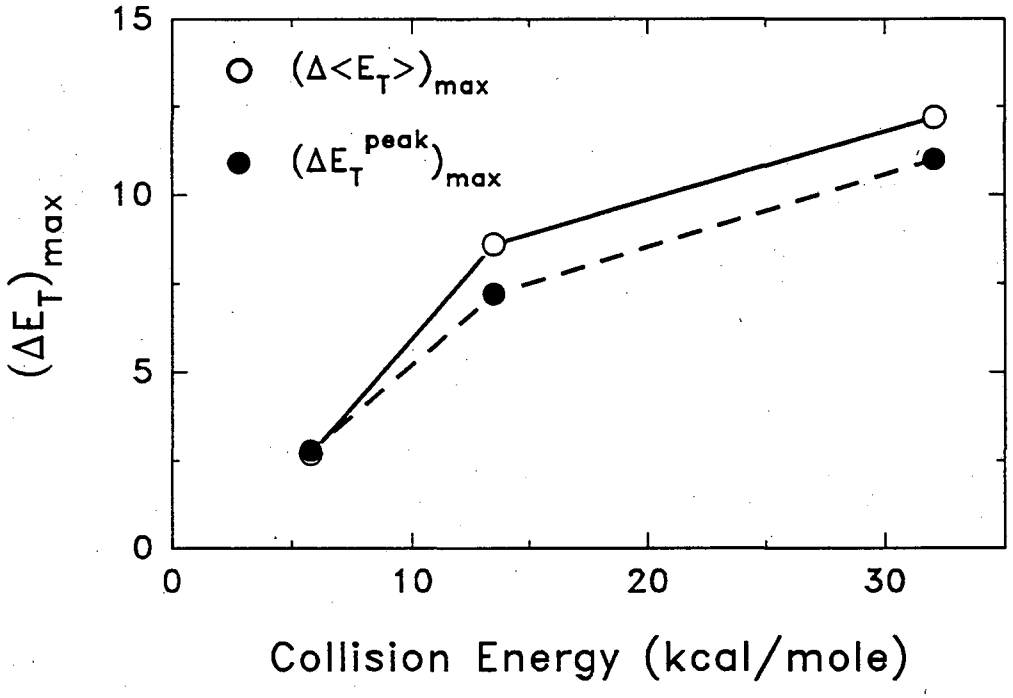
15
10
5
0
0
10
20
30
$(\Delta E_T)_{max}$
$(\Delta \langle E_T \rangle)_{max}$
$(\Delta E_T^{peak})_{max}$
Collision Energy (kcal/mole)

Figure 20

CHAPTER 3

CROSSED MOLECULAR BEAM STUDY OF THE REACTION Br + O_3

ABSTRACT

The reaction of ground-state Br($^2P_{3/2}$) atom with ozone molecule has been studied by the crossed molecular beams technique at five different center-of-mass (CM) collision energies ranging from 5 kcal/mole to 26 kcal/mole. The product translational energy distribution and the BrO product center-of-mass angular distribution have been derived from the experimental data. The product translational energy release is large, and the average translational energy release ranges from 40%-60% of the total available energy. The BrO product is forward and sideways scattered in the center-of-mass frame. With the increase of the collision energy, the fraction of the total available energy channeled into the translational energy of products is increased, and the BrO product is also scattered into more forward direction with respect to the Br atom. The translational energy release is found to depend strongly on the center-of-mass scattering angles, with the translational energy release in the forward direction in the center-of-mass frame larger than that in the backward direction. It is concluded that the Br + O_3 reaction is a direct reaction. The Br atom would most

likely attack a terminal oxygen atom of the ozone molecule. The exit channel on the BrO_3 potential energy surface is believed to have strong repulsion to cause the large translational energy release among the products. The detailed comparison of the experimental results for the Cl + O_3 and the Br + O_3 reactions shows that the two reactions have similar reaction mechanisms. The electronic structure of the ozone molecule plays the central role in determining the reaction mechanisms of these ozone reactions with the atomic radicals.

I. INTRODUCTION

The reaction $Br + O_3 \rightarrow BrO + O_2$ is important in stratospheric chemistry along with the reaction $Cl + O_3 \rightarrow ClO + O_2$.[1] They play the key roles in catalytic ozone destruction cycles. It is currently believed that the ClO dimer and ClO/BrO mechanisms in which the two reactions are involved are responsible for most of the Antarctic stratosphere ozone loss.[2-6] The reaction $Br + O_3$ is one of the initial steps in the ClO/BrO cycle of the ozone destruction.

A large number of kinetic studies on ozone reactions with radicals such as the $Cl + O_3$ and $Br + O_3$ reactions have been carried out.[7-13] Measurements made in these studies of reaction rate constants and their temperature dependencies have provided a valuable data base for modeling stratospheric chemistry and also have given some insight into the reaction mechanisms of these reactions. For atom $X + O_3$ ($X=O(^3P)$, F, Cl, and Br) reactions, the pre-exponential factors were found to be very similar and, thus, were insensitive to the reaction exothermicity.[10,12,13] The rate coefficients for atom $X + O_3$ reactions correlated with the electron affinities of the radical atoms instead of with the reaction exothermicity.[10] It was then suggested that the transition state structures of these reactions were insensitive to reactant X, and that the bond lengths and frequencies of the transition state resembled those for the stable ozone molecule.[10,11,12] It was also suggested that the $X + O_3$ reactions proceeded via early transition states that best resembled reactant ozone.[10,11,12] Therefore, based on the information from the

kinetic studies, the reaction Br + O_3 is expected to be very similar to the reaction Cl + O_3.

McGrath and Norrish carried out the pioneer flash photolysis study on Cl_2-O_3 and Br_2-O_3 systems.[14] Their flash photolysis light was filtered by a soda glass filter so that only the Cl_2 or the Br_2 molecule, and not the O_3 molecule in the Cl_2-O_3 or Br_2-O_3 mixture, could be dissociated. For the Br_2-O_3 system, BrO absorption was observed after the shortest time delay. The v" = 0 progression of BrO absorption was predominant, however, BrO absorption bands with v" up to 4 were also visible in the experiments. It is clear that the BrO product formed in the Br + O_3 reaction had considerable vibrational excitation, which was quite similar to the Cl + O_3 reaction. Clyne and Cruse[7] studied the Br + O_3 → BrO + O_2 reaction by detecting the ground-state BrO ($X^2\Pi$) radical using time-resolved electronic absorption spectrophotometry in a discharge-flow system. The absorption spectrum of the BrO radical produced in the Br + O_3 reaction showed the absence of the hot bands with v" ≥ 1. However, due to the much longer time delay (~5 ms) in this experiment, the vibrationally excited BrO radical from the Br + O_3 reaction probably had already relaxed down to the ground vibrational state (v" = 0).

There has been almost no theoretical study on the Br + O_3 reaction. However, due to the similarity of the Br + O_3 and the Cl + O_3 reactions, the semi-empirical study of the Cl + O_3 reaction by Farantos and Murrell[15] could still provide some information about the mechanism of the Br + O_3 reaction. An early

transition state in a collinear collision pathway in which the Cl atom attacked along the line of one O-O bond was located on the ClO_3 potential energy surface (PES) constructed semi-empirically by the authors. Classic trajectory calculations were carried out on this PES at the collision energy corresponding to the Maxwellian mean energy at 300 K with the O_3 molecule in its vibrational ground state. The calculation results showed that the ClO product was predominantly forward scattered with respect to the Cl atom in the center-of-mass system. The large forward-backward asymmetry showed that there was no long-lived complex formation along this collinear pathway. The calculation results also showed that at 300 K about 49% of the total available energy went into the translational energy of the products while 20% into ClO vibrational energy. The authors also predicted that v = 1 was the most probable vibrational state of ClO but that vibrational states up to v = 8 were populated while almost all the O_2 product would be in the ground vibrational state. There was a large amount of vibrational energy in ClO due to the early transition state located in the entrance valley. The O-O bond length, however, did not change much in the reaction; therefore, there was much less vibrational excitation in the O_2 product. Michael and Payne[9] used the activated complex theory to calculate the pre-exponential factor A. They assumed a collinear approach and used the BEBO method to determine the intermediate configuration. The intermediate configuration reached was quite close to the reactants. Due to the lack of information to estimate accurately the bending frequency, the comparison between the calculated pre-

exponential factor and the experimental pre-exponential factor was not conclusive.

We have reported the crossed molecular beam study of the $Cl + O_3$ reaction in the previous paper.[16] A large fraction of the total available energy was channeled into the product translational energy. The ClO product was sideways and forward scattered with respect to the Cl atom. The translational energy release was coupled with the center-of-mass scattering angle. It was concluded that the $Cl + O_3$ reaction proceeded through a direct reaction mechanism and that the Cl atom was most likely to attack the terminal oxygen atom of the ozone molecule.

Previous kinetic studies on both the $Cl + O_3$ and the $Br + O_3$ reactions have strongly suggested that the two reactions were quite alike. In the present work, we extend our study to the $Br + O_3$ reaction to further probe the reaction mechanisms of the atom reactions with ozone molecule. We have carried out a crossed molecular beam study of the $Br + O_3$ reaction at five different collision energies. The center-of-mass angular and translational energy distributions of the products are derived from the experimental data. With the obtained dynamic information, we would like to provide more insight into the mechanism of this important reaction and also to compare this study with that of the similar reaction $Cl + O_3$ we carried out before. As far as what we know, this is the first crossed molecular beam study of the $Br + O_3$ reaction.

II. EXPERIMENTAL

The experimental setup for this study is similar to that in the Cl + O_3 study presented in the previous paper.[16] We briefly describe the conditions for this experiment in the following.

The universal crossed molecular beam apparatus used for the present study has been described in detail previously.[17,18] Continuous supersonic bromine atomic and ozone molecular beams were seeded and two-stage differentially pumped. The two beams were crossed at 90° in the main collision chamber held at a vacuum of approximate 10^{-7} torr. The scattered products were detected by a triply differentially pumped mass spectrometric detector which rotated in the plane of the two beams with respect to the center of collision. The typical electron energy of the electron impact ionizer was 180 eV, and the typical ion energy was 90 eV. The size of the collision zone was typically 3 x 3 x 3 mm^3, and under normal conditions the whole collision zone was viewed by the detector.

The bromine atom beam was produced by thermal dissociation of Br_2 in rare gas mixtures in a resistively heated high-density graphite[19] nozzle source that was designed in this laboratory by Valentini, Coggiola, and Lee.[20] The Br_2/gas mixtures were generated by passing 700 torr of helium, argon or krypton through liquid bromine (reagent grade Fisher or Mallinkcrodt, without any further purification) in a glass bubbler held at an ice/water bath (at 0 °C, Br_2 vapor pressure ≈ 60 torr). For the highest collision energy used in this experiment, 700

torr of helium gas was passed through the Br_2 bubbler held at about -9 °C (Br_2 vapor pressure ≈ 40 torr) in a constant temperature bath. The high-temperature graphite source had a nozzle of 0.12 mm diameter and was heated to approximately 1700°C. A conical graphite skimmer with an orifice 1.0 mm in diameter was positioned 7.6 mm away in the downstream of the nozzle. A set of collimating slits on the differential wall further defined the beam to 3° in full width and 3 mm x 3 mm size in the collision region. A very large fraction of Br_2 thermal dissociation (≥ 97%) had been observed by a direct measurement of $[Br]/[Br_2]$ ratio in the beam. Heating power for the high-temperature graphite source had been carefully maintained constant through out the period of the experiment to ensure a stable Br atom beam with stable beam velocity. The Br beam velocity was also occasionally checked before and after a daily reactive scattering experiment.

The ozone beam was described in detail previously.[16,21] In brief, the ozone/inert gas mixture with 7% ozone concentration and 300 torr total pressure was expanded through a 0.12 mm diameter nozzle. The nozzle tip was heated to 80 °C to minimize the formation of ozone dimers. The ozone molecular beam was skimmed by a stainless steel skimmer of a 0.5 mm diameter orifice with a nozzle-skimmer distance of 7.6 mm. The beam was further defined by the collimating slits on the differential wall before entering main chamber; this gave a 3° beam full width and a 3 mm x 3 mm beam size in the collision region.

The velocity distributions of the Br and O_3 beams were measured using the

time-of-flight (TOF) technique. The Br atom and ozone molecular beam velocity distributions were obtained from fitting the experimental time-of-flight spectra using program KELVIN[22,23] which convoluted over the known apparatus functions to determine the beam speed (v) and speed ratio ($v/\Delta v$). The typical beam parameters are given in Table 1. The collision energy was varied by seeding Br_2 and O_3 in different rare gases and by changing the concentration of Br_2 in the gas mixtures. The most-probable collision energies E_{coll} and the spread of the collision energies are listed in Table 2.

The product time-of-flight spectra from the reactive scattering were measured using the cross-correlation method with a time resolution 5μs/channel.[24] The nominal flight path from the cross-correlation wheel to the electron impact ionizer was 30.1 cm. Product BrO was monitored. The mass spectrometer was set at m/e = 95 with low resolution to detect $Br^{79}O$ isotope species, while a small amount of $Br^{81}O$ might have been collected as well. Total counting times ranged from 0.5 to 6 hours per laboratory angle.

Except for the experiment at 18.5 kcal/mole collision energy, the BrO product laboratory angular distributions were measured by modulating the ozone beam using a 150 Hz tuning folk chopper with the time-of-flight wheel removed. At a particular laboratory angle, the signal with the ozone beam on and the signal with the ozone beam off were recorded in two separate channels in a dual-channel scaler. Subtracting the beam-off signal from the beam-on signal at a particular laboratory angle simply gave the net reactive signal at that angle. The

total counting times per angle ranged from 3 to 10 minutes. For E_{coll} = 18.5 kcal/mole, the BrO angular distribution was obtained by performing area integrations over the range of the time channels of the time-of-flight peaks in the TOF spectra at the appropriate laboratory angles.

To reduce the background species entering into the detector, a cryogenic copper cold panel was placed against the differential wall inside the main scattering chamber and facing the detector. It was cooled by being tightly clamped to the liquid-nitrogen cooled cold shield in the scattering chamber. Its temperature was typically about 90 K, which was monitored by a low temperature sensor (LakeShore). It was effective to reduce the background for species such as BrO.

III. RESULTS AND ANALYSIS

Laboratory angular and time-of-flight distributions were recorded at five different center-of-mass collision energies from 5 kcal/mole to 26 kcal/mole. Experimental conditions for four collision energies are listed in Table 2. The Newton diagrams for the four collision energies are shown in Figs. 2, 7, 12, and 17. The circles stand for the maximum range of the center-of-mass recoil velocity of the BrO product if all the available energy channels into the translational energy of the products. The angular and TOF distributions were recorded at m/e

= 95, corresponding to $Br^{79}O^+$.

The product angular distribution and time-of-flight spectra were fitted using a forward-convolution method. The FORTRAN program is an improved version based on the previous program.[31] The goal of the analysis is to find the product angular and translational energy distributions in the center-of-mass frame. It starts with a trial form for the center-of-mass product flux-energy distribution. The program transforms this trial center-of-mass flux distribution into the laboratory frame flux distribution and generates the laboratory frame angular distribution and time-of-flight spectra for each experimental laboratory angle after convoluting over the measured beam velocity distributions and the known apparatus functions such as the spread of collision angles, the detector acceptance angle, and the length of the ionizer. The program scales the calculated spectra to the experimental data and makes the comparison. This is repeated so as to optimize the center-of-mass flux distribution iteratively until a best fit for the experimental data is found.

Initially, we tried to fit the data using an energy-angle separable form of the center-of-mass flux distribution. In this trial form, the center-of-mass flux distribution was expressed as a product of $T(\theta)$, the center-of-mass product angular distribution, and $P(E_T)$, the center-of-mass product relative translational energy distribution. We found that, for large laboratory angles ($\Theta > 40°$), the fittings for the time-of-flight spectra were reasonably good; however, for small laboratory angles ($\Theta < 25°$), the calculated time-of-flight spectra were clearly too

slow compared with the experimental data. A fast and forward contribution in the center-of-mass flux distribution was needed to make a satisfactory fit to our experimental data which had very good signal-to-noise ratio. It was then realized that the center-of-mass angular distribution $T(\theta)$ and the translational energy distribution $P(E_T)$ were nonseparable, i.e., the product translational energy release was dependent on the center-of-mass angle. The translational energy release in the forward direction with respect the Br atom in the center-of-mass frame was larger than that in the backward direction; thus, the BrO product was faster at small laboratory angles. This type of behavior is exactly the same as in the Cl + O_3 reaction.

To account for this coupling effect in a simplified way, we used a combination of different sets of uncoupled $T(\theta)$ and $P(E_T)$. The center-of-mass product flux distribution was expressed as the weighted sum of the products of different sets of $T(\theta)$ and $P(E_T)$:[16]

$$I_{CM}(\theta, E_T) = \sum_{i=1}^{n} w_i \cdot T_i(\theta) \cdot P_i(E_T) \qquad (1)$$

Each $P_i(E_T)$ was normalized so that $\int P_i(E_T)dE_T = 1$. The total center-of-mass angular distribution could therefore be expressed as:

$$I_{CM}(\theta) = \int_0^{\infty} I_{CM}(\theta, E_T)dE_T = \sum_{i=1}^{n} w_i \cdot T_i(\theta) \qquad (2)$$

The product translational energy distribution at CM angle θ would be expressed in Eqn. 1 with the CM angle fixed at θ.

For our purpose, a trial $I_{CM}(\theta, E_T)$ combined from two different sets of $T(\theta)$ and $P(E_T)$ was used as input to the fitting program. $T(\theta)$ was chosen in a point form because of the unique angular distribution of this reaction. $P(E_T)$ was chosen in a RRK-type functional form for the convenience of parameter adjustment. After optimizing this trial $I_{CM}(\theta, E_T)$ function, quite satisfactory fittings to the experimental data were finally reached. The calculated and experimental laboratory angular distributions at four different collision energies are shown in Figs. 2, 7, 12, and 17. The fitted and experimental laboratory time-of-flight spectra at four collision energies are in Figs. 3, 8, 13, and 18. The average translational energy releases versus center-of-mass angle and the total center-of-mass angular distributions are in Figs. 4, 9, 14, and 19. We also plot the relative translational energy distributions at various center-of-mass angles in Figs. 5, 10, 15, and 20. Using the optimized center-of-mass flux-energy distribution $I_{CM}(\theta, E_T)$, we plot the center-of-mass flux distributions in velocity space $I_{CM}(\theta, u)$ ($I_{CM}(\theta, u) \propto u \cdot I_{CM}(\theta, E_T)$) both in contour maps and in 3-dimensional surface curves in Figs. 6, 11, 16, and 21.

The overall features of the $Br + O_3$ reaction are very similar to those in the $Cl + O_3$ reaction. The laboratory angular distributions are quite broad, which are due to both the large reaction exoergicity and the large product translational energy release. At higher collision energies, the laboratory angular distributions

show a significant forward peak in front of the center-of-mass angle. With collision energy increased, the peak of the laboratory angular distribution is moved in the forward direction. There seems to be two peaks in the positive angle region of the laboratory angular distribution, especially for the high collision energies, which is different from the Cl + O_3 reaction. In the center-of-mass frame, the angular distributions are also quite broad, and they have larger intensities for the sideways scattering. The center-of-mass angular distributions do not have forward-backward symmetry. Instead, the large asymmetry with more forward contribution is present in the angular distributions. The peak of the angular distribution $T(\theta)$ shifts from 90° to 60° and finally 30° with the collision energy increased, and the peaks are becoming more predominant. We have to point out, due to the kinematics of this exothermic reaction (Figs. 2, 7, 12, and 17), forward scattered BrO product within $\Theta = 10°$ in the laboratory frame could not be well detected. Therefore we are more confident about the fitting for the wide-angle scattering in the CM frame than that for the forward scattering ($\theta < 20°$). However, experimental data at E_c = 26 kcal/mole, which is under the most favorable kinematics, allows us to obtain a quite confident fit down to CM angle 10°. The decrease of the intensity from 30° to 10° in the CM frame at E_c = 26 kcal/mole is also of high certainty. For the lower collision energies, the CM angular distribution within 20° is less certain, however, the trend of the decrease of the CM angular intensity in this region is still quite obvious.

The overall product translational energy release is large. This is especially

evident in the TOF spectra at the laboratory angles near the center-of-mass angle Θ_{CM} (~20°). There are two peaks in the TOF spectra, a forward and a backward. The center-of-mass recoil velocity of the BrO product is very large so the combined forward and backward laboratory velocities are far way from the center-of-mass velocity V_{CM}; therefore, two distinct peaks are present in the TOF spectra near the center-of-mass angle Θ_{CM}. All translational energy release probabilities $P(E_T)$ peak quite far away from 0 kcal/mole. The $P(E_T)$ curves are smooth and almost symmetric. With the collision energy increased, a larger fraction of the total available energy is channeled into translational energy. The width of the translational energy release probability $P(E_T)$ becomes wider with the increase of the collision energy. Furthermore, with the collision energy increased, the angular dependence of the translational energy release also becomes larger, i.e., the difference between the fast and slow kinetic energy releases becomes larger. These trends of the kinetic energy release are shown in Figs. 5, 10, 15, and 20 and in Tables 3 and 4.

We started the Br + O_3 study with 18.5 kcal/mole collision energy. The large intensity in the laboratory angular distribution in the negative angles (-20° - -10°) aroused our attention. To confirm that no impurity would give rise to such intensities near the Br beam, we substitute O_3 with CO_2 with the same concentration. No m/e = 95 signal was observed in the nearby region, so the Br beam was quite clean from m/e = 95 contamination. Following the experiment at 18.5 kcal/mole collision energy, we performed the reactive scattering at four

more different collision energies. At these different kinematics, the intensities at the negative laboratory angles near the Br beam remained large. Finally, our data fittings gave quite reasonable reproductions of these intensities.

The other type of possible BrO impurity was from the reaction between the chemical interest species in both beams, and it might give different translational energy distribution from that of the Br + O_3 reaction. However, in the same way as we argued in the Cl + O_3 study, we can rule out this possibility. The reaction channel of Br with O_2 in the ozone beam is too endothermic ($\Delta H^\circ \approx 63$ kcal/mole) to produce any BrO. However, the reaction $Br_2 + O \rightarrow BrO + Br$ ($\Delta H^\circ \approx -10$ kcal/mole) is energetically possible. Nevertheless, because of the large fraction of dissociation ($\geq 97\%$) of bromine molecule in the high temperature source, the residual bromine molecule in the Br beam is a very minor component; and the amount of the oxygen atom in the ozone beam is also expected to be very small.[16] Therefore, the possible Br_2 + O reaction would only produce trace amount of BrO species. Furthermore, as we argue in the following, the BrO radical produced in the Br_2 + O reaction will not interfere with the TOF spectra of the BrO product from the Br + O_3 reaction. Herschbach et al.[26] and Grice et al.[27-29] studied the Br_2 + O reaction using crossed molecular beams technique. At about 1 kcal/mole collision energy,[26,27] the Br_2 + O reaction was shown to proceed via a long-lived collision complex with small product translational energy release. At higher collision energies from 3 kcal/mole to 10 kcal/mole,[28,29] the BrO center-of-mass angular distribution of the Br_2 + O reaction still showed some forward-backward

symmetry with slightly larger intensity in the direction of the incident O atom. The BrO flux was concentrated on the poles at 0° and 180° in the center-of-mass frame, and the translational energy release was small; therefore, most of the product flux concentrated around the relative velocity vector. In our experiment, the expected collision energies for the Br_2 + O reaction would be from 2 to 13 kcal/mole, which were comparable to those in the previous experiments.[26-29] The possible BrO product from the Br_2 + O reaction had to concentrate around the relative velocity vector, however, the BrO product from the Br + O_3 reaction peaked very far away from the relative velocity vector. Therefore, even if there were BrO from the Br_2 + O reaction, it would be so slow that it would not interfere in the BrO time-of-flight spectra of the Br + O_3 reaction.

We tried to detect any evidence of the reaction channel Br + O_3 → BrO_2 + O (Fig. 1). There are two types of BrO_2 isomers: asymmetric BrOO and symmetric OBrO. OBrO is an unstable molecule but could be observed by the mass spectrometer with an electron bombardment ionizer.[30] Due to the lack of the thermodynamic data of OBrO, the threshold of the OBrO + O channel is not clear. BrOO molecule is less stable than OBrO; Br and O_2 are bonded by only about 1 kcal/mole in the BrOO molecule.[7,30-32] It may not be able to survive in the electron bombardment ionizer. The reaction channel BrOO + O would be open above about 22 kcal/mole collision energy. At over 24 kcal/mole collision energy, BrOO might under go further decomposition. We detected no signal at m/e = 111 at 26 kcal/mole collision energy. As in the Cl + O_3 reaction, we think

the reaction channel $Br + O_3 \rightarrow BrO_2 + O$ is a very minor channel.

IV. DISCUSSION

The center-of-mass angular distribution and the product translational energy release of the $Br + O_3$ reaction are very similar to those in the $Cl + O_3$ reaction, and, thus, both reactions should proceed through the similar reaction mechanism. It is clear that the reaction $Br + O_3$ is also a direct reaction. For the higher collision energies (E_{coll} = 14.5-26 kcal/mole), the center-of-mass angular distribution has a predominant forward-sideways peak and is strongly asymmetric with respect to 90° in the center-of-mass frame. It does not have the typical forward-backward symmetry that a reaction via a persistent long-lived complex has.[33] Furthermore, the strong coupling between the translational energy release and the center-of-mass angle is another clear sign of a direct reaction mechanism.

The CM angular distribution at 5 kcal/mole collision energy shows a slight forward-backward symmetry (Fig. 19). It seems to have the peak at around 90° in the center-of-mass frame. If a long-lived complex exists at this low collision energy, it is an oblate that would have this type of angular distribution,[33] and the BrO product should be ejected perpendicularly to the plane of rotation of the long-lived complex. However, there is no force acting in this direction. Most

likely the force ejecting BrO would be in the plane of the rotation. In the reaction mechanism similar to that in the Cl + O_3 reaction,[16] the Br atom is likely to attack the terminal oxygen atom of the ozone molecule in a coplanar pathway at the low collision energy, and the transition state would likely be a prolate. Because of this coplanar collision pathway, **L** and **L′** are correlated so that they would be in the similar direction, and the BrO product is expected to be ejected near this collision plane. Furthermore, because the initial orbital angular momentum **L** and the final orbital angular momentum **L′** are quite large, by the conservation of the angular momentum, they should be in the similar direction, and the initial relative velocity and the final velocity should be more-or-less parallel to each other. Again, the products are supposed to decay into the plane of the rotation of the complex instead of perpendicularly out of the plane. However, the center-of-mass angular distribution of the long-lived complex decaying in the plane of the rotation should have peaks in 0° and 180° in the center-of-mass frame, which is not the observation in our experiment. This argument again suggested that it is highly unlikely for the reaction to proceed through a long-lived complex. The difference in the center-of-mass recoil velocity of the BrO product as a function of scattering angle also strongly suggests that there is not a long-lived complex in this reaction.

When comparing the experimental results from the Br + O_3 reaction and those from the Cl + O_3 reaction,[16] one finds that the product translational energy distributions and the center-of-mass angular distributions of the two reactions are

very similar. The energy dependence of these distributions from the two reactions are also similar, so are the couplings between the translational energy distributions and the center-of-mass scattering angles. Essentially, the dynamic information (center-of-mass energy-flux distribution, i.e., double differential reactive cross section) for both reactions obtained from the crossed molecular beam studies shows that the two reactions are very much alike. The O_3 molecule is the central player to determine the reaction mechanisms. The comparison of the results from the crossed molecular beams studies of these two reactions firmly supports the suggestions from the early kinetic studies that the transition state structures of these reactions were mostly determined by the configuration of the ozone molecule.[10-12] This comparison also agrees with the results from the theoretical calculations which showed that the intermediate configuration was quite like the stable ozone molecule.[9,14] The conclusion from the two crossed molecular beam studies reinforces the argument by Schaefer and co-workers that the electronic structure of the O_3 molecule plays an important role in the reaction mechanism.[34] The O_3 molecule is characterized as a diradical with the two unpaired π electrons in the terminal oxygen atoms.[35] The center oxygen atom of the O_3 molecule has a closed outer shell with 8 electrons, and the terminal oxygen atom has only 7 outer electrons with a half-filled π orbital perpendicular to the plane of the ozone molecule. The two terminal atomic O2pπ orbitals form the pair of the π molecular orbitals $1a_2$ and $2b_1$. The HOMO of the O_3 molecule is $1a_2$ orbital, which is fully occupied by the 2 terminal O2pπ electrons.

As argued previously,[16,34] it is unlikely for the Br atom to strike the central oxygen atom to make the reaction happen, because of the high repulsion of the lone pair of electrons on the central oxygen atom. This is confirmed by the fact that the BrO CM angular distribution is peaked predominantly sideways instead of in the backward direction. It is also unlikely for the Br atom to insert into the O-O bond. Previous kinetic studies suggested that in this reaction the structure of the transition state quite resembled that of the stable ozone molecule.[10-12] The similarity of the results from the crossed molecular beam studies of both the Br + O_3 and the Cl + O_3 reactions indicates that the configurations of the transition states in these two reactions are similar. This implies that the Cl or Br atom probably does not insert to the O-O bond to make the structure of the transition state quite different from that of the stable ozone molecule.

The Br atom is very likely to attack the terminal oxygen atom. One way is that the Br atom attacks the π orbital on the O_3 molecule perpendicularly from above the plane of the ozone molecule. This vertical approach is the favorite way in the frontier orbital theory.[39,40] Similar to the Cl + O_3 reaction, if the singly occupied p orbital on the Br atom descends vertically to the π orbital on the terminal oxygen atom, there is a net overlap between the two orbitals, and a σ bond in this direction is expected to form between the Br atom and the terminal O atom of the ozone molecule. This type of interaction is symmetry-allowed. This collision pathway has a large impact parameter b, and the BrO product is expected to be scattered in the forward direction. With the increasing collision

energy, the forward scattering would become stronger. However, in our experimental results, BrO is predominantly forward **and** sideways scattered, and the intensities of the BrO product in the forward angles (0°-20°) are not very large even with about five times increase of the collision energy from 5 kcal/mole to 26 kcal/mole. The significant amount of large angle scattering, especially in high collision energies, could not be explained by this consistent large impact parameter approach either. In this picture, the impact parameter is nearly constant, and the approach geometry is nearly identical; the translational energy release is therefore not expected to vary much with the CM angle. The strong angular dependence of the translational energy shown in the experimental results could not fit into this picture. Therefore, this reaction pathway does not contribute to wide-angle reactive scattering; this reaction pathway alone could not give rise to the strong dependence of the product translational energy release on the center-of-mass scattering angle; and it can not account for the whole picture of the Br + O_3 reaction mechanism. Nevertheless, it can fairly well describe the forward reactive scattering. As we discussed in the Cl + O_3 study, if two possible reaction pathways are involved in the Br + O_3 reaction, this out-of-plane reaction pathway, in which the Br atom attacks the terminal oxygen of the ozone molecule perpendicularly to the ozone molecule plane, could well account for the forward scattering channel.

If we assume the similar reaction mechanism of the Cl + O_3 reaction that the Br atom attacks a terminal oxygen atom in the plane of the ozone molecule,

the experimental results could be well explained, especially for the sideways and wide-angle scattering. If the Br atom approaches the terminal oxygen atom of the ozone molecule in a coplanar pathway with the singly occupied p orbital on the Br atom oriented perpendicularly to the collision plane (i.e., as a π orbital), this singly occupied p orbital of the Br atom would have net overlap with the π orbital on the terminal O atom, and this type of interaction is also symmetry-allowed. In this reaction approach, the Br atom has a large range of attacking angles which correspond to a large range of impact parameters and thus a wide range of CM angles into which the product BrO could be scattered. If the Br atom approaches the ozone molecule along the direction of the terminal and terminal O atoms, the impact parameter would be small, and some backward scattered BrO would be expected. Because this is a head-on type of collision, it would lead to more internal excitation of the reaction intermediate and cause less translational energy release in the backward direction. However, in this in-plane pathway, attacking of the Br atom other than in this small impact parameter approach could cause forward and sideways scattering (e.g., along the terminal O atom and central O atom direction, or perpendicularly to this direction). There is quite a strong repulsion force acting on the separating products, and the translational energy release is very large. Even with the increase of the collision energy, the BrO product is still pushed sideways by such a strong force. The large translational energy release and the low forward scattering intensities within the CM angle 20° at all collision energies could be consistently explained by this

repulsive force.

At low collision energy (5 kcal/mole), the sideways repulsion is stronger than the forward impulse from the Br atom, and most of the BrO product is sideways scattered. When the collision energy is increased, the forward impulse becomes stronger and overcomes the sideways repulsion, the forward peak starts to be predominant. It is noticed that, with the increase of the collision energy, the increase of the translational energy release for the small angle scattering is larger than that for the large angle scattering (Fig. 22 and 23). This might be understood in two ways. First, the large angle scattering corresponds to the small impact parameter (small b) approach, which causes more vibrational excitation of the reaction intermediate. The small angle scattering, however, corresponds to the large impact parameter (large b) collision, which leads to less vibrational excitation of the intermediate. When the collision energy is increased, the small b collision could still distribute the initial translational energy into the vibrational energy of the products. However, the large b collision is more efficient to channel the initial translational energy into the translation of the products. Second, the translational energy release pattern has also to meet the constraint of the conservation of the angular momentum. Because of the small initial rotational angular momentum, the total angular momentum is almost determined by the initial orbital angular momentum. Since small b collision has a relatively small orbital angular momentum, thus, small total angular momentum, consequently, the final orbital angular momentum and, thus, the relative velocity of the

products and the translational energy of the products have to be relatively small to meet this constraint. However, the large b collision allows larger total angular momentum and large final orbital angular momentum, therefore, large relative velocity of the products and larger translational energy release. The increase of the width of the $P(E_T)$ curve with the collision energy might be due to the increased excitation of the reaction intermediate with the increased collision energy.

Similar to the Cl + O_3 reaction, two possible reaction mechanisms might also exist in the Br + O_3 reaction. Besides the coplanar approach in which the Br atom attacks a terminal oxygen atom of the ozone molecule in the plane, the out-of-plane reaction pathway in which the Br atom collides vertically to the ozone molecule plane might also exist. As we have discussed, this collision pathway would give largely forward scattering, and it can not account for the wide angle scattering, thus, not the complete picture of the reaction mechanism. However, this out-of-plane channel might account for the forward scattering very well. Because of the large impact parameter in this approach, the product translational energy is larger relative to that in the wide angle scattering. It is noticed that the increase of the translational energy release with the collision energy at small center-of-mass angles is larger than that at wide center-of-mass angles, i.e., that the trend of the increase at small angles is different from that at the large angles (Fig. 22). At wide center-of-mass scattering angles, the translational energy release increases gradually, but at small center-of-mass scattering angles, the

translational energy release increases rapidly. It almost seems that at E_{coll} = 5 kcal/mole the forward scattering channel with large translational energy release is not open, and the forward scattering channel seems to have a higher reaction barrier than the wide-angle scattering channel. In a large impact parameter collision such as in the out-of-plane approach, the orbital angular momentum **L** is large, therefore, there is fair amount of translational energy tied up to rotation. This amount of translational energy is consumed into the rotation as the centrifugal energy and can not be used to break the chemical bond. For E_{coll} = 5 kcal/mole, this amount of energy is estimated to be about 1 kcal/mole. In addition to this rotational energy, there is also a reaction barrier of about 1.5 kcal/mole.[13] Therefore, at low collision energy E_{coll} = 5 kcal/mole, the translational energy is not very effective for the reaction with large impact parameter. However, with the increase of the collision energy up to E_{coll} = 26 kcal/mole, the translational energy tied up to the rotation increases only up to about 4 kcal/mole, and it is much smaller than the collision energy. Therefore, at high collision energies, the effect of the translational energy consumed in the rotation becomes much smaller, and the forward scattering from the out-of-plane collision (with large impact parameter) becomes open and becomes predominant as well. However, for the large angle scattering which has to come from the in-plane collision, the impact parameter is smaller, and the translational energy tied to rotation plays a smaller role. Therefore, there is only small dependence on the collision energy for the large angle scattering. Of course, the analysis for the out-

of-plane collision is also suitable for the large impact parameter collision in the in-plane approach. However, in the coplanar approach, the dependence on the impact parameter should be smooth and may not be very strong, so the large dependence of the translational energy release on the scattering angle may not only come from the in-pane pathway. The out-of-plane approach may indeed have a larger reaction barrier than the in-plane approach, so the forward scattering (out-of-plane pathway) has different collision energy dependence from the wide-angle scattering (in-plane pathway). At the low collision energy (5 kcal/mole), the out-of-plane channel is almost not open, however, at high collision energy, with a wide range of acceptance angles, this channel becomes significant. To summarize, the in-plane collision causes the sideways and wide angle scattering; it causes the forward scattering as well. However, an additional collision channel, the out-of-plane channel, is also possible. This channel results largely the forward scattering. It does not seem to have significant contribution at low collision energy E_{coll} = 5 kcal/mole, however, at higher collision energies, the out-of-plane channel may become quite predominant.

The experimental results for the Br + O_3 reaction are very similar to those for the Cl + O_3 reaction. The general features of the Br + O_3 experimental results have some qualitative agreement with the conclusions from the semi-empirical calculations by Farantos and Murrell on the Cl + O_3 reaction.[15] The Br + O_3 reaction is a direct reaction, and no long-lived complex is involved. The coplanar reaction pathway in the Br + O_3 reaction is similar to the collinear reaction

pathway given by the functional form of the ClO_3 potential energy surface. However, the center-of-mass angular distributions are quite different. The calculation showed a predominant forward scattering of the ClO product with respect to the Cl atom at about 1 kcal/mole thermal energy. The experimental CM angular distribution at 5 kcal/mole collision energy, the lowest in our experiment, is peaked sideways. Only with the increase of the collision energy to 14.5 kcal/mole and finally to 26 kcal/mole, the CM angular distribution shifts to the forward direction. The angular dependence of the kinetic energy release was not demonstrated in the calculations. This angular dependence becomes larger with larger collision energy, as does the kinetic energy release. One possible reason for these discrepancies is that the semi-empirical ClO_3 potential energy surface did not have a strong enough repulsion on the exit channel. The semi-empirical PES may not be sufficient; an *ab initio* calculation on the Br + O_3 reaction is very valuable.

The two product channels, $BrO(^2\Pi) + O_2(^3\Sigma_g^-)$ and $BrO(^2\Pi) + O_2(^1\Delta_g)$, are energetically possible at all collision energies. When E_{coll} is above 6.4 kcal/mole, the third product channel $BrO(^2\Pi) + O_2(^1\Sigma_g^+)$ is also open (Fig. 1). All the three channels are spin-allowed. Furthermore, all the three product channels are correlated with the reactants and are symmetry-allowed. For the Cl + O_3 reaction, early experiments have shown no or very little formation of the electronically excited $O_2(^1\Delta_g)$ and $O_2(^1\Sigma_g^+)$ channels.[16,41,42] Actually, besides in the Cl + O_3 reaction, the absence or the very minor presence of the electronically excited

oxygen molecule product seems to be a general case in the radical and ozone reaction systems such as $O(^3P) + O_3$,[43] $H(^2S) + O_3$,[43] and $NO(^2\Pi) + O_3$.[43,44] This phenomenon might be understandable from the point of view of the electronic structure of the ozone molecule. In all these reactions, the radical likely attacks a terminal oxygen atom; the O-O bond between this terminal oxygen atom and the central oxygen atom cleaves; the remaining O-O part from the ozone molecule would undergo minimum energy and electronic structure change to form the O_2 molecule. Therefore, the most likely state of the O_2 molecule would be the ground state $O_2(^3\Sigma^-_g)$ because the old π orbitals on this O-O part remain unchanged. It is unlikely for the electronically excited O_2 molecule to form in the reaction, because, in order to form the excited singlet O_2 molecule, the unpaired electron on the central oxygen atom that is just released from the breaking of the O-O σ-bond has to undergo large rearrangement to pair with the previously unpaired π electron on the terminal oxygen atom. If the radical attacks the central oxygen atom, a large change of the O-O electronic structure could occur, and the electronically excited O_2 might form;[45] however, this approach again will encounter a very high barrier. Following the above analysis, it would be quite reasonable to speculate that almost no electronically excited O_2 molecule would be produced in the $Br + O_3$ reaction. The translational energy release probability $P(E_T)$ for the $Br + O_3$ reaction is quite smooth. It is unlikely for the electronically excited O_2 product to form which might have quite different type of $P(E_T)$ from that of the ground- state O_2 product. However, because of the vibrational and

rotational excitations of the products and the time-of-flight resolution in our experiment, it is difficult to tell whether or not the electronically excited O_2 product is formed just by inspecting the translational energy release $P(E_T)$.

Another reaction channel, $Br + O_3 \rightarrow BrOO(^2A) + O(^3P)$ ($\Delta H^\circ \approx 22$ kcal/mole), is open at the high collision energy 26 kcal/mole. This channel is also spin-allowed. However, we have not observed any evidence of this channel. In the coplanar pathway, when the Br atom attacks one terminal oxygen atom on the ozone molecule to form the asymmetric BrO_3 intermediate, it would be the O-O bond between this terminal oxygen atom and the central oxygen atom that is weakened the most and is being broken because of the strongest perturbation from the Br atom; so it is very unlikely for the other O-O bond to break to form the weakly-bond BrOO product. If the lifetime of the asymmetric BrO_3 were quite long, there might be some small possibility to break the other O-O bond after the redistribution of the internal energy of the BrO_3 intermediate and to form BrOO. However, our conclusion that the lifetime of the asymmetric BrO_3 intermediate is very small implies that there is a very small probability for the BrOO channel in the $Br + O_3$ reaction. Certainly, other collision pathways would encounter a much higher barrier, and BrOO is unlikely to be generated in the range of the collision energies in our experiment.

The Br atoms could be in two spin-orbit states $Br(^2P_{3/2})$ and $Br(^2P_{1/2})$. The excited state $Br(^2P_{1/2})$ is separated by 10.5 kcal/mole from the ground state $Br(^2P_{3/2})$.[46] Before the supersonic expansion, under the assumption that the Br

atoms are in the thermal equilibrium, about 3% of the Br atoms are in the spin-orbit excited state $Br(^2P_{1/2})$ at 2000 K temperature. In general, the $Br(^2P_{3/2})$ atom is found to be more reactive than the excited $Br(^2P_{1/2})$ atom.[47] Based on the study by Clyne and Nip,[48] in which the reaction rate constant of the $Cl(^2P_{3/2}) + O_3$ reaction measured at 298 K was found to be slightly larger than that of the $Cl(^2P_{1/2}) + O_3$ reaction measured at the same temperature, the reactivity of the ground-state $Br(^2P_{3/2})$ with ozone is expected to be larger than or at least equal to that of the spin-orbit excited state $Br(^2P_{1/2})$. If $Br(^2P_{1/2})$ is highly reactive, there should be 10.5 kcal/mole more energy release. However, we could not see any abnormal extra energy release in the translational energy distributions. $Br(^2P_{1/2})$ is in a very small amount and is expected to have smaller reactivity; we can conclude that all the dynamic information obtained in this crossed molecular beam study is exclusively from the ground-state $Br(^2P_{3/2}) + O_3$ reaction. There are two possible spin-orbit states of the product BrO in the ground electronic state $^2\Pi$: $BrO(^2\Pi_{3/2})$ and $BrO(^2\Pi_{1/2})$, which are separated by 900 cm^{-1}.[49] The time-of-flight resolution and the spread of the collision energies in our experiment prevented us from getting any information about the fine-structure population of the BrO product.

From the translational energy distribution of the $Br + O_3$ reaction, we can tell that, besides the large translational energy release, the BrO product is also vibrationally and rotationally excited. Following the analysis of the reaction mechanism, the O_2 product might remain internally cool because of its spectator

role. If the O_2 product indeed has little rotational and vibrational energy, from the translational energy distribution, it is reasonable to speculate that a substantial amount of energy is channeled into the BrO vibration. The vibrationally excited BrO radical from the Br + O_3 reaction could certainly promote its reaction with certain atmospheric species in stratospheric chemistry.

V. CONCLUSIONS

We have studied the Br + O_3 reaction using the crossed molecular beam method at five different collision energies from 5 kcal/mole to 26 kcal/mole. The center-of-mass product angular distribution and the translational energy distribution have been derived from the experimental data. The product translational energy release is large, and the average translational energy ranges from 40%-60% of the total available energy. The BrO product is forward sideways scattered in the center-of-mass frame. With the increase of the collision energy, the fraction of the total available energy channelled into product translation is increased, and the BrO product is also scattered into more forward direction with respect to the Br atom. There is a strong coupling between the translational energy release and the center-of-mass angles, with the translational energy release in the forward direction in the CM system larger than that in the backward direction.

It is concluded that the Br + O_3 reaction has a direct reaction mechanism. The Br atom would most likely attack a terminal oxygen atom of the ozone molecule. The exit channel on the BrO_3 potential energy surface is believed to have a strong repulsion to cause the large translational energy release among the products. An *ab initio* calculation on the Br + O_3 reaction is valuable to compare with the results of this crossed molecular beam study.

The detailed comparison of the results for the Cl + O_3 and the Br + O_3 reactions manifests that the two reactions have the similar reaction mechanisms. In the ozone reaction with the atomic radicals, the electronic structure of the ozone molecule plays the central role to determine the reaction mechanism. It is expected that other ozone reactions with the atomic radicals such as F + O_3 , I + O_3 and O + O_3 should have the similar reaction mechanisms.

VI. REFERENCES

1. R. P. Wayne, Chemistry of Atmospheres (Clarendon Press, Oxford, 1991).
2. L. T. Molina and M. J. Molina, J. Phys. Chem. **91**, 433 (1987).
3. M. B. McElroy, R. J. Salawitch, S. C. Wofsy, and J. A. Logan, Nature **321**, 759 (1986).
4. J. G. Anderson, D. W. Toohey, and W. H. Brune, Science **251**, 39 (1991).
5. J. W. Barrett, P. M. Solomon, R. L. de Zafra, M. Jaramillo, L. Emmons, and

A. Parrish, Nature **336**, 455 (1988).

6. S. Solomon, Nature **347**, 347 (1990).

7. M. A. A. Clyne and H. W. Cruse, Trans. Faraday Soc. **66**, 2214 (1970).

8. M. -T. Leu and W. B. DeMore, Chem. Phys. Lett. **48**, 317 (1977).

9. J. V. Michael and W. A. Payne, Int. J. Chem. Kinet. **11**, 799 (1979).

10. D. W. Toohey, W. H. Brune, and J. G. Anderson, Int. J. Chem. Kinet. **20**, 131 (1988) and the references therein.

11. J. M. Nicovich, K. D. Kreutter, and P. H. Wine, Int. J. Chem. Kinet. **22**, 399 (1990) and the references therein.

12. R. Patrick and D. M. Golden, J. Phys. Chem. **88**, 491 (1984).

13. a) D. L. Baulch, R. A. Cox, R. F. Hampson Jr., J. A. Kerr, J. Troe, and R. T. Watson, J. Phys. Chem. Ref. Data. **9**, 295 (1980).

    b) D. L. Baulch, R. A. Cox, P. J. Crutzen, R. F. Hampson Jr., J. A. Kerr, J. Troe, and R. T. Watson, J. Phys. Chem. Ref. Data. **11**, 327 (1982).

14. a) W. P. McGrath and R. G. W. Norrish, Z. Phys. Chem. **15**, 245 (1958).

    b) W. P. McGrath and R. G. W. Norrish, Proc. Roy. Soc. A **254**, 317 (1960).

15. S. C. Farantos and J. N. Murrell, Int. J. Quan. Chem. **14**, 659 (1978).

16. J. S. Zhang and Y. T. Lee (to be published).

17. Y. T. Lee, J. D. McDonald, P. R. LeBreton, and D. R. Herschbach, Rev. Sci. Instrum. **40**, 1402 (1969).

18. R. K. Sparks, Ph. D. Thesis, University of California, Berkeley (1979).

19. Carborundum Co., Specialty Graphite Plant, Sanborn, New York.

20. J. J. Valentini, M. J. Coggiola, and Y. T. Lee, Rev. Sci. Instrum. **48**, 58 (1977).

21. H. F. Davis, Ph. D. Thesis, University of California, Berkeley (1992).

22. M. F. Vernon, Ph. D. Thesis, University of California, Berkeley (1983).

23. D. J. Krajnovich, Ph. D. Thesis, University of California, Berkeley (1983).

24. a) K. Sköld, Nucl. Inst. Methods **63**, 114 (1968).

b) V. L. Hirshy and J. P. Aldridge, Rev. Sci. Instrum. **42**, 381 (1971).

c) G. Comsa, R. David, and B. J. Schumacher, Rev. Sci. Instrum. **52**, 789 (1981).

25. R. J. Buss, Ph. D. Thesis, University of California, Berkeley (1979).

26. D. D. Parrish and D. R. Herschbach, J. Amer. Chem. Soc. **95**, 6133 (1973).

27. D. St. A. G. Radlein, J. C. Whitehead, and R. Grice, Molec. Phys. Lett. **29**, 1813 (1975).

28. D. P. Fernie, D. J. Smith, A. Durkin, and R. Grice, Molec. Phys. **46**, 41 (1982).

29. N. C. Firth, N. W. Keane, D. J. Smith, and R. Grice, Laser Chem. **9**, 265 (1988).

30. N. I. Butkovskaya, I. I. Morozov, V. L. Tal'rose, and E. S. Vasiliev, Chem. Phys. **79**, 21 (1983).

31. J. A. Blake, R. J. Browne, and G. Burns, J. Chem. Phys. **53**, 3320 (1970).

32. S. P. Sander and R. T. Watson, J. Phys. Chem. **85**, 4000 (1981).

33. a) W. B. Miller, S. A. Safron, and D. R. Herschbach, Discuss. Faraday Soc. **44**, 108 (1967).

b) W. B. Miller, Ph. D. Thesis, Harvard University (1969).

34. a) M. M. L. Chen, R. W. Wetmore, and H. F. Schaefer III, J. Chem. Phys. **74**, 2938 (1981).

b) M. Dupuis, G. Fitzgerald, B. Hammond, W. A. Lester, and H. F. Schaefer III, J. Chem. Phys. **84**, 2691 (1986).

35. P. J. Hay and T. H. Dunning, Jr., J. Chem. Phys. **67**, 2290 (1977).

36. S. Rothenberg and H. F. Schaefer III, Molec. Phys. **21**, 317 (1970).

37. R. P. Messmer and D. R. Salahub, J. Chem. Phys. **65**, 779 (1976).

38. P. Borowski, K. Andersson, P.-Å. Malmqvist, and B. O. Roos, J. Chem. Phys. **97**, 5568 (1992).

39. K. Fukui, Reactivity and Structure Concepts in Organic Chemistry, Vol. 2: Theory of Orientation and Stereoselection (Springer-Verlag, New York, 1975).

40. K. Fukui, in Molecular Orbitals in Chemistry, Physics and Biology, edited by P.-O. Löwdin and B. Pullman (Academic, New York, 1964), p. 513.

41. J. W. Vanderzanden and J. W. Birks, Chem. Phys. Lett. **88**, 109 (1982).

42. K. Y. Choo and M. Leu, J. Phys. Chem. **89**, 4832 (1985).

43. N. Washida, H. Akimoto, and M. Okuda, Bull. Chem. Soc. Jpn. **53**, 3496 (1980).

44. M. Gauthier and D. R. Snelling, Chem. Phys. Lett. **20**, 178 (1973).

45. A. E. Redpath, M. Menzinger, and T. Carrington, Chem. Phys. **27**, 409 (1978).

46. C. E. Moore, Atomic Energy Levels, National Stand. Ref. Data Ser. (National Bureau of Standards, Washington DC, 1971).

47. P. J. Dagdigian and M. L. Campbell, Chem. Rev. **87**, 1 (1987).

48. M. A. A. Clyne and W. S. Nip, J. Chem. Soc. Far. Trans. II **72**, 838 (1976).

49. K. P. Huber and G. Herzberg, Molecular Spectra and Molecular Structure, IV. Constants of Diatomic Molecules, (Van Nostrand Reinhold Company, New York, 1979).

VII. TABLES

TABLE I. Experimental Beam Parameters.

Beam description	Peak velocity (v_{pk}) ($x10^4$ cm/sec)	Speed Ratio ($v/\Delta v$)
Br (6% Br_2 in He)	23.7	5.7
Br (9% Br_2 in He)	19.0	5.8
Br (9% Br_2 in Kr)	10.2	7.7
O_3 (7% in He)	12.8	13.6
O_3 (7% in Ar)	6.4	12.6

TABLE II. Experimental Conditions.

Br v_{pk} ($x10^4$ cm/s)	O_3 v_{pk} ($x10^4$ cm/s)	Collision Energy E_{coll} (kcal/mole)	$\Delta E_{coll}/E_{coll}$	$\Delta E_{coll}/E_{avl}$
23.7	12.8	26	27%	12%
19.0	12.8	18.5	23%	9%
19.0	6.4	14.5	31%	10%
10.2	6.4	5	19%	3%

TABLE III. Average Translational Energy Release.

Collision Energy E_{coll} (kcal/mole)	CM Angle 10° $\langle E_T/E_{avl} \rangle$	CM Angle 40° $\langle E_T/E_{avl} \rangle$	CM Angle 120° $\langle E_T/E_{avl} \rangle$	$(\Delta\langle E_T \rangle)_{max}$ (kcal/mole)
26	.62	.56	.43	11
18.5	.58	.52	.41	9
14.5	.54	.49	.37	8
5	.39	.37	.33	2

TABLE IV. Peak Translational Energy Release.

Collision Energy E_{coll} (kcal/mole)	CM Angle 10° E_T^{peak}/E_{avl}	CM Angle 40° E_T^{peak}/E_{avl}	CM Angle 120° E_T^{peak}/E_{avl}	$(\Delta E_T^{peak})_{max}$ (kcal/mole)
26	.64	.57	.41	13
18.5	.59	.53	.38	10
14.5	.54	.48	.35	9
5	.35	.33	.30	2

VIII. FIGURE CAPTIONS

Figure 1 Energy level diagram of the Br + O_3 system. Thermodynamic values are derived from Refs. 13b, 31, and 32. The solid lines stand for the collision energies in the experiment.

Figure 2 Upper: Laboratory angular distribution of the reaction Br + O_3 at E_{coll} = 26 kcal/mole. The filled circles are for the experimental data. Error bars stand for 95% confidence limits. The solid lines are the calculated fitting curves.

Lower: The Newton diagram for the reaction Br + O_3 at E_{coll} = 26 kcal/mole. The circle stands for the maximum center-of-mass velocity of the BrO product. The Br beam is defined as 0° in the laboratory frame, and the ozone beam is 90°.

Figure 3 Laboratory time-of-flight spectra of the BrO product at E_{coll} = 26 kcal/mole. The circles are the experimental data points. The solid lines are the fitting. (a) TOF spectra in the laboratory angles from -15° to 22.5°. (b) TOF spectra in the laboratory angles from 25° to 55°.

Figure 4 Upper: Average translational energy $\langle E_T \rangle$ at different CM angles for E_{coll} = 26 kcal/mole.

Lower: Total relative center-of-mass angular distribution $I_{CM}(\theta)$ at E_{coll} = 26 kcal/mole. The maximum of the relative angular

distribution is scaled to unit.

Figure 5 Translational energy release probability $P(E_T, \theta)$ at various center-of-mass angles for E_{coll} = 26 kcal/mole. Maximum probabilities are scaled to unit. The maximum translational energy in these plots is the total available energy for the reaction at the most probable collision energy E_{coll} = 26 kcal/mole.

Figure 6 The contour map and the 3-D plot for the center-of-mass flux-velocity distribution $I_{CM}(\theta, u)$ at E_{coll} = 26 kcal/mole.

Figure 7 Same as Fig. 2 but at E_{coll} = 18.5 kcal/mole.

Figure 8 Same as Fig. 3 but at E_{coll} = 18.5 kcal/mole. (a) TOF spectra in the laboratory angles from -15° to 27.5°. (b) TOF spectra in the laboratory angles from 30° to 65°.

Figure 9 Same as Fig. 4 but at E_{coll} = 18.5 kcal/mole.

Figure 10 Same as Fig. 5 but at E_{coll} = 18.5 kcal/mole.

Figure 11 Same as Fig. 6 but at E_{coll} = 18.5 kcal/mole.

Figure 12 Same as Fig. 2 but at E_{coll} = 14.5 kcal/mole.

Figure 13 Same as Fig. 3 but at E_{coll} = 14.5 kcal/mole: TOF spectra in the laboratory angles from -15° to 45°.

Figure 14 Same as Fig. 4 but at E_{coll} = 14.5 kcal/mole.

Figure 15 Same as Fig. 5 but at E_{coll} = 14.5 kcal/mole.

Figure 16 Same as Fig. 6 but at E_{coll} = 14.5 kcal/mole.

Figure 17 Same as Fig. 2 but at E_{coll} = 5 kcal/mole.

Figure 18 Same as Fig. 3 but at E_{coll} = 5 kcal/mole: TOF spectra in the laboratory angles from 25° to 55°.

Figure 19 Same as Fig. 4 but at E_{coll} = 5 kcal/mole.

Figure 20 Same as Fig. 5 but at E_{coll} = 5 kcal/mole.

Figure 21 The contour plot of the center-of-mass flux distribution I (θ, u) at E_{coll} = 5 kcal/mole for the region where the TOF spectra have been measured.

Figure 22 Upper: The fractions of the average translational energy in the total available energy at different center-of-mass angles versus the collision energies.

Lower: The fractions of the peak translational energy release in the total available energy at different center-of-mass angles versus the collision energies.

Figure 23 The maximum difference in the average translational energy release at different center-of-mass angles versus the collision energies and the maximum difference in the peak translational energy release at different center-of-mass angles versus the collision energies.

Energy Level Diagram

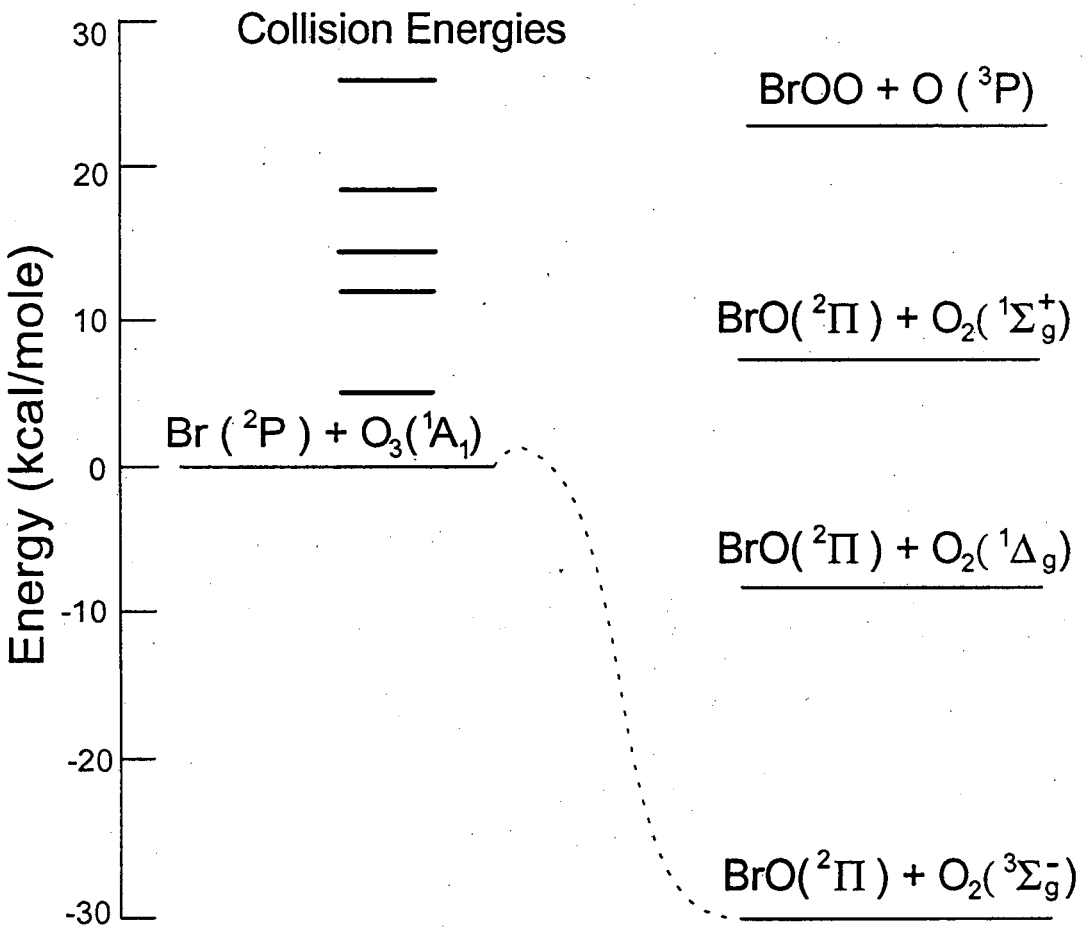

Figure 1

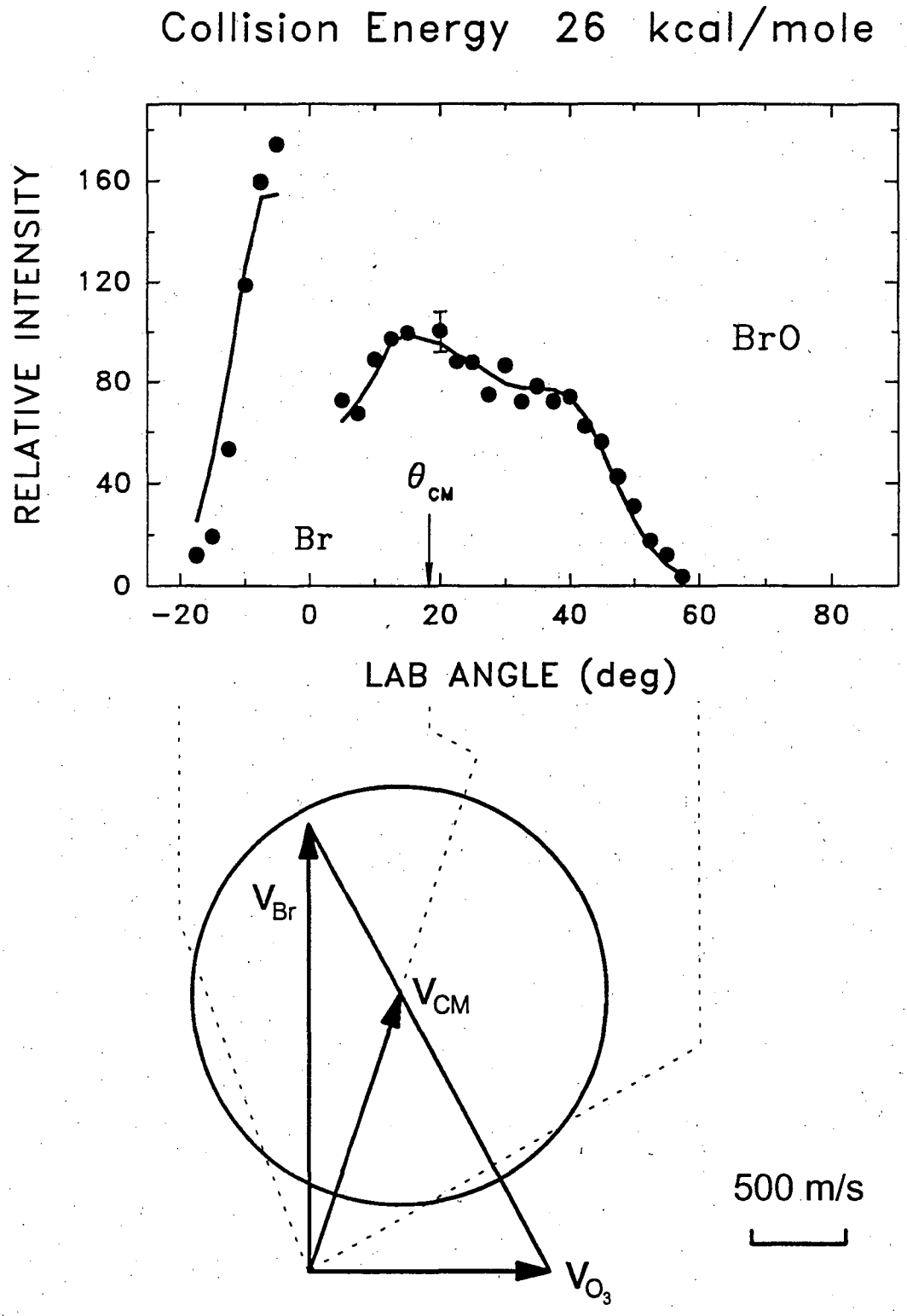
Collision Energy 26 kcal/mole
RELATIVE INTENSITY
160
120
80
40
0
−20
0
20
40
60
80
LAB ANGLE (deg)
BrO
Br
θ CM
V Br
V CM
V O3
500 m/s

Figure 2

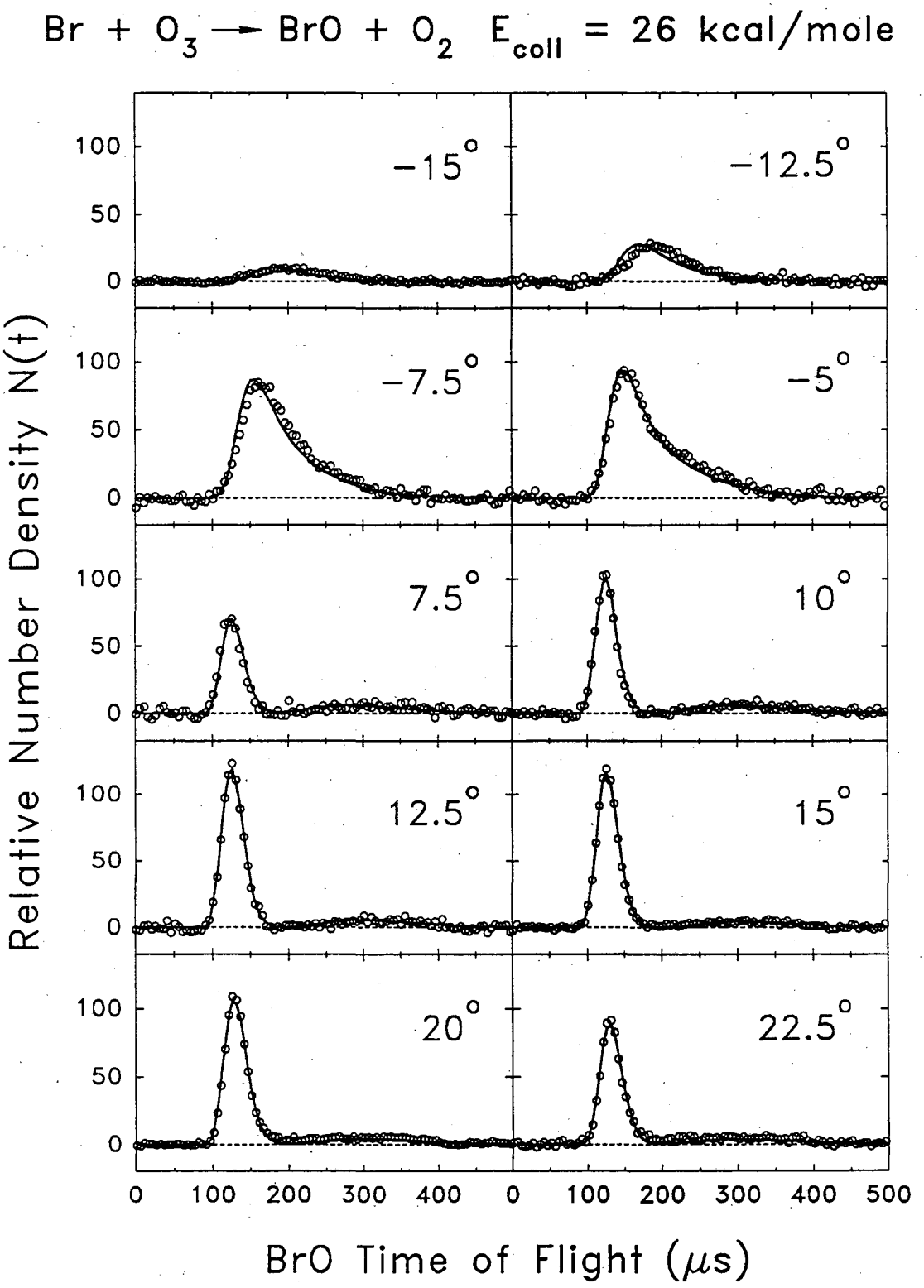
Br + O3 → BrO + O2 Ecoll = 26 kcal/mole
−15°
−12.5°
−7.5°
−5°
7.5°
10°
12.5°
15°
20°
22.5°
Relative Number Density N(t)
BrO Time of Flight (μs)
0
50
100
200
300
400
500

Figure 3a

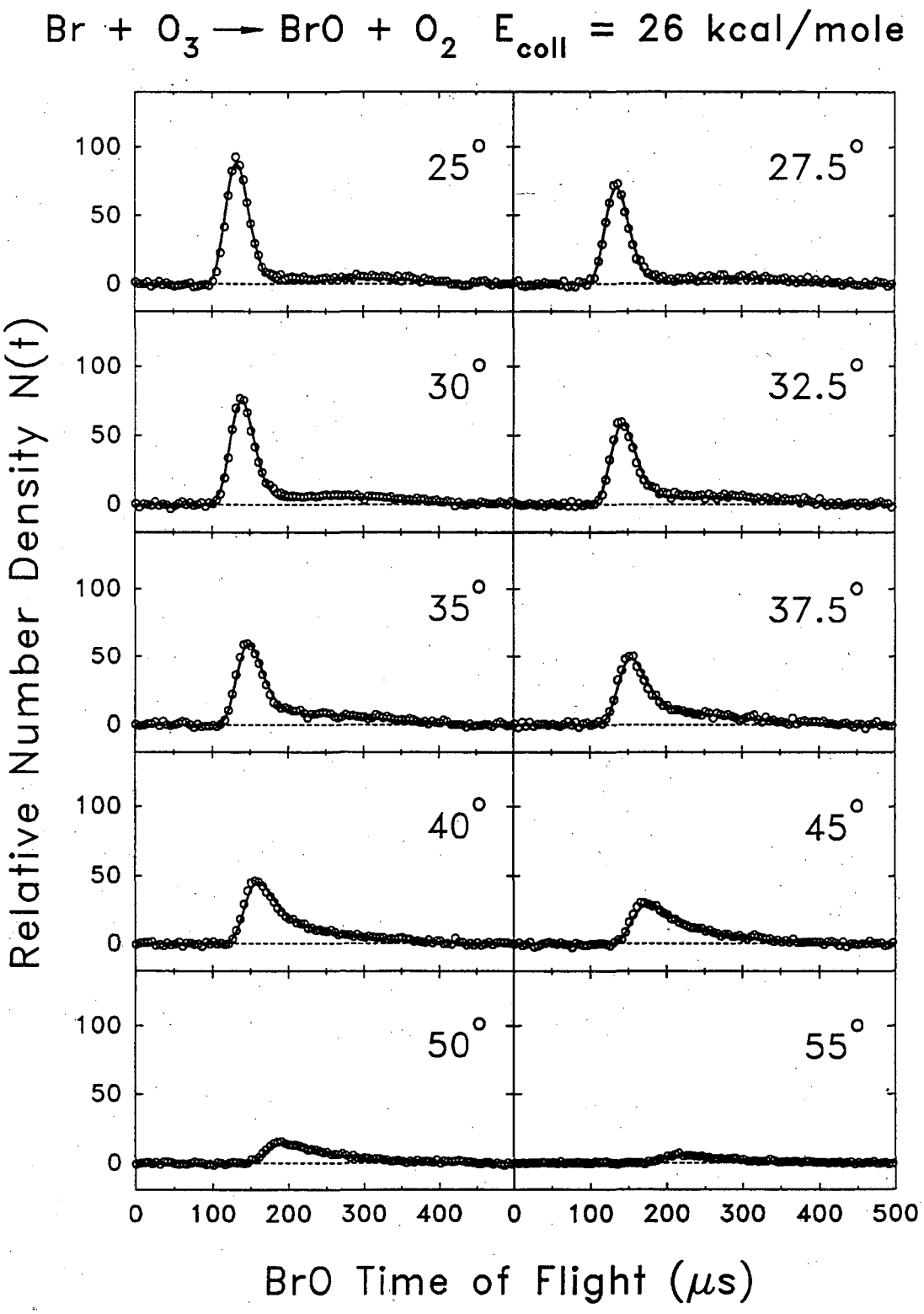
Br + O3 → BrO + O2 Ecoll = 26 kcal/mole
25°
27.5°
30°
32.5°
35°
37.5°
40°
45°
50°
55°
Relative Number Density N(t)
BrO Time of Flight (μs)

Figure 3b

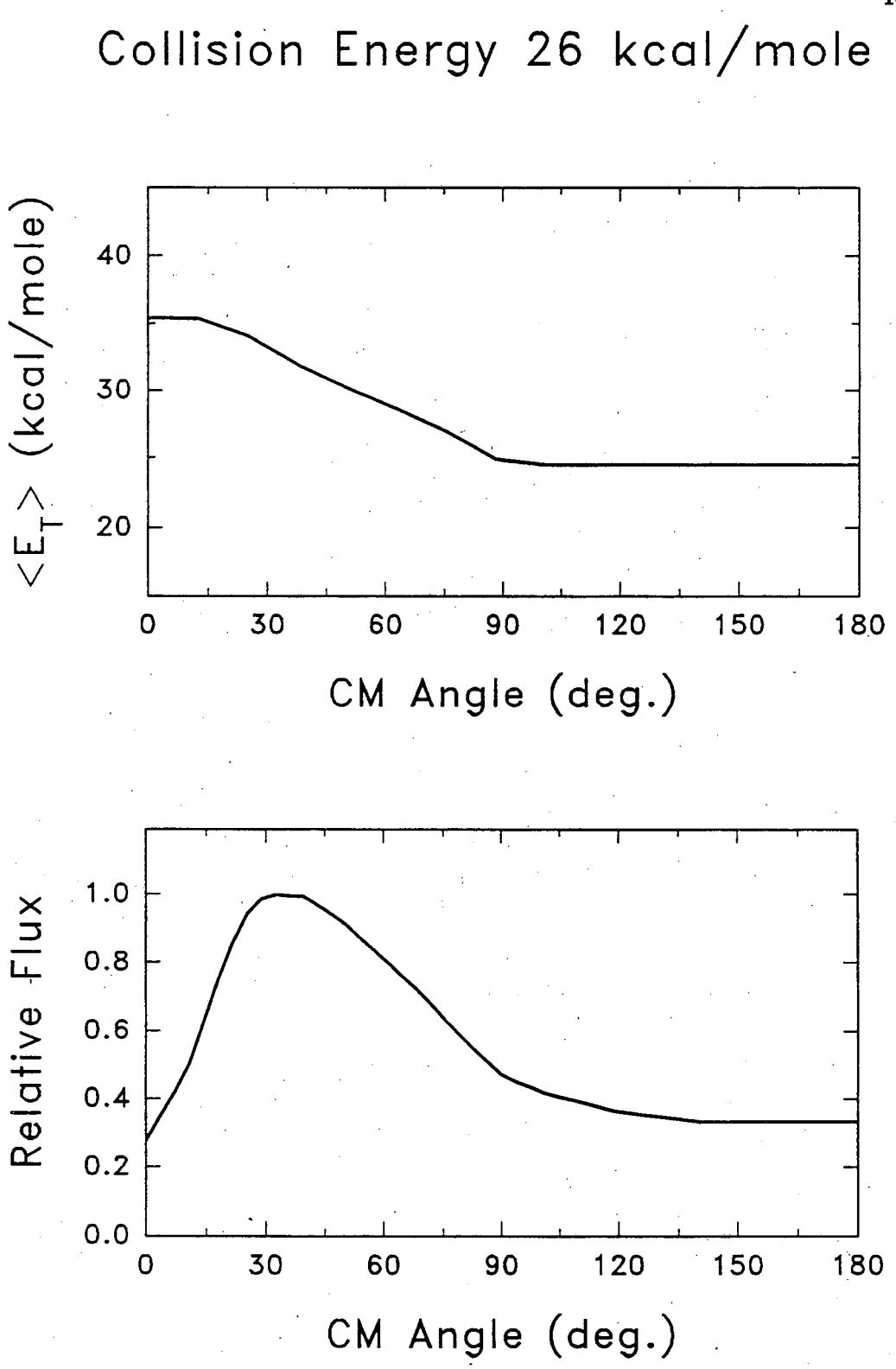
Collision Energy 26 kcal/mole
<E_T> (kcal/mole)
40
30
20
0
30
60
90
120
150
180
CM Angle (deg.)
Relative Flux
1.0
0.8
0.6
0.4
0.2
0.0
0
30
60
90
120
150
180
CM Angle (deg.)

Figure 4

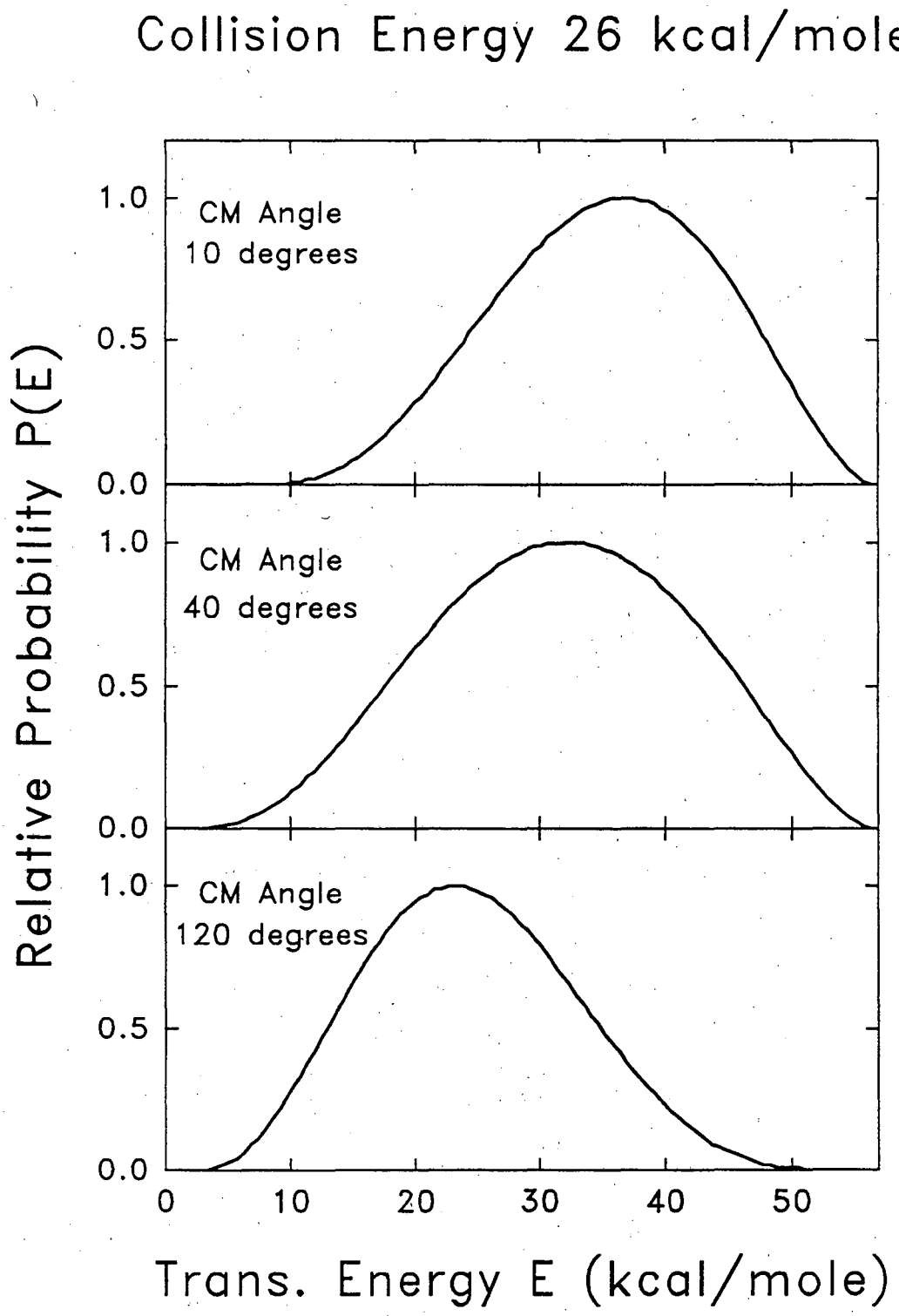
Collision Energy 26 kcal/mole
Relative Probability P(E)
CM Angle
10 degrees
CM Angle
40 degrees
CM Angle
120 degrees
1.0
0.5
0.0
0
10
20
30
40
50
Trans. Energy E (kcal/mole)

Figure 5

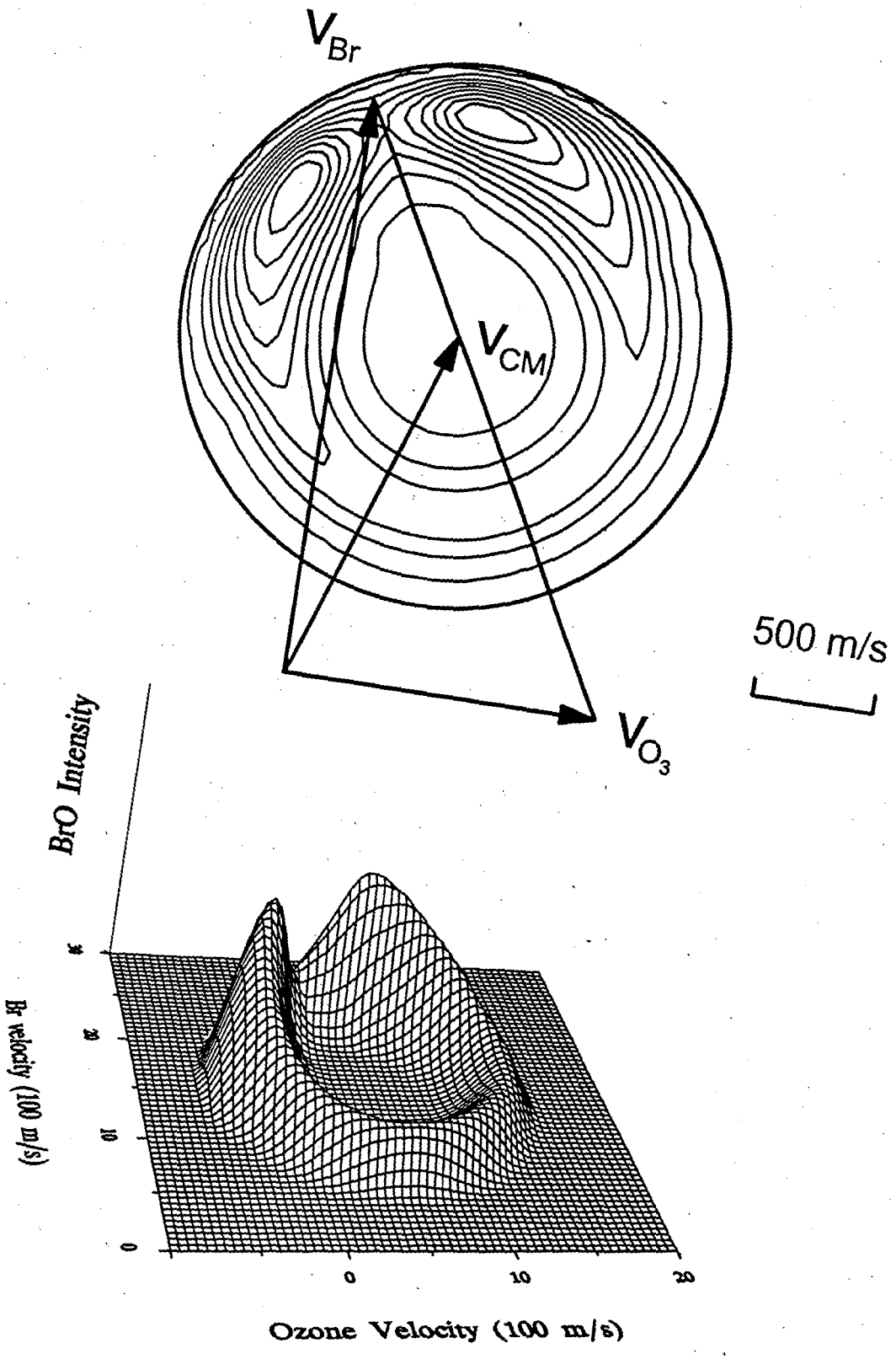
V_{Br}
V_{CM}
V_{O_3}
500 m/s
BrO Intensity
Br velocity (100 m/s)
0
10
20
0
10
20
Ozone Velocity (100 m/s)

Figure 6

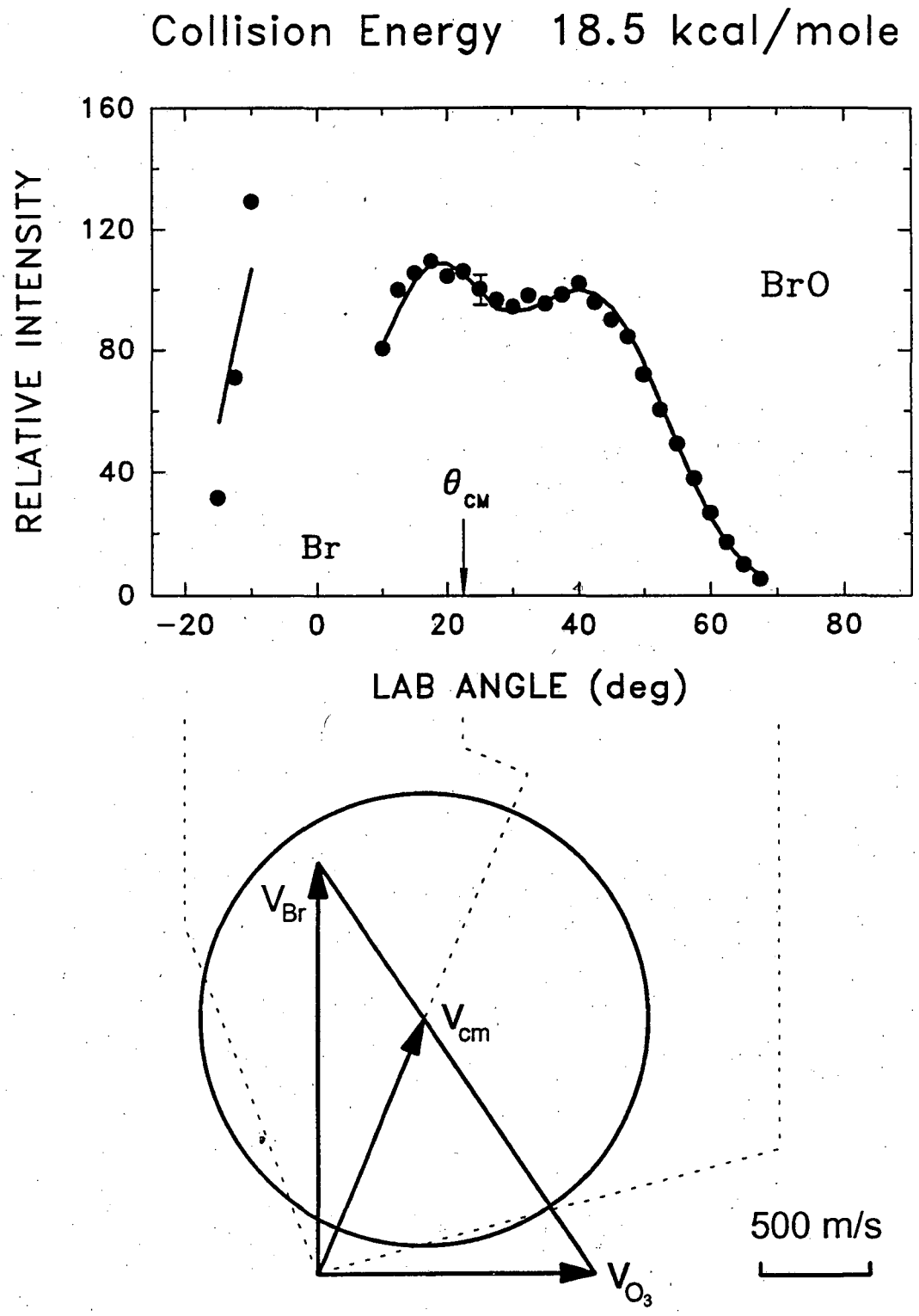
Collision Energy 18.5 kcal/mole
RELATIVE INTENSITY
160
120
80
40
0
−20
0
20
40
60
80
LAB ANGLE (deg)
BrO
Br
θ CM
V Br
V cm
V O3
500 m/s

Figure 7

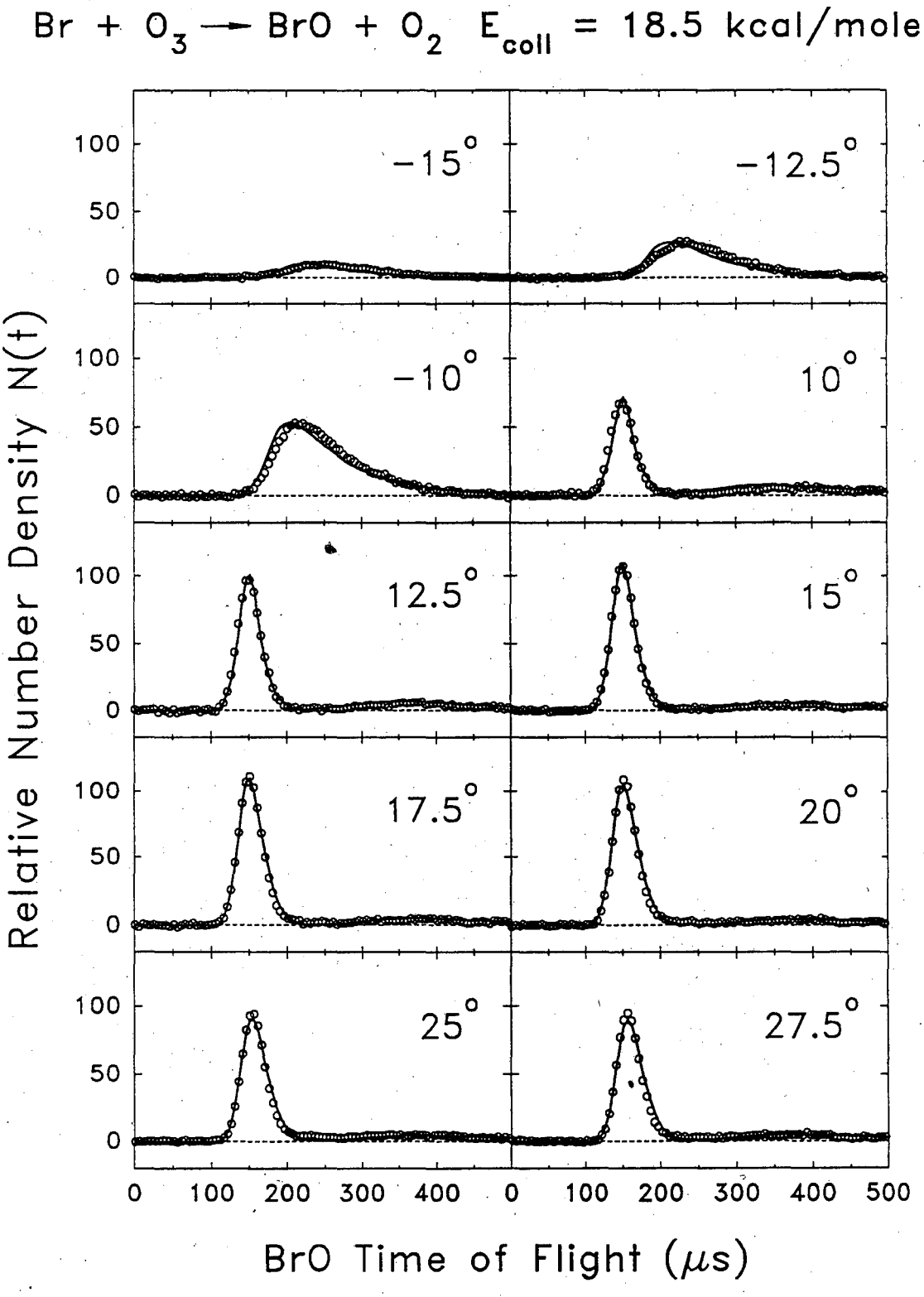
Br + O3 → BrO + O2 Ecoll = 18.5 kcal/mole
−15°
−12.5°
−10°
10°
12.5°
15°
17.5°
20°
25°
27.5°
Relative Number Density N(t)
BrO Time of Flight (μs)
0
50
100
200
300
400
500

Figure 8a

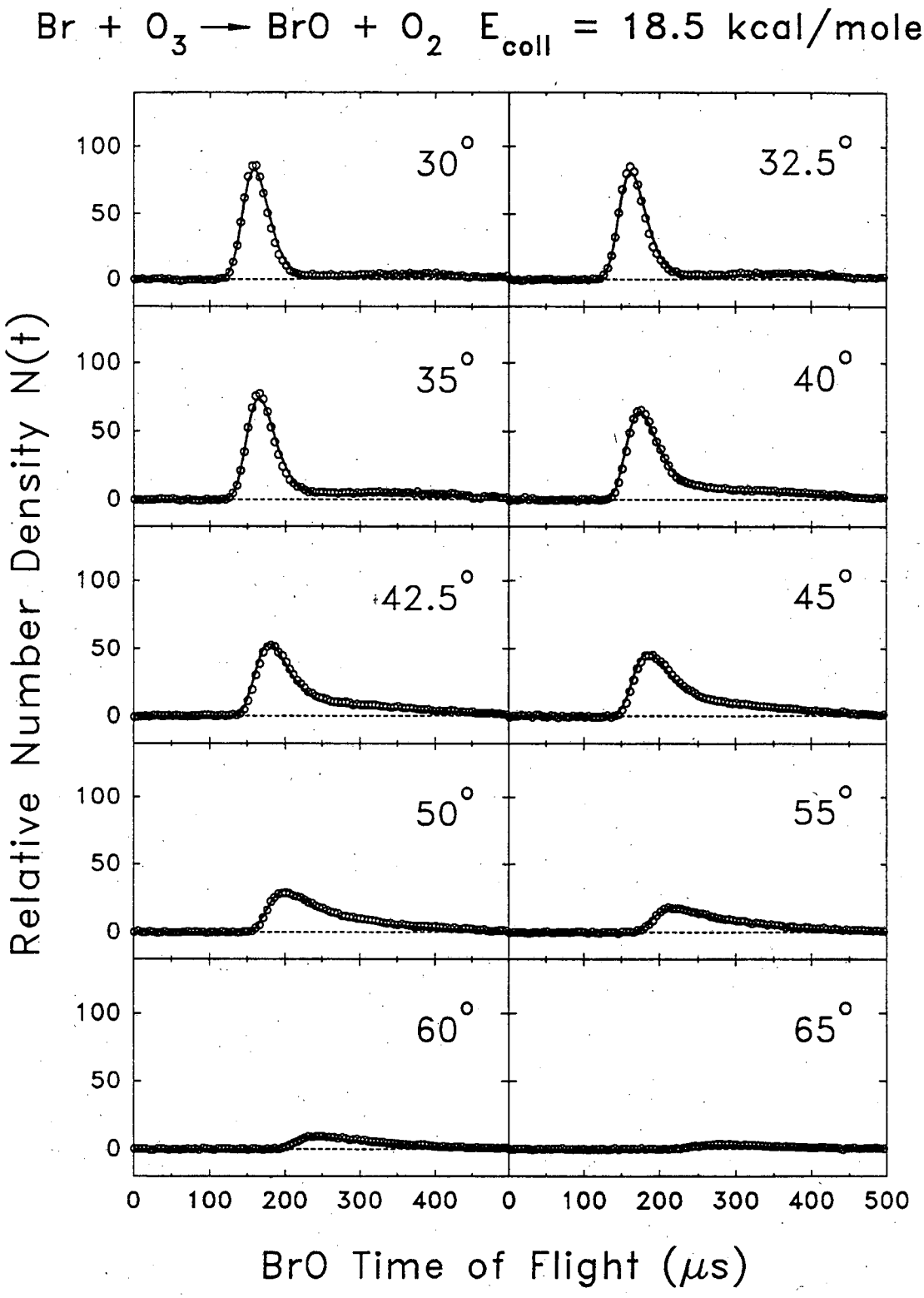
Br + O3 → BrO + O2 Ecoll = 18.5 kcal/mole
30°
32.5°
35°
40°
42.5°
45°
50°
55°
60°
65°
100
50
0
0 100 200 300 400 0 100 200 300 400 500
Relative Number Density N(t)
BrO Time of Flight (μs)

Figure 8b

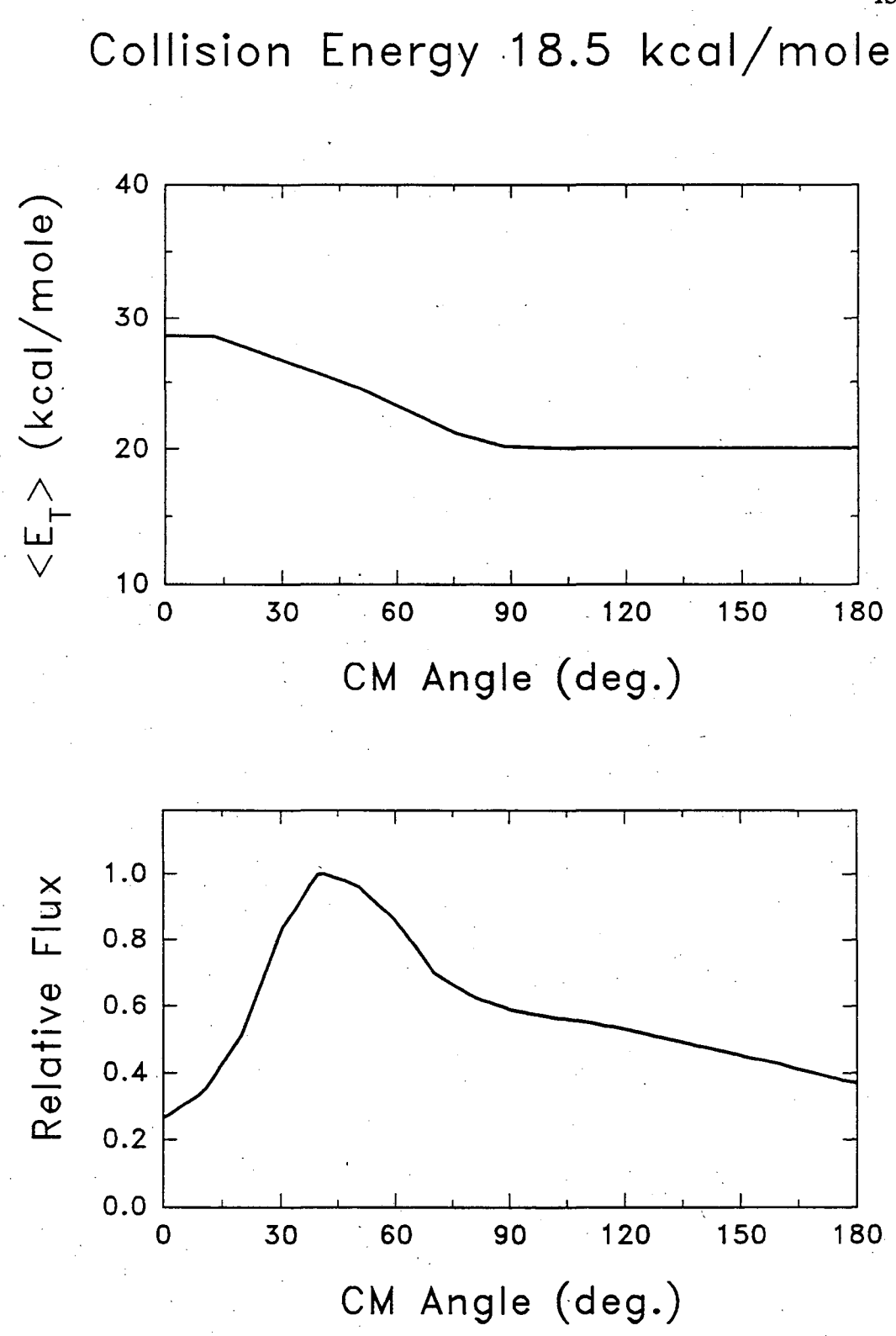
Collision Energy 18.5 kcal/mole
<E_T> (kcal/mole)
40
30
20
10
0
30
60
90
120
150
180
CM Angle (deg.)
Relative Flux
1.0
0.8
0.6
0.4
0.2
0.0
0
30
60
90
120
150
180
CM Angle (deg.)

Figure 9

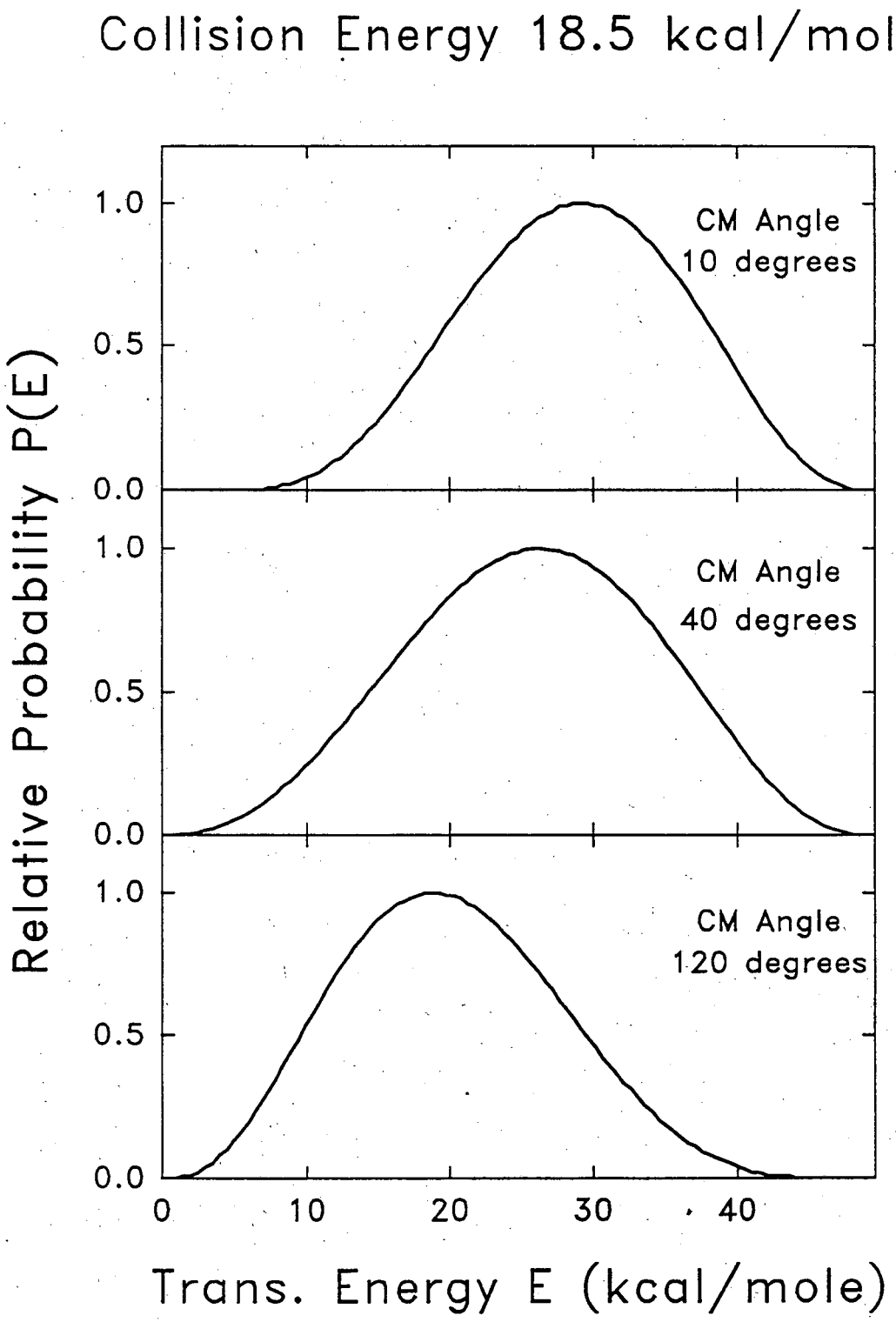
Collision Energy 18.5 kcal/mole
Relative Probability P(E)
1.0
0.5
0.0
CM Angle
10 degrees
CM Angle
40 degrees
CM Angle
120 degrees
0
10
20
30
40
Trans. Energy E (kcal/mole)

Figure 10

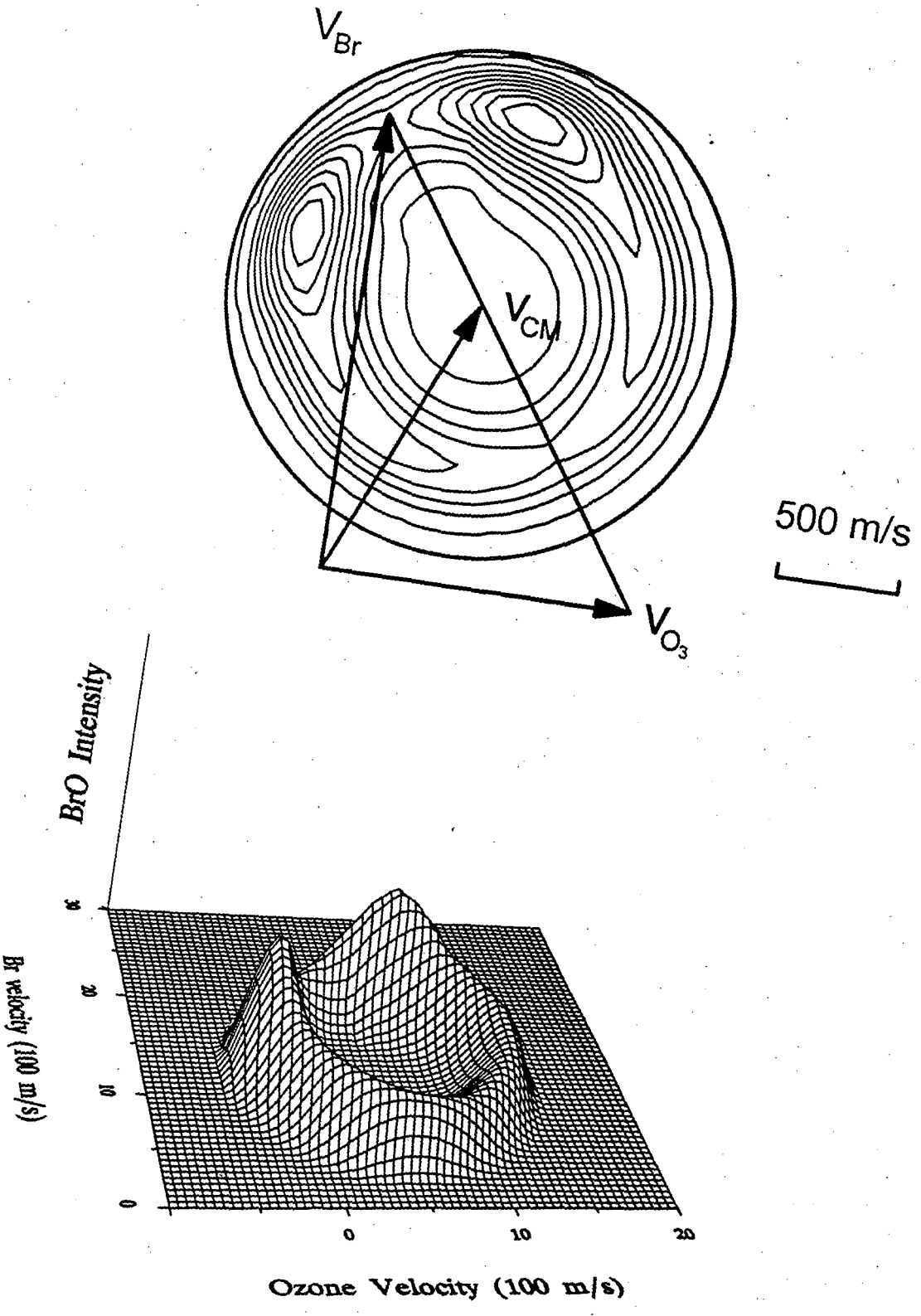
V_{Br}
V_{CM}
500 m/s
V_{O_3}
BrO Intensity
Br velocity (100 m/s)
0
10
20
Ozone Velocity (100 m/s)

Figure 11

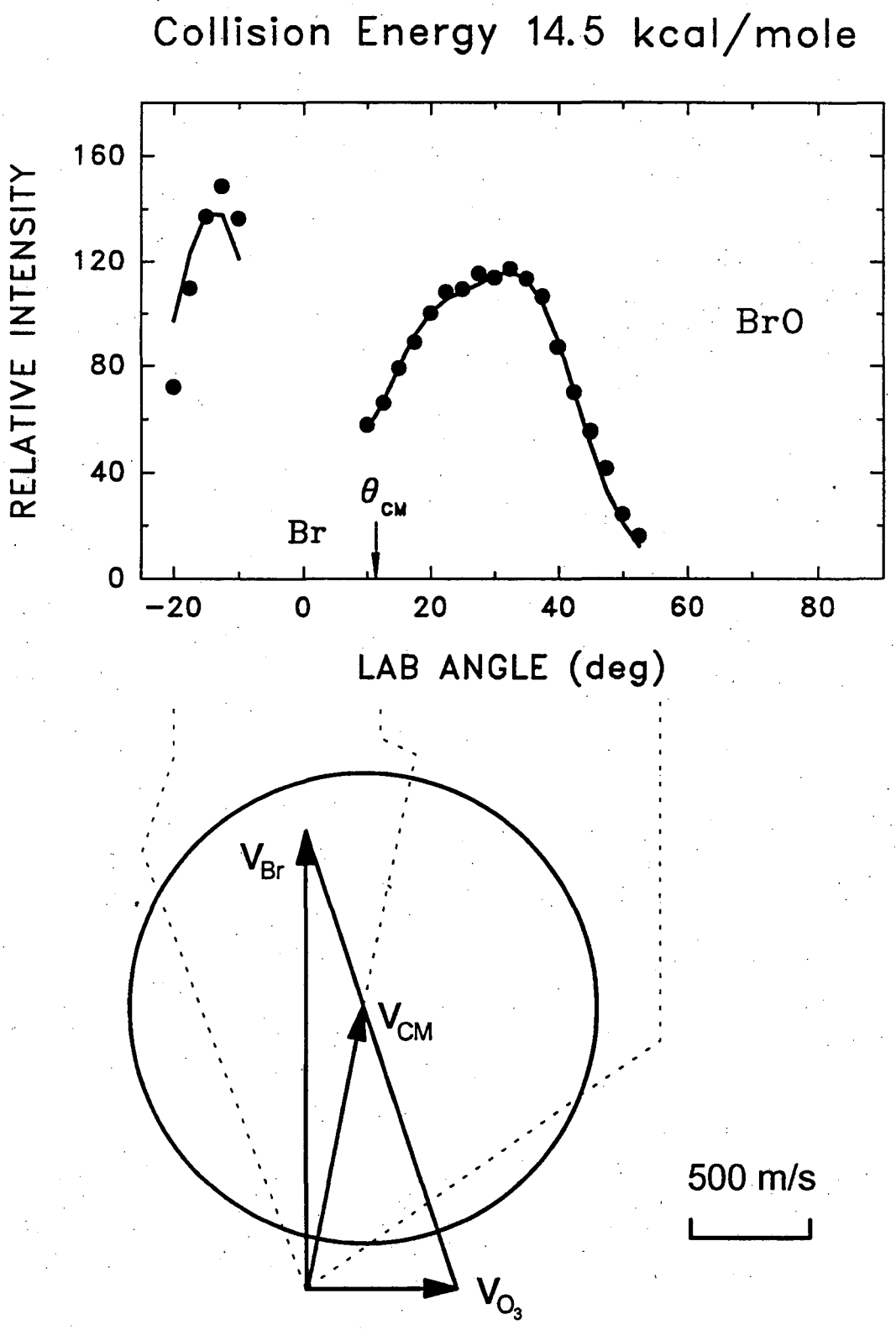
Collision Energy 14.5 kcal/mole
RELATIVE INTENSITY
160
120
80
40
0
−20
0
20
40
60
80
LAB ANGLE (deg)
BrO
Br
θ CM
V Br
V CM
V O3
500 m/s

Figure 12

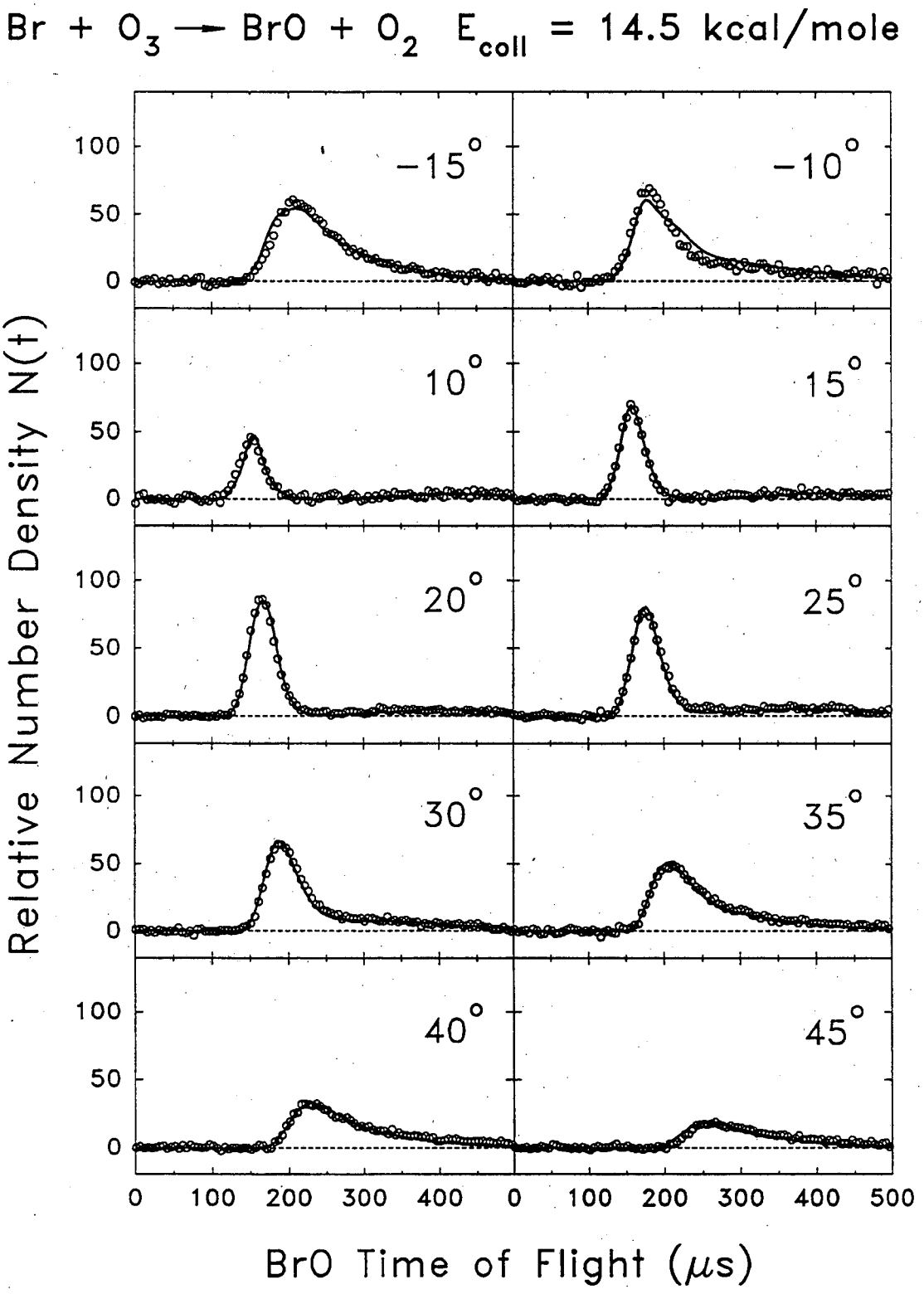
Br + O3 → BrO + O2 Ecoll = 14.5 kcal/mole
Relative Number Density N(t)
−15°
−10°
10°
15°
20°
25°
30°
35°
40°
45°
100
50
0
0 100 200 300 400 0 100 200 300 400 500
BrO Time of Flight (μs)

Figure 13

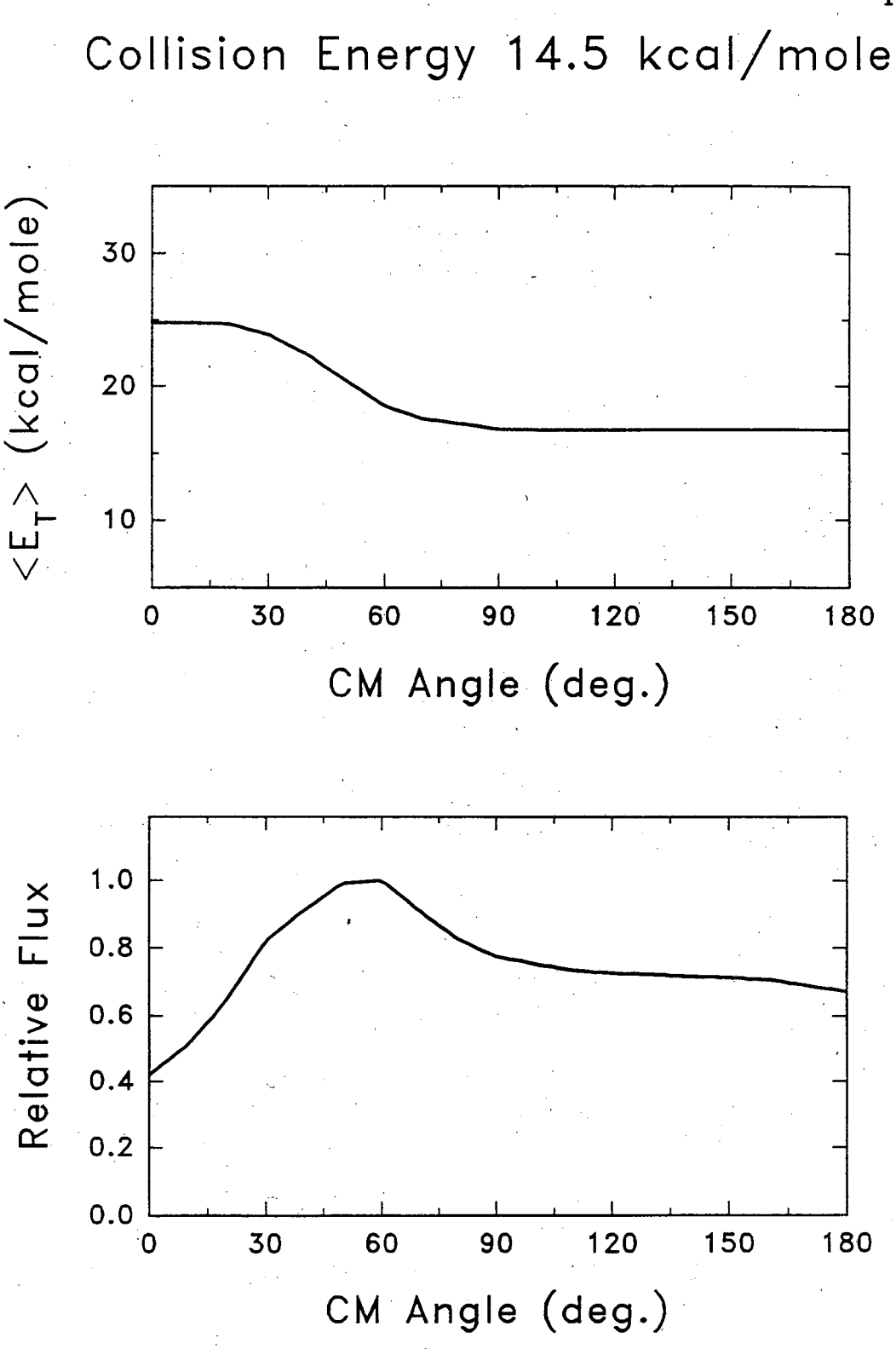
Collision Energy 14.5 kcal/mole
<E_T> (kcal/mole)
30
20
10
0
30
60
90
120
150
180
CM Angle (deg.)
Relative Flux
1.0
0.8
0.6
0.4
0.2
0.0
0
30
60
90
120
150
180
CM Angle (deg.)

Figure 14

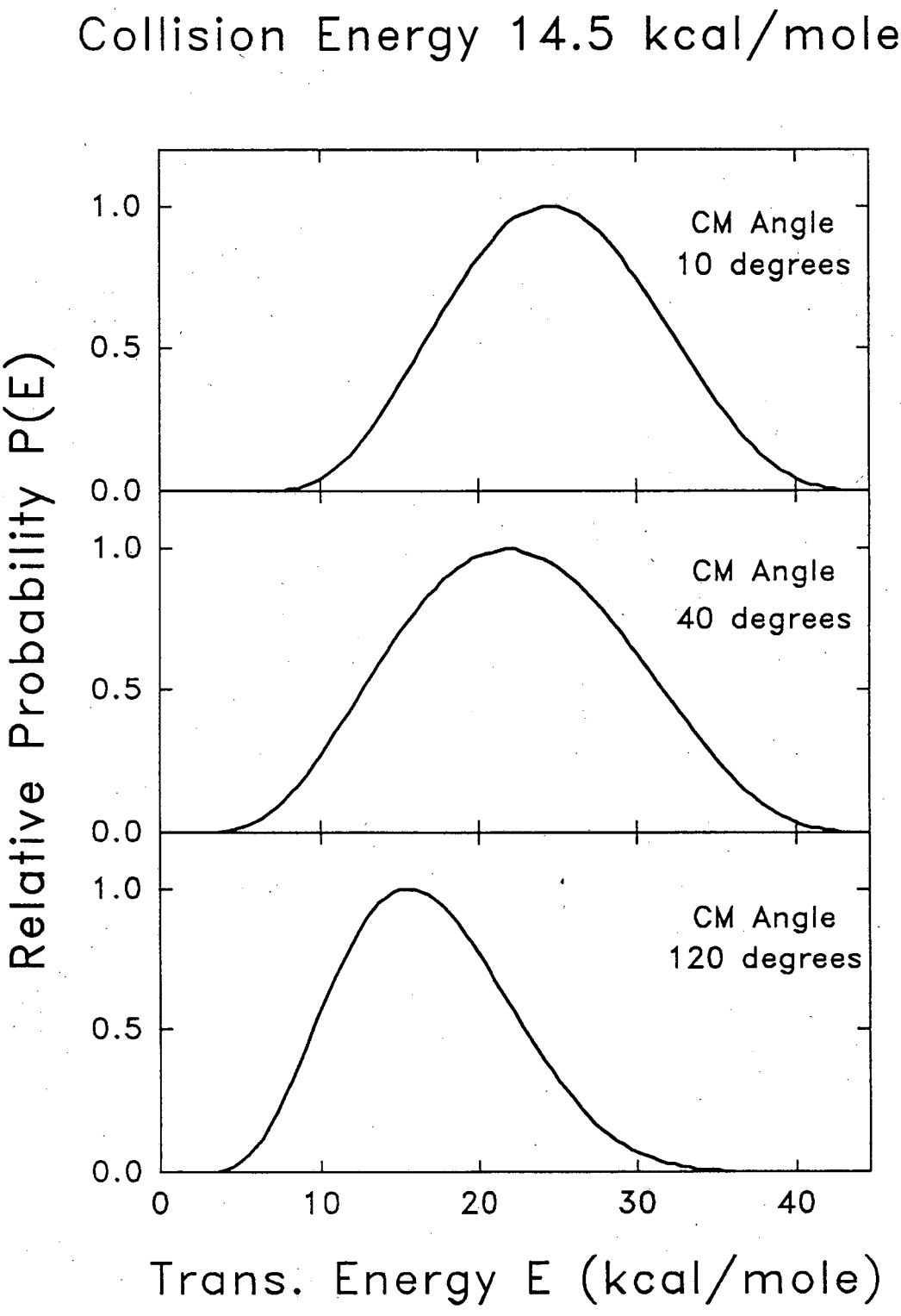
Collision Energy 14.5 kcal/mole
Relative Probability P(E)
1.0
0.5
0.0
CM Angle
10 degrees
CM Angle
40 degrees
CM Angle
120 degrees
0
10
20
30
40
Trans. Energy E (kcal/mole)

Figure 15

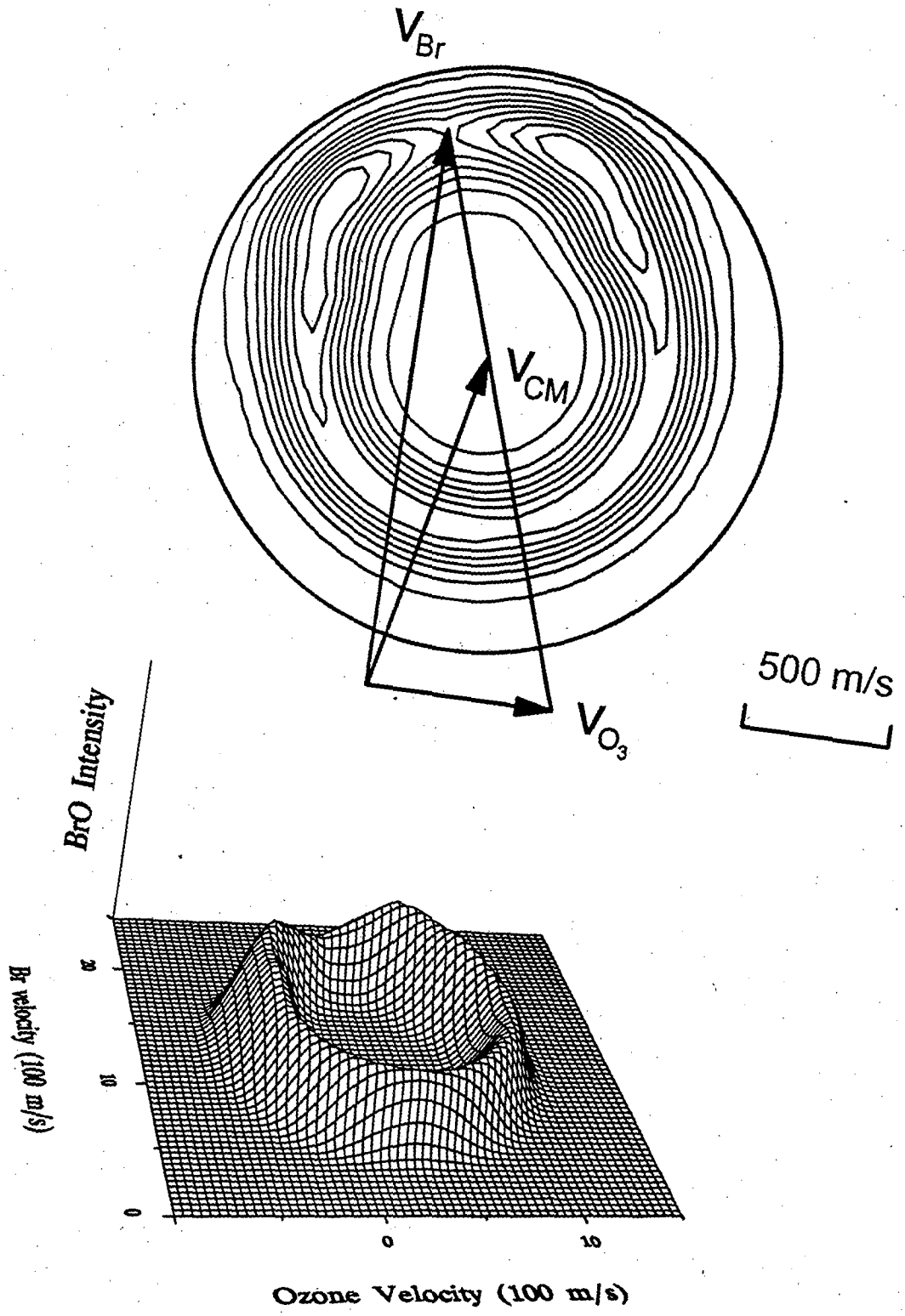
V_{Br}
V_{CM}
V_{O_3}
500 m/s
BrO Intensity
Br velocity (100 m/s)
0
10
0
10
Ozone Velocity (100 m/s)

Figure 16

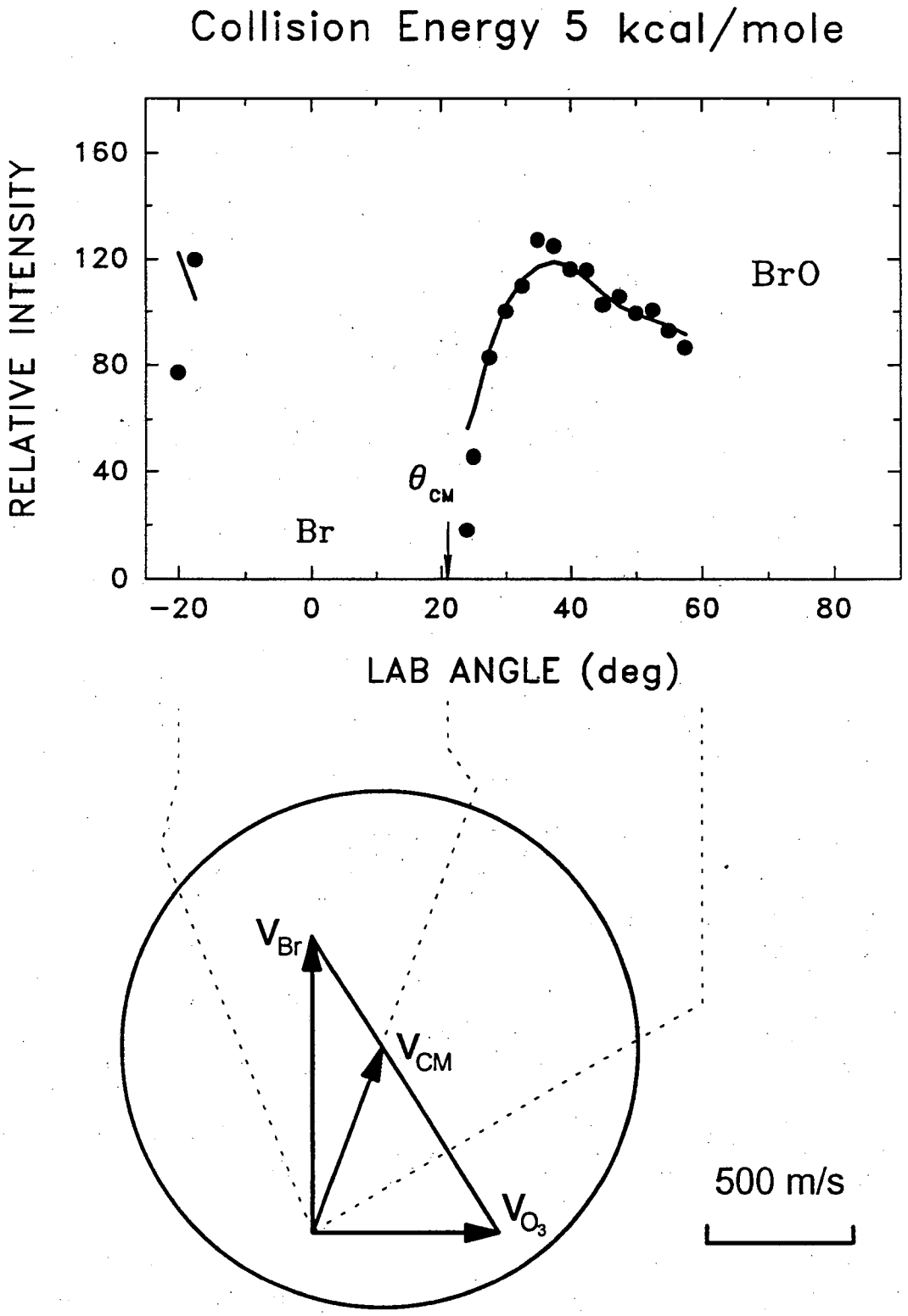
Collision Energy 5 kcal/mole
RELATIVE INTENSITY
160
120
80
40
0
−20
0
20
40
60
80
LAB ANGLE (deg)
BrO
Br
θ CM
V Br
V CM
V O3
500 m/s

Figure 17

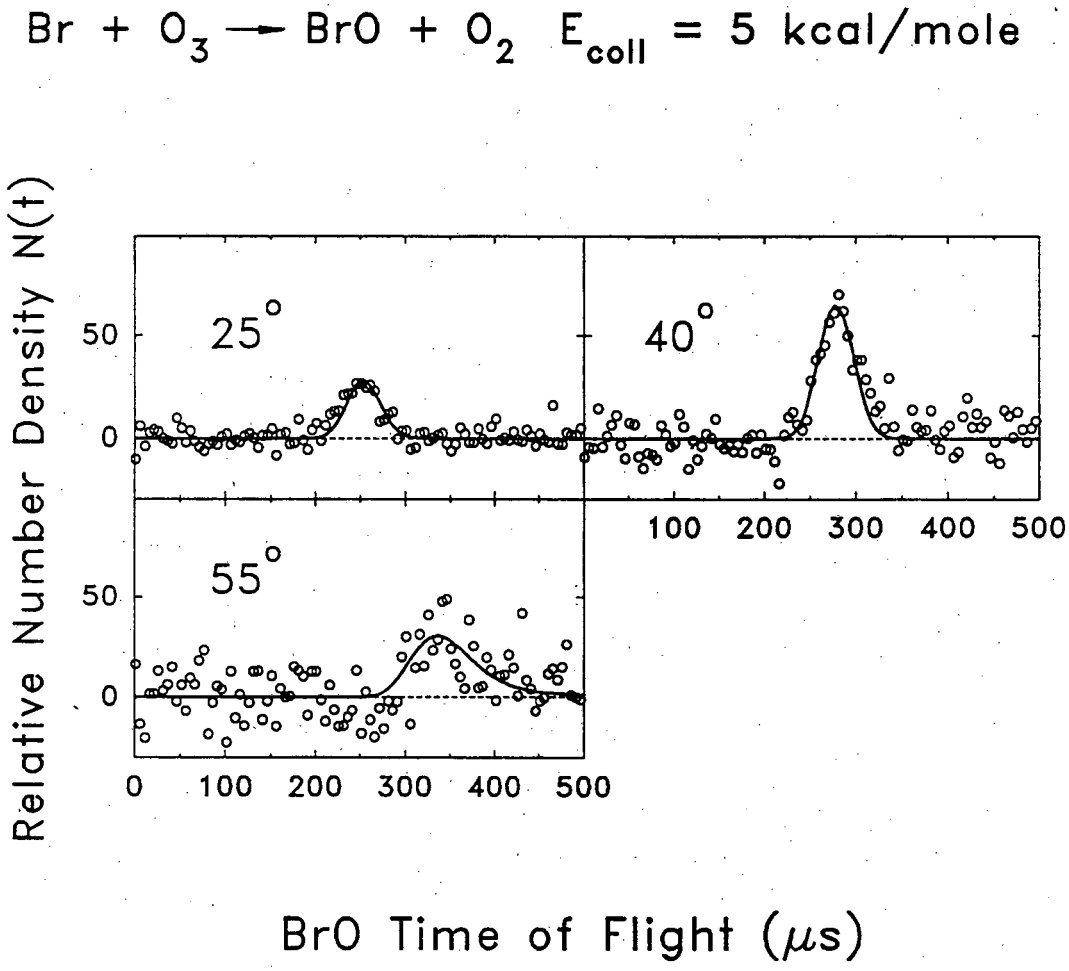
Br + O3 → BrO + O2 Ecoll = 5 kcal/mole
Relative Number Density N(t)
25°
40°
55°
50
0
100
200
300
400
500
BrO Time of Flight (μs)

Figure 18

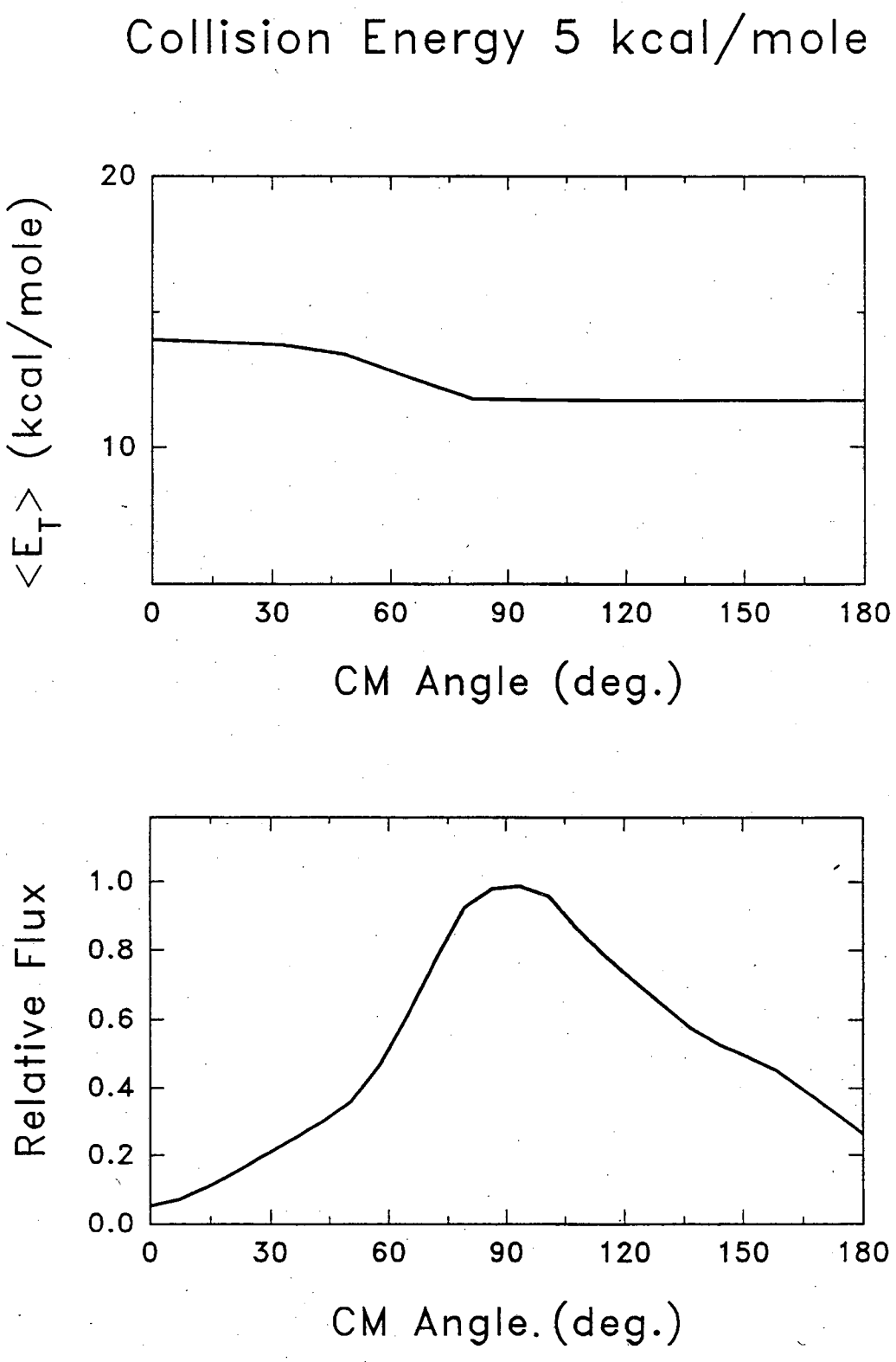
Collision Energy 5 kcal/mole
20
10
<E_T> (kcal/mole)
0
30
60
90
120
150
180
CM Angle (deg.)
1.0
0.8
0.6
0.4
0.2
0.0
Relative Flux
0
30
60
90
120
150
180
CM Angle. (deg.)

Figure 19

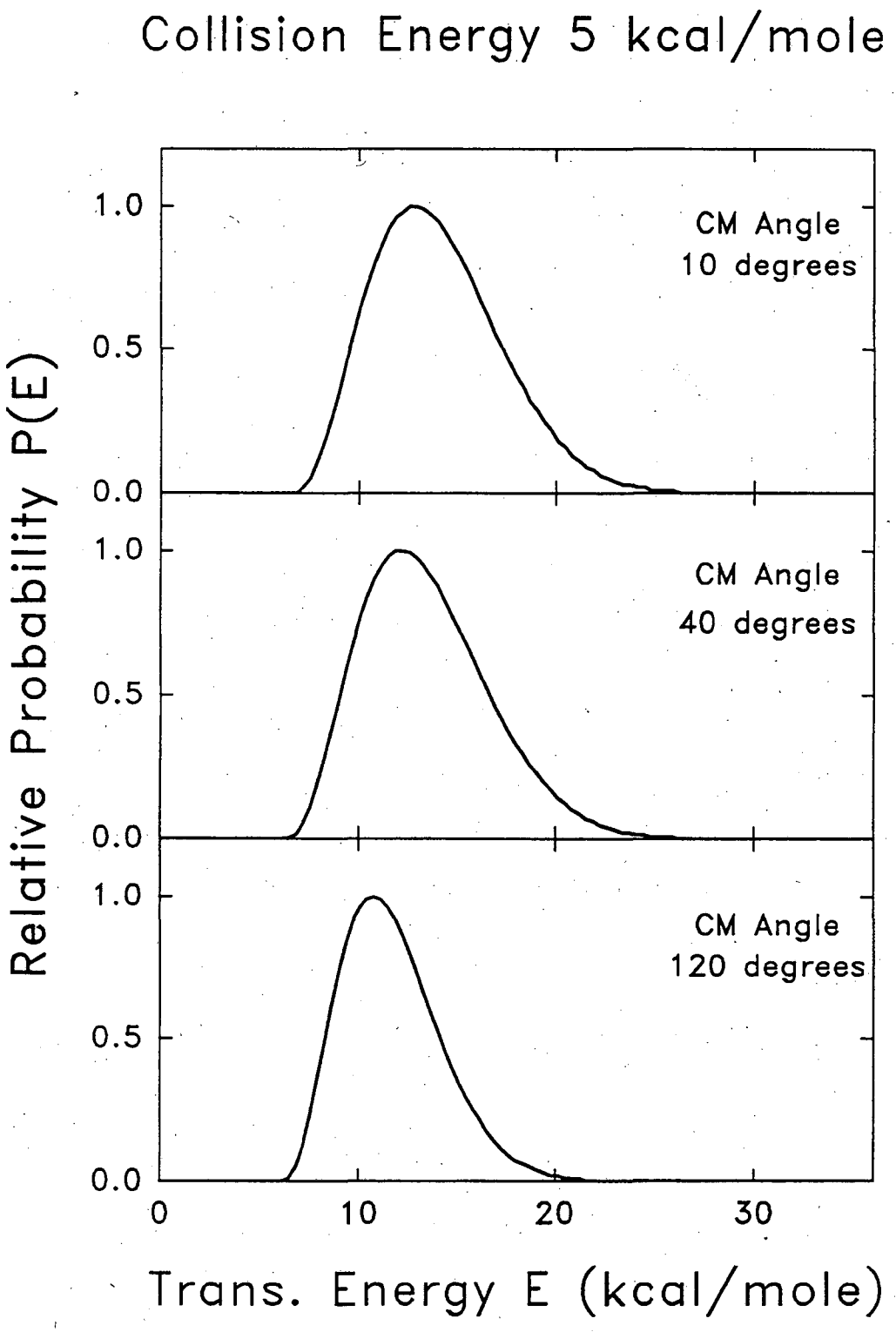
Collision Energy 5 kcal/mole
Relative Probability P(E)
1.0
0.5
0.0
CM Angle
10 degrees
CM Angle
40 degrees
CM Angle
120 degrees
0
10
20
30
Trans. Energy E (kcal/mole)

Figure 20

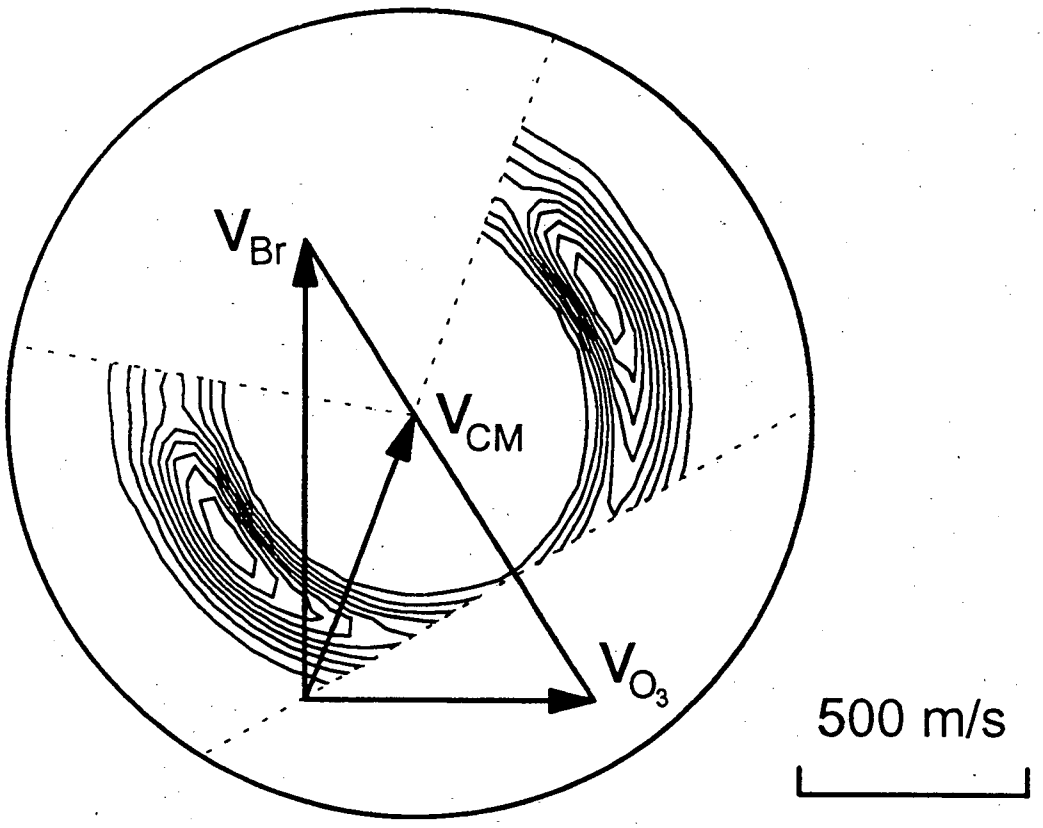

Figure 21

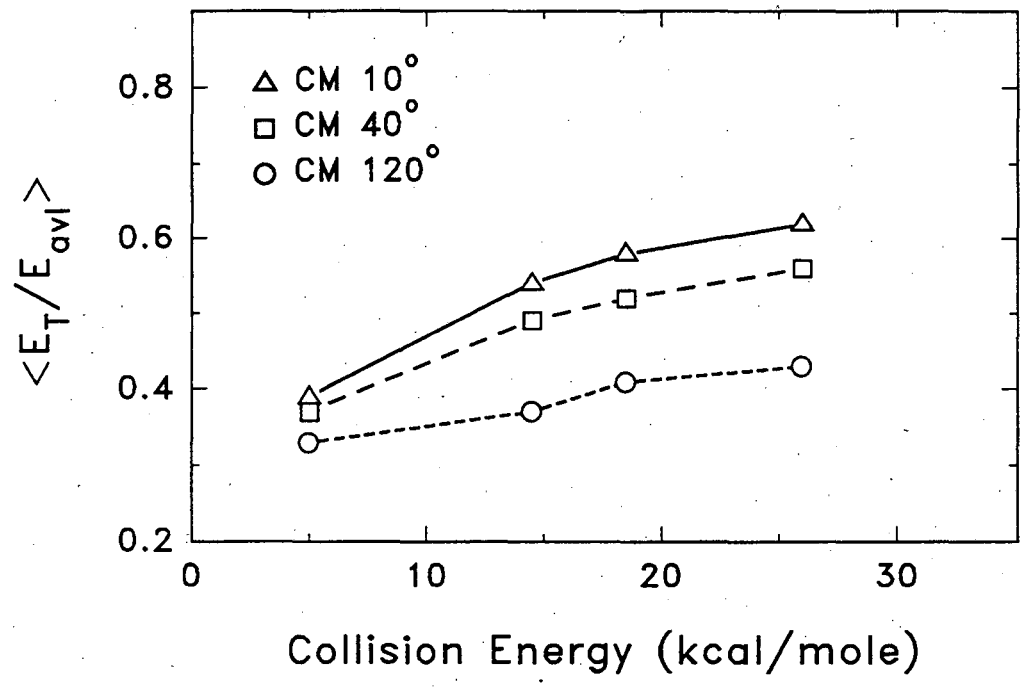
△ CM 10°
□ CM 40°
○ CM 120°
0.8
0.6
0.4
0.2
0
10
20
30
<E_T/E_avl>
Collision Energy (kcal/mole)

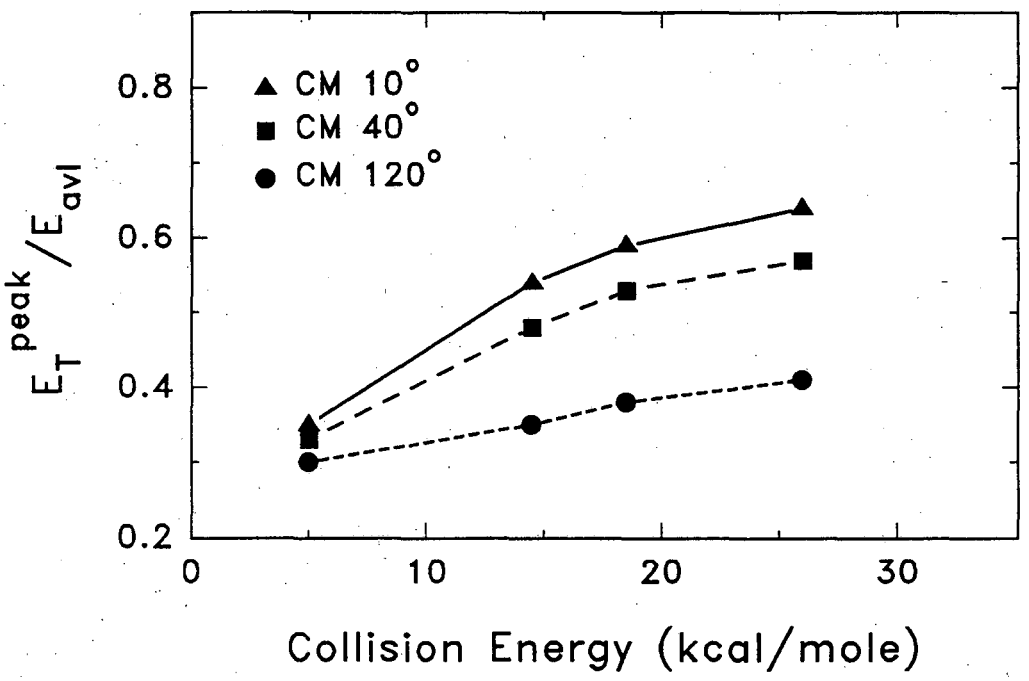
▲ CM 10°
■ CM 40°
● CM 120°
0.8
0.6
0.4
0.2
0
10
20
30
E_T^peak /E_avl
Collision Energy (kcal/mole)

Figure 22

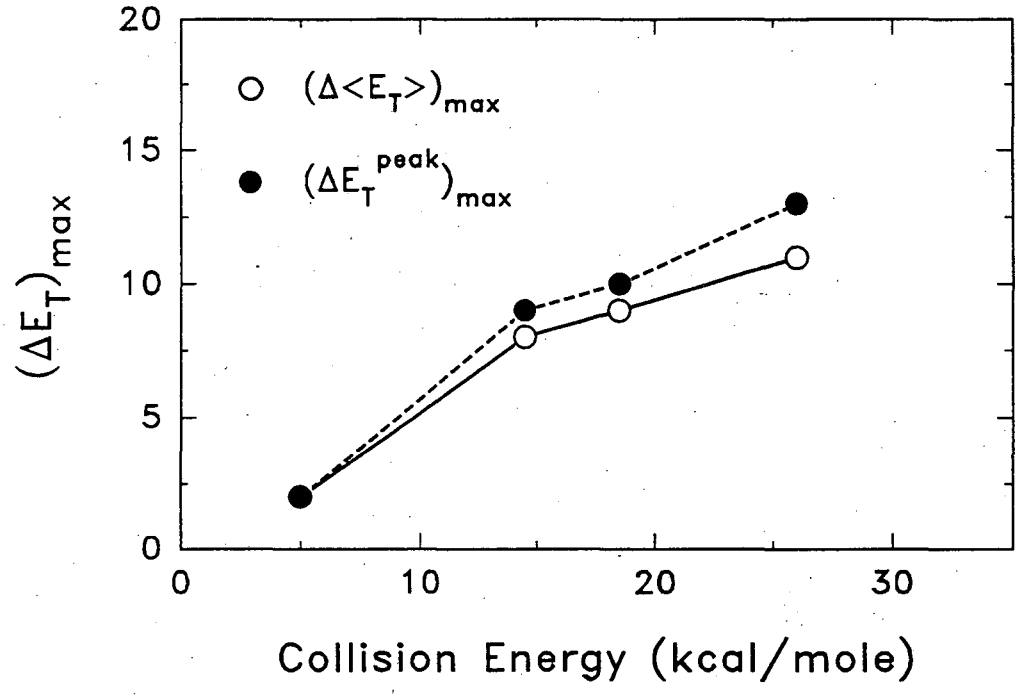
20
15
10
5
0
0
10
20
30
$(\Delta E_T)_{max}$
$(\Delta \langle E_T \rangle)_{max}$
$(\Delta E_T^{peak})_{max}$
Collision Energy (kcal/mole)

Figure 23

CHAPTER 4

CROSSED-MOLECULAR BEAM STUDY OF THE REACTION Cl + NO_2

ABSTRACT

The reaction of the chlorine atom with the nitrogen dioxide molecule has been studied using the crossed molecular beams technique at three different center-of-mass (CM) collision energies from 10.6 kcal/mole to 22.4 kcal/mole. The product center-of-mass angular distributions and translational energy distributions as well as the excitation function have been derived from the experimental measurements. The center-of-mass angular distributions have some forward-backward symmetry. The product translational energy release is generally large, and the average translational energy is over 50% of the total available energy. As the collision energy increases, the asymmetry in the angular distributions increases, and the fraction of the total energy released into translation slightly decreases. The excitation function is found to have a positive dependence on the energy; however, it does not increase rapidly with the energy. The reaction proceeds through a short-lived complex whose lifetime is less than a rotational period. The energy redistribution in the collision complex is probably not complete before the collision complex decomposes. As the collision energy

increases, the lifetime of the complex is shortened with respect to its rotational period; the forward distribution in the center-of-mass angular distribution increases; and the reaction mechanism seems to be on the transition to a direct reaction. The reaction path in which the Cl atom mainly attacks the oxygen atom instead of the nitrogen atom of the NO_2 molecule seems to be more consistent with the experimental results.

I. INTRODUCTION

The reaction $ClO + NO \rightarrow Cl + NO_2$, along with the reaction $HO_2 + NO \rightarrow OH + NO_2$, is of particular importance to the overall balance of odd oxygen in the stratosphere.[1] This is the reaction which interconnects the ClO_x family and the NO_x family in the atmosphere. The reverse association reaction $Cl + NO_2 + M$ produces both nitryl chloride ($ClNO_2$) and chlorine nitrite (ClONO), which are the possible reservoir species for the Cl atom or the ClO radical in the stratosphere.[1] Studying this reaction in detail certainly is helpful for the modeling of the stratospheric chemistry and for the understanding of the ozone destruction mechanism.

We probe the reaction mechanism by studying the reverse reaction $Cl + NO_2$ using the crossed molecular beams technique. The reaction $Cl + NO_2$ is endothermic by 8.6 kcal/mole (Fig. 1). At room temperature, only the association reaction channel is possible for the $Cl + NO_2$ approach under bulk conditions, while the reaction $ClO + NO \rightarrow Cl + NO_2$ occurs readily at thermal energy. Because of the wide use of the reliable halogen atom beam source[2,3] and the difficulty of generating intense ClO radical beam, we choose to study the reaction dynamics starting from the $Cl + NO_2$ side. The crossed molecular beams technique allows us to adjust the collision energy of the $Cl + NO_2$ reactive scattering. Using the seeded atomic and molecular beams, the collision energy could be much higher than thermal energy so the reactive channel $Cl + NO_2 \rightarrow$

ClO + NO could become open. The collision energy is adjustable so the dependence of the reaction cross section on the collision energy, i.e. the excitation function, could be probed for this endothermic reaction. We have carried out the crossed molecular beam studies on the Cl + O_3 and Br + O_3 reactions.[4,5] The ozone molecule is found to play the central role for determining the mechanism for these two reactions. We would like to study the reaction of another triatomic molecule NO_2, with the central oxygen atom in the ozone molecule replaced by the central nitrogen atom in the nitrogen dioxide molecule. We hope to compare the Cl + NO_2 reaction with the Cl + O_3 reaction, and we hope it might provide with us some more insight into the mechanisms of the atmospheric chemical reactions.

The Cl + NO_2 system has been previously studied from two approaches. When starting from the Cl + NO_2 side, because of the large endoergicity, only the association process is possible at room temperature under bulk conditions. There are two possible products in the association reaction:

$$Cl + NO_2 + M \rightarrow ClNO_2 + M \qquad (1)$$

$$\rightarrow ClONO + M \qquad (2)$$

The total reaction rate constant as well as the individual reaction rate constants have been measured.[6-11] Reaction (2) which produces chlorine nitrite ClONO was found to be faster than reaction (1) which produces nitryl chloride $ClNO_2$.[10]

Tevault and Smardzewski studied the matrix reaction of the chlorine atom with the NO_2 molecule.[12] Both the $ClNO_2$ and the ClONO species were detected by infrared absorptions; presence of a possible OClNO species was also suggested. There was indication that the ClONO species underwent intramolecular rearrangement to produce the more stable $ClNO_2$. The fact that both ClONO and $ClNO_2$ products were observed in the low temperature (~10K) matrix study implied that addition of the Cl atom to either the oxygen atom or the nitrogen atom on the NO_2 molecule had almost no energy barrier, which was typical for the radical and radical recombination reactions. The authors also pointed out that evidence for any Cl_2 + NO_2 reaction products was absent. Burrows, Tyndall and Moortgat recently obtained a Fourier transform infrared (FTIR) matrix isolation spectrum of a photolyzed gas-phase mixture of Cl_2 and NO_2.[13] Both ClONO and $ClNO_2$ were again observed, and ClONO was evidently of larger quantity than $ClNO_2$.

Using the FTIR method, Niki *et al.*[14] identified chlorine nitrite (ClONO) and nitryl chloride ($ClNO_2$) in gas phase as the reaction products of the Cl + NO_2 + M association reaction in the photolysis of Cl_2-NO_2 mixtures. A UV irradiation dissociated Cl_2, and the FTIR spectra of the products were taken during the irradiation time. From the data accumulated in a short time, 20s, an upper limit of 20% of the $ClNO_2$ yield in the primary process, correspondingly, a lower limit of 80% for the ClONO yield were determined. It was then concluded that the addition of the Cl atom to the O atom rather than the N atom of NO_2 was the

major reaction path, although this was thermochemically less favorable (see Fig. 1). Leu[9] found the branching ratio for the formation of the two possible isomers to be ClONO ($\geq 75\%$) and $ClNO_2$ ($\leq 25\%$) using a static photolysis system coupled with the FTIR spectrophotometer, which was in good agreement with Niki *et al.*'s measurements.[14] In the IR spectroscopy experiments, ClONO was found either to decompose heterogeneously on the surface or to rearrange to the more stable $ClNO_2$. Chang, Baldwin and Golden[15] calculated low-pressure limit rate constants for the three-body reactions (1) and (2) using Troe's method.[16] The ratio of the rate constants of reaction (1) and (2) was found to be 1 to 4, which was in excellent agreement with the experimental results of Niki *et al.*[14] and Leu.[9] In their simple rationale,[15] assuming similar association rate constants for forming the two types of energized reaction intermediates and similar deactivation rate constants of the two energized reaction intermediates to form the final stable products, they found that the overall rate constants for the final products were inversely proportional to the dissociation rate constants of the excited reaction intermediates back to the reactants. By virtue of the deeper well of the more stable molecule, the overall rate to form the more stable molecule was therefore expected to be smaller. Using the simplified RRK expression, and realizing that the larger entropy of ClONO resulted a smaller pre-exponential factor, the smaller overall production of the more stable $ClNO_2$ could be explained in this simple model. Lately, Patrick and Golden[17] calculated again the association rate constants for ClONO and $ClNO_2$ using Troe's method, and agreement with the

experimental results was still reached.

An extensive amount of work was also carried out on studying the kinetics of the ClO + NO reaction.[10, 18-23] It was well established that there was a negative temperature dependence of the reaction rate constant, i.e., a negative activation energy. In order to explain the negative temperature dependence, Leu and DeMore[20] proposed a mechanism involving formation of an intermediate complex. In this reaction, according the RRK theory, the dissociation rate constant of the intermediate complex back to the reactants, k_r, increased more rapidly with temperature than the dissociation rate constant of the intermediate complex to the products, k_p. The overall reaction rate constant therefore decreased with increasing temperature, i.e., showed a negative temperature dependence. However, this type of assumption required that k_r, the rate constant for dissociation of the intermediate into the original reactants, to be at least comparable in magnitude to k_p, the rate constant for dissociation of the intermediate into the products, i.e., $k_r \sim k_p$. According to the RRK theory, the rate constant could be expressed in the form $k = A(\varepsilon^+/E^*)^{s-1}$, where A is the pre-exponential factor, ε^+ is the excess energy above the critical configuration, E^* is the internal energy of the energized intermediate and s is the number of active vibrational modes. In order to obtain comparable k_r and k_p, the pre-exponential factor A_r should be much larger than A_p. However, it was difficult to confirm this condition. If the reaction intermediate was like chlorine nitrite ClONO, it was unclear how the pre-exponential factors for the ClO + NO and Cl + NO_2 channels

could be very different.

Menon and Sathyamurthy[24] deconvoluted the rate constant data for the ClO + NO → Cl + NO_2 and BrO + NO → Br + NO_2 reactions using a new generalized Lloyd's secant method to find the excitation function, i.e., the energy dependence of the reaction cross section σ(E). They found that, essentially, a model of an almost zero threshold energy and a sharply decaying excitation function ($\sigma = A \cdot E^{-b}$, $b > 0.5$) seemed to provide an adequate explanation of the negative activation energies for the ClO + NO → Cl + NO_2 and BrO + NO → Br + NO_2 reactions. However, this explanation fitted into the mechanism suggested by Leu and DeMore.[20] If indeed an intermediate complex of certain stability and lifetime was involved in the reaction, a decaying excitation function for the exoergic reaction ClO + NO → Cl + NO_2 was quite straightforward according to the RRKM theory.

Phillips[25,26] carried out approximate, quasi-classical trajectory calculations of the rate constants for a number of bimolecular radical-radical reactions, including the ClO + NO reaction, over the temperature range 10-600 K. The potential energy surface was chosen such that the reaction proceeded through a configuration corresponding to a bound complex, which was typical for gas-phase radical-radical reactions. The intermediate complex was expected to have a life-time comparable to or longer than the rotational period. The calculated rate constants had relatively good agreement with the experimental data. This model was also consistent with the mechanism proposed by Leu and DeMore.[20]

There is some information about the UV-photodissociation of the stable nitryl chloride $ClNO_2$ molecule.[27-30] The transitions at 248 nm and 308 nm of the $ClNO_2$ molecule are located on the NO_2 moiety. The major products of the $ClNO_2$ photodissociation at the two laser wavelengths were Cl atom plus ground and electronically excited NO_2 molecules, while very minor NOCl + O channel was observed.[27-30] In the photofragment translational spectroscopy study by Covinsky and Lee,[30] no ClO product was detected. The Cl + NO_2 products were likely coming from the repulsive excited electronic states, because the angular distribution of the products was polarized and the product translational energy release was quite large.[30] Thermal dissociation of the $ClNO_2$ molecule from the ground electronic state into Cl + NO_2 was also extensively studied.[31-34] The ClO + NO channel is not open at thermal energy, besides, the Cl + NO_2 channel is strongly statistically favored. For the chlorine nitrite ClONO molecule, however, no information for the thermal dissociation is available. The UV-absorption spectrum of ClONO was measured, and two likely dissociation processes, ClO + NO channel and Cl + NO_2 channel, were also pointed out;[35] however, no work was done to find the exact product yields. Overall, according to the statistical theory, with high enough vibrational energy at which both ClO + NO channel and Cl + NO_2 channel are open, the dissociation of the less stable ClONO into the ClO + NO product channel should be more likely than that of the more stable $ClNO_2$ into the ClO + NO product channel.

The reaction Cl + NO_2 → ClO + NO is endoergic (ΔH_0° = 8.6 kcal/mole).

The decay of the reaction intermediate complex into products ClO and NO is less statistically favored than the decay of the intermediate into the reactants Cl and NO_2. The cross section for an endoergic reaction typically displays a positive dependence on the collision energy, i.e., the excitation function increases with the collision energy. By studying the translational energy dependence of the reaction cross section, i.e. the excitation function, as well as the product angular distribution and translational energy distribution for the endoergic reaction channel, we hope to gain some more insight into the dynamics of this endoergic reaction. The powerful crossed molecular beams technique allows us to study the chemical reactions under single collision conditions and allows us to adjust the collision energy to probe the translational energy dependence of the reaction cross section. We have carried out the crossed molecular beam study of the reaction $Cl + NO_2 \rightarrow ClO + NO$ at three collision energies 10.6 kcal/mole, 16.0 kcal/mole and 22.4 kcal/mole, which are 2.0 kcal/mole, 7.4 kcal/mole and 13.8 kcal/mole, respectively, above the reaction endoergicity or the reaction threshold (The reaction barrier for the reverse reaction $ClO + NO \rightarrow Cl + NO_2$ was expected to be zero.[24] In general, the reaction barriers for the radical-radical reactions are very small[36,37]). The product angular distribution and translational energy distribution in the center-of-mass system are derived from the experimental data for each collision energy. With all the information from the crossed molecular beam study of the $Cl + NO_2 \rightarrow ClO + NO$ reaction, we hope to understand more about the reaction mechanism of this important atmospheric chemical reaction and the

mechanism of its reverse reaction $ClO + NO \rightarrow Cl + NO_2$.

II. EXPERIMENTAL

The universal crossed molecular beam apparatus used for the present study has been described in detail previously.[38,39] The two-stage differentially pumped supersonic chlorine atomic and nitrogen dioxide molecular beams were crossed at 90° in the main collision chamber held at a vacuum of about 10^{-7} torr. The scattered products were detected by a triply differentially pumped mass spectrometric detector which rotated in the plane of the two beams with respect to the center of collision. The mass spectrometric detector is composed of a Brink's[40] type electron impact ionizer, an Extrel quadrupole mass spectrometer, and a scintillation-based Daly ion detector.[41] The typical electron energy was 180 eV, and the typical ion energy was 90 eV. The size of the collision zone was typically 3 x 3 x 3 mm^3, and under normal conditions the whole collision zone was viewed by the detector.

The chlorine atom beam was produced by thermal dissociation of Cl_2 in rare gas mixtures in a resistively heated high-density graphite[42] nozzle source designed in this laboratory by Valentini, Coggiola and Lee.[2,3] Mixtures of 10% Cl_2 in argon, 10% Cl_2 in 8% argon and 82% helium, 5% Cl_2 in helium were used as seeded gas mixtures for this experiment. The high-temperature graphite source

had a nozzle of 0.12 mm diameter and was heated to approximately 1400 °C. A conical graphite skimmer with an orifice diameter of 1.0 mm was positioned 7.6 mm away in the downstream of the nozzle. A set of collimating slits on the differential wall further defined the beam to a 3° full width and 3 mm x 3 mm size in the collision region. The total stagnation pressure of the beam was typically 800-1100 torr measured outside of the machine right before the gas mixture entered the molecular beam source. A reasonable fraction of Cl_2 thermal dissociation had been observed by a direct measurement of $[Cl]/[Cl_2]$ ratio in the beam with the Cl^+ signal corrected by subtracting the contribution from the undissociated Cl_2. The fraction of Cl_2 dissociation was smaller than in our previous experiment[4] because a different graphite tube was used and the source was operated at a lower temperature. The residual Cl_2 species was not a problem in this experiment, which we will discuss in detail later. Heating power for the high-temperature graphite source had been carefully maintained constant through out the period of the experiment to ensure a stable Cl atom beam with stable beam velocity.

The NO_2 atom beam was produced by passing 400 torr of helium through solid nitrogen dioxide (NO_2/N_2O_4) in a glass bubbler held at a constant temperature bath (-20°C to -35°C, FTS Multicool System, model number MC-4-60A-1). The seeded NO_2 molecular beams were typically composed of 10-20% NO_2 in He. NO_2/N_2O_4 used in the experiment was from Matheson; it was transferred into the glass bubbler without any further purification in the open air

inside a ventilation hood. Any NO impurity in the reagent was quickly oxidized to NO_2 during the transferring process. Furthermore, NO_2 reagent in the bubbler was purged by the carrier gas for at least half hour, so the volatile impurity such as NO, if there were still any, would be minimized for the following reactive scattering experiment. The NO_2/He gas mixture was expanded through a 0.12 mm diameter nozzle into the source region. The nozzle tip was heated to around 200°C to minimize the formation of N_2O_4 and larger clusters.[43] No N_2O_4 and larger clusters were detected in the molecular beam with the mass spectrometric detector looking directly into the beam. The NO_2 molecular beam was skimmed by a stainless steel skimmer of 0.5 mm orifice with a nozzle-skimmer distance of 7.6 mm. The beam was further defined by the collimating slits on the differential wall before entering the main chamber, this gave 3° beam full width and 3 mm x 3 mm beam size in the collision region.

The velocity distributions of Cl and NO_2 beams were measured with the time-of-flight (TOF) technique. A 17.8 cm diameter stainless steel wheel with four 0.78 mm slots equally spaced around its circumference was installed in front of the detector. The wheel was spun at 300 Hz speed and the modulated beam was sampled straight into the detector through a 0.18 mm aperture. A home-made 4096-channel multichannel scaler (MCS)[44] interfaced with a computer accumulated the data. The flight path from the wheel to the effective center of the ionizer was experimentally determined to be 29.8 cm. After the correction of the experimental time-of-flight spectra using the appropriate offset time (ion flight time, wheel

trigger time offset etc.), the Cl atom and NO_2 molecular beam velocity distributions were obtained from fitting the experimental time-of-flight spectra using program KELVIN[45,46] which convoluted over the known apparatus functions to determine the beam speed (v) and speed ratio ($v/\Delta v$). The typical beam parameters are listed in Table 1.

Product TOF spectra from the reactive scattering were measured using the cross-correlation method.[47] A 17.8 cm diameter cross-correlation wheel was mounted in front of the detector to replace the four-slot single-shot wheel and was spun at 392 Hz. The wheel has two identical 255-bit pseudorandom sequences of open and closed slots and was photoetched by PCM Products based on Lee group specifications. When spun at 392 Hz, the wheel gives nominal 5 μs/channel time resolution in the TOF spectra and 50% transmission. The detector was stationed at a particular laboratory angle to measure the product velocity distribution. Product ClO was monitored. The mass spectrometer was set at m/e = 51 with low resolution to detect more abundant $Cl^{35}O$ isotope species while a small amount of $Cl^{37}O$ might have been collected as well. Total counting times for the time-of-flight spectra ranged from 2 to 8 hours per angle. Finally, we have to point out, when measuring ClO time-of-flight spectra near the Cl beam (within ~10° of the Cl beam), small amount of slow effusive background from the Cl beam source showed up in the spectra. To correct this background, ClO time-of-flight spectra near the Cl beam with the NO_2 beam on and with the NO_2 beam off were measured, and the corrected ClO product time-of-flight

spectra were obtained by simply subtracting the NO_2 beam-off spectra away from the NO_2 beam-on spectra at the same laboratory angle. However, there was only one time-of-flight spectrum (for laboratory angle 10°, at E_{coll} = 22.4 kcal/mole) that needed to be corrected for this background in the whole experiment.

ClO product angular distributions were measured by modulating the NO_2 beam using a 150 Hz tuning folk chopper (Bulova) with the time-of-flight wheel removed. At a particular angle, the signal with NO_2 beam on and the signal with NO_2 beam off were recorded in two separate channels in a dual-channel scaler (Joerger, model VS) with a appropriate gating originated from the tuning folk chopper. Subtracting beam-off signal from beam-on signal at a particular laboratory angle simply gave the net reactive signal at that angle. To correct for long-term drifts of the experimental conditions, a reference angle (typically the one with near maximum intensity) was chosen. After a sequence of measurements at every 6-10 angles, data was taken at this reference angle twice. The set of data was then normalized by taking a linear interpolation based on the time at which a given angle was measured and the time between normalization measurements. Counting time at each angle in each normalization sequence ranged from 1 min to 4 mins, while the total counting times per angle summed from all the normalization sequences ranged 8-40 mins.

To reduce the background species entering into the detector, a cryogenic copper cold panel was placed against the differential wall inside the main scattering chamber and facing the detector. It was cooled by being tightly

clamped to the liquid-nitrogen cooled cold shield in the scattering chamber. Its temperature was typically about 90 K, which was monitored by a low temperature sensor (LakeShore). It was effective in reducing the ClO background for both time-of-flight and angular measurements.

In order to obtain relative cross section for the reaction at different collision energies, we need to scale the product number densities at different energies and normalize them with the relative reactant flux factor $n_{Cl}n_{NO_2}v_{rel}$ as well. To account for changes of the experimental conditions such as reactant flux, all these scaling and normalization factors were measured in one day's experiment, which we will discuss in detail later.

Because an intermediate complex is likely involved in this endoergic reaction $Cl + NO_2 \rightarrow ClO + NO$, and because statistically the dissociation rate constant of the intermediate complex back into the reactants is larger than that into the products, the time-of-flight spectra and laboratory angular distribution of the Cl atom, especially at wide scattering angles due to the so-called "failed reaction", would give rich information about the intermediate complex. We therefore have made the measurement of time-of-flight spectra of Cl atom. Because of the significant amount of undissociated Cl_2 in the Cl beam, the elastically and in-elastically scattered Cl_2 molecule by NO_2 also gave rise to m/e 35 signal; however, the contribution of m/e 35 signal from the small amount of ClO product was negligible. Because of the contribution from the undissociated Cl_2 molecule, it was virtually impossible to measure the Cl angular distribution

using a tuning fork. Time-of-flight spectra of both the Cl atom (m/e = 35) and Cl_2 molecule (m/e = 70) were measured at the same laboratory angle. The TOF peaks of Cl and Cl_2 were fairly well separated, especially in the wide scattering angles. The TOF peak in the m/e 70 spectra from the Cl_2 in/elastic scattering was carefully scaled to that in the m/e 35 spectra corresponding to the contribution from Cl_2 at the same laboratory scattering angle, it was then subtracted from the m/e 35 spectra to give the corrected time-of-flight spectra of the Cl atom from in/elastic scattering off the NO_2 molecule. The Cl angular distribution was obtained by the integration over the areas of the corrected Cl time-of-flight peaks in the spectra from different laboratory angles. We could double check this procedure by taking the time-of-flight spectra of Ar in the mixture of 10% Cl_2, 8% Ar and 82% He. Because Ar and Cl have similar mass, their in/elastic scattering spectra with NO_2 were expected to be almost identical. Indeed, the measured Ar time-of-flight spectra were very similar to the corrected time-of-flight spectra of Cl atom at the same laboratory angle.

III. RESULTS AND ANALYSIS

The product angular distributions and time-of-flight spectra were fitted using a forward-convolution method. The FORTRAN program was an improved version based on the previous program.[48,49] The goal of the analysis is to find the

product angular and translational energy distributions in the center-of-mass frame. It starts with a trial form for the center-of-mass product flux-energy distribution, i.e. the center-of-mass double differential cross section (DDC). In this case, the center-of-mass product flux-energy distribution $I_{CM}(\theta, E_T, E_c)$ (where θ is the center-of-mass angle, E_T is the product translational energy and E_c is the collision energy) is assumed to have an energy-angle separable form and expressed as a product of $T(\theta)$, the center-of-mass product angular distribution, and $P(E_T, E_c)$, the center-of-mass product relative translational energy distribution, and $S_r(E_c)$, the collision energy dependence of the relative reaction cross section, i.e., the excitation function:

$$I_{CM}(\theta, E_T, E_c) = T(\theta) \cdot P(E_T, E_c) \cdot S_r(E_c) \qquad (3)$$

The program transforms this trial center-of-mass flux distribution into the laboratory frame flux distribution using the transformation Jacobian: $I_{Lab}(\Theta,v) = I_{CM}(\theta,u) \cdot v^2/u^2$ and generates the laboratory frame angular distribution and time-of-flight spectra for each experimental laboratory angle after convoluting over the measured beam velocity distributions and the known apparatus functions such as the spread of collision angles, the detector acceptance angle and the length of the ionizer. The program scales the calculated spectra to the experimental data and makes the comparison. This is repeated so as to optimize the $T(\theta)$, $P(E_T, E_c)$ and $S_r(E_c)$ iteratively until a best fit for the experimental data is found.

A RRK functional form was chosen for $P(E_T, E_c)$ for the convenience of parameter adjustment. In this functional form, $P(E_T, E_c)$ is expressed in the following:

$$P(E_T, E_c) = (E_T - B)^p (E_{avl} - E_T)^q \qquad (4)$$

where E_{avl}, $E_c - E_0$, is the total energy available to the products. The threshold energy E_0 is taken to be the reaction endoergicity (ΔH_0° = 8.6 kcal/mole) because the energy barrier for the reverse reaction is expected to be negligible .[24,36,37] $T(\theta)$ was chosen in a point form. The parameters p, q and B in the $P(E_T, E_c)$ form as well as $T(\theta)$ are optimized to give the best fit to the experimental data.

In the crossed molecular beam experiment, the spread in beam velocities and intersection angles gives rise to a spread in relative velocities and hence in collision energies. Each beam velocity and intersection angle combination corresponds to a different kinematic configuration (Newton diagram) over which the calculated time-of-flight spectra and the angular distribution must be averaged. Since the reaction cross section of an endoergic reaction is typically strongly dependent on the collision energy, each Newton diagram is also weighted according to its collision energy E_c using the excitation function $S_r(E_c)$ (see Eqn. 3). The most probable energies, corresponding to the most probable kinematic configurations, are listed in Table 1. The values of the relative collision

energy spread $\Delta E_c/E_c$ for different collision energies are also listed in Table 1. For an endoergic reaction, the maximum translational energy of the products depends strongly on the collision energy E_c. Therefore, a $P(E_T, E_c)$ with a unique value of E_{avl} is used for each kinematic configuration in the analysis. Each unique $P(E_T, E_c)$ is normalized to its own area so that $\int P(E_T, E_c)dE_T = 1$.

We obtain the excitation function $S_r(E_c)$ in the following way. Initially, we use a constant as the trial functional form for excitation function $S_r(E_c)$ and make reasonable fits to the experimental data for the three nominal collision energies. The relative center-of-mass reaction cross sections S_r for the most probable collision energies are then obtained by integrating the CM frame product flux at the most probable energies:

$$S_r(E_c) = 2\pi \int_0^\infty \int_0^\pi P(E_T, E_c)\, T(\theta) \sin\theta \, dE_T \, d\theta \, (E_c) \qquad (5)$$

The calculated $S_r(E_c)$ values are used as the initial multiple-point excitation function. The Newton diagrams are weighted with this trial excitation function $S_r(E_c)$. Iteratively this trial excitation function $S_r(E_c)$ is modified to fit the relative ratios of the laboratory angular distributions at the different nominal collision energies.

The experimental laboratory angular distribution $N_{exp}(\Theta)$ is scaled and normalized before being used for the fitting of the excitation function. Because

the product laboratory angular distributions at different collision energies were measured in a period of several weeks, there might have been certain fluctuations in both the Cl beam intensity and the NO_2 beam intensity. In order to compare the integrated product flux at different collision energies, one day was spent on measuring the intensities of both beams and the ClO product signals at two laboratory angles at each collision energy for which a complete product laboratory angular distribution was already measured. The signals at the two angles were divided by the corresponding signals from the complete angular distributions, which gave two scaling factors. The experimental laboratory angular distribution $N_{exp}(\Theta)$ at each collision energy was then scaled by the average of the two corresponding scaling factors and further normalized by the data counting time. Finally, to account for changes in the reactant flux in the different beam conditions for the different collision energies, the experimental angular distributions were further normalized by relative reactant flux factors $n_{Cl}n_{NO_2}v_{rel}$, where n_{Cl} is the number density of the Cl beam, n_{NO_2} is the number density of the NO_2 beam, and v_{rel} is the relative velocity. Relative reactant number densities were obtained by directly measuring the reactant count rates with the detector directly looking into each beam, respectively. This was straightforward for the number density of the NO_2 beam; however, extra measurement was needed for determining the number density of the Cl beam. Because of the undissociated Cl_2 in the Cl beam, some of the measured Cl^+ (m/e = 35) signal was from the Cl_2 molecule at the high operational nozzle temperature. The ratio of Cl^+/Cl_2^+ was

measured at low nozzle temperature (~200°C, for eliminating Cl_2 dimer and other larger clusters) where the Cl^+ signal could only come from the dissociative ionization of the Cl_2 molecule. This measurement was taken at the same mass spectrometer resolution as for the high temperature measurement. It was then assumed the similar dissociative ionization pattern for the Cl_2 molecule at high temperature. The corrected Cl atom number density was then obtained by subtracting the calculated Cl^+ contribution from the Cl_2 molecule away from the total original Cl^+ count rate.

After the above scaling and normalization procedures, the experimental laboratory angular distributions $N_{exp}(\Theta)$ for different collision energies, with the same relative product signal scale and data counting time, as well as with the normalized relative reactant flux, were finally obtained and used for the excitation function calculation. At each most probable collision energy, the laboratory angular distribution $N_{cal}(\Theta)$, which is calculated from the laboratory frame flux distribution $I_{lab}(\Theta, E_T, E_c)$ transformed from the center-of-mass flux distribution $I_{CM}(\theta, E_T, E_c)$, is scaled to the normalized experimental laboratory angular distribution $N_{exp}(\Theta)$, using the least-squares fit expressed in the following:

$$\frac{d}{dz}\sum_i [N_{exp}(\Theta_i) - z\,N_{calc}(\Theta_i)]^2 = 0 \qquad (6)$$

The input $S_r(E_c)$ is then modified so that the least-squares scaling parameters z

agree to within 2-3% with the values in the excitation $S_r(E_c)$ for the corresponding collision energies, which indicates that the derived excitation function $S_r(E_c)$ fits the experimental data. Because the experimental angular distributions $N_{exp}(\Theta)$ were normalized, the scaling parameters z, therefore $S_r(E_c)$, are accordingly normalized for the relative reactant flux and for the same product signal scale. Finally, we would like to point out, in order to fit the time-of-flight spectra and angular distribution for E_c = 22.4 kcal/mole, the highest collision energy, we have to extrapolate the excitation function beyond the highest collision energy in our experiment to around E_c = 30 kcal/mole.

After optimizing this trial $I_{CM}(\theta, E_T, E_c)$ function, satisfactory fittings to the experimental data were finally achieved. The time-of-flight spectra and laboratory angular distribution for each collision energy are fitted with the optimized functions $P(E_T, E_c)$ and $T(\theta)$ as well as $S_r(E_c)$. Furthermore, the final calculated relative cross sections for each most-probable collision energy using the optimized fitting functions agree well with the optimized excitation function $S_r(E_c)$. The calculated and experimental laboratory angular distributions are shown in Figs. 2, 8, and 14. The fitted and experimental laboratory time-of-flight spectra are in Figs. 3, 9, and 15. The center-of-mass translational energy distributions $P(E_T)$ for the most-probable collision energies and the center-of-mass angular distributions are plotted Figs. 4, 10, and 16. Using the optimized center-of-mass flux-energy distribution $I_{CM}(\theta, E_T, E_c)$, we plot out, for the three most-probable collision energies, the center-of-mass flux distributions in velocity space $I_{CM}(\theta, u)$ ($I_{CM}(\theta, u)$

$\propto u \cdot I_{CM}(\theta, E_T)$) both in contour maps (Figs. 5, 11, and 17) and in 3-dimensional surface curves (Figs. 6, 12, and 18).

For all the three collision energies, the product translational energy release probabilities $P(E_T, E_c)$ are quite a large fraction of the total available energy. This is clearly shown in the time-of-flight spectra near the center-of-mass angles Θ_{CM}. For example, for collision energy 16.0 kcal/mole, the time-of-flight spectra at laboratory angles 40° and 50° show two separated peaks. As shown in the translational energy distributions, both the average kinetic energy and the peak kinetic energy are larger than 50% of the total available energy in the experiment for all the three collision energies. For lower collision energy such as 10.6 kcal/mole and 16.0 kcal/mole, the peak translational energy is close to the limit of the total available energy. The translational energy release probabilities for these two collision energies are interestingly shifted toward larger energy; there is small probability for low translational energy release. At the highest collision energy in our experiment, 22.4 kcal/mole, the peak in the $P(E_T, E_c)$ curve is moved toward lower energy slightly, but the overall translational energy release is still quite large.

The product ClO is scattered in a large range of laboratory angles for the higher collision energies shown in the laboratory angular distributions, despite 8.6 kcal/mole endoergicity. There are two peaks in all the three laboratory angular distributions. This is quite reasonable because of the large translational energy release. It is also noticed that, with the increase of the collision energy, the

difference of the intensities of the two peaks becomes larger and the two peaks are separated further apart. The forward peak in small angles close to the Cl beam becomes more predominant with the increase of the collision energy. The optimized center-of-mass angular distributions show certain forward-backward symmetry in the center-of-mass frame with large intensities located around 0° and 180° in the center-of-mass frame. However, the center-of-mass angular distributions are not completely symmetric with respect to 90° in the center-of-mass system, since there are obviously larger intensities in the forward direction with respect to the Cl atom than in the backward direction. With the increase of the collision energy, the forward part in the angular distribution increases as well. This is clearly manifested in the change of T(0°)/T(180°), the ratio between the center-of-mass intensity at 0° and that at 180°. It increases from 1.1 for E_c = 10.6 kcal/mole to 2.2 for E_c = 16.0 kcal/mole and finally to 2.7 for E_c = 22.4 kcal/mole. The ratio T(0°)/T(90°) increases with the collision energy too. It changes from 2.8 to 9.0 and 9.3 with the increase of the collision energy from 10.6 kcal/mole to 16.0 kcal/mole and 22.4 kcal/mole.

Laboratory angular distributions for wide angle in/elastic scattering of the Cl atom are measured and shown in Figs. 7, 13, and 19. The intensities of the in/elastic scattering of the Cl atom decrease normally in small laboratory angles near the Cl beam (see Fig. 7); however, the intensities in the angular distributions near the NO_2 beam, from laboratory angles 60° to 80°, increase again. Polynomial fitted curves shown in these figures are used only for the guideline of the data

points; no forward convolution fittings are carried out. However, we can still see that the center-of-mass angular distributions of the elastic and inelastic scattering of the Cl atom would be similar to those for the ClO reactive product. There should be large intensities around 180° in the center-of-mass frame in the CM angular distributions of the Cl atom in/elastic scattering.

Because of the significant amount of Cl_2 present in the Cl beam, we investigate whether Cl_2 would react with NO_2 as well. The possible reaction channel is $Cl_2 + NO_2 \rightarrow Cl + ClNO_2$ ($\Delta H_0^\circ \approx 24$ kcal/mole), which is readily open at $E_c = 31$ kcal/mole, the highest collision energy for Cl_2 and NO_2 scattering in our experiment. The reaction channel $Cl_2 + NO_2 \rightarrow Cl + ClONO$ ($\Delta H_0^\circ \approx 40$ kcal/mole) is too endoergic to be observed in our experiment. We try to detect $ClNO_2$ product at m/e = 81; however, we could not find any meaningful signal. The molecule-molecule reaction $Cl_2 + NO_2 \rightarrow Cl + ClNO_2$ certainly is slow. If there is a reaction barrier besides the reaction endoergicity, which is likely for a molecule-molecule reaction, it is not very surprising that we could not detect any evidence of this reaction at the collision energy of 31 kcal/mole.

To complete the picture of the reactive scattering of the reaction $Cl + NO_2 \rightarrow ClO + NO$, besides detecting one product ClO, we would also like to take data for the other product NO. However, the elastically and inelastically scattered parent NO_2 molecules generate a large amount of m/e = 30 signals. This makes the detection of the small amount of reactive scattered NO signals imbedded in the large background signals virtually impossible.

IV. DISCUSSION

The center-of-mass angular distributions of the reaction $Cl + NO_2 \rightarrow ClO + NO$ suggest that the reaction proceeds through a short-lived complex.[50,51] The angular distributions have some forward-backward symmetry in the center-of-mass frame; however, a more forward distribution is also quite evident. For a reaction which proceeds through a persistent long-lived complex that lives for more than one rotational period of the complex, the angular distribution is symmetric in the center-of-mass frame, and the intensities at both 0° and 180° are the same[51]. In the case of the reaction $Cl + NO_2 \rightarrow ClO + NO$, however, the asymmetry is quite obvious. With the increase of the collision energy, the asymmetry is further increased. It seems that, at the lowest collision energy 10.6 kcal/mole, the lifetime of the complex is close to and slightly smaller than a rotational period of the complex, since it is the most symmetric in all the three collision energies. With the increase of the collision energy, the lifetime of the complex is further shortened, which is demonstrated by the increase of the asymmetry. However, the significant intensities around 180° in all three collision energies manifest certain lifetime of the complex. The reaction $Cl + NO_2 \rightarrow ClO + NO$ can not be a direct reaction. The reaction intermediate stays on for a short period of time less than a rotational period, but the time is otherwise long enough for the intermediate complex to rotate to some extent so that the product decayed

from the complex into the wide angles is observed. Because of the nature of the short lifetime, a large fraction of the intermediate complex would decay before the complex has the time to finish one rotation, especially for the higher collision energy at which the lifetime is further shortened. Overall, it seems that the intermediate complex lives a time shorter than its rotational period. It decays fast while it is rotating. A large fraction of the products are spread in the forward direction; however, a small fraction of products are also generated in the backward direction when the intermediate complex rotates to certain extent.

If the reaction proceeds through the ClONO configuration, in which the Cl atom adds onto an oxygen atom of the NO_2 molecule, the potential well along the reaction coordinate is about 17 kcal/mole deep (Fig. 1), which may not be of enough depth to sustain a long-lived reaction complex. However, this potential well is still deep enough for the reaction to proceed through a short-lived complex. The reaction may proceeds through the $ClNO_2$ configuration as well. In this approach, the Cl atom adds onto the nitrogen atom of the NO_2 molecule. The potential well depth is about 33 kcal/mole (Fig. 1). It is deeper than that in the ClONO configuration; the reaction intermediate complex is expected to have a longer lifetime. However, the $ClNO_2$ configuration is considered unlikely as the intermediate for the reaction $Cl + NO_2 \rightarrow ClO + NO$. From the experimental angular distributions, we know that the lifetime of the intermediate of the reaction is quite short, less than a rotational period; however, for the $ClNO_2$ intermediate to produce the ClO + NO products, a rearrangement of this reaction complex to

a configuration similar to that of ClONO is required. This process is unfavorable in the time scale shorter than a rotational period. It is also less favorable statistically since the more statistically favored dissociation channel of the $ClNO_2$ configuration, the Cl + NO_2 channel, requires no rearrangement of the intermediate complex. Associated with the experimental results from Niki *et al.*[14] and Leu[9], which showed that ClONO product was found to be the major product of the Cl + NO_2 association reaction, it is reasonable to consider the reaction Cl + NO_2 → ClO + NO mainly proceeds through the intermediate complex of the ClONO configuration.

It is unlikely for the backward scattering of the ClO product in the center-of-mass frame to come from a direct reaction channel. The attack of the Cl atom on either one of the two oxygen atoms on NO_2 molecule has large range of acceptance angles; it is impossible for the ClO product to be solely scattered in the backward direction. If Cl attacks the nitrogen atom on NO_2 molecule, a rearrangement of the collision complex is required to form the ClO and NO products. The collision complex rotates while the rearrangement takes place, the backward ClO product again can not come from a direct reaction mechanism. Furthermore, the laboratory angular distributions of in/elastic scattering of Cl atom supports a short-lived complex mechanism as well. If a direct reaction mechanism took place in the reaction Cl + NO_2 → ClO + NO, the angular distribution of in/elastic scattering of the reactant Cl atom would be expected to decreases more or less monotonically with the increase of the laboratory angles

away from the primary Cl beam. In this direct reaction mechanism, the intensities of in/elastic scattering of Cl atom in the backward direction should be extremely low and quenched because the reactive scattering occurs mainly at small impact parameters. However, our experimental results show the increase of the backward scattering in the laboratory angular distributions (Figs. 7, 13, and 19). This could only be explained by a non-direct reaction mechanism. The collision complex lives for a short period of time, the reactant Cl atom decayed from the decomposition of the complex in the non-reactive channel, from the so-call "failed reaction",[52] is spread into a wide range of angles while the complex rotates. Because of the effect of the solid angle the detector sustains, very large intensities show up around 0° and 180° in the center-of-mass system; correspondingly, there are large intensities of in/elastic scattering of Cl atom in the backward direction in the laboratory angular distributions. Overall, the laboratory angular distributions of in/elastic scattering of Cl support a mechanism involved with a short-lived collision complex.

The asymmetric center-of-mass angular distributions that we obtained indicate that the majority of the collision complexes decompose in a time less than one rotational period.[50] At lower collision energy, the angular distributions show more forward-backward symmetry, which indicates that the lifetime of the collision complex increases relative to its rotational period as the collision energy decreased. We can make some estimation on the rotational period at different collision energies by using ClONO configuration as that of the collision complex.

Using the structure information of NO_2 molecule[53] and ClONO molecule,[54] and for the sake of simplicity, taking the case in which the Cl atom attacks the NO_2 molecule in a plane in the trans-ClONO configuration, we assume an impact parameter of 1.1 Å. Because of the supersonic cooling in the molecular beam, the rotational angular momentum of NO_2 molecule is assumed to be negligible so that the total angular momentum **J** is almost equal to initial orbital angular momentum **L**. At the collision energy E_c = 22.4 kcal/mole, initial orbital angular momentum $|\mathbf{L}| = \mu b v_{rel} \approx 110\ \hbar$, where μ is the reduced mass of the reactants, b is the impact parameter of the entrance channel, and v_{rel} is the relative velocity of the reactants. The moment of inertia about the rotation axis of the collision complex, I, is about 180 amu.·Å^2, assuming the ClONO configuration for the complex. The rotational period of the complex, $\tau_{rot} = 2\pi I/L$, is about 1.5 ps in the present model. At the collision energy E_c = 16.0 kcal/mole, $\tau_{rot} \approx$ 2.0 ps; while at the collision energy E_c = 10.6 kcal/mole, τ_{rot} is estimated to be ≈ 2.5 ps.

The product translational energy release in the center-of-mass frame is much larger compared with that in a usual reaction via a persistent long-lived complex in which the energy is completely randomized.[55] Although some initial translational energy is expected to be tied up in the rotation energy of the reaction complex and is eventually released as the product translational energy, the amount of this type of energy is not very large compared to the total energy release. The maximum amount of rotation energy of the collision complex that can be released into product translational energy is reached if the orbital angular

momentum of the products, **L'**, is equal to the total angular momentum **J**. For E_c = 22.4 kcal/mole, using the same parameters for estimating the lifetime of the complex, the maximum amount of energy that could be tied up in rotation of the complex is estimated to be ~ 3 kcal/mole, and it is quite small compared to the average and peak translational energy release at this collision energy. For E_c = 16.0 kcal/mole, this amount of energy is estimated to be ~ 2 kcal/mole, which is still not a significant fraction of the observed translational energy release. Conservation of angular momentum seems to play a bigger role for the reaction near the threshold energy; for E_c = 10.6 kcal/mole, the amount of energy tied up in rotation of the complex is about 1 kcal/mole, a significant amount of the translational energy release. However, because the complex could decompose leaving a fair amount of rotational excitation in the products (i.e., the final rotational angular momentum, **j'**, is not small), the final orbital angular momentum $|\mathbf{L}'|$ might be smaller than the total angular momentum, and the energy release into the translation of the products from the energy of the complex rotation may become smaller. If we use the peak translational energy release from the experiment results to calculate the relative velocity of the products and assume the impact parameter for exit channel to be similar to that for the entrance channel, we can estimate the final orbital angular momentum $L' = \mu' b' v'_{rel}$ and the rotational energy associated with it. All the rotational energies associated with the final orbital angular momentum are small, in a fraction of one kcal/mole. Therefore, the amount of energy that is tied up in rotation of the complex could

not account for the large translational energy release in the products, at least not for the high collision energies. The large product translational energy release might be associated with the short lifetime of the intermediate complex. During the short lifetime of the intermediate complex, the chemically excited intermediate complex does not have enough time to randomize all its internal energy; only few internal modes (vibration and internal rotation) are excited by the redistribution of the excess internal energy. The process of the randomization of the internal energy, intramolecular vibrational relaxation (IVR), is competing with the lifetime of the intermediate complex. The reaction complex does not have sufficient amount of time to redistribute effectively its excess internal energy, so there still leaves a large amount of energy coupled with the translational mode. The large product translational energy release in the center-of-mass system is therefore consistent with the short lifetime of the intermediate complex.

The incompleteness of the internal energy randomization can be further checked by looking at the time-of-flight spectra of the Cl atom from the decay channel of the collision complex back to the reactants Cl and NO_2. If energy redistribution in the ClONO intermediate complex were complete before the unimolecular decay, the reactants formed from this reverse channel would have very small center-of-mass frame recoil velocities and correspondingly very small translational energy release. However, for all three collision energies, the translational energy probabilities of in/elastically scattered Cl atom, which are obtained from satisfactory forward-convolution fittings to the time-of-flight

spectra of in/elastically scattered Cl atom, show peaks near the respective collision energy limit, i.e., the translational energies of the in/elastically scattered Cl atom are very large and close to the elastic scattering limit. Cl atom does not lose too much energy after colliding with NO_2 molecule to form the collision complex and then decaying from the collision complex. This certainly implies that the energy redistribution in the reaction intermediate is not complete. There is another check of the conclusion. For the reaction at E_c = 16.0 kcal/mole, a mixture of Cl_2, Ar and He was used for generating the Cl beam. Because of the similar mass of both Cl and Ar, Ar in the Cl beam serves as a internal reference for the in/elastic scattering. The time-of-flight spectra of in/elastic scattering of Ar were also measured along with those of Cl in/elastic scattering. The time-of-flight spectra of the in/elastically scattered Ar are very similar to that of the in/elastically scattered Cl atom (see Sec. II). This again suggests that a collision complex with completely statistically randomized internal energy does not form. This also suggests that the Cl addition cross section is substantially smaller than the in/elastic scattering cross section.

It is very interesting to look at the excitation function of this reaction. As shown in Fig. 20 (the filled circles are for the excitation function derived from the experiment), there is a rapid increase of the relative reactive cross section shortly above the reaction threshold; however, the increase of the cross section slows down, and the energy dependence of the cross section becomes flattened out above about 10 kcal/mole excess energy over the reaction threshold. The relative

reactive cross sections can be expressed as the following:

$$S_r = \sigma_{add}[\eta_{ClO}/(\eta_{ClO} + \eta_{Cl})] \quad (7)$$

where σ_{add} is the cross section for forming the collision adduct, η_{ClO} is the rate constant for the unimolecular decay of the collision complex into the products ClO and NO and η_{Cl} is the rate constant for the unimolecular decay of the collision complex back to the reactants Cl and NO_2. The value $\eta_{ClO}/(\eta_{ClO} + \eta_{Cl})$ is therefore the relative probability of decomposition of the collision complex into the products, i.e., the branching ratio for the collision complex to decay to the products. For an endoergic reaction, the branching ratio for the product channel increases rapidly with the increase of the excess energy. This could be understood by the energy dependence of the rate constants for both ClO and Cl channels using RRKM theory. Each rate constant η_i reflects the density of states at the transition state for a given pathway. For an endoergic reaction, the density of states at the product transition state increases faster with energy in the threshold region than the density of states at the reactant transition state; therefore the branching ratio of the product channel increases more rapidly with energy. The density of states depends strongly on the number of active vibrational modes in the transition state as well as the frequencies of those vibrational modes. With a smaller number of active vibrational modes, the

difference between the densities of states for the endoergic product channel and the exoergic reactant channel becomes smaller; the branching ratio for the product channel does not increase very rapidly either. This is easily shown by using the classical formula for the rate constant in the RRK theory: $\eta = A(\varepsilon^+/E^*)^{s-1}$, where ε^+ is the excess energy, E^*-E_0, at the transition state and s is the number of active vibrational modes.[56]

If we assume that the cross section for forming the collision adduct σ_{add} does not depend strongly on collision energy, the calculated branching ratio would well represent the relative reactive cross section using Eqn. 7. Noticing that the experimental excitation function does not increases rapidly with the excess energy, a reduced number of active vibrational modes might be involved in the energy redistribution in the collision complex. We carried out RRKM calculations[56,57] for the branching ratio of the product channel. The vibrational frequencies used in our calculation are taken from references 58 and 59 as well as from references 12 and 13. The branching ratios calculated with more than two active vibrational modes in the transition state do not flatten out around the excess energy from 10 kcal/mole to 20 kcal/mole; they still rapidly increase beyond 20 kcal/mole of excess energy, and they do not quite reproduce the experimental excitation function. Only the branching ratio calculated using two active low frequency vibrational mode in the transition state fits the experimental data very well (Fig. 20, the two sets of data are scaled at both excess energy E = 0 kcal/mole (relative cross section $S_r = 0$) and excess energy E = 21.4 kcal/mole

(relative cross section S_r = 1.)). The fact that reduced-mode RRKM calculation reproduces the experimental excitation function quite well does not necessarily mean that the small number of vibrational modes are in microcanonical equilibrium prior to the unimolecular decomposition. As the analysis for the center-of-mass angular distributions and translational energy distributions shows, the redistribution of the internal energy, i.e., intramolecular vibrational relaxation, in the collision complex, is competing with decomposition of the complex in this reaction. In principle, RRKM theory can not apply in this case. Therefore, the number of active modes used in the RRKM calculation is just a relative measure of the extent of intramolecular energy redistribution prior to the decay of the collision complex to the ClO and NO products. There are five possible vibrational modes in the transition state; however, there are only two used in the RRKM calculation to well reproduce the experimental excitation function. This is the indication that the energy redistribution in the collision complex is not completed before the complex undergoes decomposition. The experimental excitation function, which is well reproduced by the reduced-mode RRKM calculation, along with the product center-of-mass angular and translational energy distributions derived from the experimental data, confirms that the reaction Cl + NO_2 → ClO + NO proceeds through a short-lived complex. The experimentally derived excitation function, with the explanation from the reduced-mode RRKM calculation, and the product angular and translational energy distributions are quite consistent under the same model.

In reaching to a reduced-mode mechanism for this reaction, we have assumed that the cross section for Cl addition on to NO_2, σ_{add}, does not depend strongly on the collision energy. Because there is no energy barrier for the association reaction of Cl + NO_2[12] and the collision energy is very large (at least 10 kcal/mole) for the entrance channel of the association reaction, we do not think the cross section σ_{add} for Cl addition would strongly depend on the collision energy; at least, it would not increase very rapidly with the collision energy.

In a "line-of-centers" model for an endoergic reaction,[60] the reaction occurs if the kinetic energy along the line-of-centers exceeds the threshold energy E_0. The kinetic energy off the line-of-centers is used to overcome the centrifugal barrier, i.e., some amount of kinetic energy is taken as the rotational energy of the collision intermediate. The reaction cross section does not increase steeply as a step function above the reaction threshold E_0 because some kinetic energy is tied up in the rotational energy during the collision process. The energy dependence in this simple model can be expresses as: $\sigma_r(E_c) = \sigma(1 - E_0/E_c)$, when $E_c > E_0$ and $\sigma_r = 0$, when $E_c \leq E_0$. This function could be interpreted as the relative probability for the reactants to reach the critic configuration which leads to the products in a unit probability. It may also be considered as the relative probability of forming the collision adduct which decays to the products with unit probability. We calculate the relative cross section using this simple model (with E_0 = 8.6 kcal/mole), to compare with the experiment excitation function, this curve $\sigma_r(E_c)$ is further scaled so that $\sigma_r = 0$, at $E_c = E_0$; $\sigma_r = 1$, at E_c-E_0 = 21.4 kcal/mole. These

results are shown in Figure 21. Surprisingly, the experimental excitation function agrees with calculated reactive cross section dependence of energy using the line-of-centers model. However, this result may still be consistent with the result from the reduced-mode RRKM calculation. All the calculations suggest that the energy redistribution is incomplete, and the decomposition of the short-lived collision complex is very fast.

Finally we would like to inspect the effects of the electronic structures of both NO_2 and Cl on the reaction mechanism. The highest occupied molecular orbital (HOMO) on NO_2 molecule is $6a_1$.[61-63] It is half-filled with the unpaired electron mainly residing on the nitrogen atom. If the Cl atom attacks on the nitrogen site, because of the non-bonding nature of this orbital on the nitrogen atom, it may not quickly lead to the reaction channel ClO + NO; however, we can see that this approach is effective to form collision complex. It seems that the Cl atom needs to attack on the oxygen atom to cleave the N-O bond and to form ClO + NO products. The center-of-mass angular distributions from the experimental results support the mechanism that the Cl atom mainly attacks the oxygen atom of the NO_2 molecule. As we have seen, with the increase of the collision energy, the forward distribution in the CM angular distribution increases. This behavior can not come from the reaction approach in which the Cl atom collides with the nitrogen atom of the NO_2 molecule. The approach of the Cl atom towards the nitrogen atom has small impact parameter; it would mainly lead to backward scattered products in a direct reaction mechanism.

Furthermore, since the lifetime of the complex decreases with the increase of the collision energy; the adduct of the Cl on the nitrogen atom of the NO_2 molecule is less likely to finish one rotation before it decomposes, and the reaction mechanism is shifted to be close to a direct reaction. Following these arguments, if the Cl atom mainly attacks the nitrogen atom, with the increase of the collision energy, the backward scattering should be increased instead of the forward scattering. Therefore, the experimental angular distributions strongly indicate that the Cl atom attacks the oxygen atom of the NO_2 molecule. With the increase of the collision energy, the lifetime of the collision complex decreases; the forward stripping component in the center-of-mass angular distribution increases, and the reaction mechanism is shifted towards a direct reaction.

V. CONCLUSION

The reaction $Cl + NO_2 \rightarrow ClO + NO$ has been studied at three different collision energies. The product center-of-mass angular distributions and translational energy distributions as well as the excitation function have been derived. The center-of-mass angular distributions have some forward-backward symmetry; however, as the collision energy increases, the asymmetry in the angular distributions increases. The product translational energy release is generally large, with the average translational energy over 50% of the total

available energy. As the collision energy increases, the fraction of the total energy released into translation slightly decreases. The excitation function is found to have a positive dependence on the energy; however, it does not increase rapidly with the energy. The reaction proceeds through a short-lived complex whose lifetime is less than a rotational period. The energy redistribution in the collision complex is probably not complete before it decomposes. As the collision energy increases, the lifetime of the complex is shortened with respect to its rotational period; the forward distribution in the center-of-mass angular distribution increases; the reaction mechanism seems to be on the transition to a direct reaction. The reaction path in which the Cl atom mainly attacks the oxygen atom instead of the nitrogen atom of the NO_2 molecule seems to be more consistent with the experimental results.

VI. REFERENCES

1. R. P. Wayne, Chemistry of Atmospheres (Clarendon Press, Oxford, 1991).
2. J. J. Valentini, Ph. D. Thesis, University of California, Berkeley (1976).
3. J. J. Valentini, M. J. Coggiola, and Y. T. Lee, Rev. Sci. Instrum. **48**, 58 (1977).
4. J. S. Zhang and Y. T. Lee, to be published.
5. J. S. Zhang, T.T. Miau, and Y. T. Lee, to be published.
6. T. C. Clarke, M. A. A. Clyne, and D. H. Stedman, Trans. Faraday Soc. **62**,

3354 (1966).

7. M. S. Zahniser, J. S. Chang, and F. Kaufman, J. Chem. Phys. **67**, 997 (1977).

8. S. Glavas and J. Heicklen, J. Photochem. **31**, 21 (1985).

9. M. T. Leu, Int. J. Chem. Kinet. **16**, 1311 (1984).

10. W. B. DeMore, D. M. Golden, R. F. Hampson, C. J. Howard, M. J. Kurylo, M. J. Molina, A. R. Ravishankara, and S. P. Sander, JPL Publication 87-41 (1987) and the references cited therein.

11. A. R. Ravishankara, G. J. Smith, and D. D. Davis, Int. J. Chem. Kinet. **20**, 811 (1988).

12. D. E. Tevault and R. R. Smardzewski, J. Chem. Phys. **67**, 3777 (1977).

13. J. P. Burrows, G. S. Tyndall, and G. K. Moortgat, J. Phys. Chem. **92**, 4340 (1988).

14. H. Niki, P. D. Maker, C. M. Savage, and L. P. Breitenbach, Chem. Phys. Lett. **59**, 78 (1978).

15. J. S. Chang, A. C. Baldwin, and D. M. Golden, J. Chem. Phys. **71**, 2021 (1979).

16. J. Troe, J. Chem. Phys. **66**, 4758 (1977).

17. R. Patrick and D. M. Golden, Int. J. Chem. Kinet. **15**, 1189 (1983).

18. M. A. A. Clyne and R. T. Watson, J. Chem. Soc. Faraday Trans. I **70**, 2250 (1974).

19. M. S. Zahniser and F. Kaufman, J. Chem. Phys. **66**, 3673 (1977).

20. M. T. Leu and W. B. DeMore, J. Phys. Chem. **82**, 2049 (1978).

21. M. A. A. Clyne and A. J. MacRobert, Int. J. Chem. Kinet. **12**, 79 (1980).

22. G. W. Ray and R. Watson, J. Phys. Chem. **85**, 2955 (1981).

23. Y. P. Lee, R. M. Stimpfle, R. A. Perry, J. A. Mucha, K. M. Evenson, D. A. Jennings, and C. J. Howard, Int. J. Chem. Kinet. **14**, 711 (1982).

24. A. Menon and N. Sathyamurthy, J. Phys. Chem. **85**, 1021 (1981).

25. L. F. Phillips, J. Phys. Chem. **94**, 7482 (1990).

26. L. F. Phillips, J. Comput. Chem. **11**, 88 (1990).

27. H. H. Nelson and H. S. Johnston, J. Phys. Chem. **85**, 3891 (1981).

28. B. Y. Oh, Ph. D. Thesis, University of California, Berkeley (1988).

29. W. N. Sisk, Ph. D. Thesis, University of California, Berkeley (1990).

30. M. H. Covinsky, Ph. D. Thesis, University of California, Berkeley (1990).

31. H. F. Cordes and H. S. Johnston, J. Amer. Chem. Soc. **76**, 4264 (1954).

32. H. D. Knauth and H. Martin, Z. Naturforsch. **33 A**, 1037 (1978).

33. G. M. Wieder and R. A. Marcus, J. Chem. Phys. **37**, 1835 (1962).

34. W. Tsang, Int. J. Chem. Kinet. **5**, 947 (1973).

35. L. T. Molina and M. J. Molina, Geophys. Res. Lett. **4**, 83 (1977).

36. R. D. Levine and R. B. Bernstein, Molecular Reaction Dynamics and Chemical Reactivity (Oxford University Press, Oxford, 1987).

37. I. W. M. Smith, Kinetics and Dynamics of Elementary Gas Reactions (Butterworths, London, 1980).

38. Y. T. Lee, J. D. McDonald, P. R. LeBreton, and D. R. Herschbach, Rev. Sci. Instrum. **40**, 1402 (1969).

39. R. K. Sparks, Ph. D. Thesis, University of California, Berkeley (1979).

40. G. O. Brink, Rev. Sci. Instrum. **37**, 857, 1626 (1966).

41. a) N. R. Daly, Rev. Sci. Instrum. **31**, 264 (1960).

b) H. M. Gibbs and E. D. Commins, Rev. Sci. Instrum. **37**, 1385 (1966).

42. Carborundum Co., Specialty Graphite Plant, Sanborn, New York.

43. H. F. Davis, A. G. Suits, and Y. T. Lee, J. Chem. Phys. **96**, 6710 (1992).

44. P. S. Weiss, Ph. D. Thesis, University of California, Berkeley (1986).

45. M. F. Vernon, Ph. D. Thesis, University of California, Berkeley (1983).

46. D. J. Krajnovich, Ph. D. Thesis, University of California, Berkeley (1983).

47. a) K. Sköld, Nucl. Inst. Methods **63**, 114 (1968).

b) V. L. Hirshy and J. P. Aldridge, Rev. Sci. Instrum. **42**, 381 (1971).

c) G. Comsa, R. David, and B. J. Schumacher, Rev. Sci. Instrum. **52**, 789 (1981).

48. R. J. Buss, Ph. D. Thesis, University of California, Berkeley (1979).

49. G. N. Robinson, R. E. Continetti, and Y. T. Lee, J. Chem. Phys. **89**, 6226 (1988).

50. G. A. Fisk, J. D. McDonald, and D. R. Herschbach, Faraday Discuss. Chem. Soc. **44**, 228 (1967).

51. a) W. B. Miller, S. A. Safron, and D. R. Herschbach, Faraday Discuss. Chem. Soc. **44**, 108 (1967).

b) W. B. Miller, Ph. D. Thesis, Harvard University (1969).

52. D. O. Ham, J. L. Kinsey, and F. S. Klein, Faraday Discuss. Chem. Soc. **44**,

164 (1967).

53. K. M. Ervin, J. Ho, and W. C. Lineberger, J. Phys. Chem. **92**, 5405 (1988) and references therein.

54. S. C. Bhatia and J. H. Hall, Jr., J. Chem. Phys. **82**, 1991 (1985).

55. S. A. Safron, N. D. Weinstein, and D. R. Herschbach, Chem. Phys. Lett. **12**, 564 (1972).

56. P. J. Robinson and K. A. Holbrook, Unimolecular Reactions (Wiley, New York, 1972).

57. RRKM algorithm of W. L. Hase and D. L. Bunker, Quantum Chemistry Program Exchange, University of Indiana, Bloominton, Indiana.

58. B. Janowski, H.-D. Knauth, and H. Martin, Ber. Bunsenges. Physik. Chem. **81**, 1262 (1977).

59. M. E. Jacox, J. Phys. Chem. Ref. Data **19**, 1387 (1990).

60. Reference 36, pages 59-60.

61. C. R. Brundle, D. Neumann, W. C. Price, D. Evans, A. W. Potts, and D. G. Streets, J. Chem. Phys. **53**, 705 (1970).

62. J. E. DelBene, J. Chem. Phys. **54**, 3487 (1971).

63. C. P. Blahous III, B. F. Yates, Y. Xie, and H. F. Schaefer III, J. Chem. Phys. **93**, 8105 (1990).

VII. TABLES

TABLE I. Experimental conditions.

Cl v_{pk}[a] ($\times 10^4$ cm/s)	Cl Beam Speed Ratio	NO_2 v_{pk} ($\times 10^4$ cm/s)	NO_2 Beam Speed Ratio	E_{coll} (kcal/mole)	$\Delta E_{coll}/E_{coll}$
26.4	6.4	15.7	12.5	22.4	24%
21.1	7.0	15.2	11.6	16.0	20%
13.0	9.8	16.7	11.9	10.6	13%

a. Peak velocity.

TABLE II. Relevant quantities of the reaction.

E_{coll} (kcal/mole)	$\langle E_T/E_{avl} \rangle$	$n_{Cl}n_{NO_2}v_{rel}$ [a]	S_r (arb. units)
10.6	.57	.34	.39
16.0	.57	.84	.82
22.4	.54	1.0	1.0

a. Relative reactant flux (arbitrary units).

b. Relative reactive cross section scaled to 1.0 for E_{coll} = 22.4 kcal/mole (Excess energy $E = E_{coll} - E_0$ = 13.8 kcal/mole) in this table.

VIII. FIGURE CAPTIONS

Figure 1. Energy level diagram of the reaction Cl + NO_2 → ClO + NO. Two type of collision intermediate, ClONO and $ClNO_2$, are shown. Three collision energies in our experiment are also shown in the diagram.

Figure 2. Upper: Laboratory angular distribution of the reaction Cl + NO_2 at E_{coll} = 22.4 kcal/mole. The filled circles are from the experimental data. Error bars stand for 95% confidence limits. Solid line is the calculated laboratory angular distribution from the optimized center-of-mass differential cross section functional forms. The laboratory angular distribution is scaled to unit relative reactant flux, and the maximum in this angular distribution is further scaled to 1.0.

Lower: The Newton diagram for the reaction Cl + NO_2 at the most probable collision energy E_{coll} = 22.4 kcal/mole. The circle stands for the maximum center-of-mass recoil velocity of the ClO product at the most probable collision energy. The Cl beam direction is defined as 0° in the laboratory frame, and correspondingly the NO_2 beam direction is at 90°.

Figure 3. Laboratory time-of-flight spectra of the ClO product at indicated laboratory angles for the reaction Cl + NO_2 → ClO + NO at E_{coll} = 22.4 kcal/mole. The circles are the experimental data points, while the solid lines are for the calculated spectra.

Figure 4. Best fit translational energy distribution $P(E_T)$ and center-of-mass angular distribution $T(\theta)$ for the reaction $Cl + NO_2 \rightarrow ClO + NO$ at E_{coll} = 22.4 kcal/mole. The nominal total available energy is 13.8 kcal/mole.

Figure 5. Contour map for the ClO product center-of-mass flux-velocity distribution, superimposed on the nominal Newton diagram for the most probable collision energy E_{coll} = 22.4 kcal/mole.

Figure 6. 3-D surface plot for the ClO product center-of-mass flux distribution at E_{coll} = 22.4 kcal/mole.

Figure 7. Laboratory angular distribution of in/elastically scattered Cl. The distribution is in arbitrary units. The filled circles are data points from the integrated Cl time-of-flight spectra. The solid line is a polynomial fit which is only for the purpose of guideline.

Figure 8. Same as in Figure 2 but at E_{coll} = 16.0 kcal/mole.

Figure 9. ClO time-of-flight spectra at indicated laboratory angles for reaction $Cl + NO_2 \rightarrow ClO + NO$ at E_{coll} = 16.0 kcal/mole.

Figure 10. Same as in Figure 4 but at E_{coll} = 16.0 kcal/mole. The nominal total available energy is 7.4 kcal/mole.

Figure 11. Same as in Figure 5 but at E_{coll} = 16.0 kcal/mole.

Figure 12. Same as in Figure 6 but at E_{coll} = 16.0 kcal/mole.

Figure 13. Same as in Figure 7 but at E_{coll} = 16.0 kcal/mole. Notice also that the intensity is normalized to a different scale.

Figure 14. Same as in Figure 2 but at E_{coll} = 10.6 kcal/mole.

Figure 15. Same as in Figure 3 but at E_{coll} = 10.6 kcal/mole. Because the collision energy is very close to the reaction threshold, the reaction cross section is small and the center-of-mass recoil velocity is also small, therefore, only three time-of-flight spectra of the ClO product were measured.

Figure 16. Same as in Figure 4 but at E_{coll} = 10.6 kcal/mole. The nominal total available energy is 2 kcal/mole.

Figure 17. Same as in Figure 5 but at E_{coll} = 10.6 kcal/mole.

Figure 18. Same as in Figure 6 but at E_{coll} = 10.6 kcal/mole.

Figure 19. Laboratory angular distribution of in/elastically scattered Cl at E_{coll} = 10.6 kcal/mole. The intensity at laboratory angle 70° is scaled to 1.

Figure 20. Excitation function $S_r(E)$ of the reaction $Cl + NO_2 \rightarrow ClO + NO$. The filled circles are the experimentally derived values. The solid curve is from reduced-mode RRKM calculations. The threshold energy E_0 is 8.6 kcal/mole. The total available energy $E = E_{coll} - E_0$. Both sets of data are scaled at E = 0 kcal/mole with $S_r = 0$ and at E = 21.4 kcal/mole with $S_r = 1$.

Figure 21. Same as in Figure 20, except that the solid curve is from calculations using line-of-centers model.

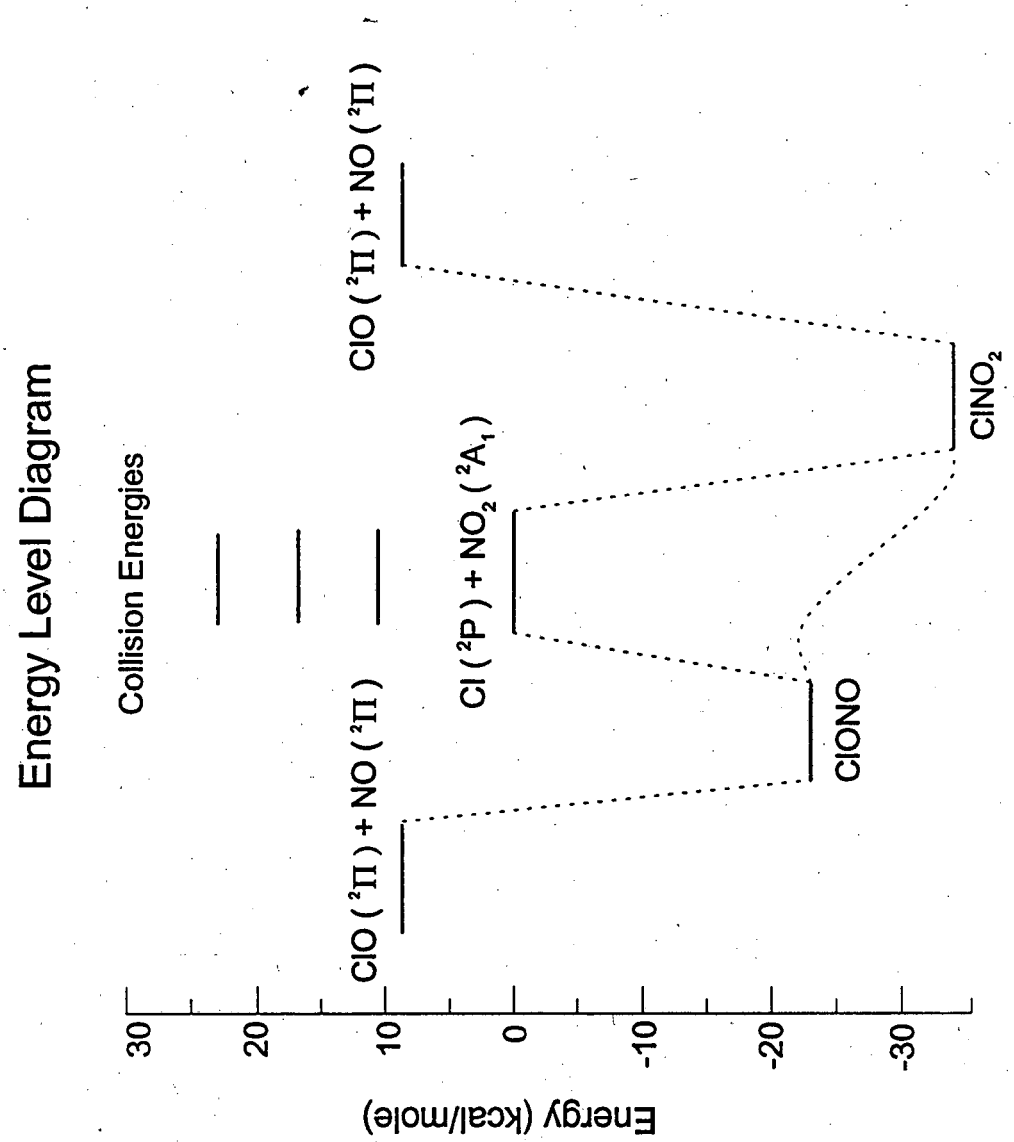
Energy Level Diagram
Collision Energies
ClO ($^2\Pi$) + NO ($^2\Pi$)
Cl (^2P) + NO_2 ($^2A_1$)
ClO ($^2\Pi$) + NO ($^2\Pi$)
ClONO
$ClNO_2$
Energy (kcal/mole)
30
20
10
0
-10
-20
-30

Figure 1

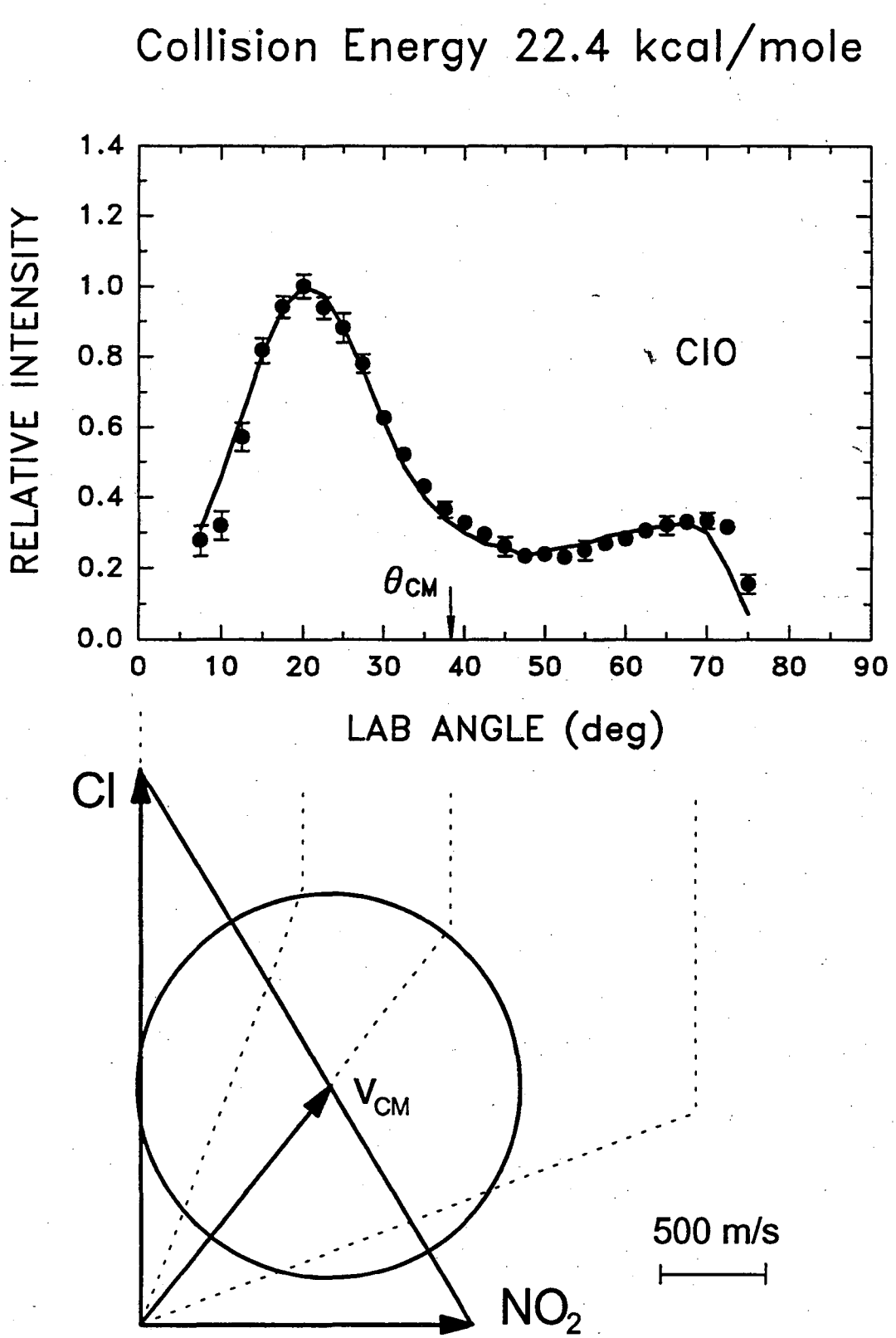
Collision Energy 22.4 kcal/mole
RELATIVE INTENSITY
1.4
1.2
1.0
0.8
0.6
0.4
0.2
0.0
ClO
θ_{CM}
0
10
20
30
40
50
60
70
80
90
LAB ANGLE (deg)
Cl
V_{CM}
500 m/s
NO_2

Figure 2

$$Cl + NO_2 \rightarrow ClO + NO \quad E_{coll} = 22.4 \text{ kcal/mole}$$

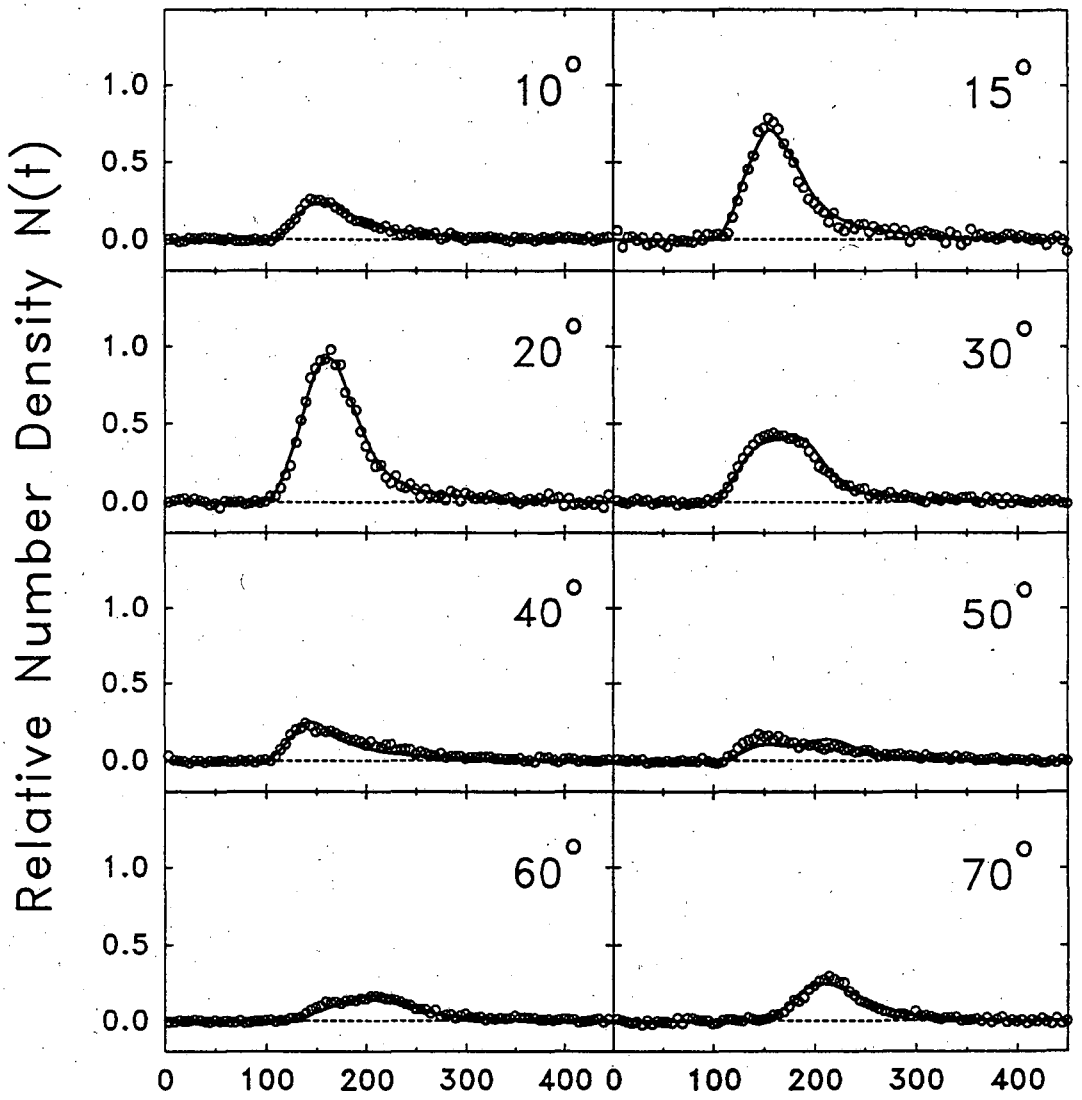

Figure 3

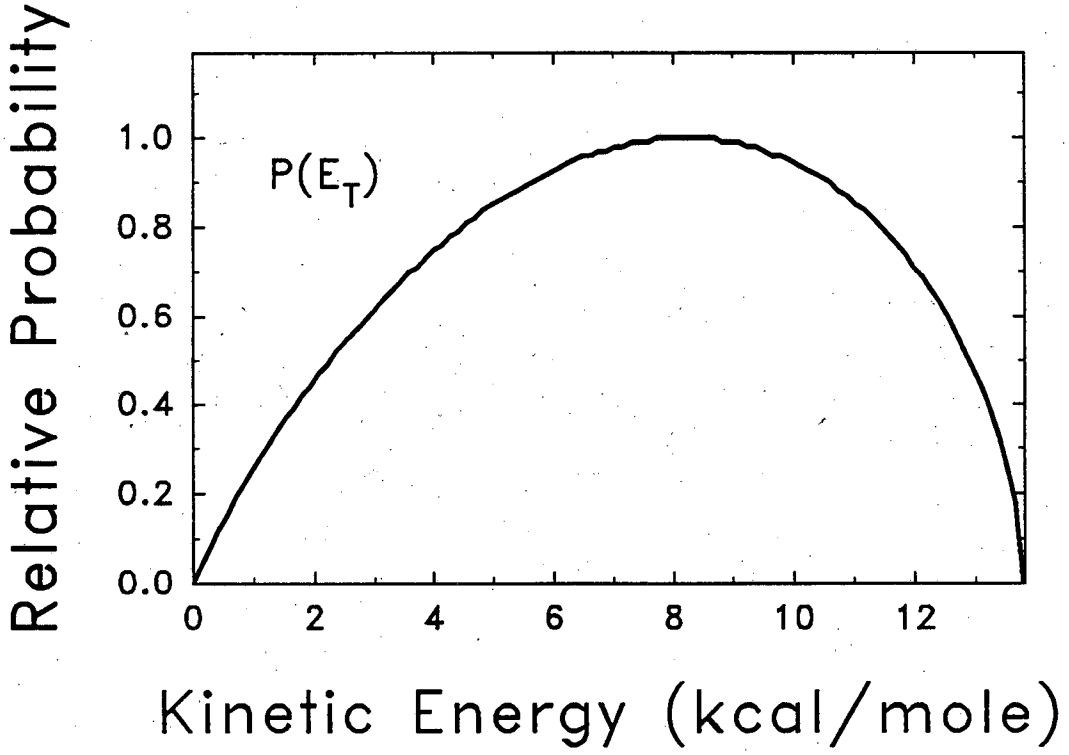
Relative Probability
P(E_T)
1.0
0.8
0.6
0.4
0.2
0.0
0
2
4
6
8
10
12
Kinetic Energy (kcal/mole)

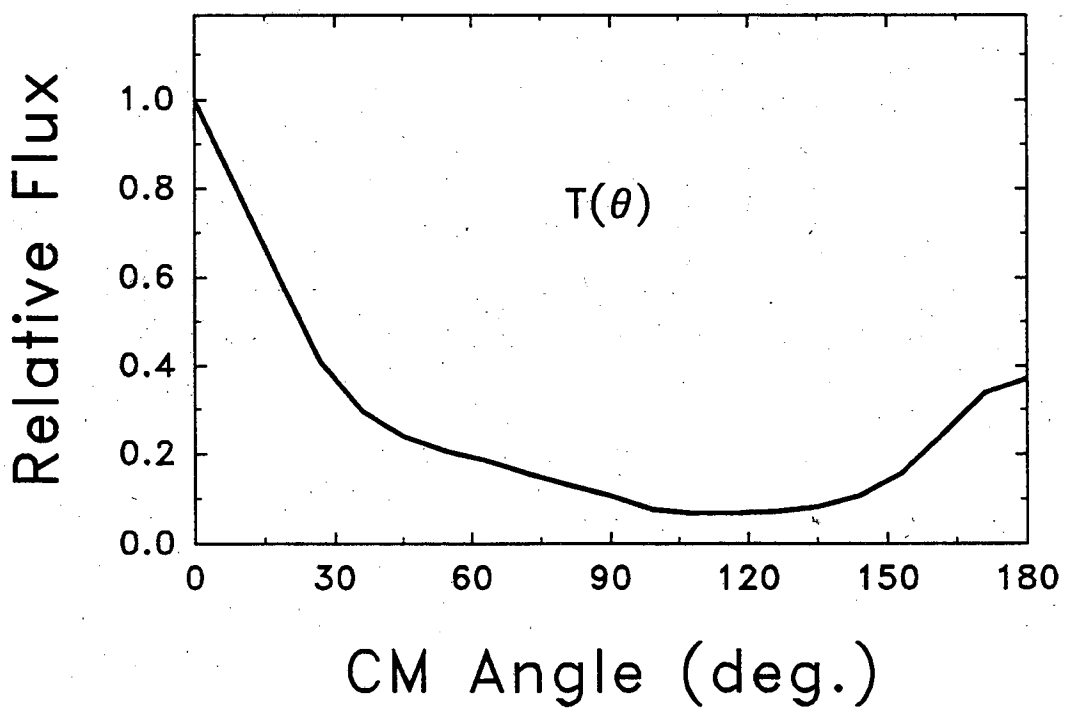
Relative Flux
T(θ)
1.0
0.8
0.6
0.4
0.2
0.0
0
30
60
90
120
150
180
CM Angle (deg.)

Figure 4

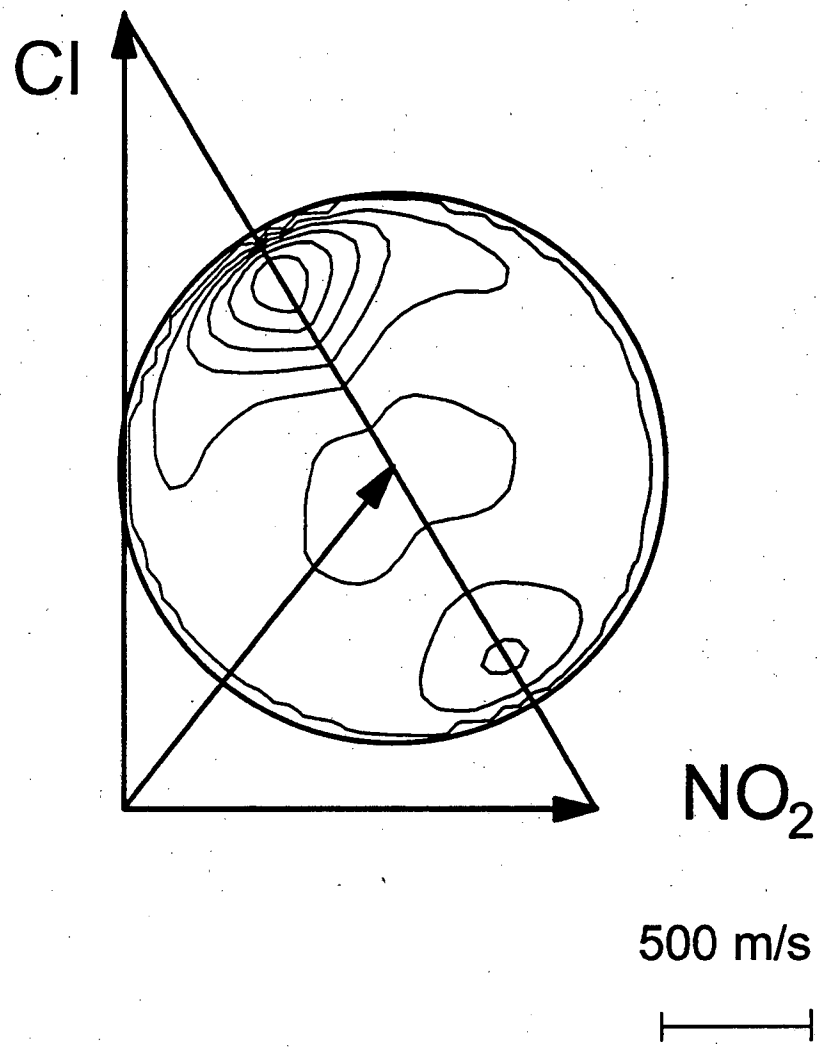

Figure 5

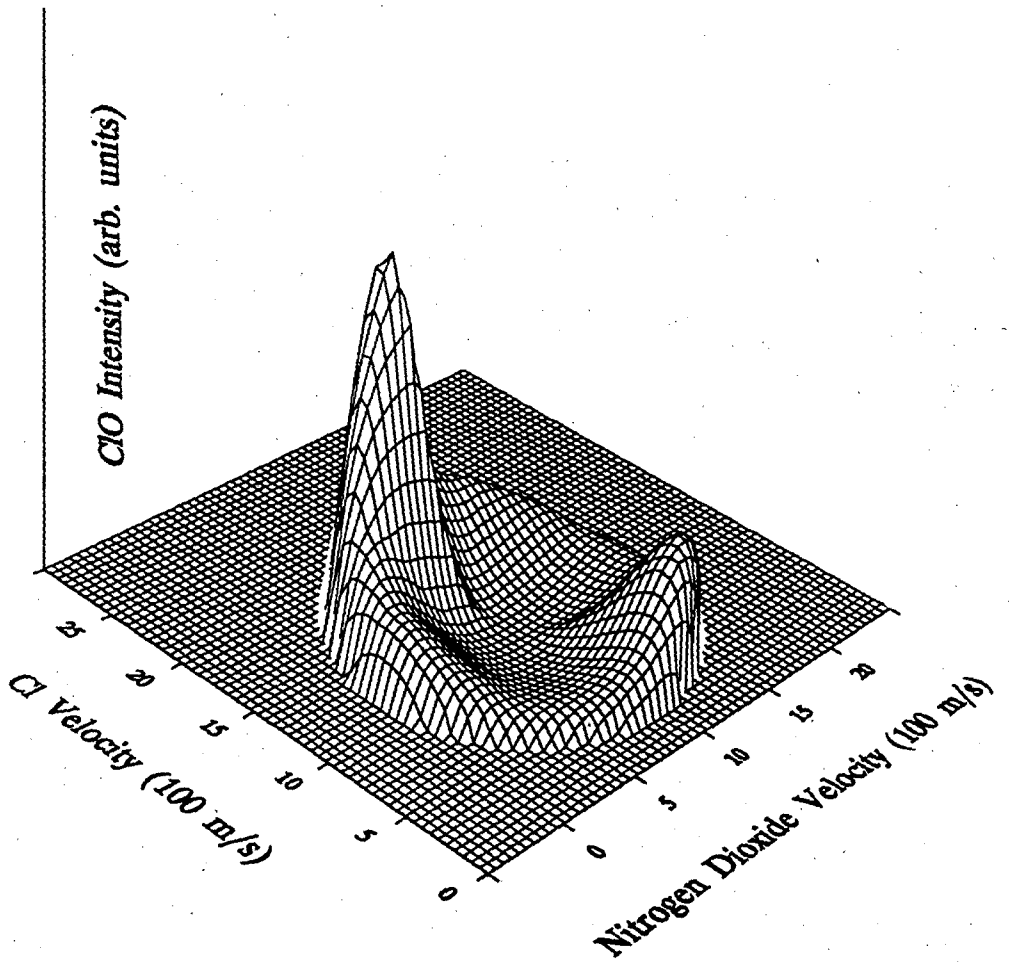
ClO Intensity (arb. units)
Cl Velocity (100 m/s)
25
20
15
10
5
0
Nitrogen Dioxide Velocity (100 m/s)
0
5
10
15
20

Figure 6

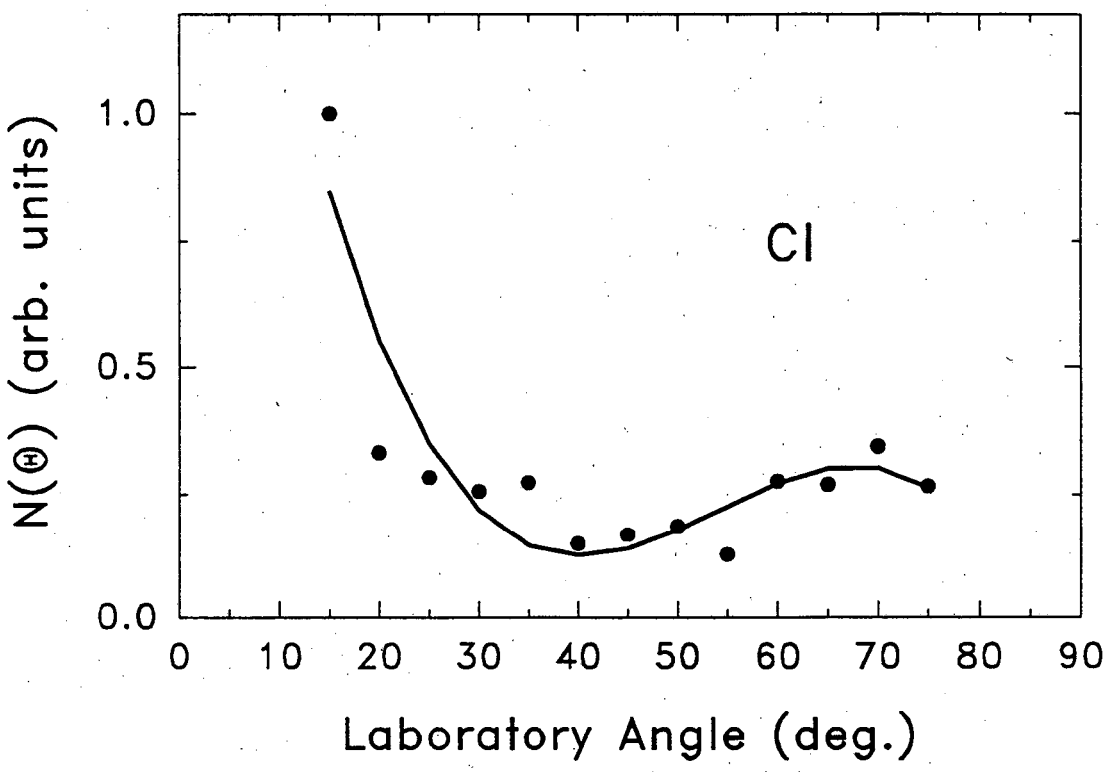
N(Θ) (arb. units)
1.0
0.5
0.0
Cl
0
10
20
30
40
50
60
70
80
90
Laboratory Angle (deg.)

Figure 7

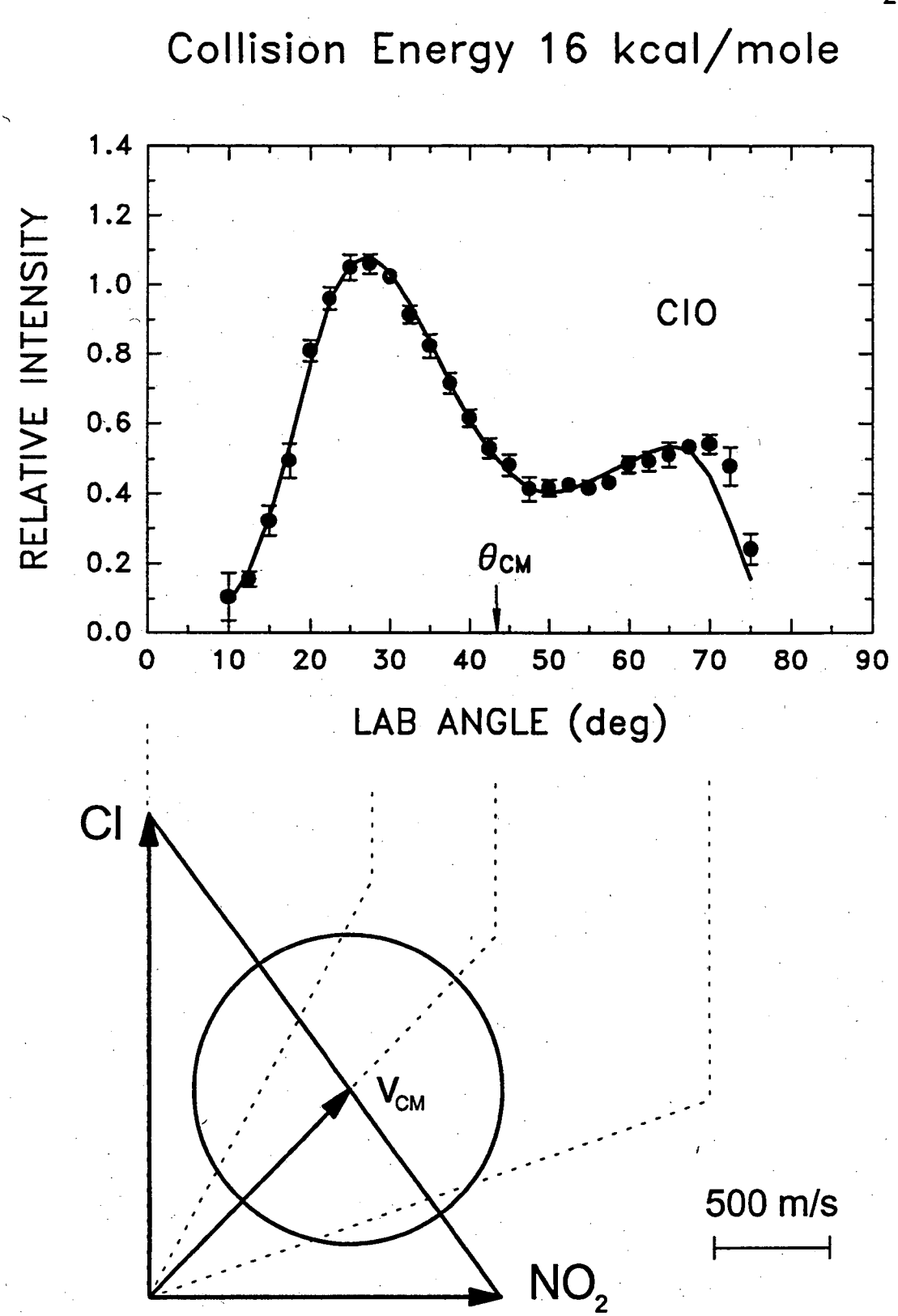
Collision Energy 16 kcal/mole
RELATIVE INTENSITY
1.4
1.2
1.0
0.8
0.6
0.4
0.2
0.0
ClO
θ_{CM}
0
10
20
30
40
50
60
70
80
90
LAB ANGLE (deg)
Cl
V_{CM}
500 m/s
NO_2

Figure 8

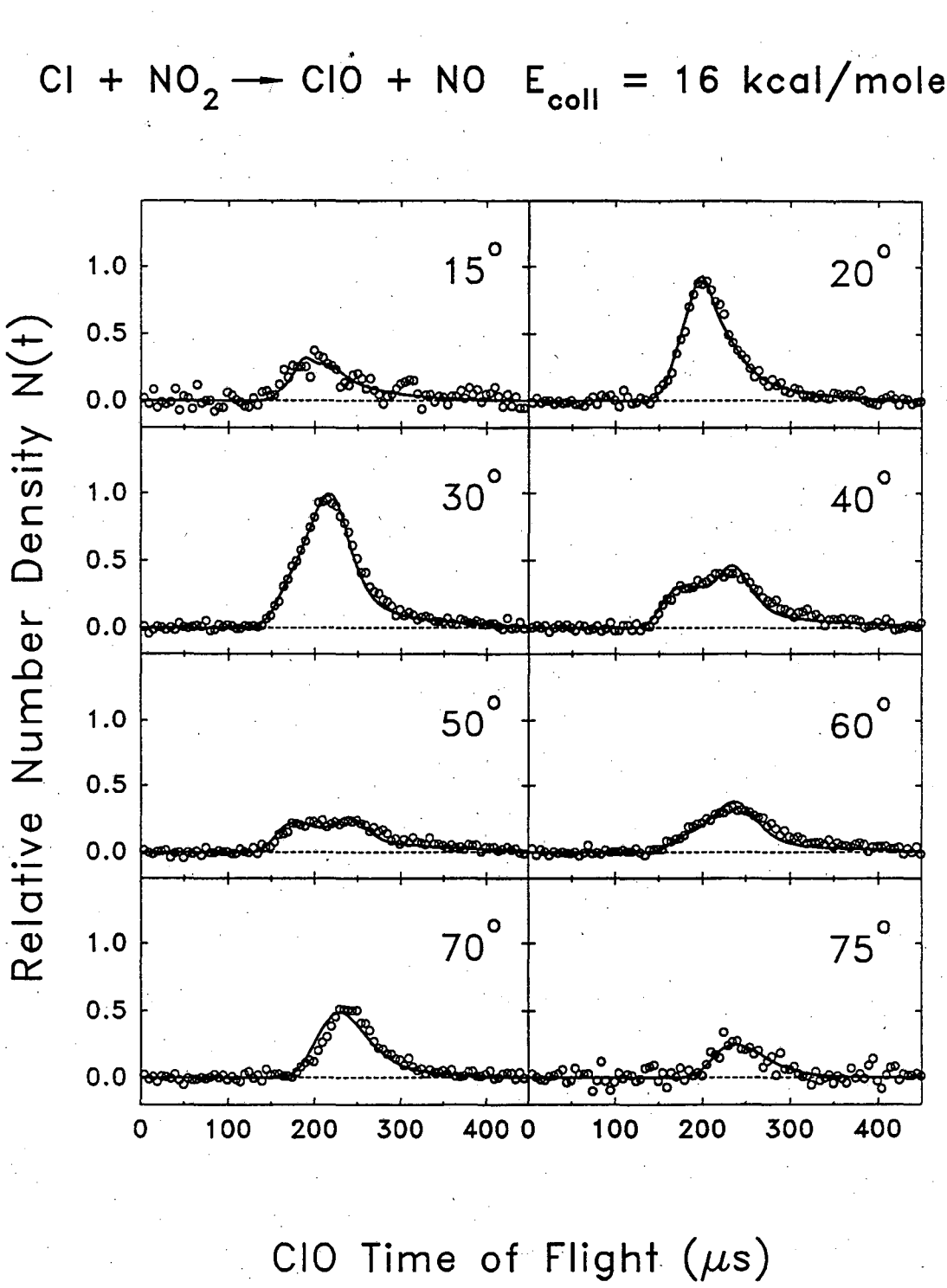
Cl + NO2 → ClO + NO E coll = 16 kcal/mole
15°
20°
30°
40°
50°
60°
70°
75°
1.0
0.5
0.0
0
100
200
300
400
Relative Number Density N(t)
ClO Time of Flight (μs)

Figure 9

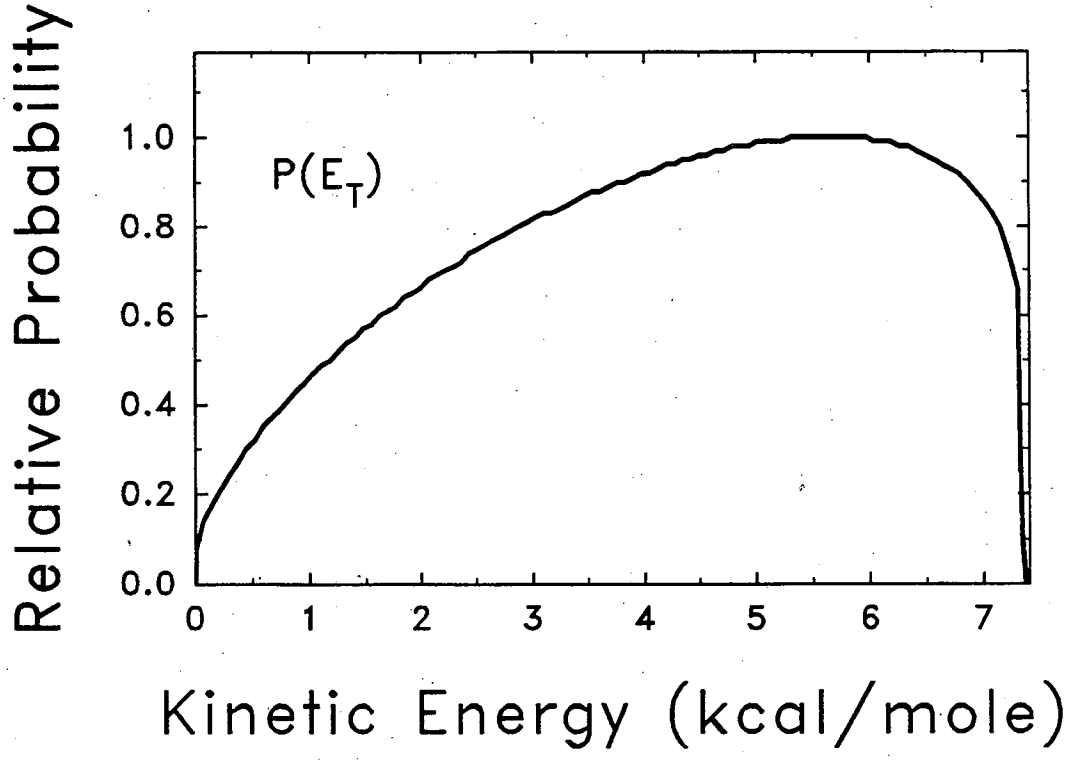
Relative Probability
P(E_T)
1.0
0.8
0.6
0.4
0.2
0.0
0
1
2
3
4
5
6
7
Kinetic Energy (kcal/mole)

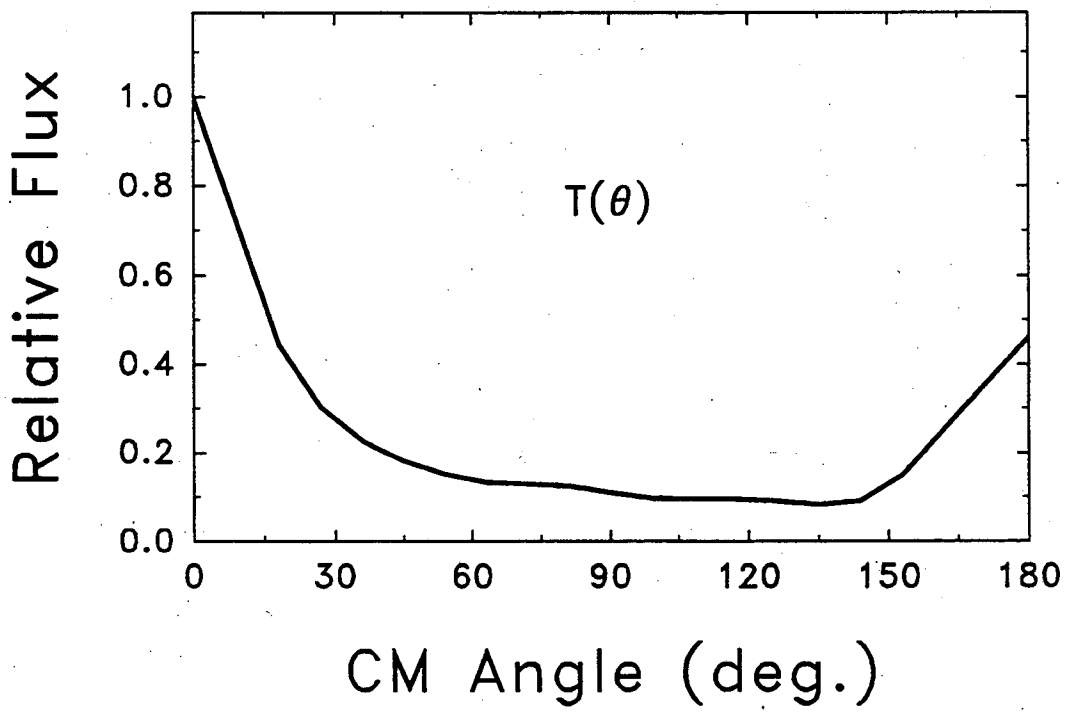
Relative Flux
T(θ)
1.0
0.8
0.6
0.4
0.2
0.0
0
30
60
90
120
150
180
CM Angle (deg.)

Figure 10

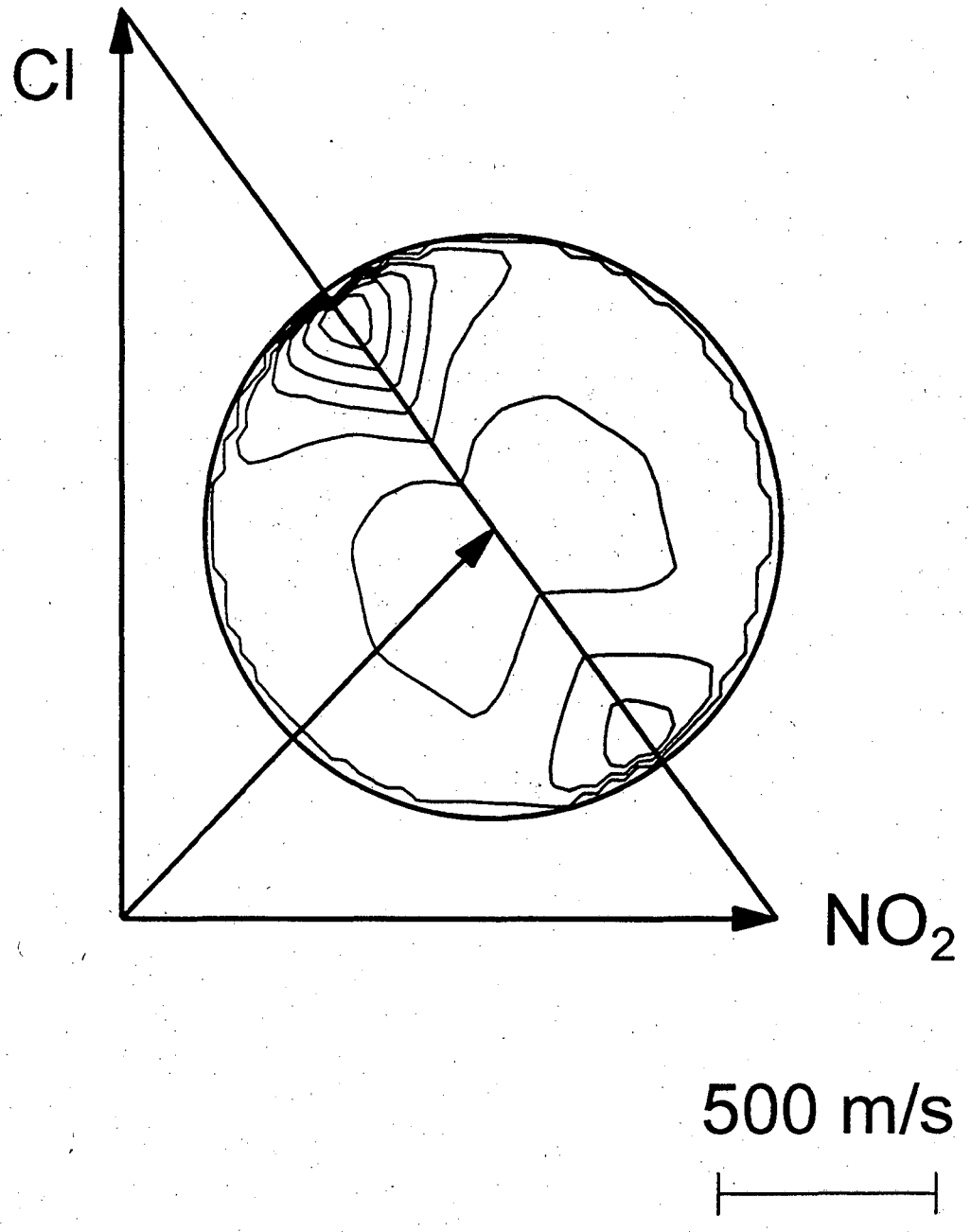

Figure 11

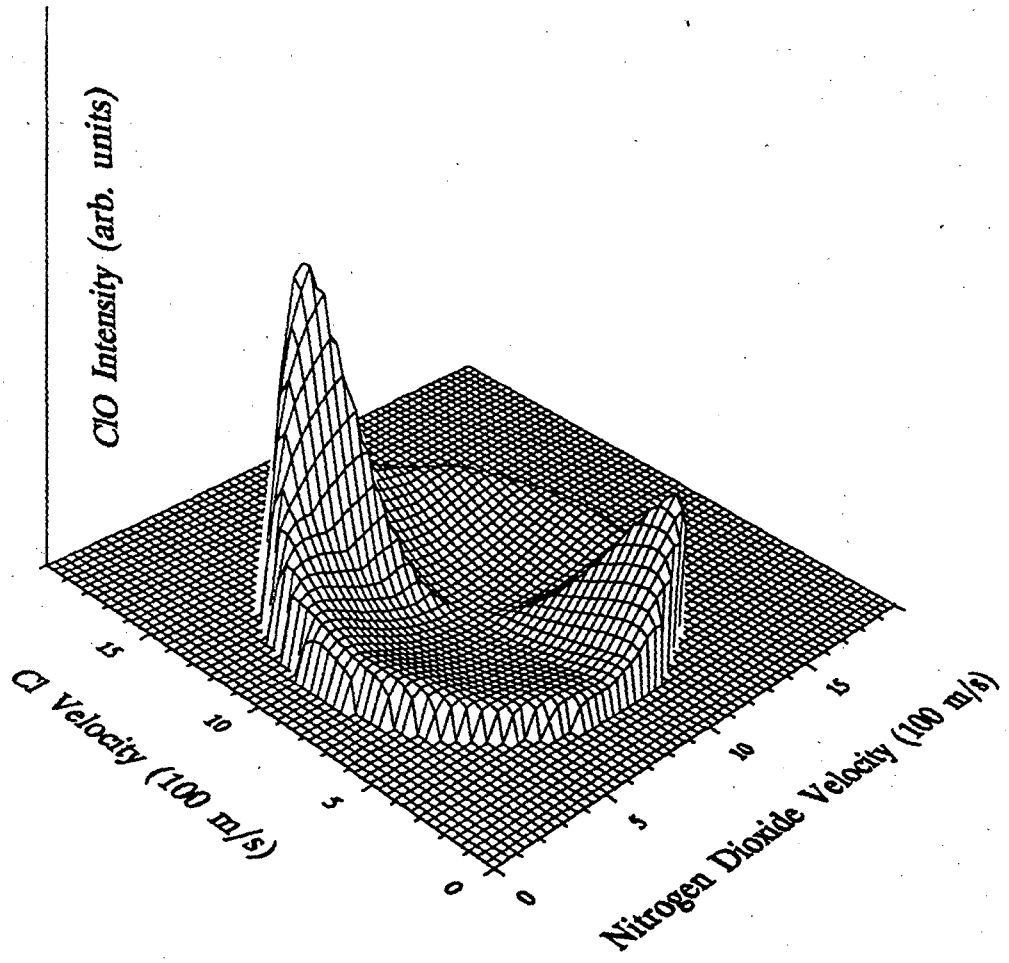
ClO Intensity (arb. units)
Cl Velocity (100 m/s)
0
5
10
15
Nitrogen Dioxide Velocity (100 m/s)
0
5
10
15

Figure 12

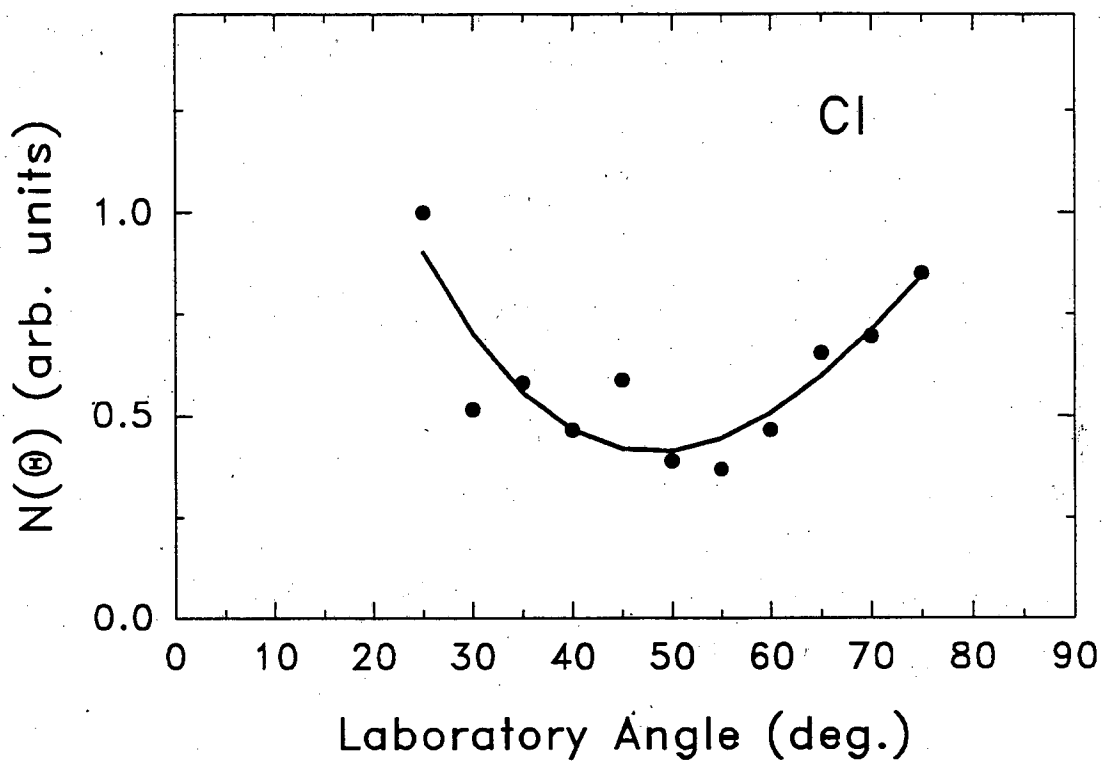
Cl
N(Θ) (arb. units)
1.0
0.5
0.0
0
10
20
30
40
50
60
70
80
90
Laboratory Angle (deg.)

Figure 13

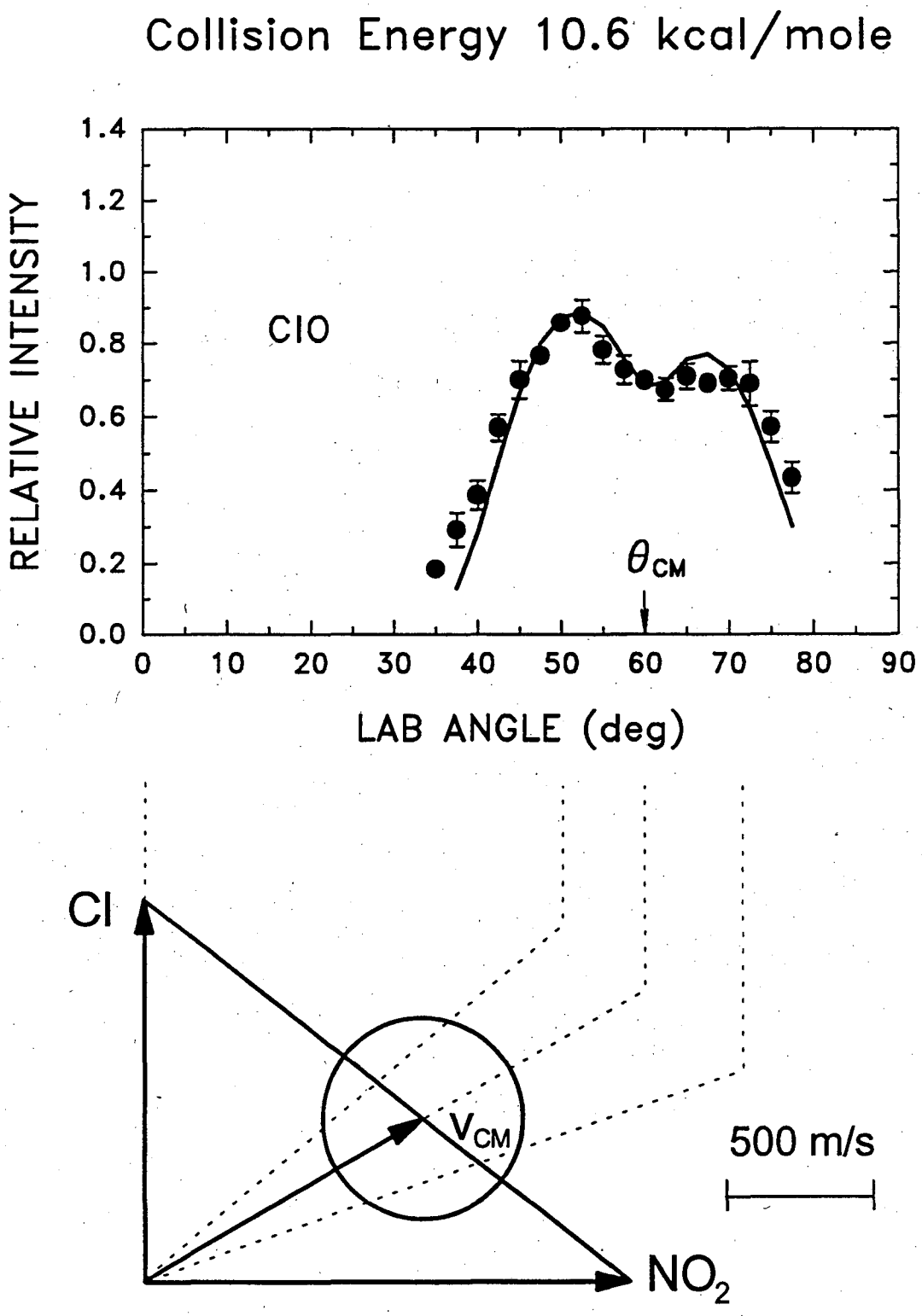
Collision Energy 10.6 kcal/mole
RELATIVE INTENSITY
1.4
1.2
1.0
0.8
0.6
0.4
0.2
0.0
ClO
θ_{CM}
0
10
20
30
40
50
60
70
80
90
LAB ANGLE (deg)
Cl
V_{CM}
500 m/s
NO_2

Figure 14

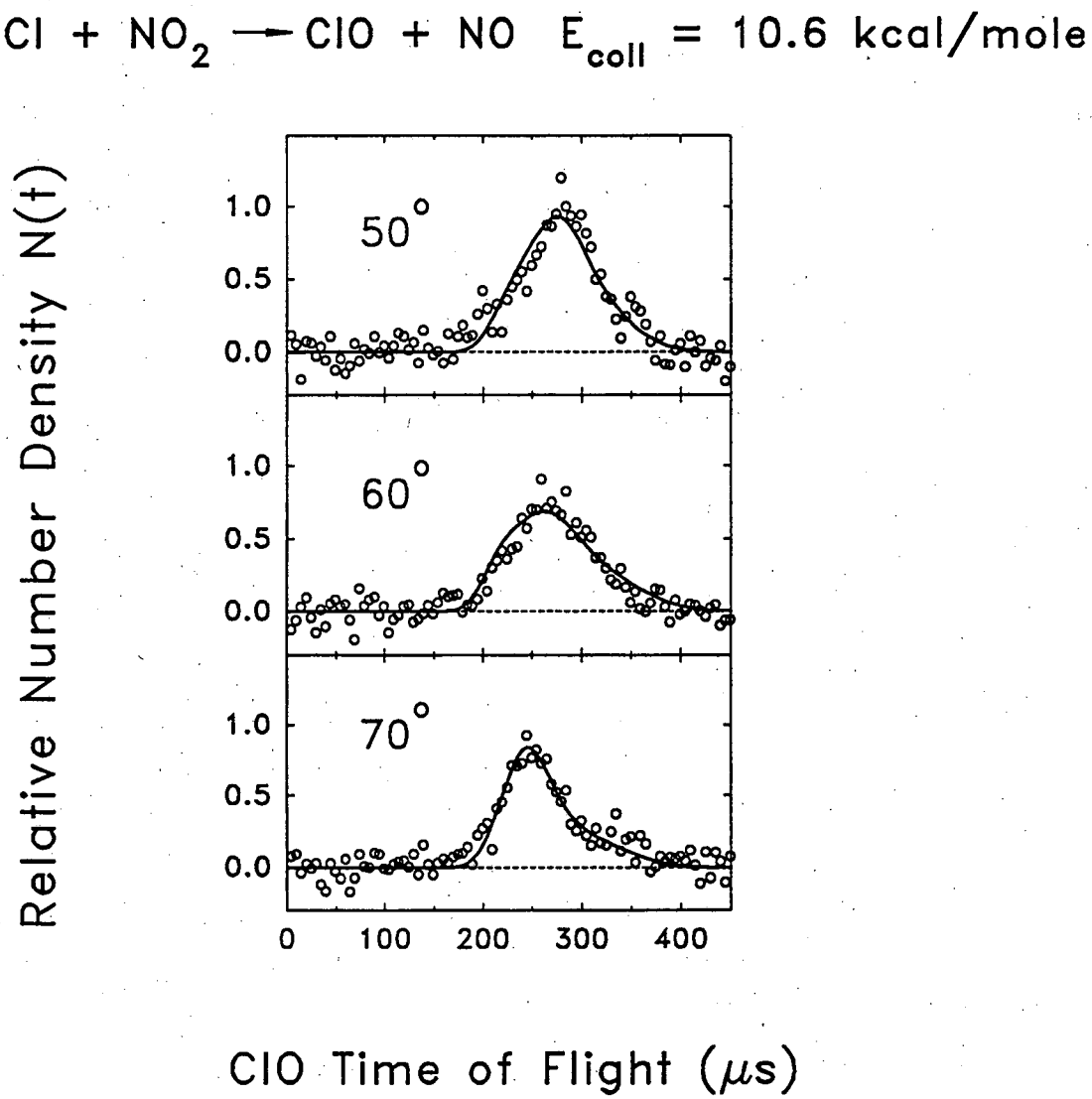
Cl + NO2 → ClO + NO Ecoll = 10.6 kcal/mole
Relative Number Density N(t)
50°
60°
70°
1.0
0.5
0.0
0
100
200
300
400
ClO Time of Flight (μs)

Figure 15

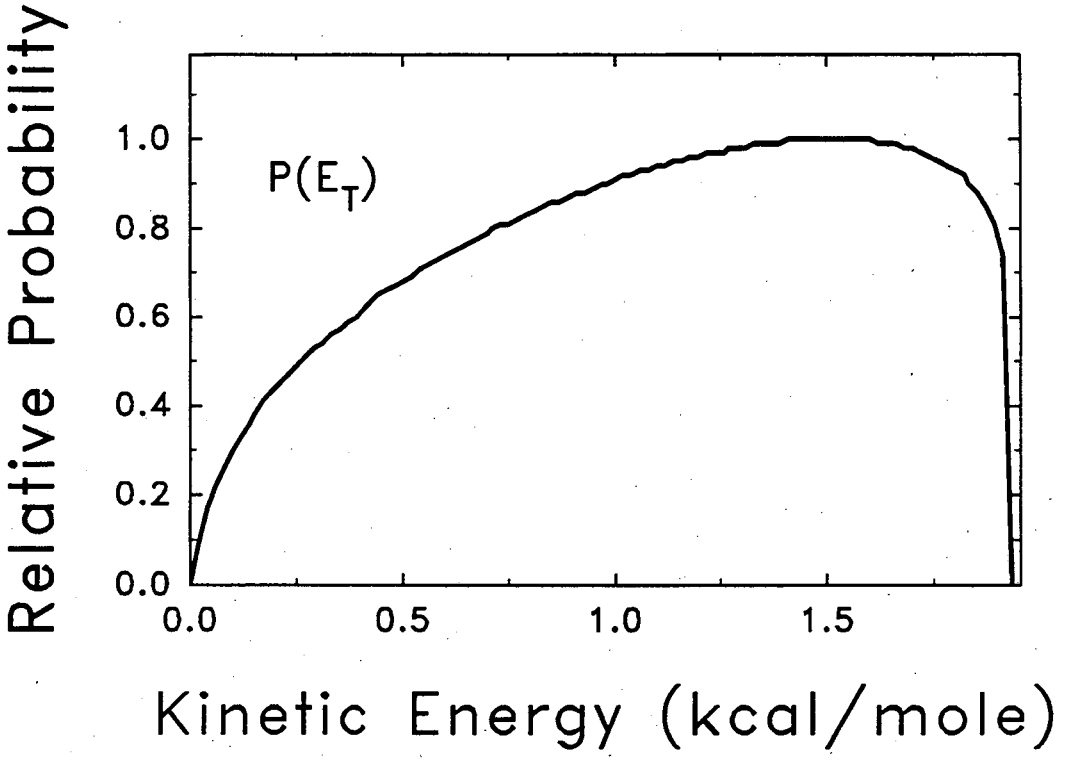
Relative Probability
1.0
0.8
0.6
0.4
0.2
0.0
P(E_T)
0.0
0.5
1.0
1.5
Kinetic Energy (kcal/mole)

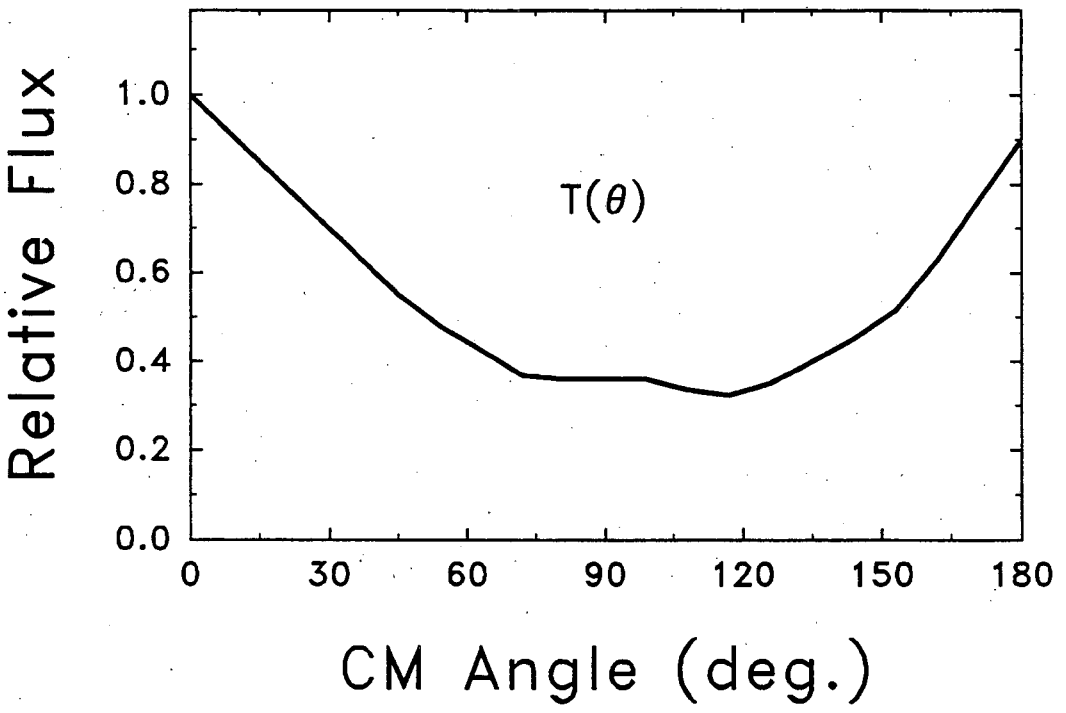
Relative Flux
1.0
0.8
0.6
0.4
0.2
0.0
T(θ)
0
30
60
90
120
150
180
CM Angle (deg.)

Figure 16

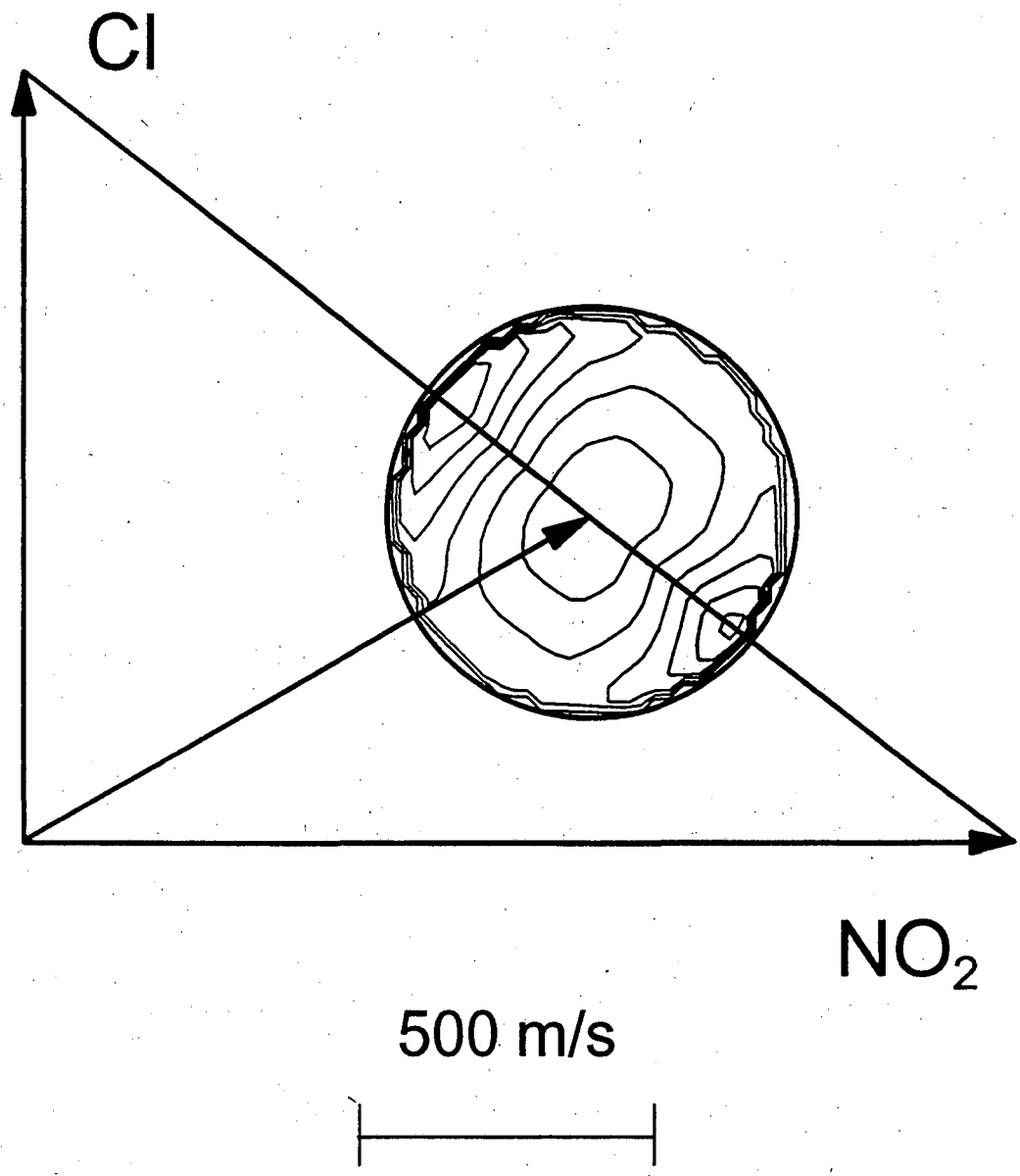

Figure 17

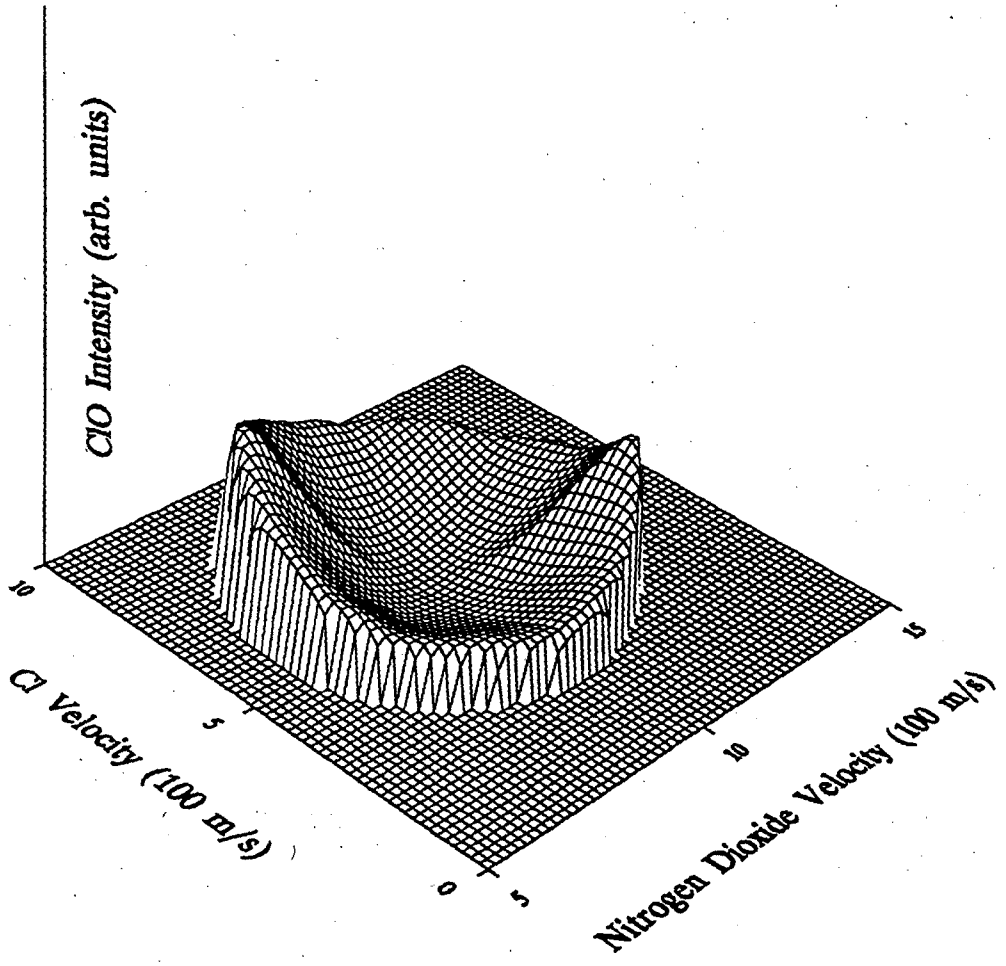
ClO Intensity (arb. units)
Cl Velocity (100 m/s)
10
5
0
5
10
15
Nitrogen Dioxide Velocity (100 m/s)

Figure 18

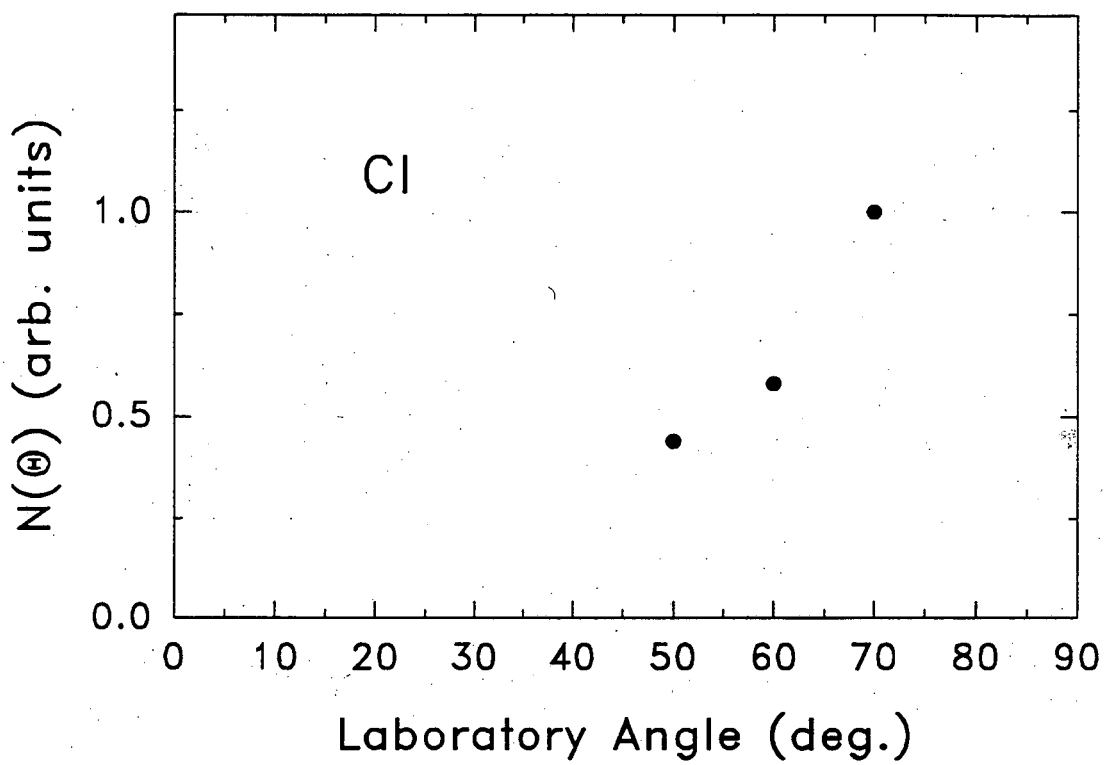
Cl
N(Θ) (arb. units)
1.0
0.5
0.0
0
10
20
30
40
50
60
70
80
90
Laboratory Angle (deg.)

Figure 19

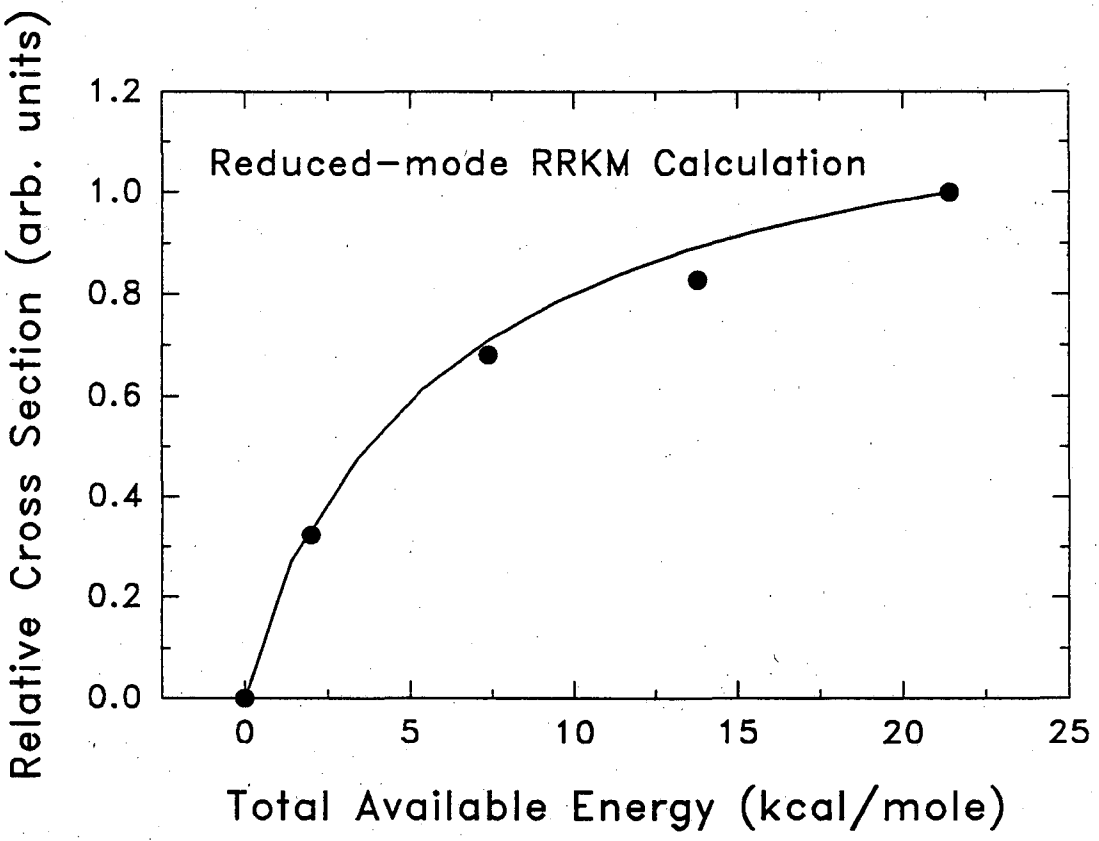
Reduced–mode RRKM Calculation
Relative Cross Section (arb. units)
Total Available Energy (kcal/mole)
0.0
0.2
0.4
0.6
0.8
1.0
1.2
0
5
10
15
20
25

Figure 20

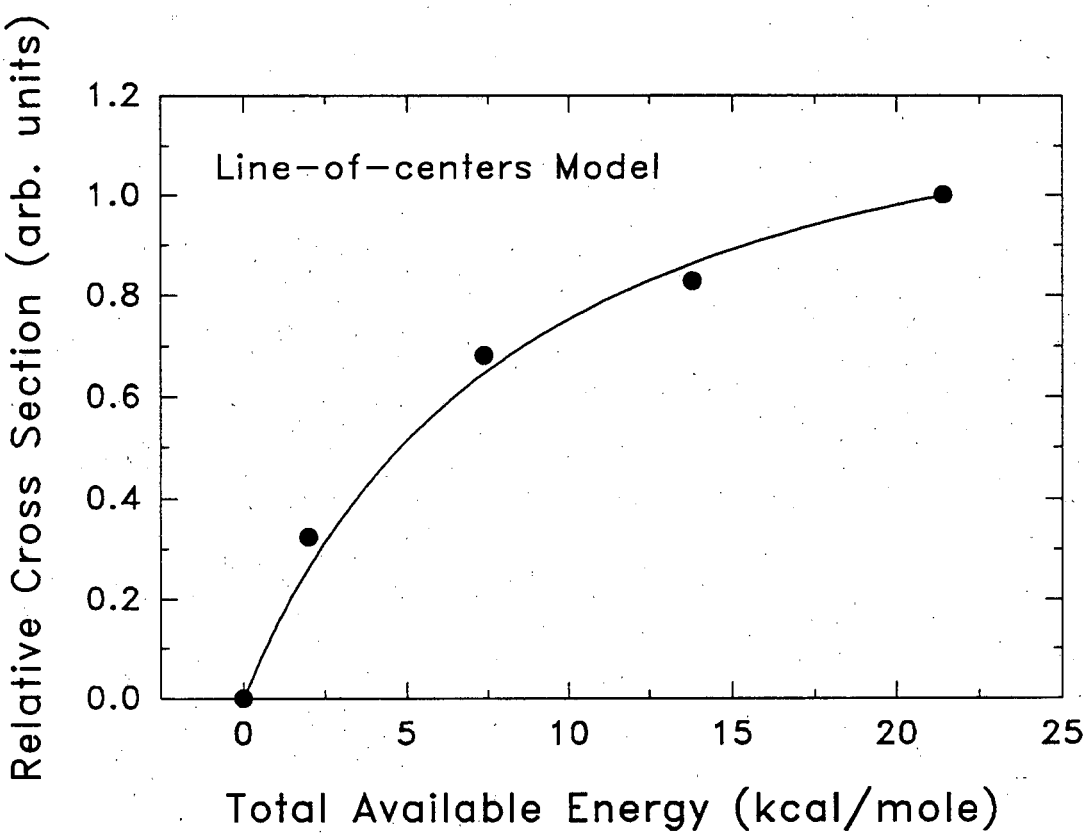
Line-of-centers Model
Relative Cross Section (arb. units)
Total Available Energy (kcal/mole)
0.0
0.2
0.4
0.6
0.8
1.0
1.2
0
5
10
15
20
25

Figure 21

LAWRENCE BERKELEY LABORATORY
UNIVERSITY OF CALIFORNIA
TECHNICAL INFORMATION DEPARTMENT
BERKELEY, CALIFORNIA 94720